TECHNISCHE UNIVERSITÄT MÜNCHEN

Lehrstuhl für Messsystem- und Sensortechnik

A kinematic measurement framework to investigate the modular organization of finger movements

Reinhard Gentner

Vollständiger Abdruck der von der Fakultät für Elektrotechnik und Informationstechnik zur Erlangung des akademischen Grades eines

Doktor-Ingenieurs

genehmigten Dissertation.

Vorsitzender:	Univ.-Prof. Dr. rer. nat. habil. B. Wolf
Prüfer der Dissertation:	
	1. Univ.-Prof. Dr.-Ing. habil. A.W. Koch
	2. Univ.-Prof. Dr. med. J. Claßen, Universität Leipzig

Die Dissertation wurde am 02.06.2009 bei der Technischen Universität München eingereicht und durch die Fakultät für Elektrotechnik und Informationstechnik am 07.12.2009 angenommen.

TECHNISCHE UNIVERSITÄT MÜNCHEN

Lehrstuhl für
Messsystem- und Sensortechnik
Technische Universität München
Univ.–Prof. Dr.–Ing. Alexander W. Koch

Dissertation

A kinematic measurement framework to investigate the modular organization of finger movements.

Reinhard Gentner

TECHNISCHE UNIVERSITÄT MÜNCHEN

Lehrstuhl für
Messsystem- und Sensortechnik
Technische Universität München
Univ.–Prof. Dr.–Ing. Alexander W. Koch

A kinematic measurement framework to investigate the modular organization of finger movements.

Reinhard Gentner

Abstract

In this thesis a measurement framework is described which allows a coherent analysis of cortical finger movement representations, human motor behavior, motor learning, and simulated finger movements. The results obtained with this framework suggest that synergistic joint movement patterns (modules), extracted from movements after stimulation of the primary motor cortex exhibit similarity to the kinematic features of voluntary grasping movements. Intensive training of a musical motor skill or short term repetitions of a single stereotyped movement result in a skill related adaptation of the modules. However, modules, resulting from simulated random muscle activation patterns are not sufficient to generate human grasping movements. The results support the hypothesis of a modular architecture of the nervous system, including neuronal cortical networks.

Zusammenfassung

In der vorliegenden Arbeit wird ein Messsystem beschrieben, das eine kohärente Analyse von kortikalen Bewegungsrepräsentationen der Hand und Finger, menschlichem motorischen Verhalten, motorischem Lernen und simulierten Fingerbewegungen ermöglicht. Die erzielten Ergebnisse deuten darauf hin, daß synergistische Kopplungen der Fingergelenke (Module), die von Bewegungen nach Stimulation des primär motorischen Kortex abgeleitet wurden, ähnlich zu willkürlichen kinematischen Greifmustern sind. Intensives Training musikalischer Fähigkeiten oder kurzzeitiges Wiederholen einer stereotypen Bewegung führen zu einer Anpassung der Module an die trainierte Fähigkeit. Aus simulierten, zufälligen Muskelaktivierungen resultierende Module sind jedoch nicht geeignet, menschliche Greifbewegungen zu reproduzieren. Die Ergebnisse unterstützen die Hypothese eines modularen Aufbaus des Nervensystems unter Einbeziehung neuronaler kortikaler Netzwerke.

Acknowledgements

First of all thanks to my family, especially my parents, Helga and Rudolf Gentner, and Doreen for their invaluable support during the entire thesis. The work for this thesis was carried out in Department of Neurology of the "Bayerische Julius-Maximilians Universität" in Würzburg in collaboration with the Institute for Measurement Systems and Sensor Technologies of the "Technische Universität München". Many thanks to Professor Claßen, who has given me excellent guidance and outstanding support throughout the thesis. I am grateful to Professor Dr. Alexander W. Koch for the possibility to conduct the thesis under his guidance. Many thanks for the continuous support and guidance. Thanks to Prof. Dr. Reiners for the support during the development of the sensor glove. I am grateful for the friendly and always good relationship to the other team members: Kristin Aufm Kampe, Su-Yin Dang, Susanne Gorges, Jenifer Jennings, Andre Nagel, Cigdem Önal, Claus Reinsberger, Julian Rumpf, Katja Stefan, Astrid Übelmesser, Katharina Wankerl, David Weise, and Daniel Zeller. Especially, I want to thank my students and collaborators who significantly contributed to this thesis: Andre Arnold, Eivind Bardalen, Daniel Dees, Wael Farhan, Andreas Gutsche, Ahmed Hefny, Katja Kessler, Helmut Kramer, Matthias Mahrenholz, Dan Qui, Florian Segor, Olga Sidorova and Florian Stumpf. Finally, many thanks to all participants in the neurophysiological studies, especially all musicians.

Contents

1 Introduction

Hand movements are the most complex movements in nature. Many of our cultural and technological achievements marking us as human depend on skilled use of the hand [263]. Tool use [167, 150], tool manufacturing [261], writing, music [5], arts, speech [188, 49, 10], possibly our entire culture [261, 263] would not exist without the human hand and the neural machinery underlying its control [145, 184, 31]. When we use our hand hundreds of times per day we are not aware of having the privilege of owning the greatest and most sophisticated motor apparatus among all species [168]. It is only when we observe the clumsy movements of a child, or the motor challenges faced by individuals with neurological disorders that we become aware of the inherent difficulties of motor control.

These difficulties arise from the high complexity of the human hand with 27 bones, 18 joints, and 39 intrinsic and extrinsic muscles [151] with over 20 degrees of freedom [227], muscle force transmissions to one or more finger or finger segments [205], tendon couplings , short and long loop reflex pathways [212] and millions of cortical and subcortical neurons connected to the muscles (Figure 1A and B). Despite years of research in the field of motor control and

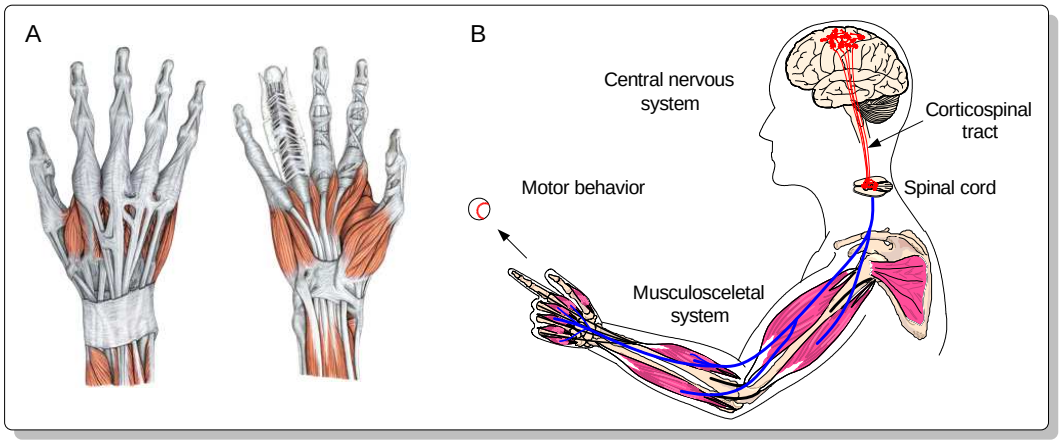

Figure 1: (A) Dorsal (left) and palmar view of the hand system. (Images are taken from [236].) (B) Schematic overview of the biomechanical and neuronal control architecture to generate finger movements.

recent advances in neurophysiological techniques such as transcranial magnetic stimulation (TMS) [14], no coherent understanding of control mechanisms and the capability to acquire and store new motor skills exists. Furthermore, as knowledge continues to grow in different research areas such as physics of the musculoskeletal system, neurophysiological studies to explore neural control, and investigations of motor behavior, it becomes more challenging to link these aspects of the motor system and to maintain a cohesive framework within which to describe motor function or to interpret the role of certain brain regions [216]. However, such a cohesive framework is a premise to understand the human motor system and to progress in the fields of rehabilitation [253, 64], neural prosthetics [171] and humanoid robotics [202].

1.1 Aim of the thesis

The aim of this thesis was to bring together several different research areas and study the neural mechanisms of finger movement control from neurophysiological, behavioral, and computational viewpoints in a single cohesive measurement framework. To accomplish this, the first aim of the thesis was to develop a measurement system consisting of several components for data collection and analysis, namely

- a custom developed, high resolution sensor glove to record finger movements,
- an experimental setup to record and analyze finger movements after transcranial magnetic stimulation (TMS), a non-invasive and painless method to stimulate the human brain (the neurophysiologial component),
- a virtual-reality, sensor glove based finger movement training system with database support (a behavioral component),
- a software system to assess grasping movements (a behavioral component), and
- a dynamic hand model to simulate the effect of muscle activity on finger movements (the computational component).

While the first aim mainly was theory formation and the technical development of the measurement framework, the second aim of the thesis was to apply the measurement framework to investigate

- the relationship between grasping movements and organization of the primary motor cortex,
- traces of musical skills in the central nervous system,
- short term motor learning with the training system, and
- the relationship between muscle activity and finger movements with the simulation model.

All thesis related publications are listed in the Chapter "Thesis related publications". The organization of the thesis to cover these points is described in the next chapter.

1.2 Organization of the thesis

The following chapters 1.3 - 1.4 explain the biological underpinnings of the human hand from an evolutionary perspective and highlight the control problem that the central nervous system has to solve in order to generate purposeful finger movements. These features are then embedded in a motor control theory (Chapter 1.7), which is used as a computational model for the analysis and interpretation of the results throughout the thesis. This theory states that finger movements are generated by combining basic movement patterns of multiple joints. Such basic movements will later be introduced as kinematic modules.

The remainder of the thesis is divided into two main parts. In the first part, the components of the measurement framework are explained (Figure 2). The topic of Chapter 2.1 is the development of a high resolution, flexible and low-cost sensor glove system, which

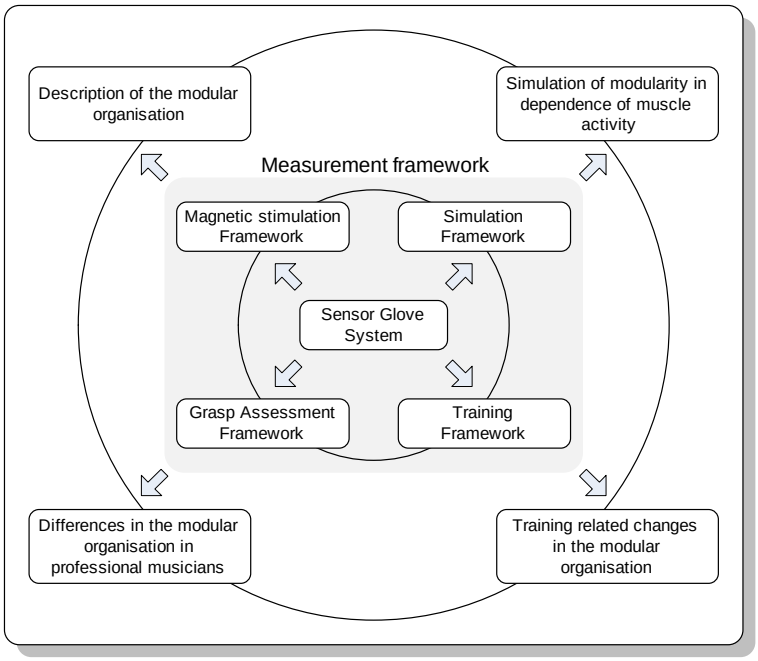

Figure 2: The thesis consists of two parts. The first is the technical development of a measurement framework for finger movements (grey shaded region). The second aim is the evaluation of the measurement framework to investigate neuronal principles of finger movement control.

represents the basic data acquisition instrument for assessment of finger movements. The neuro-navigation based magnetic brain stimulation environment, experimental setup and analysis methods are presented in Chapter 2.2. This element of the measurement framework represents the neurophysiological component to 'read out' kinematic representations of finger movements from the primary motor cortex. Furthermore, mathematical tools to extract and analyze kinematic modules are introduced. The behavioral element of the framework, the grasp-assessment system, is described in Chapter 2.3. This component allows the comparison of kinematic data obtained from magnetic brain stimulation to voluntary movements to build a bridge between motor cortex organization and grasping movements actively generated by the central nervous system. The finger movement training system, presented in Chapter 2.4, was developed to examine plasticity effects after finger movement training in conjunction with the brain stimulation environment. It consists of a database, and a fully featured virtual-reality based software system to visualize, record, and analyze the performance of subjects during training of a target movement. Finally, the first steps towards a simulation framework for the validation of the results from the other components are described in Chapter 2.5. In this chapter the development of a dynamic hand model controlled by 24 muscles is explained.

The second part of the thesis (outer circle in Figure 2) consists of empirical studies to examine the modular organization of the human CNS within the developed measurement framework. Each chapter represents a standalone project, containing different elements from the framework. The first study (Chapter 3.1) describes kinematic features of finger movements after TMS in healthy adults. The results are compared to other established methods such as functional magnetic resonance imaging. Characteristics of finger movements with respect to random data, movements after stimulation of the brachial plexus, passive finger movements and voluntary grasping movements are described and discussed. The

second study in Chapter 3.2 addresses the effect of learning a musical instrument on the organization of the primary motor cortex by investigating the change of finger movements after TMS due to years of intensive musical practice. This study was conducted with the help of professional violin players and showed that neuronal traces of motor skills can be highlighted with the measurement framework and can be directly linked to the trained movement repertoire. In the third study (Chapter 3.3), the developed finger movement training system is evaluated and the effect of short term learning of complex finger movements on the organization of the motor cortex is described. Finally in the fourth study presented in Chapter 3.4, the simulation environment is evaluated. The kinematic effect in terms of finger movements due to random muscle activity is investigated and compared to the results from empirical data. At the end of the thesis (Chapter 4), the results of all studies are summarized.

To understand the rationale of analysis and interpretation of the results, the evolutionary development of the human hand and the neural architecture controlling finger movements must be considered. These are introduced in the next chapter.

1.3 Evolutionary aspects of the human hand and its neural control

The human hand and its neural control architecture is not an one-off product of nature [168] but the product of millions of years of evolution. The earliest primates in the Paleocene (65-58 mio years ago) were equipped with five-rayed paws adapted to life in the trees, climbing and locomotion [263]. Two critical modifications in the musculoskeletal system contributed to the launching of the hominid line 3-5 million years ago. The first was the adoption of a bipedal gait, and the second were subsequent changes in the upper limb, altering the repertoire of hand movements in ways that favored tool use [261, 263, 267]. From this period, another one million years elapsed, until the production of tools was possible [261], a feature discerning humans from non-human primates [150]. Thus, the anatomic development of the hand, fingers and muscles [211] was not the only factor contributing to manual dexterity. In support of this notion it was emphasized that different types of non-human primates, although having a remarkable similar hand anatomy [184, 31, 263, 168], differ largely in their ability to generate dexterous finger movements [184, 31]. These observations highlight the importance of the neural machinery controlling finger movements. Especially, there is growing evidence that the expression of the motor system, especially direct cortico-motoneuronal connections, are a surrogate marker for manual dexterity [140, 184, 145, 31].

In addition to differences in the corticospinal tract, the intrinsic organization of the primary motor cortex presynaptic to the corticospinal tract is equally important [149]. In humans, intracortical motor maps in the primary motor cortex have developed during evolution to grossly somatotopic, multiple representations of movements, both repeated and highly interspersed with other representations [82, 178, 266, 195, 208]. Evidence for the importance of the full expression of the motor system comes from the observation that small infarctions [207] or locally distinct inactivations in the primary motor cortex [35, 209] abolish dexterous finger movements while unskilled movements remain intact. Similar conclusion can be derived from onthogenesis. In humans, skilled voluntary control of movements develops post-natally with the emergence of motor skills over the first 18-24 post-natal months [73]. The increase in dexterity can be neurophysiologically linked to the emergence of motor maps in the primary motor cortex [73, 160] and maturation of the corticospinal tract [76, 149].

Thus, in addition to neuroanatomic evolutionary changes, parallel development of the neural system, especially the full expression and integrity of the motor system supports the capacity to produce dexterous movement. As a consequence of this evolutionary development, the resulting biological human hand retains many structural and functional features of the ancestral appendage [211], which must be considered to understand the control mechanisms of the human hand. These features are reviewed in the next chapter.

1.4 Synergistic nature of finger movements

Although nonhuman primates, and specifically humans are clearly capable of more sophisiticated finger movements, the vast majority of movements we execute simply consists of grasping for objects [206], where fingers act synergistically with other fingers, the wrist, and the arm. Beyond grasping, the fine finger movements used in manipulating small objects, typing or playing musical instruments are performed less frequently. Although the fingers are commonly assumed to move independently during such tasks, recordings show that these sophisticated performances entail simultaneous motion of multiple digits. Even when asked to move individual fingers, both nonhuman primates and humans show some degree of simultaneous motion in neighboring fingers [137, 227, 205, 71], whether moving the fingers isotonically [96, 204] or applying forces isometrically [187, 268].

This synergistic nature of finger movements may result from biomechanical constraints such as tissue couplings [96, 137, 211], tendon interactions [143], finger dynamics, neuromuscular compartmentalization [211] and multi-tendoned muscles [205]. For example, in humans the flexor digitorum profundus, the flexor digitorum superficialis and the extensor digitorum each give tendons to all four fingers [206, 236] causing considerable co-movements of all fingers. The independence of finger movements during voluntary control is not only modulated by biomechanical factors but also by the spinal and cortical neural organization including convergence of different neurons on the same muscle [44, 174, 82, 178, 265, 232, 104, 135, 65, 234] divergence of the output of a single neuron to several motoneuron pools in the spinal cord and muscles [221, 184, 208, 113, 146, 153, 74] and horizontal interconnections between neurons in the primary motor cortex [105, 186, 65, 94, 72, 125, 12]. As a consequence of the entire neuroanatomic organization, the activation of neuronal populations [94, 82, 178, 265] or even a single neuron in the primary motor cortex [34] results in most cases in complex muscle activation patterns and synergistic movements.

In addition to the phyolgenetic and onthogenentic development of the hand system, fast changes in the neural system during motor skill learning or motor adaptation must be considered.

1.5 Plasticity of the nervous system

One of the most intriguing aspects of the behavior of primates is their remarkable flexibility in motor behavior including learning of new motor skills or adaptation to novel environments. Functional and structural reorganization of the neural system are seen as mechanisms by which this flexibility can be expressed by the nervous system [118, 175, 172, 129, 111, 42, 39, 22]. Especially the intracortical connectivity of the primary motor cortex has been identified as an anatomical substrate subserving motor skill learning and adaptation [118, 160, 163, 47, 40, 30, 3]. Motor maps in human primary motor cortex appear sensitive to both long-term

[129, 172] and short-term experience. For example, repetition of an individual movement [47], two movements together [110], finger movement sequences [1], adaptation to novel dynamic environments [217], as well as peripheral nerve lesions [121, 196] or an ischaemic nerve block [120] lead to a reorganization of the primary motor cortex.

All these findings have led to the notion that especially the primary motor cortex provides a neural substrate for the storage of motor skills and adaptation by changing its connection pattern between regions controlling task-related muscle synergies [118, 160, 3]. While reorganization of the spinal circuitry may also contribute to motor learning [108, 149], it is conceivable to think of the primary motor cortex and other cortical structures as the main substrate for dexterous finger movements and motor learning.

1.6 Synergies as the neurophysiological substrate for motor control

The enormous complexity of the biological hand and the adaptive nature of the nervous system controlling the hand raises the question, how the central nervous system (CNS) succeeds in generating dexterous finger movements. In essence, the control challenge is that there are much more control variables (degrees of freedom) than are needed for the solution of a task [20, 203]. For example, moving the hand from one point to another can usually be accomplished by a variety of combinations of rotations at the shoulder, elbow and wrist, and therefore a variety of muscle activation pattern [220, 78]. Bernstein gave emphasis to the biomechanical degrees of freedom of joint space, together with those arising from the muscles. In principle, however, the question of the coordination solution for the degrees of freedom problem pertains to all levels of analysis of the system [170], also to the neural level. At this level, the control problem is even more complex [213]. At one extreme there are as many degrees of freedom as neurons. The answer proposed by Bernstein was that the CNS groups several variables (movement, muscles, or neurons) together in functional synergies [20]. Each synergy can then be controlled by a single command and, therefore, the components forming a functional synergy are constrained to act as a unit. This reduction of control variables therefore reduces the number of parameters to be controlled by the CNS.

Experimental support for synergies has been obtained during voluntary behavior through computational analysis of muscle activities or movement kinematics in amphibians [241, 55, 52, 46, 45] nonhuman primates [36, 173] and humans [54, 53, 109, 107, 33, 197, 198, 151, 95, 189, 106, 21]. For instance, using factor analysis, the human gait can be described by combinations of just five muscle activation patterns independent of body weight [109] and perturbations [107]. Similarly, principal component analysis (PCA) has revealed that static hand postures [197, 117] and entire reach-to grasp movements [151, 198] can be reconstructed by weighted combinations of just a few main patterns of covariation in joint rotations or muscle activation patterns. Further, neurophysiological support for a synergistic operation of the central nervous system comes from studies employing electrical [25, 89, 166] or chemical [194, 243] neuronal stimulation. However, with one exception [51], the evidence was obtained exclusively through direct stimulation of the spinal cord, and most of these studies were performed in amphibians or rats and not humans.

An important question in that context is how many synergies are present in the CNS. If the number of synergies is smaller than the number of output variables (for example joints or muscles), not all possible output patterns can be generated. Consider, for example, 4 synergies controlling 10 individually movable joints. Then the nervous system can only

compute joint combinations lying in the four dimensional subspace of the 10 dimensional joint space. As a consequence, the movement patterns the CNS can generate are constrained and no individual movement of a joint is possible without co-movements of other joints. While several authors argue for this or similar scenarios [78, 235, 54, 24, 23], others give the concern that a smaller number of control elements does not solve or simplify the control problem [139], cannot explain the abundance of human movements [20, 139], or may simply be an artifact of optimal properties of the neural controller [239, 238, 237, 148].

Conversely, if there were as many synergies as corticospinal neurons, the activity of each joint or each muscle could be controlled individually. This, however, does not imply that a single signal is sent to a single muscle as often proposed or seen as an alternative to synergies. Based on the evolutionary considerations and neural organization of the motor cortex, spinal cord, muscles, and joints, a one-to-one relationship between neurons and joints or muscles cannot exist [91, 211, 34]. Rather the activity of individual neurons can be flexibly combined in a way to generate movement of only one joint or activity of only one muscle. This scenario would provide the CNS with an enormous flexibility but also at high computational costs and energy demands. Such a control principle would not require any type of representation or reorganization. However, learning related effects on the organization of the motor cortex [118] and neuroanatomical considerations clearly speak against such a control system.

The model developed and evaluated in this thesis is between these extreme positions and combines certain aspects of both views. The argumentation is based on the principle of economy or cost minimization [220, 218]. Here it is assumed that the neural organization is continuously [175] pushed into a state of optimal energetic organization to account for the individual degree of dexterity. Within this principle, the number of synergies stored in the CNS may be larger than the number of output variables (joints or muscles), but smaller than the number of neurons. During execution of a movement, the neural controller selects the synergies which allow the most efficient execution of the task. For example during grasping, mainly two synergies might be activated, one that corresponds roughly to the simultaneous motion of all the joints in the opening and closing of all the digits and, the other to the degree of flexion of the fingertips toward the palm or extension of the fingertips away from the palm [197]. This explains why synergies are experimentally found in human behavior [54], but is also consistent with the uncontrolled manifold concept [214, 139] and optimal control theory [239]. While, in principle, more synergies could participate in a task, they are only activated if fine adjustment are necessary [197, 210]. Consequently, the synergies used more often to generate human behavior are more prominently (and perhaps redundantly) represented in the motor system, while synergies that are needed less frequently might be represented less strongly. In this way the CNS reduces computational demands and saves energy. Motor learning or the development of finger dexterity might then result in an adaptation of the synergistic structure to facilitate the execution of the newly learned skill [172]. The upper limit of finger dexterity might be constrained by biomechanical and neural couplings, as described in Chapter 1.4. Interestingly, kinematic [251] and spatial [172, 111, 180] demands of a skill to be learned determine the amount of reorganization of the primary motor cortex, suggesting the presence of a threshold at which reorganization of the neural control structure is more efficient as the re-combination of the skilled movements by existing synergies. Another prediction is that it might be possible,e.g. by motor learning or with high concentration at very low speed (high computational costs), to compensate for some of the biomechanical and neural constraints to move (and therefore control) each finger joint individually [238].

The entire concept fits into the phylogenetic and onthogenetic development of the human hand. When the hand was used for living in the trees and grasping, the neural system was optimized for the necessary movement repertoire, which mainly required efficient closure and opening of all fingers [263]. A neural system which produces this fundamental mode of finger movements with muscles moving several fingers at a time driven by a single control signal might have been the logical and most efficient way to achieve the goals, as opposed to a system with several channels to control each joint individually [208, 206]. During million years of evolution, additional synergies might have been developed on top of the existing systems, making more individual finger movements possible.

In the next chapter, these considerations are formalized and put into a mathematical description.

1.7 Definition of modularity

In this thesis an ensemble of cortical neurons in the primary motor cortex producing a certain synergistic movement is defined as a kinematic module (Figure 3B). Within this definition, a module consists of cortical, subcortical, spinal and biomechanical elements. Because the primary motor cortex is one of the most important cortical areas responsible for finger movements and can be investigated relatively easily using neurophysiological techniques such as TMS, here the cortical contribution is restricted to this area.

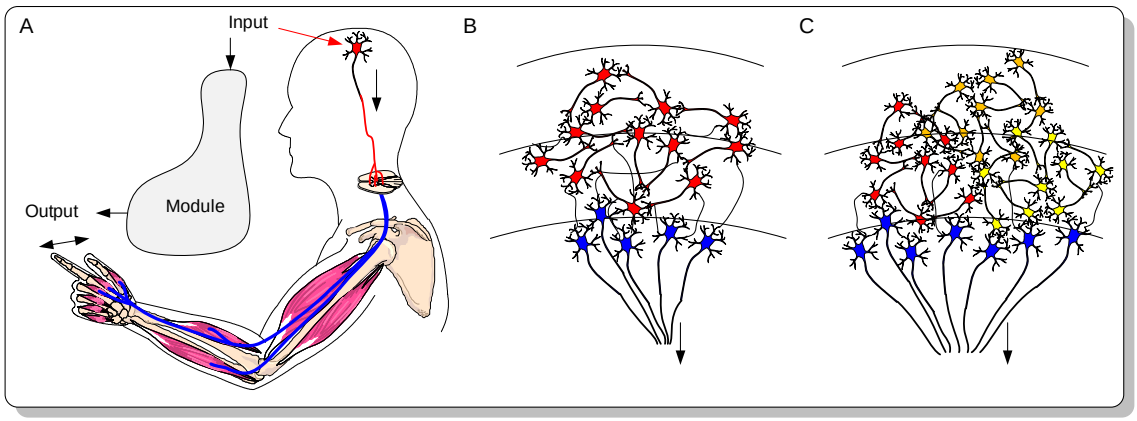

Figure 3: Definition of modularity. (A) The theoretically smallest cortical contribution to a module is a single neuron in the primary motor cortex whose activity results in a certain finger movement pattern, the output of a module. (B) More realistically, not a single neuron but a network of interconnected neurons is the cortical contribution to a module. (C) Different neuronal networks may overlap or share certain regions.

At one extreme (neglecting the cortical cytoarchitecture), only a single cortical neuron (Figure 3A) contributes to a module. There might then be as many modules as neurons projecting from the primary motor cortex to the spinal cord. As a consequence there would be many modules having the same kinematic output, i.e. a high kinematic redundancy. However, as outlined above it is reasonable to think of neuronal networks [70], located presynaptic to corticospinal projecting neurons as a potential cortical contribution to a module (Figure 3B). These neuronal circuits are activated during natural behavior by signals, for example from premotor regions [66, 181] or passively by transcranial magnetic stimulation (TMS) over the primary motor cortex [116]. Thus, the kinematic output of the modules as defined here contains information on the organization of the primary motor cortex.

At the cortical level one network might not be completely separated from the other networks, but instead may overlap or share cortical regions [208, 56, 77] as illustrated in Figure 3C. To execute finger movements, the neural controller must coordinate the activity of all networks. The effect of this coordination, the desired movement, is a blend of the outputs of the modules activated individually. Blending may occur at all levels of the modules. First there may be cortical interactions [70, 72] between two activated modules by horizontal connections or convergences on pyramidal output cells. Second, interactions between circuits of the spinal cord may occur [72]. Third, peripheral (muscle, tendons, bones, tissue, etc.) interactions may determine the final shape of the output of several active modules. While the enormous complexity would suppose a highly non-linear interaction between modules [48], experimental data suggest that the combined action can be successfully treated by linear algebra [72, 165, 243, 55], i.e. the kinematic output of the modules are scaled and summed. Mathematically the generation of finger movements can then be written as linear combinations of n modules:

$$\mathrm{mov}(t) = \sum_{i=1}^{n} c_{ij}(t)\vec{m}_i \tag{1.1}$$

where $\mathrm{mov}(t)$ is the configuration of the fingers at time t, $\vec{m}_i$ is the i^{th} p-dimensional synergy and c_{ij} a corresponding scaling coefficient at time t. The execution of grasping movements

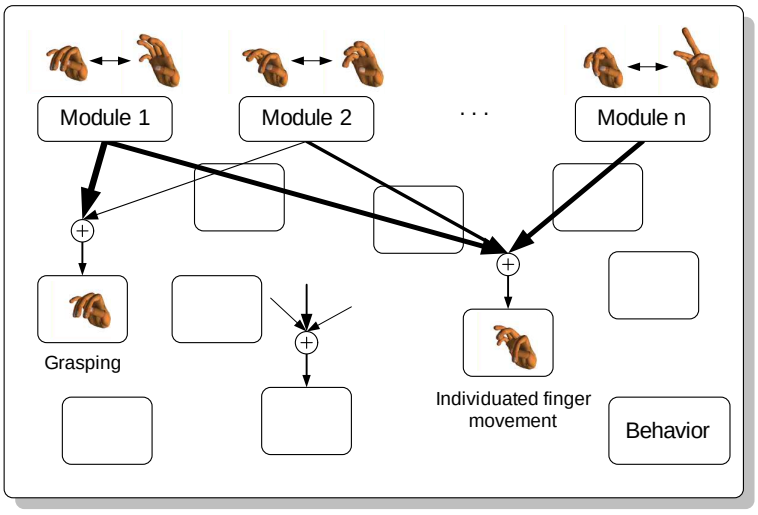

Figure 4: Principle how movements may be generated by the combination of modules. Due to cortical, subcortical and biomechanical interactions, the kinematic output of two modules can be additively combined to generate grasping movements (left) or individual finger movements. The thickness of the arrows indicate the size of the contribution of a module to generate the movement.

at one time step, for example, can then be generated by a large weighting coefficient of a module whose output is a synergistic flexion of multiple fingers and only small weighting coefficients of other modules. Individual movements might be produced by an increase of weighting coefficients of additional modules whose actions are blended to result only in the movement of the desired finger (Figure 4). In this model, computational costs and energy consumptions are reflected by the number of combinations of the modules needed for a task and by the size of the weighting coefficient values for the modules during the behavior. Thus, indirectly, the shape of the kinematic output of the modules determines computational costs. According to Figure 4 (the arrow thickness encodes the size of the weighting coefficients), grasping movements, therefore, may be executed at less costs and energy than individual

finger movements.

However, until now, no evidence for such a modular organization has been found in humans. Critical support for this model is provided for the first time in humans in Chapters 3.1 - 3.4. In the next chapter, the development and evaluation of a high resolution sensor glove is described. Kinematic modules will later be extracted from joint angle data collected with the sensor glove.

2 The measurement framework

This part of the thesis covers the development of the measurement framework to record and analyze finger movements. In the following chapter, the development of a sensor glove system, the basic data acquisition instrument, is described.

2.1 The sensor glove system

Generally, sensor gloves have been used to record and analyze voluntary human finger movements in healthy subjects [117, 138, 151, 197, 257] and patients [136, 137, 185]. The sensor glove serves as basic data acquisition device for the measurement framework.

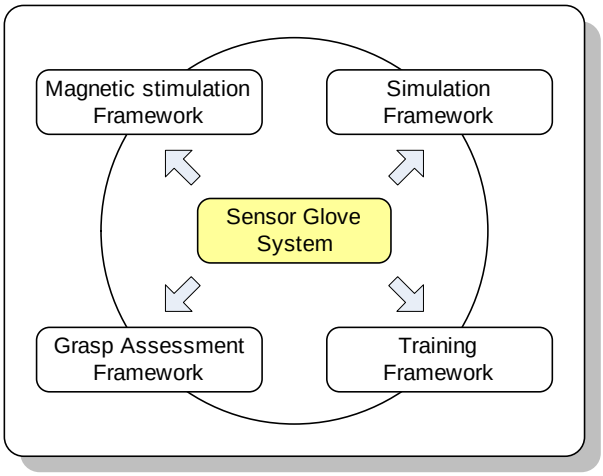

Several groups and companies have developed [103, 226, 244, 262], commercialized or evaluated [63, 128, 156, 264] different sensor gloves over the past 15 years. Here, a novel sensor glove equipped with 10 sensors for recording flexion and 4 sensors for recording abduction movements is described and evaluated. The sensors were modified in order to enhance measurement accuracy and to increase sensor linearity. Repeatability tests as introduced by Wise and colleagues [264] yielded similar accuracy results compared to other glove designs [63, 226, 264]. As a consequence, sensor linearization calibration time was reduced from several minutes to ≈10 s.

2.1.1 Available sensor glove systems

In general, sensor gloves differ in several factors, namely the type of sensors used, the number of sensors, the linearity of the sensors, the sensor resolution, the sampling rate, the data transfer technique to the host computer, the availability for the left and right hand and the price (see Table 1).

The first commercially available sensor glove was the VPL Dataglove (1986). In 1989, the patent of the VPL Dataglove was bought from Mattel to develop the PowerGlove, an inexpensive sensor glove designed for computer games. After the production stop in the 1990's, the P5 Glove, a further development of the PowerGlove, was released. Additionally, sensor gloves were developed for virtual reality (VR) applications, gesture recognition, goniometry and the recording of grasping movements. Some of these gloves are the 5DT Glove Ultra series (5DT), the DG5-VHand, the X-IST Glove (NoDNA), the TUB Glove, the Pinch Glove,

Figure 5: Overview of available sensor gloves.

the Didji Glove, the HumanGlove (Humanware), the SIGMA Glove, the ShapeHand (Measurand) and the CyberGlove (Immersion), see Figure 5. From these, several have been tested for their applicability to quantitatively assess human finger movements for rehabilitational purposes or for the study of motor control. In this field of application, the accuracy and repeatability demands, which do not only depend on the technical characteristics of a sensor glove, but also on factors such as the fit of the glove to the subject's hand, are high [264]. For the current application the sensor glove should not only allow accurate measurements (stability of the sensor signal, repeatability of movements), be easy to apply (comfortable during donning, doffing and use) and rapidly calibrated, but also be available for left and right hands and for different hand sizes. At least 14 sensors including abduction sensors with a spatial resolution of $<0.1°$ and a sampling rate of at least 40 Hz are necessary. To maximize flexibility (for example to sample electromyographic activity and finger kinematics with a single A/D converter) the glove should be provided with an analogous output of the sensor signals. The requirements are summarized in the bottom line of Table 1.

None of the available sensor gloves was perfectly suited for the measurement framework. Therefore, a novel sensor glove adapted for the current requirements was developed and evaluated. The glove can be manufactured for different hand sizes, can detect movements $<0.1°$, and is extremely cheap. Moreover, to enhance measurement accuracy and to increase sensor linearity the sensors were modified and adapted to the specific needs. In the following chapters (see Figure 6) the evaluation and modifications of the sensors, the sensor glove material, the conditioning circuits and the software interface is described in detail.

After the technical characteristics, the repeatability and the subjective comfort is assessed and compared to other sensor gloves. Finally, further developments and optimizations are discussed.

2.1.2 Sensor type selection

A variety of sensors have been employed to measure joint angle, including strain gauges, fiber optics, inductive sensors, capacitive sensors, Hall effect sensors or resistive bend sensors. Their working mechanisms are shortly summarized:

Name	No. of sensors	Resolution (°)	Sample rate (Hz)	Analog output	Both hands	Different sizes	Price
Cyber Glove II	18, 22	0.5	90	no	yes	no	8900 €
X-IST Glove	5, 14, 15	-	60	no	yes	no	2913 €
Power Glove	10	-	-	no	-	-	-
Human Glove	22	0.4	-	no	-	no	-
Shadow Monitor	5	0.06 - 3	-	no	yes	yes	-
Didji Glove	10	-	-	no	-	no	3200 €
SIGMA Glove							
P5 Glove	5	0.5	60	no	yes	no	99 $
5DT Glove Ultra	5, 14	0.2	60	no	yes	no	4700 €
DG5-VHand	5	-	100	no	-	no	785 $
TUB Glove	24	0.2	20 - 100	no	no	no	-
VPL Data Glove	10	-	-	no	no	no	9000 €
Pinch Glove	-	-	-	no	yes	no	1899 $
Shape Hand							
Requirements	min. 14	< 0.1	> 40	yes	yes	yes	< 1000 €

Table 1: Characteristics of available sensor gloves and requirements for the sensor glove needed for the measurement framework.

- The use of fiber optics to measure bend requires a light source such as a light emitting diode and a photo detector. The amount of bend is proportional to the attenuation of detected light in specially treated sections of fiber that pass over the tops of the finger joints. Disadvantages of this sensor types include the complexity of glove construction and price [225].

- The physical construction of a typical linear inductive sensor consists of a movable core of magnetic material and three coils comprising the static transformer [132]. One of the three coils is the primary coil and the other two are secondary coils. When an AC excitation signal is applied to the primary coil, voltages are induced in the two secondary coils. The magnetic core inside the coil winding assembly provides the magnetic flux path linking the primary and secondary coils. When the magnetic core is displaced from the neutral position, an electromagnetic imbalance occurs, leading to a proportional output voltage across the secondary coils.

- Joint angles can also be measured by capacitive sensors, which consist of two layers of conductive polymer separated by a dielectric. Each conductive layer is arranged as a comblike fashion, such that the overlapping electrode surface is proportional to the amount of sensor bending [169, 132]. The bending angle can be determined using the direct proportionality of the capacitance and the overlapping surface of the two sensor electrodes.

- Hall-effect sensors, which detect magnetic fields, can be configured as proximity sensors to provide a linear output proportional to distance from a magnetic source [127]. By

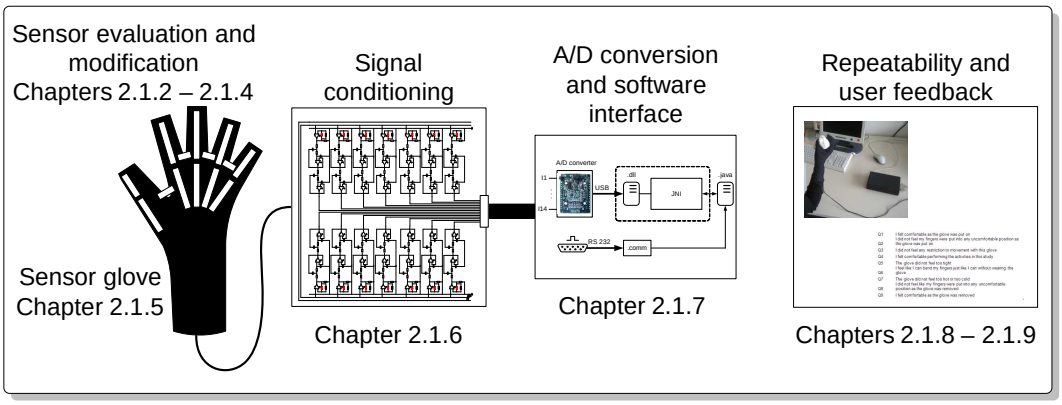

Figure 6: Overview of the chapters describing the sensor glove development.

placing a series of sensors on the back of a glove in a predefined pattern, the joint angle can be computed from the changing field strengths measured by the sensors when the fingers bend.

- Strain gages detect stretch produced by joint rotation. The design of strain gage-based sensors consists of specially designed structures that perform in a predictable and repeatable manner when a force, load or weight is applied. The applied input is translated into a voltage by the resistance change in the strain gages. The amount of change in resistance indicates the magnitude of deformation in the transducer structure and hence the stretch that is applied [255]. Strain gages may have very high accuracy, but are expensive and often difficult to handle [225].

- Resistive bend sensors (Figure 7A) consist of thin flexible substrate that is coated with a carbon/polymer based ink [86, 15]. When the coated film is bent, the ink separates into many micro cracks which upon movement open and close to the specific bending of the material causing a change in electrical conductivity [80] as shown in Figure 7B. Increasing bend angle is generally associated with increased resistance which can be converted to voltage signal changes by electrical circuits [79]. However, resistive bend sensors do not allow reliable measurements due to their non-linear characteristics and unstable behavior [225].

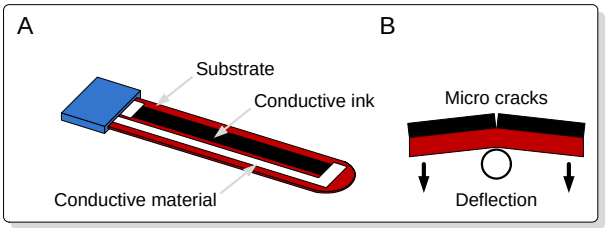

Figure 7: (A) Elements of a resistive bend sensor. (B) Principle of work.

While each technology has advantages and disadvantages, resistive bend sensors were selected for the following reasons:

- Signal conditioning is simple. For the simplest circuit only one additional resistor is needed to build a voltage divider [79].

- The sensor length can be adapted by cutting the sensor and re-establishing the electrical contacts, for example using conductive silver.

- Cost factor: The costs for one sensor amounts to only 4-10€ which results in <150€ for a glove with 14 sensors.
- Sensors are lightweight, improving user comfort.

Sensors from three different manufacturers were evaluated according to their signal stability and the sensor type with best stability was used. Subsequently, to increase measurement reliability and linearity, sensors were modified as described in the following sections.

2.1.3 Sensor stability

Because of dynamic effects of the conductive ink and the substrate of the sensor, resistance generally does not remain stable when constantly bent to a static position. To quantify this effect, sensors from 3 manufacturers, namely Flexpoint (FP, 2" sensor without overlaminate), Abrams Gentile (AG) and Spectra Symbol (SS; here the plastic substrate on the back of the sensor was thinner than in commercially available sensors) were evaluated and the sensor type with the most stable signal was chosen. In an experimental setup, each sensor was attached to a manual goniometer (1° resolution) as illustrated in Figure 8A. After remaining in the neutral (0°) position for 10 s, the goniometer (and with it the sensor) was bent (≈500 ms movement duration) and adjusted at a bending position of 60° for 40 s. Subsequently, it was returned to the baseline position for 10 s. To quantify the step response behavior of each sensor, the mean of 15 measurements was used. The ratios of the signal value (which was proportional to the resistance of the sensor) as obtained immediately after the bending (T0) and the signal value 1, 5, 10, 20 and 30 s (T1 - T5) afterwards, were calculated. All sensors exhibited a similar step response curve as illustrated in Figure 8B, C and D.

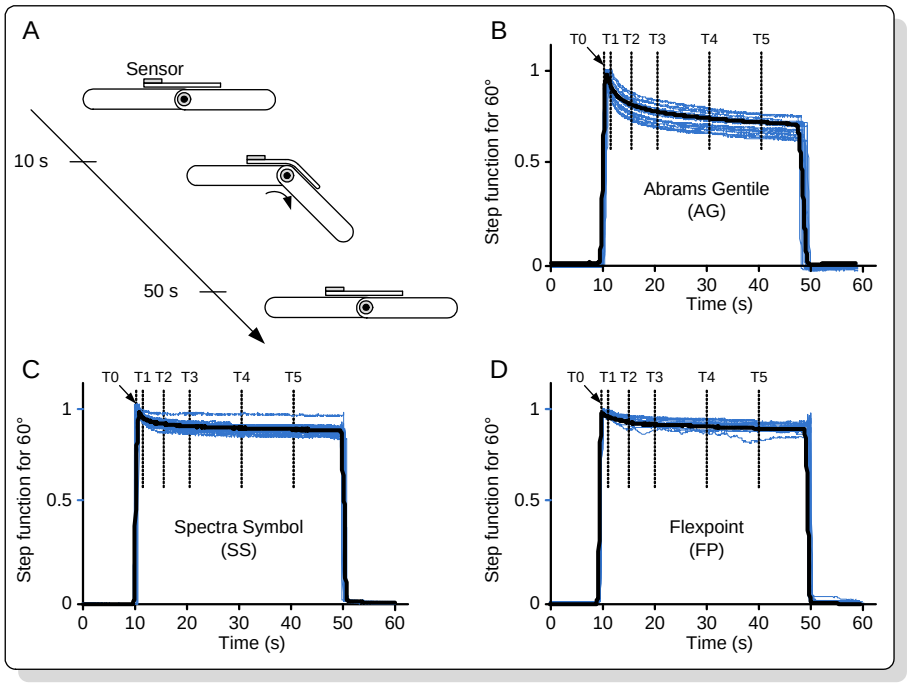

Figure 8: Step response of resistive bend sensors from three manufacturers.

Each sensor reached a peak resistance value just as it was bent, with an immediate decay in resistance over time. Compared to the initial peak resistance, the resistance of the AG sensor decayed after 30 s (T5) for 28.6 ± 4.1 % and the resistance of the SS sensor decayed

for 13.0 ± 2.7 %. The mean decay of the FP sensor 30 s after bending was 9.3 ± 2.4 %. The decay was highly significant different between sensors (ANOVA, F = 164.95, p << 0.001) which could be attributed to significant differences between all sensor types (p < 0.001, two tailed unpaired t-tests). Since the FP sensors showed the best stability, they were chosen as the preferred sensors.

In an attempt to further enhance the sensor stability, a thin unplasticised polyvinyl chloride (PVC) foil with a width of 4 mm and a thickness of 0.2 mm was fixed over the carbon layer on the front side of the Flexpoint bend sensor using an instant adhesive (Pattex Plastik, Henkel, Duesseldorf, Germany). The sensor was then turned around and flexed in the opposite direction so that the attached plastic foil was squeezed when bent. After this modification, which was termed Modification 1, the step response was reassessed as described above. As a consequence, the mechanical stiffness somewhat increased but the sensor resistance decayed for only -0.8 ± 2.2 % (see Figure 9) of the step function rise, significantly less compared to the original FP sensor (p << 0.001, two-tailed unpaired t-test at T5). The other two sensor types were also modified and tested but showed worse results.

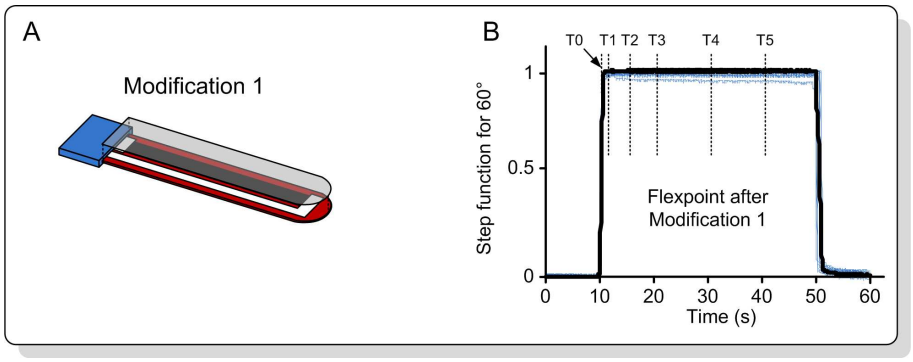

Figure 9: (A) Modification of sensors. (B) Step response after modification was enhanced.

To test if this effect was specific only for the selected sensor, the resistance variation of six additional sensors during 40 s of bending at 60° was tested before and after Modification 1. The mean of three measurements before and after Modification 1 for each sensor was used for further analysis. Additionally, to assess the change of the sensor resistance over a longer time period, three of the six sensors were tested in a condition lasting 60 min. Here, the sensor remained in the neutral position for 1 min, was bent to 60° for 58 min and finally was returned to baseline for 1 min. Again, the mean of three measurements for each sensor before and after Modification 1 was used for analysis. The ratios of the signal value immediately after the bending (T0), and the signal value 10, 20, 30, 40 and 50 min (T6 - T10) afterwards were calculated.

Before Modification 1, the resistance of all six sensors continuously decreased for 6.3 ± 1.4 % at T5 (Figure 10A and Table 2 for details for T1-T4). Three of the six sensors were monitored during 58 min of bending. Results indicate that the resistance continuously decayed for ≈30 min (T8) and then stayed stable. At the end of the measurement, 50 min after the bending (T10), the mean decay was 16.8 ± 4.9 % (Figure 10C). After Modification 1, the sensor resistance decreased to -1.0 ± 0.8 % at T5 (Figure 10B), ≈6 times lower in magnitude than the original sensors. Moreover, the resistance of three of the six sensors remained stable (-1.9 ± 1.0 %) until the last measurement at 50 min (T10) after the step response (Figure 10D). Detailed results of individual sensors are shown in Table 2.

Because this modification removed a major drawback of resistive bend sensors for reliable

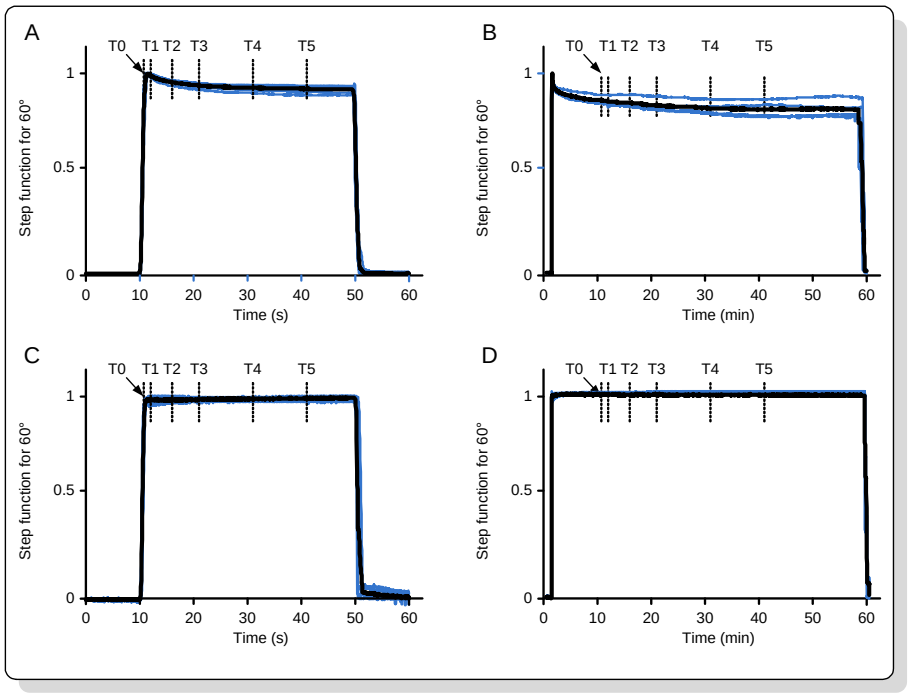

Figure 10: The change of sensor resistance was recorded before (A) and after (C) Modification 1 during 40 s of bending to ≈60° in six sensors (grey lines indicate the mean out of three measurements from each sensor and black lines indicate the mean of all sensors). Three of the six sensors were also tested before (B) and after (D) Modification 1 in a condition lasting 60 min. In both conditions, Modification 1 considerably reduced the decay of the sensor resistance after the step function.

measurements of human finger movements, the sensors for the sensor glove were modified as described above and all further results are based on FP sensors after Modification 1. A second undesired characteristic of resistive bend sensors, the non-linear behavior, was compensated by Modification 2, which is introduced in the next chapter.

2.1.4 Sensor linearity

The procedure to establish the relationship between change of sensor signal and the bend angle is commonly referred to as calibration and is realized after A/D conversion by software or by manual processing of the sensor signals. The relationship is influenced by

- the change of sensor resistance when bent,
- the hand size of the person wearing the glove,
- the transfer characteristic of the conditioning circuit and
- the software mapping routines.

Linear sensors, a linear transfer characteristic of the conditioning circuit and a linear mapping of the sensor signals in joint angle are desirable. The advantage is that calibration can be performed using only two values at specific joint angles. Furthermore, the sensor resolution after analog/digital (A/D) conversion is constant across the whole range of joint angles. Resistive bend sensors generally exhibit a non-linear relationship. Therefore, an attempt was

Original sensors

Decay after step function 60 s (%)

	T0	T1	T2	T3	T4	T5
t(s)	0	1	5	10	20	30
Sensor						
#1	0.0	1.6	3.6	4.7	5.1	5.2
#2	0.0	0.5	3.6	4.9	5.6	6.2
#3	0.0	0.1	3.5	5.7	7.4	8.1
#4	0.0	1.8	4.3	5.4	6.7	7.2
#5	0.0	1.0	3.5	5.2	6.0	6.7
#6	0.0	0.3	1.4	1.8	3.6	4.2
Mean	0.0	0.9	3.3	4.6	5.7	6.3

Decay after step function 60 min (%)

	T0	T6	T7	T8	T9	T10
t(min)	0	10	20	30	40	50
Sensor						
#1	0.0	10.8	11.5	13.1	13.0	11.8
#2	0.0	15.1	18.2	20.4	21.8	21.5
#3	0.0	14.0	16.8	17.2	15.7	17.0
#4						
#5						
#6						
Mean	0.0	13.3	15.5	16.9	16.8	16.8

Sensors after Modification 1

Decay after step function 60 s (%)

	T0	T1	T2	T3	T4	T5
t(s)	0	1	5	10	20	30
Sensor						
#1	0.0	-0.4	-0.3	-0.6	-1.2	-1.6
#2	0.0	-0.2	-1.2	-1.4	-1.9	-2.1
#3	0.0	0.8	2.3	1.5	0.4	0.0
#4	0.0	-0.4	-1.2	-2.4	-1.6	-0.8
#5	0.0	-0.8	-1.0	-0.5	-0.5	-0.4
#6	0.0	-0.4	-0.6	-0.8	-0.9	-1.1
Mean	0.0	-0.2	-0.3	-0.7	-1.0	-1.0

Decay after step function 60 min (%)

	T0	T6	T7	T8	T9	T10
t(min)	0	10	20	30	40	50
Sensor						
#1	0.0	-1.9	-2.3	-2.5	-2.5	-2.5
#2	0.0	-2.4	-2.6	-2.6	-2.6	-2.4
#3	0.0	-0.1	-0.0	-0.3	-0.7	-0.7
#4						
#5						
#6						
Mean	0.0	-1.5	-1.6	-1.8	-1.9	-1.9

Table 2: Sensor signal decay over time before and after Modification 1. For each sensor the mean values out of 3 trials are shown. Positive values indicate a decrease and negative values an increase with respect to T0.

made to enhance the linear relationship of sensor resistance of modified FP sensors and bend angle. The challenge of sensor linearization appears in several applications such as in temperature measurement systems using temperature sensitive resistors. A common approach is to linearize these sensors by placing resistances in parallel to the resistors. The value of the parallel resistance is chosen to maximize the linearity of the temperature-resistance relationship. The same procedure was adopted here. As a first step, the relationship between sensor resistance and bend angle, the "calibration curve" was assessed experimentally. A sensor after Modification 1 was placed over a gonimeter which was adjusted to 0, 15, 30, 45, 60, 75 and 90°. In each case the corresponding sensor resistance R_{Sensor} was recorded. The procedure was repeated three times and the mean values constituted the calibration curve

(black dots in Figure 11A). The calibration curve was mathematically approximated by a quadratic function according to

$$R_{Sensor}(Angle) = f(x_1) = p_2 \cdot x_1^2 + p_1 \cdot x_1 + p_0, \tag{2.2}$$

where $p_2 = 0.00083794, p_1 = 0.094847$ and $p_0 = 4.1643$ form the function coefficients determined by a least squares fitting algorithm (red line in Figure 11A). With this functional, the sensor resistance can be described as a non-linear function of the bend angle $x_1 \in \{0, 90°\}$. This interpolation procedure was used to smooth the data and to evaluate the sensor resistance-angle relationship at more points than measured. If a parallel resistance $R_{Parallel}$ is added, the final sensor resistance $R_{Sensor,new}$ does not only depend on the bend angle x_1 but also on the value of the parallel resistance x_2. Thus, the function which describes the calibration curve in dependence of $R_{Parallel}$ is given by

$$R_{Sensor,new}(Angle, R_{Parallel}) = g(x_1, x_2) = \frac{f(x_1) \cdot x_2}{f(x_1) + x_2} = \frac{p_2 \cdot x_1^2 \cdot x_2 + p_1 \cdot x_1 \cdot x_2 + p_0 \cdot x_2}{p_2 \cdot x_1^2 + p_1 \cdot x_1 + p_0 + x_2}. \tag{2.3}$$

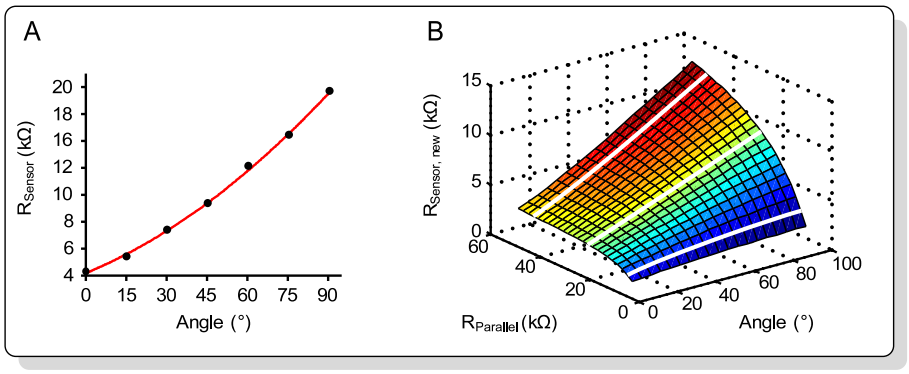

Figure 11: (A) Calibration curve for a sensor after Modification 1. (B) Effect of a parallel resistance on the calibration curve.

This map is visualized in Figure 11B. White lines indicate the calibration curves for $R_{Parallel} = 1, 20$ and 50 kΩ. Obviously, the calibration curve for large parallel resistances (left white line) approaches the original calibration curve while it converges to zero and changes its slope to the opposite direction, if the parallel resistance is small (right white line in Figure 11B). Between these two extremes, a value of the parallel resistance exists, at which the linearity of the calibration curve is maximal (middle white line in Figure 11B). To determine this optimal value of $R_{Parallel}$ exactly, the linearity of the calibration curves for fixed parallel resistances was numerically quantified as a fit to a linear regression model. The goodness of a linear regression for a given parallel resistance $x_2 = k$ can be assessed as the residuum e_i, which denotes the difference between resistance at $g(x_1 = i, x_2 = k)$ and resistance predicted by a linear regression $\hat{y}(x_1, x_2 = k)$ of g evaluated at $x_1 = i,\ i \in \{0, 90\}$ (Figure 12):

$$e_i = g(x_1 = i, x_2 = k) - \hat{y}(x_1 = i, x_2 = k). \tag{2.4}$$

Further, the squared sum of the residuum over all considered data points $\sum e_i^2$ for a given parallel resistance $x_2 = k$ can be expressed as part of the data variance [32]:

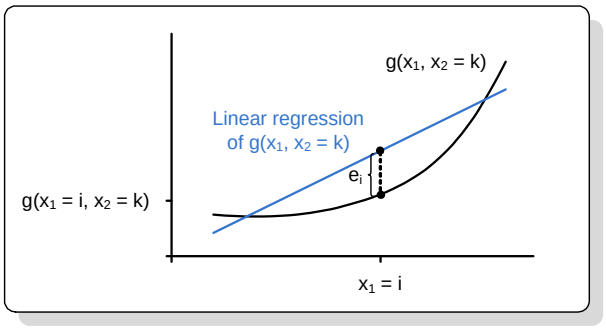

Figure 12: Measure of linearity of the calibration curve for a given parallel resistance.

$$\frac{\sum_{x_1=0}^{90}(g(x_1,k)-\overline{g}(x_1,k))^2}{n-1} = \frac{\sum_{x_1=0}^{90}(g(x_1,k)-\hat{y}(x_1,k))^2 + \sum_{x_1=0}^{90}(\hat{y}(x_1,k)-\overline{g}(x_1,k))^2}{n-1}. \tag{2.5}$$

This equation indicates that the variance of $g(x_1, k)$ evaluated for a specific step size $\frac{1}{n}$ for x_1 can be formulated as the sum of the variance explained by the linear regression model and the residual variance. Thus, the quotient

$$r^2 = \frac{\sum_{x_1=0}^{90}(g(x_1,k)-\hat{y}(x_1,k))^2}{\sum_{x_1=0}^{90}(g(x_1,k)-\overline{g}(x_1,k))^2} \tag{2.6}$$

is a marker of how much variance of the data points can be explained by a linear model for a given parallel resistance $x_2 = \mathrm{k}$. r^2 values close to 0 indicate a non-linear relationship inherent in the data, whereas values close to 1 indicate high linearity. The exact value of the optimal resistance $R_{Parallel}$ maximizing linearity of the calibration curve was found by minimizing the error function

$$\min_{x_2}(\mathrm{errfcn}(x_2)) = \min_{x_2}(1-r^2) \tag{2.7}$$

by a least squares optimization algorithm using a step size of $\frac{1}{n} = 0.001$.

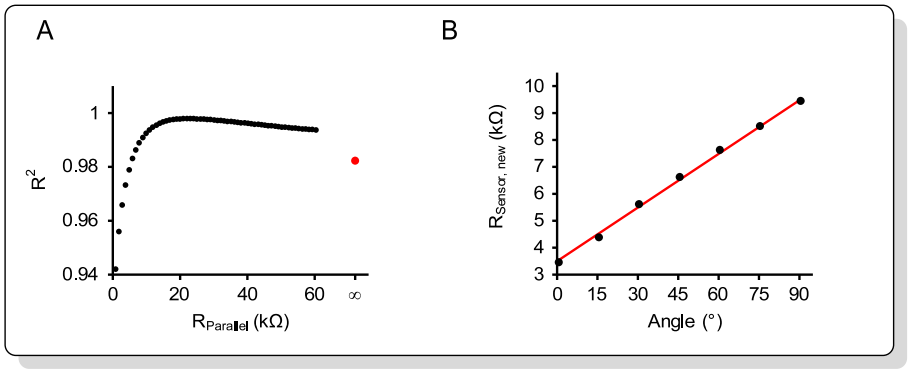

Figure 13: (A) Values of 1 - errfcn(x_2) for parallel resistances from 0 - 60 kΩ. (B) Empirically assessed calibration with a parallel resistance of 20 kΩ and linear regression.

Figure 13A shows calculated r^2 values for different parallel resistances ranging from 1 to 60 kΩ. The maximum r^2 value was determined by the optimization algorithm as $R_{Parallel} =$ 22.68 kΩ. For implementation, a resistance with a value of 20 kΩ was placed parallel to the sensor and a new empirical calibration curve was determined (Figure 13 red line indicates linear regression with $r^2 = 0.9975$). For abduction sensors, a resistance value of $R_{Parallel} =$ 47 kΩ was chosen analogously. This second modification was termed Modification 2.

2.1.5 Glove material and sensor arrangements

The sensors after Modification 2 were embedded in a glove, custom fabricated out of a stretchable grade of Lycra. On the dorsal side of the hand, two layers of Lyrca were sewed together so that the sensors could be inserted between the layers (Figure 14B). Ten 2" sensors after Modification 2 were placed over the dorsal aspects of the metacarpal (MCP) and proximal interphalangeal (PIP) joints. For the thumb, the sensors were placed over the MCP and interphalangeal (IP) joint. The end of the proximal sensor was allowed to overlap with the distal sensor so that the sensors could be optimally placed over the MCP and PIP joints (Figure 14C). To ensure that the sensors could not leave their position at one end, they were fixed to the glove stuff (arrows in Figure 14A, B and C). Abduction (ABD)

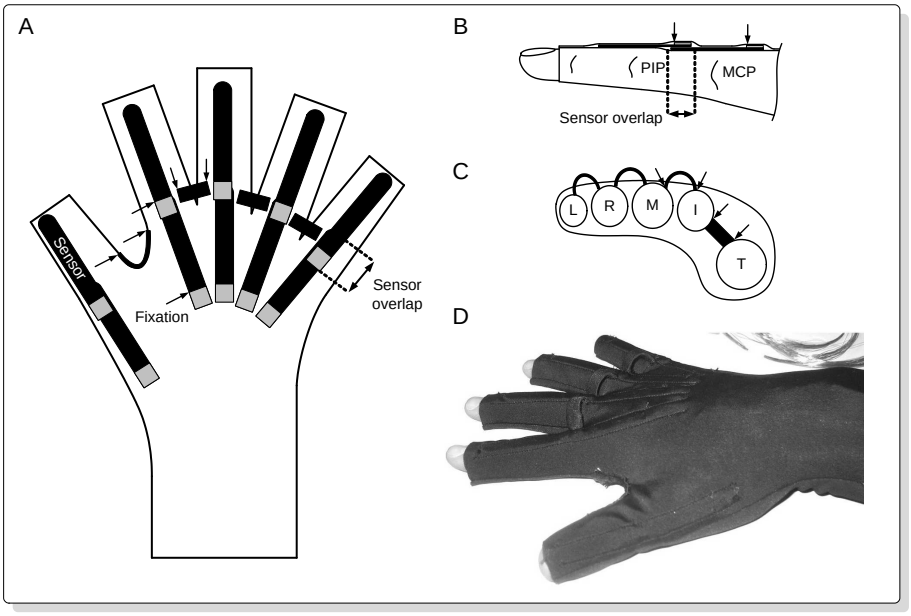

Figure 14: The sensor glove with 14 sensors to measure flexion and abduction movements. (A) Top view of the glove. To ensure that the sensors could not leave their position, they were fixed to the glove stuff (black arrows). (B) Frontal view of the glove (T indicates the thumb, I the index finger, M the middle finger, R the ring finger and L the little finger). (C) Section through the middle of a finger.

sensors consisted of four 1" sensors from the same manufacturer and were placed in a half-circle configuration between the Index-Middle, Middle-Ring and Ring-Little fingers (Figure 14B). If two fingers were abducted, the fixed ends of the sensors were pulled apart causing an increase in bending radius and thus a reduction of sensor resistance. The Thumb-Index abduction sensor was fixed to the glove material between thumb and index finger.

Since the calibration curve of the sensors changes when bent about a different radius [225] the linearity of the 14 sensors embedded in the glove may differ in subjects with different

hand sizes. To address this point, all sensors were manually calibrated in two male subjects with a medium to large hand size and in one female subject with a small hand size. For each subject, the procedure took ≈30 min to complete. The mean r^2 values of all subjects ranged from 0.9855 to 0.9980 with an overall mean of 0.9915 ± 0.0031, indicating a high degree of linearity in all joints. The calibration curves for all subjects and the linear regression for the mean values across subjects are illustrated in Figure 15. The mean r^2 value across joints of

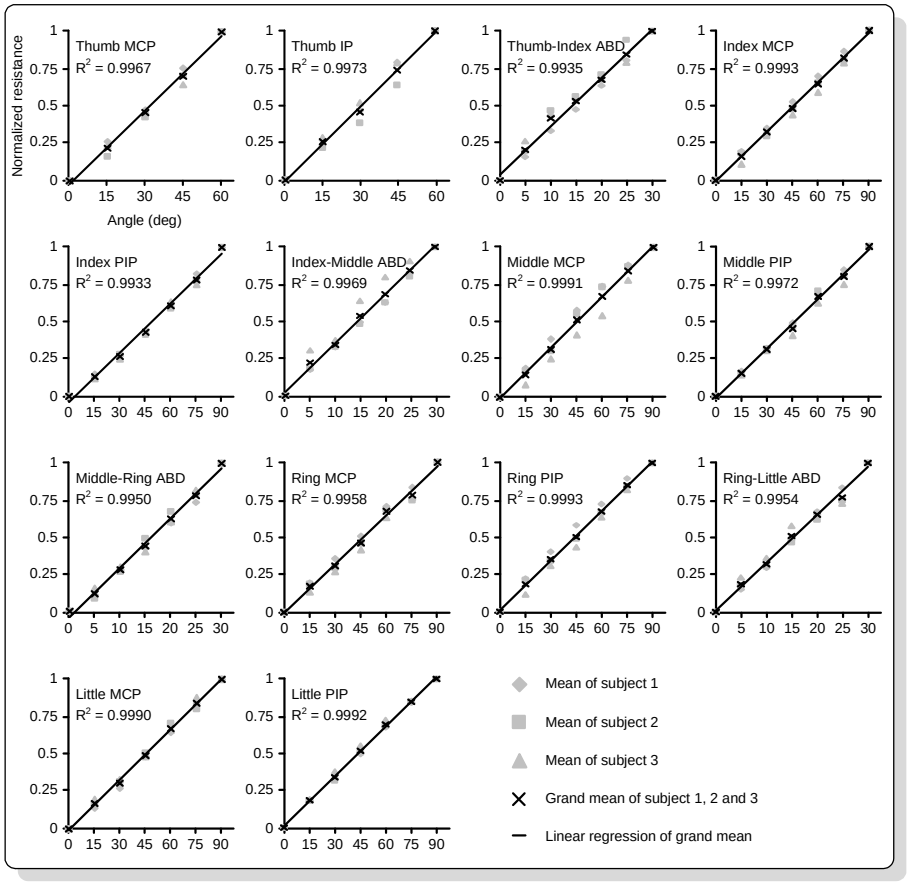

Figure 15: Mean out of three empirically established normalized calibration curves for all joints in three subjects after Modification 2. r^2 values of the mean calibration curve confirmed an acceptable degree of sensor linearity.

the female subject with small hand size (0.9881 ± 0.0086) tended to be somewhat smaller than in the male subjects with larger hand sizes (0.9942 ± 0.0058 and 0.9921 ± 0.0064, respectively) but the differences did not reach statistical significance (ANOVA, F = 2.78, p = 0.07). Thus, the degree of linearity after Modification 2 is only mildly affected by different hand sizes. To obtain absolutely optimal characteristics, the modification parameters may be optimized for gloves manufactured for small and large hands, respectively. Therefore, 4 gloves pairs (left and right hand) for different hand sizes were produced.

2.1.6 Sensor signal conditioning

Before A/D conversion, the measured variable, here the change of sensor resistance during bending must be converted into voltage signals. As noted in chapter 2.1.4, the transfer characteristic of the conditioning circuit, i.e. the relationship between the sensor resistance and the output voltage, should be linear for calibration. Furthermore it should be possible to power the conditioning circuit by the USB interface from a conventional personal computer

with a voltage supply between 0 and 5 V. Besides a low noise in the output signal, the gain of the conversion should be adaptable. Among the many possibilities to meet these requirements, operational amplifier (op-Amp) circuits are especially suited [79]. A non-inverting amplifier circuit was selected, because it combines a linear relationship between output voltage and sensor resistance without the need of a symmetric powering of the op-Amp. The relationship between sensor resistance and output voltage U_{amp} is given by

$$U_{amp}(R_{Sensor,new}) = U_c \cdot (1 + \frac{R_{Sensor,new}}{R_v}),$$

where $R_{Sensor,new}$ is the sensor resistance after Modification 1, U_c is a constant input voltage of the non-inverting op-Amp input and R_v is a resistance which value affects the gain of the amplifier.

Commonly, high frequency noise in the output signal of the non-inverting amplifier is present, which can distort the glove signals and can lead to measurement errors [83]. The source of the noise can be every part of the circuit such as the sensors, inductive or capacitive couplings in the wires or the op-Amps. Another issue to be considered is the sampling theorem in A/D applications. The input signal must be band limited to less than the half the sampling frequency to avoid aliasing. This task is usually accomplished with sharp low-pass filters designed to provide adequate attenuation at at least half the sampling frequency [83]. Since the frequency of finger movements is anatomically restricted to maximum 15-20 Hz [5], and the sampling frequency of the used A/D converter is 50 Hz, the filter was designed to have an edge frequency of 20 Hz. For the current application, a 4^{th}-order Butterworth filter in a Sallen-Key configuration with a sharp falloff of 80 db/decade [152] was developed.

Generally, the characteristics of a filter are completely described by its transfer function $H(s)$, calculated as the Laplace transform of the relationship between input and output voltage:

$$H(s) = \frac{U_{out}(s)}{U_{in}(s)} = \frac{a_m s^m + a_{m-1} s^{m-1} + \cdots + a_1 s + a_0}{b_n s^n + b_{n-1} s^{n-1} + \cdots + b_1 s + b_0} \tag{2.8}$$

where $s = \sigma + j\omega$ is the complex frequency variable [83]. The transfer function $H(s)$ can also be written as a rational function of s with appropriate scaling coefficients a_k, $k = 0 \ldots m$ and b_l, $l = 0 \ldots n$. The degree n of the denominator determines the order of the filter (first order, second order, etc.). By varying the parameters of $H(s)$ (i.e. changing the electronic parts of the circuit), filter characteristics including system stability, edge frequency, amplitude attenuation, and phase shift can be influenced. Especially the position of the poles (the zeros of the denominator) are important to design the desired filter characteristics. Figure 16A shows the hardware implementation of a Sallen-Key 2^{nd}-order low-pass filter with the transfer function

$$H(s) = \frac{U_{out}(s)}{U_{in}(s)} = \frac{1}{R_1 C_1 R_2 C_2 s^2 + (R_1 C_2 + R_2 C_2)s + 1}. \tag{2.9}$$

Higher-order filters must not be treated separately, because a polynomial in s of any length can be factored into a series of quadratic terms (plus a single first-order term if the polynomial is odd, [152]). Therefore, a 4^{th}-order low-pass filter can be built by cascading two 2^{nd}-order filters:

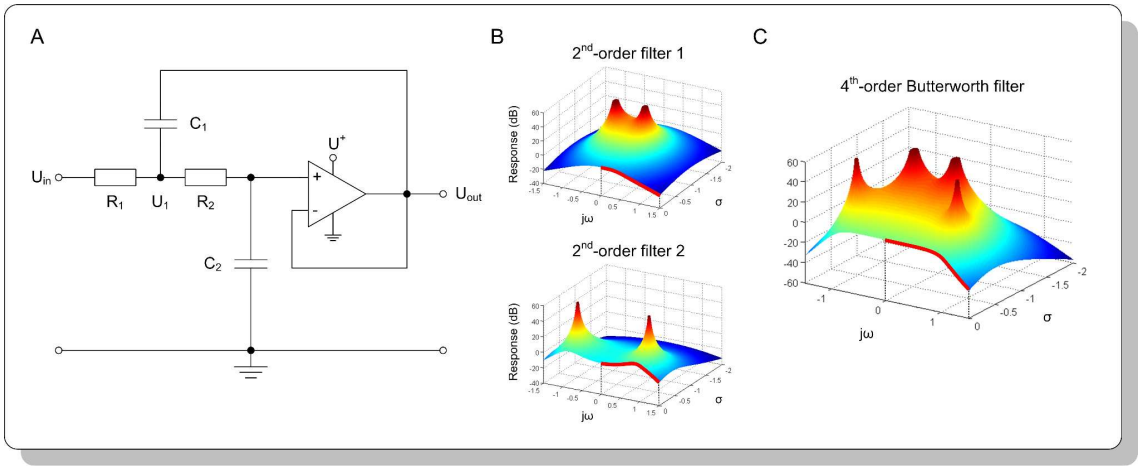

Figure 16: (A) Hardware implementation of a 2nd-order low pass filter. (B) Amplitude of the transfer function of two different 2nd-order low pass filter. (C) Amplitude of the transfer function of the cascaded filters from B resulting in a 4th-order Butterworth filter.

$$H(s) = H_1(s) \cdot H_2(s) = \frac{1}{R_1C_1R_2C_2s^2 + (R_1C_2 + R_2C_2)s + 1} \cdot \frac{1}{R_3C_3R_4C_4s^2 + (R_3C_4 + R_4C_4)s + 1}. \tag{2.10}$$

In the current application, the frequency behavior of the 4th- order filter is determined by the pole locations of the two 2nd-order filters, i.e. the values of the resistances and capacitors. Several concepts for pole placement exist, each leading to different filter characteristics. Examples are the Bessel, the Chebychev or the Elliptic filter. A type of filter which is common to many applications requires a response that is maximally flat in the passband, but cuts off as sharply as possible afterwards. Such a behavior, which is also desired here, can be obtained by arranging the poles with equal spacing around a semicircular locus [83, 152]. This kind of filters are called Butterworth filters. It can be accessed from data tables that the transfer function of a 4th-order Butterworth filter with an edge frequency of 1 rad/s is

$$H(s) = H_1(s) \cdot H_2(s) = \frac{1}{s^2 + 1.8478s + 1} \cdot \frac{1}{s^2 + 0.7654s + 1}. \tag{2.11}$$

Thus, for the first 2nd-order filter the following equations must hold:

$$\begin{aligned} R_1C_1R_2C_2 &= 1 \\ R_1C_2 + R_2C_2 &= 1.8478, \end{aligned}$$

and for the second filter:

$$\begin{aligned} R_3C_3R_4C_4 &= 1 \\ R_3C_4 + R_4C_4 &= 0.7654 \end{aligned}$$

The resistances for both filters were initially chosen to be $R_1 = R_2 = R_3 = R_4 = 1$ kΩ. Then, the values of the capacitors are calculated to $C_1 = 1.08$ mF, $C_2 = 0.92$ mF and $C_3 = 2.61$mF, $C_4 = 0.38$ mF, respectively.

Figure 16B shows the amplitude of the transfer function of both filters across the complex s-plane. The sharp rise of the amplitude indicates the position of the poles. If only the complex part of s is considered, i.e. $s = j\omega$; $\sigma = 0$, the amplitude of the frequency response

(red lines in Figure 16B) is obtained. Note that none of the 2nd-order filters is a Butterworth filter on its own. However by cascading these two 2nd-order filters, a 4th-order Butterworth filter is implemented (Figure 16C). It can be seen that the signal amplitude of the transfer function (red line in Figure 16C) drops for 3 dB at a frequency of 1 rad/s. This frequency is called the edge frequency. To shift the edge frequency to the desired value of $\omega_0 = 20$ Hz, the capacitor values were reduced by a factor of $2\pi\omega_0$ to $C_1 = 8.61$ μF, $C_2 = 7.35$ μF, $C_3 = 20.79$ μF and $C_4 = 3.04$ μF.

For practical reasons (availability of the hardware components), the resistance values of $R_1 = R_2 = 9$ kΩ and $R_3 = R_4 = 21$ kΩ and capacitor values of $C_1 = 1$ μF, $C_2 = 0.85$ μF, $C_3 = 1$ μF and $C_4 = 0.15$ μF were chosen for the implementation. The final conditioning circuit including the non-inverting amplifier and the Butterworth filter is visualized in Figure 17.

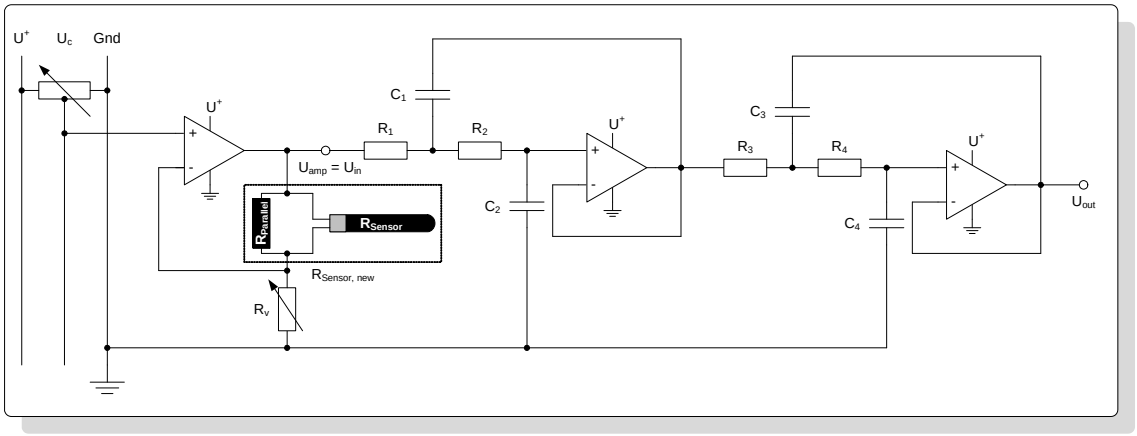

Figure 17: Complete conditioning circuit for a sensor consisting of the non-inverting amplifier and the 4th-order Butterworth filter.

The circuit is powered by a positive reference voltage U^+, for example from an USB interface. The constant reference voltage U_c for the non-inverting amplifier can be adjusted by a potentiometer which serves as a voltage divider. A resistance is placed parallel to the sensor in the feedback path of the amplifier, leading to a linear relationship between sensor resistance ($R_{Sensor,new}$) change and change of the amplifier output voltage U_{amp}. A second potentiometer R_v allows a flexible adjustment of the amplification gain. The voltage U_{amp} is then gated into the Butterworth filter to reduce signal noise and to band limit the signal for proper A/D conversion. Finally, the output voltage U_{out} is A/D converted and fed into the computer.

2.1.7 Analog / Digital (A/D) conversion

After conditioning, the analogous signals must be digitized for recording and further analysis on a computer. For most of the available sensor gloves, individual A/D converters with special transmission protocols were developed. The communication with the glove is then restricted to the functionalities and A/D conversion facilities of the glove. For the sensor glove developed here, the A/D concept is different and as flexible as possible:

- First, no individual A/D converter was developed. Instead, the glove is provided with a commercially available A/D card which comes with a number of libraries for interfacing the glove from different software programs and programming languages. For Java users, a set of routines have been developed as described later in this chapter.

- Second, the conditioning circuit is additionally provided with an analogous output of the filtered sensor signals (see Figure 18). Thus, users who already possess A/D equipment (which is the case for most neurophysiological labs) simply can plug the glove in their devices and use it with their individual software and processing routines. If, for example, the relationship between finger kinematics and muscle activity is topic of a study, the glove can be connected to the electromyographic apparatus and the signals from the two modalities can be recorded in a single file with equal sampling rate (this was done in Study 2 and 3, see later). Furthermore, for analysis, there is no need for synchronization between the glove and muscle activities.

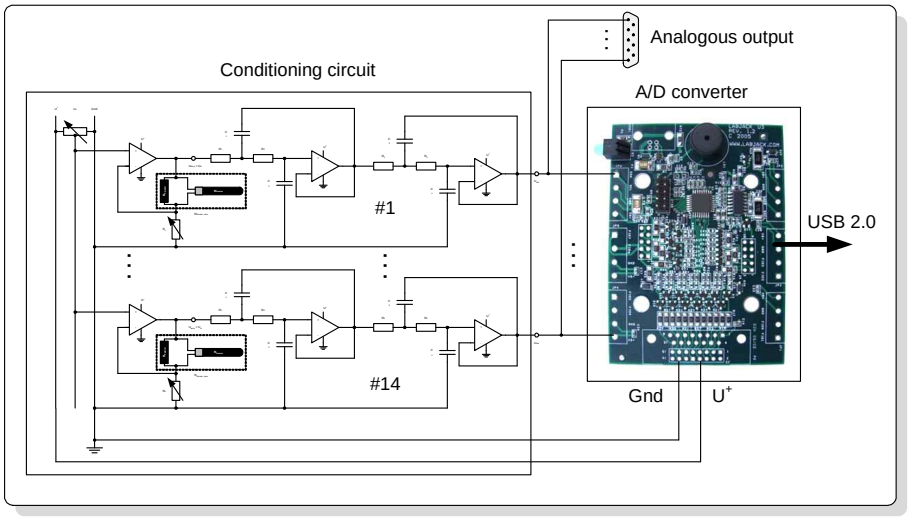

Figure 18: The conditioning circuit is connected to a commercially available A/D converter which communicates with the computer via the USB port. To maximize flexibility of data acquisition, an analogous output was provided.

A commercially available A/D converter was chosen which best met the requirements for the glove system. The card is a LabJack U3 (LabJack Corporation, Lakewood, Colorado, USA), equipped with an USB 2.0 interface, 16 A/D channels (0 - 2.44 V), 50 Hz sampling rate, 12 bit resolution and software drivers for Java, C/C++, Python, VisualBasic, LabView, and more. Additionally, the card is provided with a reference output voltage of 5 V which is used to power the conditioning circuit (see Figure 18). The cost factor is ≈125 €. To ensure the highest angular resolution, the analogous signal of the conditioning circuit was adjusted to the highest range with a maximum of 2.44 V. Within this A/D setup, the a maximum sensor resolution was between 0.01 and 0.1°.

For the measurement framework, a set of Java routines for data acquisition was developed. The Java Native Interface (JNI, [147]) was used to access the native functions of the A/D card (provided in a dynamic link library, .dll). The JNI is a feature that allows to take advantage of the Java platform, but still utilize code written in other languages. As a part of the Java virtual machine implementation, the JNI is a two-way interface that allows Java applications to invoke native code and vice versa (see Figure 19). Since JNI methods are already included in the LabJack U3, the card can directly be accessed from Java.

Therefore, only a Java library was developed which configures the A/D card for the special needs of the sensor glove. Some of the methods are illustrated in Figure 19. For example, the method 'openGlove()' enables the communication with the A/D card and configures it for the acquisition of 16 A/D channels. If the glove connection is established, the method

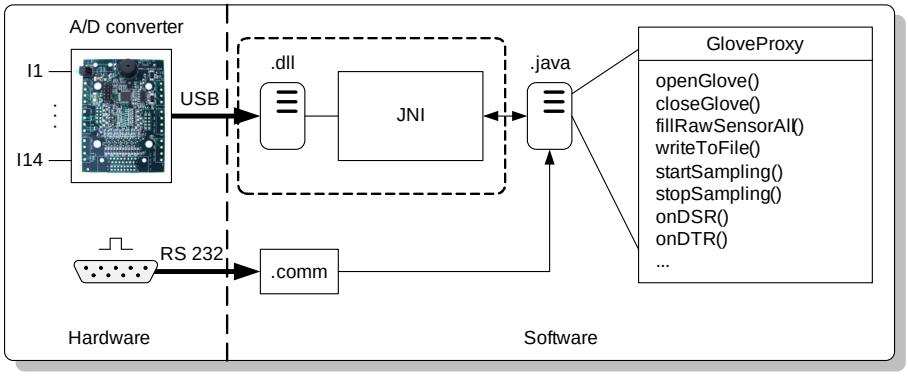

Figure 19: Software routines for accessing the A/D card were developed by using the Java Native Interface. Additional, an external trigger mechanisms to start and stop measurements with TTL-signals was implemented.

'fillRawSensorAll()' forces the LabJack to internally collect raw signals from all 16 A/D channels and to return a 16-dimensional array containing the actual voltage signals. The values of the array can be written to a data file by invoking the 'writeToFile()' method. For data recording, the function 'startSampling()' is called, which invokes the 'fillRawSensorAll()' and 'writeToFile()' methods every 20 ms (50 Hz), resulting in a data stream from the glove to a data file on the computer. Recording stops if the method 'stopSampling()' is called. Finally, the connection to the A/D card can be destroyed by the 'closeGlove()' method. To enable an external start of the data recording, the Java application was programmed to 'listen' to the 'Data Set Ready' (DSR) pin of the RS232 interface [123] (This feature was implemented using the .comm package). If a TTL signal occurs at this pin, the data recording is started ('onDSR()') by invoking the 'startSampling()' method. Similarly the measurement can be stopped by a TTL signal on the 'Data Terminal Ready' (DTR) pin of the RS232 port ('onDTR()'), which leads to a call of the 'stopSampling()' method. These and several additional methods provide basic functionality for retrieving and storing raw data from the glove as needed for the evaluation of the sensor glove. For the training system discussed in Chapter 2.4, this library served as a basis for more refined data acquisition methods.

2.1.8 Sensor glove evaluation

In addition to the technical characteristics of the glove, other factors such as the glove fit to the subject's hand determine the measurement accuracy, repeatability and reliability. Furthermore, user comfort during wearing the glove is also an important factor. In the following chapters the evaluation of these features is described.

Repeatability and accuracy compared to other sensor gloves

Four tests of repeatability, similar to those described earlier [264] were conducted in 5 subjects (3 male and 2 female): For each subject a plaster mold was fabricated to ensure that the finger joints in Test A and B could be consistently placed in the same position. Subjects were asked to create a cylindrical shaped object by squeezing a modeling mass with the thumb in opposition to the other fingers (Figure 20A). After the mass became stiff after ≈20 min, the grip posture could be repeated identically. Additionally, the 5DT-Glove Ultra and

the TUB-Glove were evaluated analogously in 4 subjects. Because it was shown that grip force affects test accuracy, we followed the recommendation by Dipietro and colleagues to instruct the subjects to grip the mold with as low force as possible and not to squeeze it [63].

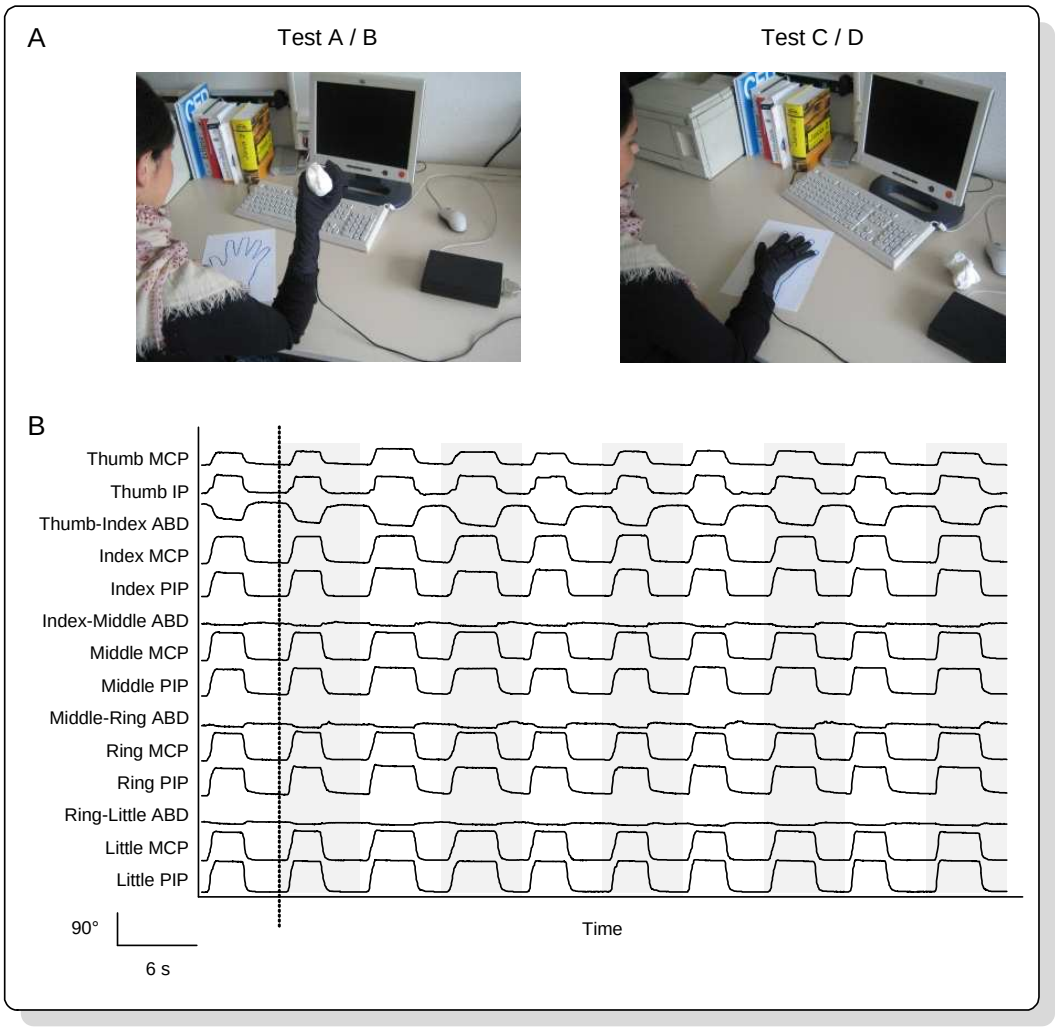

Figure 20: (A) Principle of repeatability tests. (B) Raw data for each joint in one subject. Ten data files from one block of Test C are concatenated and visualized. Different background colours indicate different data files. The dark grey shaded rectangle indicates the last 20 samples of the first data file which were used for analysis and corresponded to the flat hand position in (A).

In Test A and B (Figure 20A left) the repeatability of a roughly cylindrical grip posture was quantified, whereas in Test C and D, the consistency of a neutral flat hand position was assessed (Figure 20A right):

Test A: Mold grip and glove on between data acquisition
This test aimed to quantify the repeatability of a roughly cylindrical grip posture. The subjects's hand initially was in a flat position on the table. After a Go-Signal the subject gripped the plaster mold until data recording stopped after 6 s (see Figure 20A). Then the hand was returned to the flat position and the next trial was initiated. Ten blocks were recorded, and each block consisted of 10 trials. The subjects did not remove the glove between blocks.

Test B: Mold grip and glove off between data acquisition

Test B was analogous to Test A, except that the glove was removed and put on again before each block. Here, the influence of donning and doffing was quantified.

Test C: Flat hand and glove on between data acquisition
To assess the consistency of a neutral position, subject placed their flat hand on a table in marked finger positions. After a Go-Signal, the subject performed a flexion movement of all fingers and returned to the flat hand position after ≈3 s. Typical sensor readings obtained from one subject in Test C are shown in Figure 20B: data files from 10 trials (1 block) were concatenated and visualized. Recordings stopped after 6 s. Again 10 blocks consisting of 10 trials each were recorded.

Test D: Flat hand and glove off between data acquisition
This test was analogous to Test C, except that the glove was removed and put on again before each block.

For each subjects, the entire procedure took about 1.5 hours to complete. For repeatability analysis, the last 20 samples of each trial were averaged to reduce the data to 14 static joint angles representing the end posture of the trial (Figure 20B, dark grey shaded rectangle). As previously defined [63], the 100 trials for each test can then be represented as a 3-dimensional matrix $\mathbf{X}_{ijk}$, where i = 1...10 denotes the z^{th} trial, j = 1...10 the j^{th} block and k = 1...14 the k^{th} sensor. Accuracy of the repeatability measurements was quantified as the range (Range) and the standard deviation (SD) [63, 226]. For each repeatability test and each subject, Range was computed as

$$R_k = \max_j(\bar{\mathbf{X}}_{jk}) - \min_j(\bar{\mathbf{X}}_{jk}),$$

where

$$\bar{\mathbf{X}}_{jk} = \frac{1}{10}\sum_{i=1}^{10} \bar{\mathbf{X}}_{ijk}.$$

SD was calculated as the standard deviation of the $\mathbf{X}_{ijk}$ values. SD and Range values were averaged across joints or across subjects. The reliability between measures in each test was assessed by intraclass correlation coefficients (ICCs). ICC values were calculated for each test by randomly choosing 2 trials out of 2 randomly chosen blocks for each subject. The average angles of the last 20 samples of the 2 trials were calculated for each subject. Afterwards, the angle pairs of each joint from all subjects were pooled together and an ICC [222] was calculated for each joint. A high ICC close to 1 indicated a small fraction of variance explained by measurement errors (i.e. a high reliability). Conversely, a low ICC indicated a large fraction of variance explained by measurement errors (i.e. a low reliability). For consistency, the entire procedure was repeated 20 times resulting in 20 ICC values for each joint. The grand mean ICC was calculated by averaging all 20 ICCs.

The glove was calibrated before the experiments by using the maximum and the minimum sensor values for each joint without including hyperextension of the metacarpophalangeal joints (interphalangeal for the thumb). Calibration was necessary to adjust the sensor range to different hand sizes. The minimum and maximum values were stable across the three calibration cycles indicating that the glove fitted well to the subject's hand and did not considerably move during calibration. In the current experiments, Range and SD values were highly correlated (Figure 21A) to each other ($r > 0.99$, Pearson's correlation coefficient), as was also observed by Wise and colleagues [264]. In accordance with previous studies, the average flat hand repeatability (Range 3.29 ± 1.29°; SD 1.07 ± 0.42°) was better than

the average grip repeatability (Range 6.63 ± 1.86°; SD 2.10 ± 0.56°) and the repeatability without removing the glove (Range 4.35 ± 2.14°; SD 1.4 ± 0.65°) was better than the repeatability with removing the glove between blocks (Range 5.57 ± 2.43°; SD 1.77 ± 0.76°).

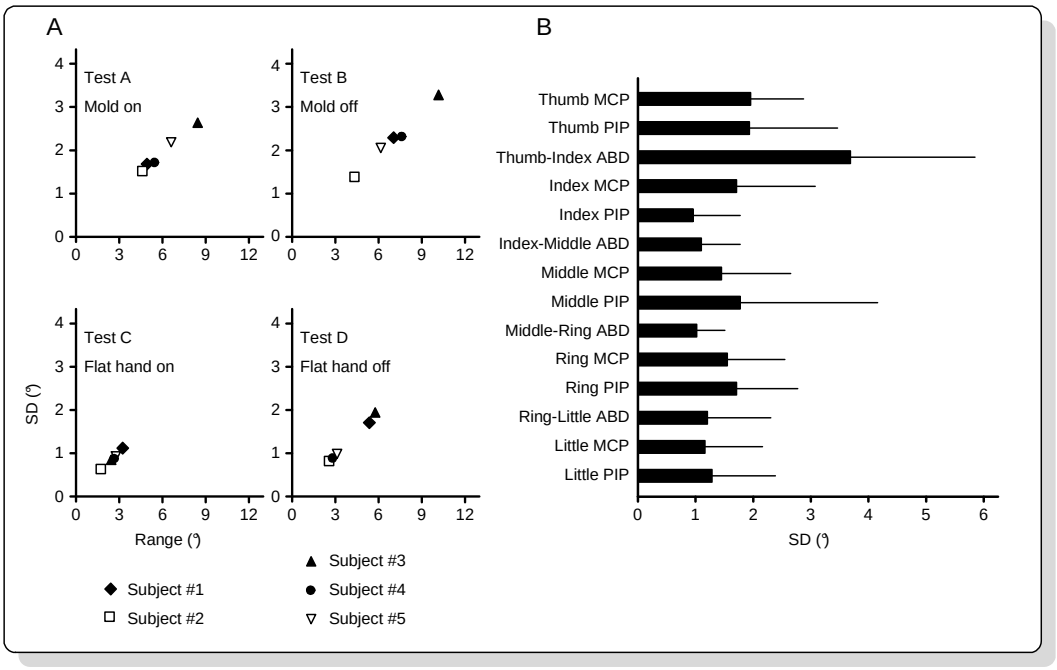

Figure 21: (A) Average Range plotted against average SD for each subject of Test A - Test D. As noted by other authors, Range and SD values were highly correlated to each other. (B) SD of each joint averaged across subjects and tests. Results were comparable to previously evaluated sensor gloves.

One of the five subjects (Subject #3) had a large hand size (>7.5) which made it difficult to don the glove over his hand consistently. This is reflected in the higher Range and SD values of this subject especially in Test B and D (Figure 21A black triangle). In Table 3 the mean repeatability values across all subjects are summarized and compared to results obtained with the 5DT-Glove Ultra, the TUB-Glove, and previously evaluated gloves.

Range and SD values were also calculated for each joint across subjects (visualization of SD values in Figure 21B). In this analysis, all joints showed comparable SD values from 0.96° to 1.93° (Range 3.05° - 6.16°), except the Thumb-Index ABD sensor, which had a somewhat higher SD of 3.65° (Range 11.01°). ICC values were computed to identify the variability between measures. ICC values close to 1 indicated a high reliability, whereas ICC values close to 0 indicated low reliability. In the current study, the overall ICC values across tests were high and ranged from 0.87 (Middle-Ring ABD) to 0.98 (Little MCP) with an overall average across tests and joints of 0.93 ± 0.05. Thus, repeatability and reliability of the sensor glove is high and lies in the range of previously evaluated sensor gloves. For evaluation of subjective and ergonomic features of the glove, a user feedback questionnaire was constructed.

2.1.9 User feedback of glove handling

A user feedback questionnaire, adapted from [226], aimed at assessing the subjective comfort of wearing and handling the glove (answers were coded as: 1 = strongly disagree, 2 = disagree, 3 = somewhat disagree, 4 = neutral, 5 = somewhat agree, 6 = agree, 7 = strongly

	Test A		Test B		Test C		Test D		Total	
	Range	SD	Range	SD	Range	SD	Range	SD	Range	SD
Subject										
#1	5.03	1.67	7.09	3.37	2.27	1.10	5.44	1.72	5.23	1.69
#2	4.67	1.49	4.43	1.40	1.86	0.62	2.57	0.83	3.38	1.09
#3	8.52	2.60	10.31	3.25	2.55	0.82	5.77	1.93	6.79	2.15
#4	5.49	1.72	7.72	2.32	2.55	0.84	2.91	0.91	4.67	1.45
#5	6.74	2.20	6.27	2.08	2.72	0.94	3.18	1.00	4.73	1.56
Mean	**6.09**	**1.94**	**7.16**	**2.26**	**2.61**	**0.86**	**3.98**	**1.28**	**4.96**	**1.59**
TUB-Glove	6.02	1.88	6.25	1.94	5.56	1.83	7.19	2.19	6.25	1.96
5DT-Glove	6.10	1.97	9.56	3.11	6.67	2.12	6.74	2.15	7.27	2.34
Wise (1990)	6.5	2.6	6.8	2.6	4.5	1.6	4.4	2.2	5.6	2.3
Dipietro (2003)	7.47	2.44	9.38	2.96	3.84	1.23	5.88	1.92	6.65	2.14
Simone (2007)	5.22	1.61			1.49	0.5			3.36	1.05

Table 3: Average Range (°) and SD (°) obtained from each subject. Mean values across subjects and test were compared to other studies. In addition, the TUB-Glove and the 5DT-Glove were evaluated in 4 subjects.

agree). Each item (see Table 4) was judged on a scale by 10 subjects.

Q1	I felt comfortable as the glove was put on.
Q2	I did not feel my fingers were put into any uncomfortable position as the glove was put on.
Q3	I did not feel any restriction to movement with this glove.
Q4	I felt comfortable performing the activities in this study.
Q5	The glove did not feel too tight.
Q6	I feel like I can bend my fingers just like I can without wearing the glove.
Q7	The glove did not feel too hot or too cold.
Q8	I did not feel like my fingers were put into any uncomfortable position as the glove was removed.
Q9	I felt comfortable as the glove was removed.

Table 4: User feedback questionnaire. Subjects indicated how strongly they agreed with the statements.

In general, subjects rated the sensor glove as positive. They felt comfortable during donning (analogue score: 6.3 ± 0.95, Q1), doffing (6.7 ± 0.48, Q9) and did not feel their fingers were put into any uncomfortable position (6.6 ± 0.52, Q2 and 6.5 ± 0.71, Q8). Over the period of wearing the glove, participants also felt comfortable (6.4 ± 0.70, Q4), denied that the glove felt too tight (6.5 ± 0.53, Q5) and denied any uncomfortable temperature changes of the hand and fingers (6.9 ± 0.32, Q7). However, due to the mechanical resistance of the glove material and the sensors, subjects felt some restrictions during wearing the glove (4.7 ± 2.11, Q3) so that the finger could not be entirely moved as if they were free (5.5 ± 1.84, Q6). The overall mean score was 6.23 ± 0.91.

To assess to which degree the increased sensor stiffness after Modification 1 affected the mobility of the joints, we additionally performed experiments on 3 subjects wearing a left and a right glove at the same time. The left glove was equipped with original sensors and the right glove with sensors after Modification 1. Subjects were instructed to move the fingers and afterwards evaluated Q3 and Q6 for both gloves. The answers to Q3 were equal between both gloves (4.67 ± 0.58 for the left vs. 4.67 ± 2.31 for the right). For Q6, the results of the glove equipped with original sensors (5.33 ± 0.58) were slightly better than that equipped with the modified sensors (5.0 ± 1.73). In summary, these results suggest that Modification 1 contributed only little to the finger joint stiffness in comparison to the glove material.

2.1.10 Summary and conclusions

Sensor gloves have a wide area of application including virtual reality, robotics or computer games. Of particular interest is their usage in rehabilitation or physiological assessments [27]. For all applications, accurate measurements, easy handling and a low price are desirable characteristics of a sensor glove. Here we presented a sensor glove, developed at the University of Wuerzburg (hence it is termed **Wii**-Glove), that appears to fulfill many of these characteristics.

Sensor resistance stability

Stability of the sensor resistance is mandatory for accurate measurements [225]. However, carbon ink based sensors show a decay of resistance over time when constantly bent. For example, Abrams-Gentile sensors (Abrams-Gentile Entertainment Inc, New York, USA) decay to ≈25 % of the initial resistance after 30 s [225], confirmed by the results obtained here), limiting their application for quantitative measurements of human finger movements. We found the decay of 2" Flexpoint sensors after 30 s to be in the range of ≈6 %, and, thus even superior to that of 3" Flexpoint sensor (decay ≈9 %), previously proposed as the optimal resistive bend sensors [225]. In separate experiments, we found that the sensor resistance further decreased to ≈18 % after 50 min of bending. This decay could be significantly reduced to a magnitude < 2 % by mounting a thin plastic foil over the sensor substrate. Thus, a major drawback of resistive bend sensors could be removed by Modification 1. That the associated increase of sensor stiffness affects user comfort to a high degree could be ruled out by the answers of question 3 and 6 of the user feedback questionnaire in which subjects answered to feel only mild restrictions of finger movements and did not feel a substantial difference between a glove with modified and a glove with original sensors.

Sensor linearity

A second desirable characteristic is a linear relationship between the final glove sensor signals (usually voltage) and bend angle, whereas the linearity depends on both, sensor resistance and conditioning circuit. Using a signal conditioning circuit that proportionally converted the sensor resistance into voltage signals reduced the source of linearity of the final signal exclusively to the sensor resistance. We obtained a linear relationship between the sensor resistance and bend angle by placing a resistor parallel to the sensor (Modification 2). Because only 2 angle-voltage pairs were needed, the sensor values at flat hand position and maximum bent, calibration time of the 14 sensors was performed within only ≈10 s. In contrast, if the

final voltage signals do not correlate linearly with the joint angles, a time consuming calibration (≈30 min in this study, ≈8 min for 5 sensors in the study of Simone and colleagues) and additional offline data processing is required [226]. Moreover, the linearity of the sensor after modification ensured a constant sensor resolution after A/D conversion over the full range of movements which again is not present if the bending signal before A/D conversion is not linearly related to the bending angle.

Linearity changed only little in subjects with different hand sizes indicating that hand size has a minor effect on linearity. However, to optimize linearity, gloves for different hand sizes (small, middle, large) may be designed each with optimal adjusted modification parameters (foil thickness and parallel resistance) for appropriate hand sizes. We will also test alternative conditioning circuits, which do not linearly convert sensor resistance into voltage signals. With such setups, linearization may be performed by the conditioning circuit directly without the need for additional resistances. To our knowledge, the **Wii**-Glove is the first glove design which utilizes linearized resistive bend sensors and therefore combines low sensor costs with ideal sensor characteristics. Furthermore, the reliability and repeatability of the glove were high.

Repeatability and reliability

While several commercial and non-commercial sensor gloves exist, only a few studies systematically addressed their reliability and accuracy [63, 156, 226, 264]. Compared to these sensor gloves, the Wii-Glove showed similar repeatability and reliability results (see Table 3). As illustrated in Figure 21, there was no substantial difference between the SD values of the MCP, PIP and ABD (except Thumb-Index ABD) joints indicating that the Range and SD values of this glove can be compared to gloves equipped with different sensor types and different number of sensors. The higher errors at the Thumb-Index ABD joint on the one hand may be related to the position of the sensor on the glove which may not be optimal. A second error source could be the repeatability protocol itself. As noted by others, the results of the repeatability tests are influenced not only by technical characteristics of the sensor glove, but also by factors like the grip strength [63] or small deviations of the thumb and finger placements. We tried to minimize these effects by instructing the subjects to grip the mold with as low force as possible and monitored a constant position of the hand. Despite these effects SD was only 1.59° reflecting high measurement repeatability. Reliability was quantitatively assessed by ICCs (ranging from 0.81 - 0.99 with a mean across joints of 0.93), which were comparable to gloves evaluated by Simone et al. [226] (ICCs from 0.79 - 0.99 with a mean of 0.95), Dipietro et al. [63] (ICCs from 0.7 - 1.0) and Mentzel et al. [156] (ICCs from 0.82 - 0.99, with a mean of 0.94, although in this study the test procedure was somewhat different). Consequently, the repeatability and reliability of the **Wii**-Glove is similar to other evaluated gloves and also lies within the measurement reliability of manual goniometry [264].

Issues related to practical application

User acceptance and applicability, assessed by a user feedback questionnaire, was high, suggesting that the modifications had not been accomplished at the cost of user acceptance. Another possibility to further optimize user comfort and to increase the physical workspace of the glove would be a wireless data transmission from the glove to the computer. However,

the **Wii**-Glove was intended to work within TMS environments, which may have a disrupting effect on wireless data transmission due to its large and rapidly changing magnetic fields (up to 2 Tesla). Those possible external interferences were minimized by removing all electrical elements except the bend sensor from the glove. In experiments with TMS we could not find any stimulation artifact or distortion of the sensor signals indicating a reliable operation of the glove in conjunction with this neurophysiological technique. A second advantage of the distributed design was that the same conditioning circuit could be used for different gloves (e.g. for different hand sizes) further reducing costs. To maximize flexibility, the conditioning unit was provided with an analogous output for each sensor. Therefore, it can be connected to any A/D converter allowing, for example, the simultaneous and synchronous recording of electromyographic signals and finger movements with already present hardware equipment. Finally, sensor resolution (≈0.1°) of the -Glove could be optimized by potentiometers of the conditioning circuit and was higher than in most other sensor gloves (ranging from 0.2° to 0.5°). For example, the CyberGloveII has a nominal resolution of 0.5°, which may not be optimal for recording small finger movements such as after TMS [87].

Optimization of modification parameters

A general disadvantage of resistive bend sensors is the abrupt loss of sensitivity when bent in opposite direction, which is needed, for example, to measure metacarpophalangeal hyperextension. Here we also found that the sensitivity decreased and the linear relationship of the sensors was not preserved for hyperextension movements. However, for a new prototype glove, the optimization procedure was repeated using a plastic foil with 0.1 mm thickness (Modification 1) and a simulated parallel resistance of 1 kΩ (Modification 2) in one subject. As illustrated in Figure 22, the linearity was maintained in the range of -30° hyperextension to 90° flexion of the MCP (IP and 60° maximum flexion for the thumb) joints with these parameters (mean r^2 across all MCP and IP joints of 0.9965 ± 0.0048).

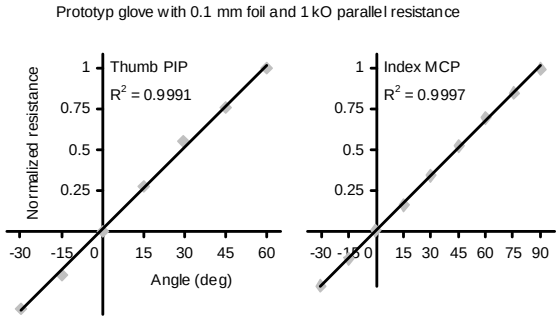

Figure 22: The optimization procedure using a plastic foil with 0.1 mm thickness (Modification 1) and a parallel resistance of 1 kΩ (Modification 2) mounted in a prototype was repeated. Results show that the linearity was maintained in the range of -30° hyperextension to 90° flexion. Examples for the Thumb IP and Index MCP sensor are shown.

Thus, the modification concept is capable of resolving another disadvantage of resistive bend sensors. To our knowledge, this is the first demonstration that the whole range of finger movements in humans can be measured with linearized resistive bend sensors. Because hyperextension movements were not measured in the current study, the present results are not influenced. In future, sensor gloves with these optimal modification parameters will be constructed and used.

Conclusions

The **Wii**-Glove provides reliable, linear, high resolution joint angle signals. Elements of the glove incurred material costs of < US $ 500, a factor of ≈10 - 20 less than the price of some commercially available sensor gloves. We also found flawless operation of the glove in the presence of large magnetic fields associated with TMS. Finally, user acceptability was comparable to previously described sensor gloves. The fact that it can easily be produced for different hand sizes for the left and right hand makes it a flexible measurement system which may also be adaptable to study movements in non-human primates such as monkeys. The next chapter describes the application of the glove to record stimulation induced finger movements.

2.2 The magnetic stimulation framework

The neuro-navigation based magnetic brain stimulation environment represents the neurophysiological component of the measurement framework to 'read out' the kinematic representations of finger movement from the primary cortex.

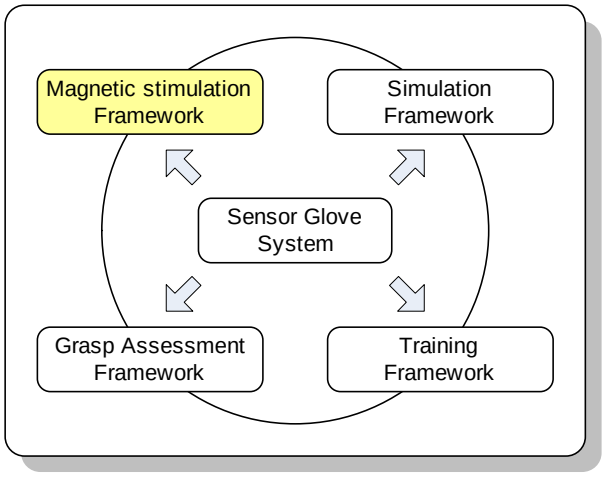

As a neurophysiological technique, transcranial magnetic stimulation (TMS) is used. This technique is non-invasive, painless and has a number of unique physiological features that distinguish it from other techniques such as intracortical microstimulation. These properties suggest that TMS leads to current injection into a small, but extended neuronal circuit, inducing a naturalistic neuronal activation pattern [116]. If moderate intensities are employed, TMS over the primary motor cortex preferentially activates intracortical horizontal fibres which link up an extended cortical network presynaptic to the corticospinal projection neurons, the single-most important anatomical substrate for individuated dexterous finger movements. Thus, TMS is an ideal method to excite the input of the modular structure defined in Chapter 1.7. Since the interpretation of the results critically depend on the nature of excitation, the technical and physiological characteristics of this technique are explained in more detail in the next chapters.

2.2.1 Transcranial magnetic stimulation (TMS)

While the first reported application of magnetic fields to the human brain ranges back into the late 1890s, the quantitative application of transcranial magnetic stimulation (TMS) in human subjects was first described in 1985 [14], see Figure 23A. Since then, the field of TMS has been steadily growing [258]. Nowadays applications of TMS range from clinical assessment of disease related parameters over research in neurophysiology, rehabilitation to the treatment of psychiatric disorders [191]. If the motor system is studied, the effect of TMS usually is examined by muscle responses and the change of the muscle response amplitude due to experimental interventions or diseases. However, studying only the magnitude of a single or a small number of muscles might not be sufficient to understand the mechanisms underlying the human motor system. A more convenient approach would be to look at parameters that capture the synergistic action of all muscles. This attempt has been taken in the measurement framework. Instead of studying single muscle activity, the kinematics of TMS-evoked finger movements and their modular characteristics are the main objective here. Before the methodological details are described, a short introduction to TMS is given.

Technical foundations of TMS

Modern magnetic stimulators consist of two main components: a capacitive high-voltage, high-current charge-discharge system and a magnetic stimulating coil that produces pulsed fields of 1-4 Tesla in strength with durations of approximately a millisecond for single-pulse stimulators [252, 260]. The charge-discharge system is composed of a charging unit, storage capacitor, switching circuitry, and control electronics (Figure 23B). With the capacitor first charged to 2-3 kV, the gating of the thyristor into the conducting state will cause the discharging of the capacitor through the coil (I_{Coil} in Figure 23B). The resulting current waveform is typically a damped sinusoidal pulse that lasts about 300 ms and has a peak value of 5-10 kA [193]. The maximum magnetic field is set up within ≈ 200 μs [191]. With the standard monophasic stimulation, the thyristor blocks at the moment when the energy swings back over the coil and the capacitor is completely discharged by a diode resistor combination parallel to the coil (I_R in Figure 23B). For biphasic stimulation the electrical circuit is slightly different [260].

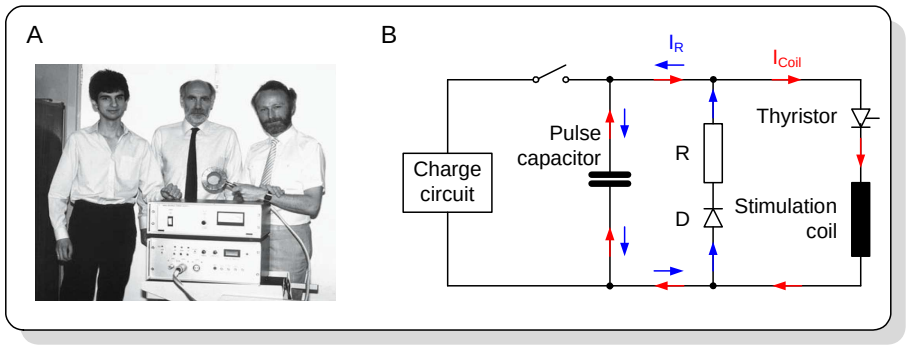

Figure 23: (A) Historical image (1985) of the first applicable magnetic single pulse stimulator. From left to right: Dr. Reza Jalinous, Prof. Ian Freeston, Prof. Anthony Barker (from [99]). (B) Principle electronics of a monophasic magnetic stimulator.

During discharge of the capacitor through the coil a time t and distance r dependent magnetic field $\mathbf{H}$ around the coil windings builds up according to the Biot-Savart law

$$\mathbf{H}(r,t) = \frac{\mathbf{B}(r,t)}{\mu_0} = \frac{1}{4\pi} \mathrm{I}_{\mathrm{Coil}}(t) \oint_C \frac{dl(r') \times (r - r')}{|r - r'|^3}, \tag{2.12}$$

where r represents the vector from the origin of a coordinate system to a position within the cortex and r' is the vector from the origin to the coil center. The integration is performed with the vector dl along the coil windings C and μ_0 is the permeability of free space. In contrast to electrical brain stimulation, the magnetic fields painlessly pass the skin and the bones [14] and, similar to a transformer, induce an electrical field in the brain tissue which is proportional to the change of the magnetic field (Figure 24A):

$$\nabla \times E = -\frac{\partial \mathbf{B}(r,t)}{\partial t}. \tag{2.13}$$

Regarding the induced electric field, models of the current induced in a flat volume conductor show that the resulting electric field is parallel to the surface (Figure 24B) at all points [191, 240]. However, note that the brain is much more complex and more inhomogenous such that the direction of the electrical field might be different [223].

To enhance the focality of the induced electrical field, the coil geometry is normally selected as a figure-of-8-shape. Because of the rules of magnetic induction, the resulting magnetic

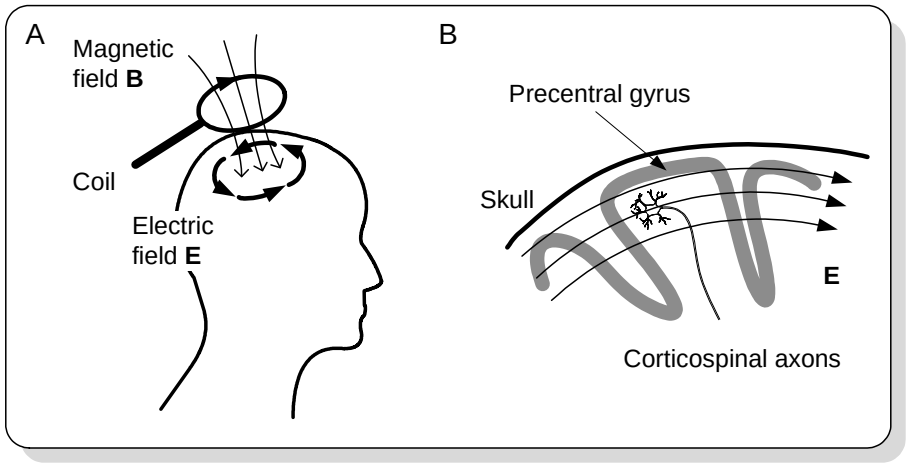

Figure 24: Principles of TMS. (A) Current in the coil generates a magnetic field that induces an electric field **E**. (B) A schematic lateral view of the precentral gyrus in the right hemisphere. A pyramidal axons together with a typical orientation of the intracranial **E** field are shown. (Adapted from [192])

field of the twin coils simply is the sum of the magnetic fields of each of the wings [191]. The maximum electrical field of the coil is then obtained at the junction of the wings and typically stimulates a cortical area of a few centimeters in diameter [193, 260]. The induced electric field is able to depolarize neurons preferentially at the axon (Figure 24B) rather than the cell body or other parts of the neurones [192]. The physiological mechanisms of TMS are described in greater detail in the next chapter.

Physiology of excitation

Neurons communicate between each other by changing their state due to chemical or electrical events at their inputs. The state change of a neurons is referred to as an action potential which denotes an abrupt increase of the membrane potential. An action potential occurs if the intra-cellular ion concentration receives a certain amount of excitatory post synaptic potentials. The resulting electrical wave then passes along the membrane of the axon and excites connected neurons (see Chapter A.1). Thus, physiologically, information between neurons is transmitted by electrical waves, generated by biological depolarization of the neuron.

In order to passively stimulate a neuron, the depolarization must be initiated by the stimulus, for example the electrical field induced by magnetic stimulation. It is assumed that the depolarization of the neuron most likely is initiated at the axon near the soma [144]. The axon's membrane is depolarized if the spatial derivative of the electric field parallel to the neuron's axon (for transversal fields much higher electrical fields are needed) exceeds a certain value within a certain length of time [192, 258]. Thus, an axon which runs parallel to a constant electric field will not be stimulated since the potential at all points along its length will be equal (Figure 25A). However, if the axon is bent it will cut the electric field lines with the result that the potential at points along the axon near the bend will differ and favor stimulation at this point (Figure 25B bottom left). Within this condition, calculations of electric field gradients suggest that the site of activation is at the bent of the axon [258, 260]. Excitation might also occur if the equipotential lines of the electrical field changes cross the straight axon (Figure 25C). Furthermore, the axon might be depolarized, if the electrical

field parallel to the axon changes (Figure 25D). In all cases the passively induced local depolarization leads to a global depolarization of the neuron and therefore to the generation of an action potential. If the brain is stimulated, the induced electric field depolarizes a

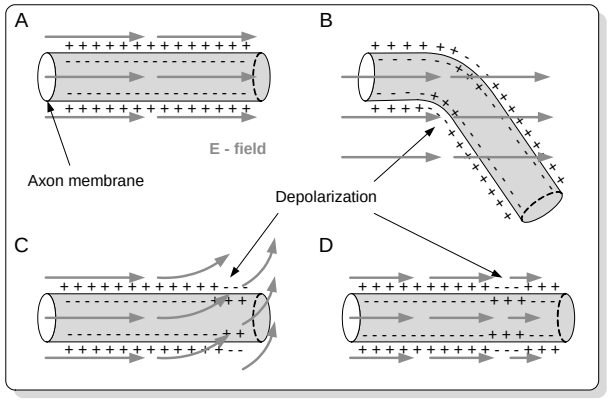

Figure 25: Physiology of excitation. (A) An axon which runs parallel to an electric field will not be stimulated. Excitation occurs if the axon is bent (B), if the equipotential lines of the electrical field changes cross the straight axon (C) or if the electrical field parallel to the axon changes (D). (Adapted from [260])

large number of neurons, which may differ in function depending on the underlying cortical microstructure. In the following chapter, the physiology of stimulating the primary motor cortex is explained.

Stimulation of the primary motor cortex

The mechanisms of stimulation of the primary motor cortex are best investigated among all brain areas. One of the main reason is that a direct stimulation effect (muscle activities or movements) can be observed with relatively low stimulation intensities [82, 208, 116]. Basically, the cytoarchitecture of the primary motor cortex can be subdivided in six (I - VI) vertically arranged and overlapping layers, containing different types of neurons and different connection topologies [184]. Layer I is closest to the surface of the brain, whereas layer VI is the deepest layer. For brain stimulation, layers V and II-III are most relevant [144, 116]. In layer V pyramidal cells are located, projecting with their axons to neurons in the spinal cord or directly to motor neurons (also to other cortical and subcortical structures). These cells are believed to be the main output cells of the primary motor cortex and an origin of the corticospinal tract [184]. In the upper layers II-III, neurons with horizontally oriented axons exist, which are densely interconnected and project onto corticospinal output cells or to other cortical and subcortical areas [184]. Thus, the excitation of neurons could in principle occur at several cortical layers (grey matter) or even downstream at the cortical white matter. However, this appears to be less likely [68]. Indeed, studies recording descending volleys with chronically implanted electrodes in the spinal cord [59] showed that electrical and magnetic stimulation evoke several descending volleys separated in time by $\approx$1.5 ms [223, 259] suggesting that neurons located in different cortical layers are excited by a single pulse.

The first volley is called the direct (D) wave and the following are called indirect (I) waves [6]. Figure 26A illustrates the effect of direct and indirect waves on the muscle evoked potential (MEP). A single suprathreshold stimulus evokes a D-wave followed by several I-waves (upper right subset in Figure 26A). The waves propagate to the spinal cord and induce excitatory

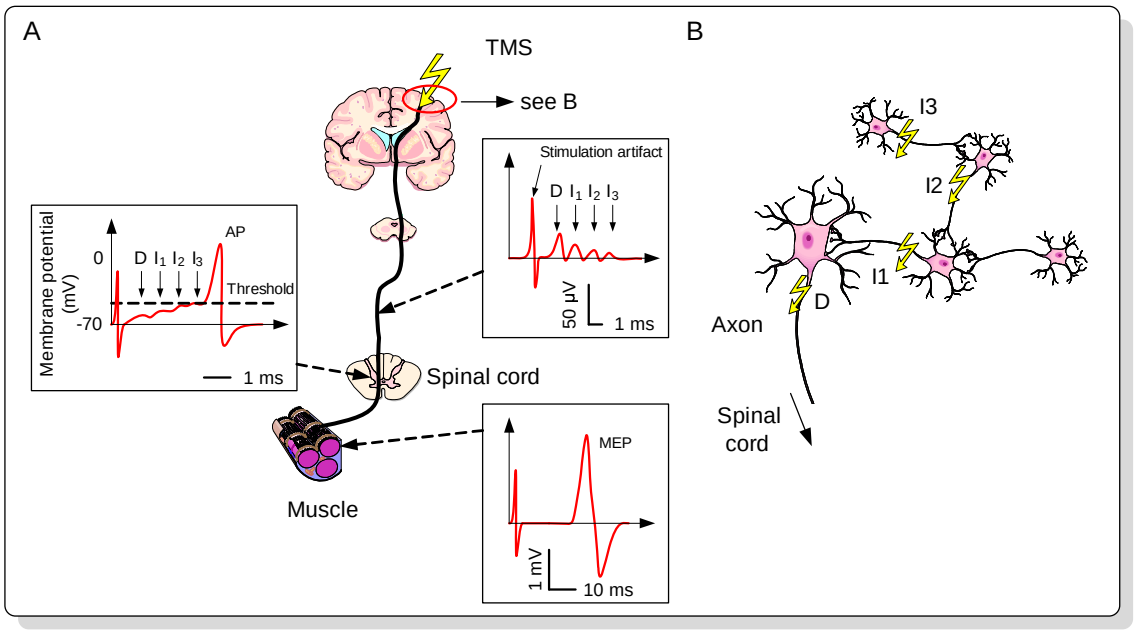

Figure 26: Stimulation of the primary motor cortex. (A) Principle of MEP generation. (B) Cortical sources of excitation.

postsynaptic potentials (EPSP) in the spinal motoneuron. The depolarizing effects of the EPSPs accumulate and lead to an action potential in the motoneuron if a certain threshold is exceeded (left subset in Figure 26A). The motoneuron transmits the signal to the target muscle, where a motor evoked potential (MEP), a summed muscle action potential, can be observed (lower right subset in Figure 26A) [223].

Figure 26B illustrates the possible origins of D and I-waves [144]. The D-wave is believed to be set up from the direct stimulation of pyramidal cells located preferentially in layer V of the cortical cytoarchitecture [191]. Conversely, the indirect waves are likely generated in the upper cortical layers and excite the pyramidal output neurons trans-synaptically, i.e. indirect. The first I-wave might originate from stimulation of neurons separated one synapse from pyramidal cells, the second I-wave separated two synapses and so on [144]. Precisely which neuronal connections might be involved in I-wave generation is unknown. A candidate for I-wave origin is the intrinsic motor cortical circuitry located in layers II-III [191, 223]. Support for this site of stimulation comes from the characteristics of the induced electric field which especially is suited to excite the horizontal (parallel to the cortex surface) oriented axon collaterals of these neurons [223]. Since the I-waves depend on the state of the cortex such as wakefulness, are sensitive during execution of skilled finger movements [116] and reflect learning processes [47], a high proportion of I-wave components (i.e. information from intrinsic neurons presynaptic to pyramidal cells) in the MEP is desirable.

The size of the recruitment of D- and I-waves is influenced by the direction of the induced electric field [59]. The direction of the electric field depends on the current flow through the coil and the orientation of the coil over the scalp (Here, a figure-of-8 coil [114] is assumed). If the electric field induced in the brain is oriented vertically from lateral to medial, preferentially D-waves, and at higher stimulation intensities, also I1-, I2- and I3-waves are recruited [223, 259]. Conversely if the induced electric field (and the induced current) points from posterior to anterior, an I1-wave is preferentially generated [61, 223]. If the stimulation intensity is raised, later I-waves and finally D-waves are recruited [62]. With anterior to posterior induced electric fields higher stimulation intensities are needed [259, 60] and I3-waves

are preferentially generated [61]. In addition to the orientation of the induced electric field and the stimulation intensity, the recruitment is influenced by the type of the coil [60] and the stimulation mode, i.e. monophasic vs. biphasic [124, 58, 59]. The mechanisms explained here relate to figure-of-8 coils and monophasic stimulators.

In summary, to ensure that a presynaptic stimulation occurs, the coil should be oriented so that an electrical field in the brain is induced which is directed from posterior to anterior. With the Magstim monophasic stimulator this is ensured if the coil handle points backwards. The best stimulation is obtained if the handle additionally is tilted about 45° relative to the sagittal plane [159, 223]. Furthermore, the stimulation intensity should be kept as low as possible. Studies have shown that with a posterior to anterior induced electric field intensities at 1.4 times the resting motor threshold (RMT, the minimum stimulation intensity at which a muscle response occurs [190]) mainly I waves are recruited [62]. Here, the upper limit of stimulation intensity is set 1.4 times RMT. Finally, a monophasic stimulator using a figure-of-8 coil should be used. If these conditions are met, the MEP and TMS evoked movements reflect intrinsic properties of the primary motor cortex and thus learning dependent organization [47]. Note that due to the transsynaptic stimulation of pyramidal tract neurons, the resulting MEP or movement is not only composed of excitatory, but of a mixture of excitatory and inhibitory potentials [245, 223]. The next section describes the experimental setup of the recording of finger movements after TMS.

2.2.2 Description of the experimental setup

The subject must be comfortably seated with the hand secured at a semipronated position in a cast with the elbow joint in a flexed position such that the hand is approximately 30 - 40 cm in front of the chest (Figure 27A). Electromyographic (EMG) activity is recorded from the right abductor pollicis brevis (APB) muscle and from the abductor digiti minimi (ADM) muscle in a belly tendon montage (Figure 27B). Finger kinematics are measured

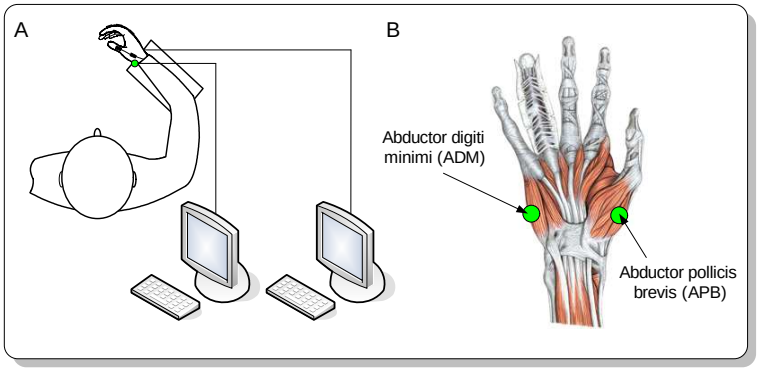

Figure 27: (A) Experimental setup up for magnetic stimulation. Electromyography and a sensor glove is used for measurement of muscle activity and finger movements, repsectively. (B) Electrodes for electromyography are placed over the abductor digiti minimi (ADM) and abductor pollicis brevis (APB) muscle.

with a sensor glove (e.g. the **Wii**-Glove) which must be pulled over the EMG electrodes. For the long fingers (I: index, M: middle, R: ring, L: little), sensor values from the proximal interphalangeal joints (PIP: I PIP, M PIP, R PIP, L PIP), metacarpophalangeal joints (MCP: I MCP, M MCP, R MCP, L MCP), and, for the thumb, from the MCP (T MCP) and thumb-index abduction (T-I ABD) sensors are considered for analysis.

Next, the frameless MR-guided neuronavigational device (Brainsight, Rogue Research, Montreal, Canada) which is used to increase accuracy in coil positioning and angulation is set up. Trackers must be adjusted to the head of the subject and to the stimulation coil in order to detect the relative coil position with respect to the head (see Figure 28). Using anatomical

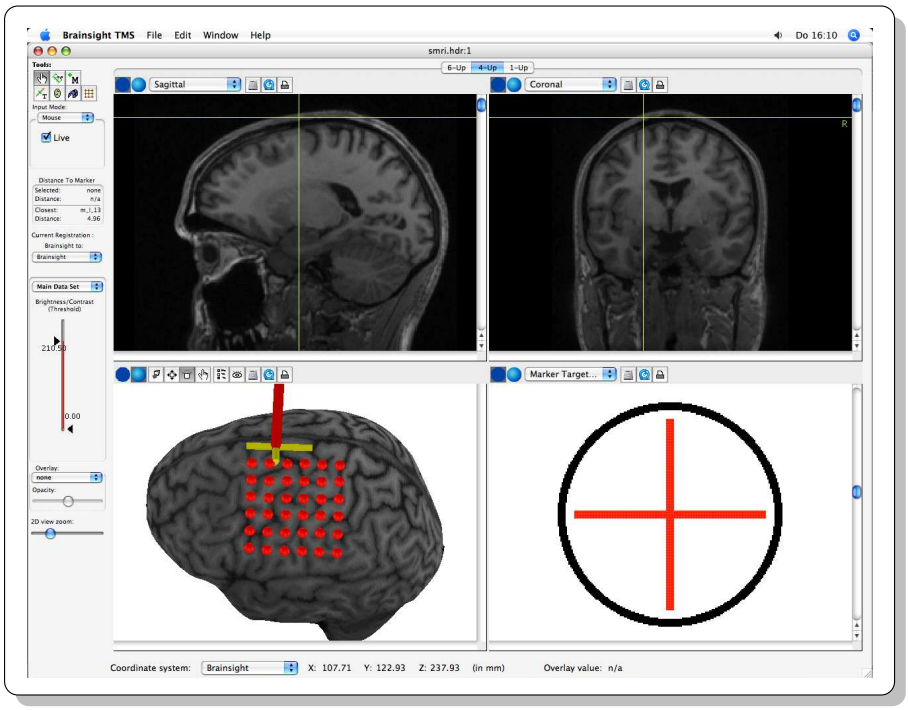

Figure 28: A frameless, MR-guided neuronavigational device is used to increase accuracy in coil positioning.

landmarks, the head geometry of the subject is matched to template (Montreal Neurologic Institute MNI) or individual MR-images of the subject. The position of the coil can then be visualized with respect to the MR-images. In the 3D-reconstruction of the MR images, a total of 100 stimulation sites arranged as a grid with 1 cm spacings on the surface of the scalp are determined and saved as markers in the navigation software. The 30 (or 36) best suited markers are selected for stimulation (Figure 29). This grid is selected on the basis of the optimal position of the magnetic coil for eliciting motor evoked potentials (MEPs) at a moderately suprathreshold stimulation intensity in the resting APB muscle. At this site, termed the hotspot, the resting motor threshold (RMT) is determined as the minimum stimulation intensity needed to produce a response of at least 50 μV in the relaxed APB in at least five of ten consecutive trials [190]. The stimulation intensity should be set to < 1.4 RMT in order to minimize direct stimulation of output neurons, which occurs inevitably at higher stimulation intensities (see previous chapter). Initially, the 30 grid points surrounding the hotspot should be selected. To ensure that the mapping grid covers all sites where finger movements can be elicited by TMS, points lying outside the grid should be stimulated. If this is the case, the grid position must be moved until no visually observable finger movements can be evoked outside the border of the stimulation grid. The sequence of stimulation points should be random to avoid systematic effects originating from the subsequent stimulation of neighboring points. Fifteen to 20 TMS pulses at inter stimulus intervals of at least 6 s are sufficient for each stimulation site. This type of experiments is commonly referred to as 'cortical mapping' [155].

The complete experimental setup is shown in Figure 29. A trial (consisting of a TMS pulse,

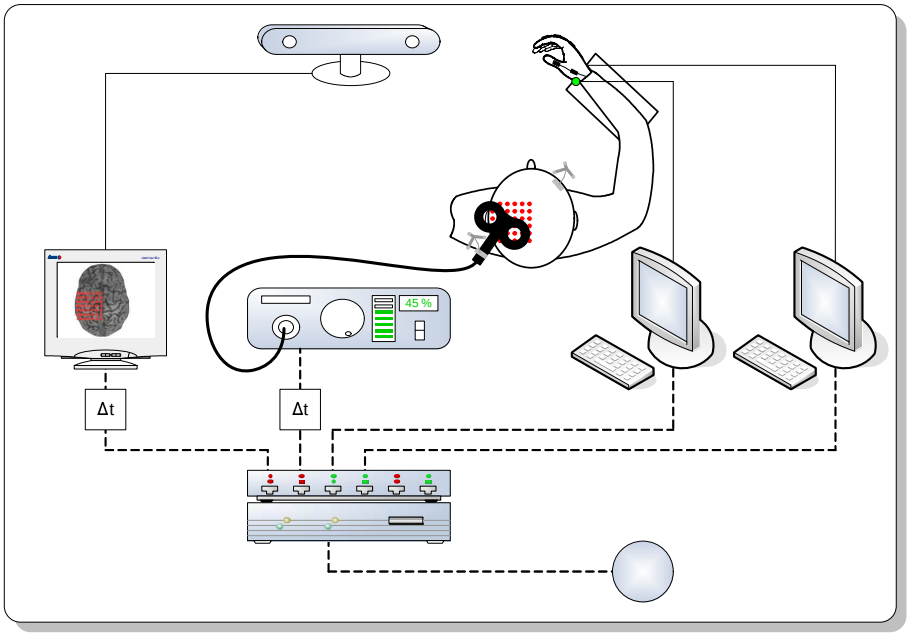

Figure 29: Complete experimental setup including the neuro-navigation system, the magnetic stimulator and the experiment control electronics. The coil is positioned over a randomly selected stimulation point and 15 stimuli are applied at each point. The resulting finger movements are recorded by the data glove and stored on a computer.

the recording of EMG and sensor glove signals and the recording of the actual coil position) is initiated by a TTL signal, released manually by a foot switch or software based at predefined intervals. The TTL pulse triggers the EMG recording system and the sensor glove by a positive flank at the DSR pin of the RS232 port (see Chapter 2.1.7). Alternatively, if the **Wii**-Glove is used, the sensor signals and EMG activity can be recorded with the same A/D converter. The TMS pulse and the trigger for recording the coil position is delayed (Δt) by a Master 8 (A.M.P.I., Jerusalem, Israel) for some hundreds of milliseconds. During the recordings, the subject should be instructed to keep the hand and fingers in a relaxed position. Muscle relaxation is monitored by audio feedback.

2.2.3 Experiment management software

To automatize and standardize the sensor data acquisition, a Java based graphical user interface was developed (Figure 30). The sensor glove signals are stored in -ascii format files in data folders with predefined conventions. The parent folder name consists of the name and first name of the subject and the date (Figure 30A). In a subfolder 'Data', each stimulation site is represented as a folder with its spatial coordinates in matrix notation ranging from '11' to '65'. The information on the subject (name, first name, age, handedness) and the main data folder can be entered in a graphical user interface mask as displayed in Figure 30B. After the 'OK' button is clicked, the empty subject and data folder are created and the main user interface is opened. The main user interface consist of three areas which communicate with each other (Figure 30C). First, in the data folder area the actual basic folder is displayed or can be changed. If the actual folder corresponds to the naming convention as described above (see also Figure 30A) and is selected, the software displays the stimulation folders according to their coordinates as circles with red background color in the second area, the visualization of the stimulation sites. For example, the folder '11' is drawn in the upper left corner (first

Figure 30: (A) Data structure for storage of TMS-evoked movements. For each grid point, a corresponding data folder exists. (B) Graphical user interface mask to set up the data folders and store information on the subject. (C) Main user interface for stimulation. A new stimulation point can be selected manually by clicking on the circles or randomly by the computer. Orange circles denote already stimulated points and the blue circle is the currently selected point. Sensor glove recordings can be triggered by signals at the RS232 port.

row and first column) of the matrix and the folder '66' in the lower right corner (sixth row and sixth column). Each circle object is programmed to have a mouse listener and therefore is sensitive for mouse interactions. If the user clicks on a circle, the color of the circle changes from red to blue, indicating that the selected circle and the corresponding subpath (e.g. '11') is the actual storage folder for the sensor glove data. Furthermore, if a folder already contains -ascii data from the glove, the software recognizes it and changes the color of the circle to orange. In this way, the user is always aware of the already stimulated sites. A second way to select a stimulation point is to click the button 'randomly select point'. If this button is clicked an algorithm randomly selects an index of the matrix (e.g., '34') and the corresponding circle is set active with a blue background. If a folder already contains data, this folder will not be considered by the algorithm anymore. Thus, with the random selection mode, all stimulation sites can be selected iteratively until all stimulation sites contain data from the sensor glove. Every time a new stimulation point is selected, the corresponding folder is transferred to the data acquisition area of the main user interface. In the menu, the user can choose between three different sensor gloves for data acquisition, namely the **Wii**-Glove, the 5DT-Glove family and the TUB-Glove. For each glove, the corresponding drivers are loaded and the acquisition parameters can be specified. In particular, the user can select if the glove should sample a certain number of data packages, or for a certain duration or continuously. The data acquisition can be started manually by clicking on the 'start' button. However, as described in Chapter 2.1.7, all glove drivers are equipped with the feature to respond to signals on the serial (RS232) port [123]. If the button 'serial port' is enabled, the manual 'start' button is disabled and the software starts a measurement if a TTL pulse occurs at the DSR pin of the serial port. If a TTL signal occurs, the software first generates a new file name containing the stimulation site and the number of the file (e.g. '11_001.csv' for the first file in folder '11'), opens the file and streams the values from the glove continuously

into this file. If the trial is stopped (for example after the specified package limit is reached), the file is closed. The lower left area is left blank for further options, such as a camera system to record the finger movements of the subjects. In summary, the software fully automatizes the stimulation procedure, leading to a consistent data structure and minimizing acquisition time.

2.2.4 Preprocessing of kinematic data

The analysis software, a library of Matlab functions, imports the measurements from the data storage concept specified in Chapter 2.2.3. Ten sensors are considered for analysis in the current version of the library. Figure 31A shows a representative example of joint excursions (recorded with the **Wii**-Glove connected to a 1401 power A/D converter and sampled at 2 kHz) and muscle activity after TMS. The first two channels contain muscle

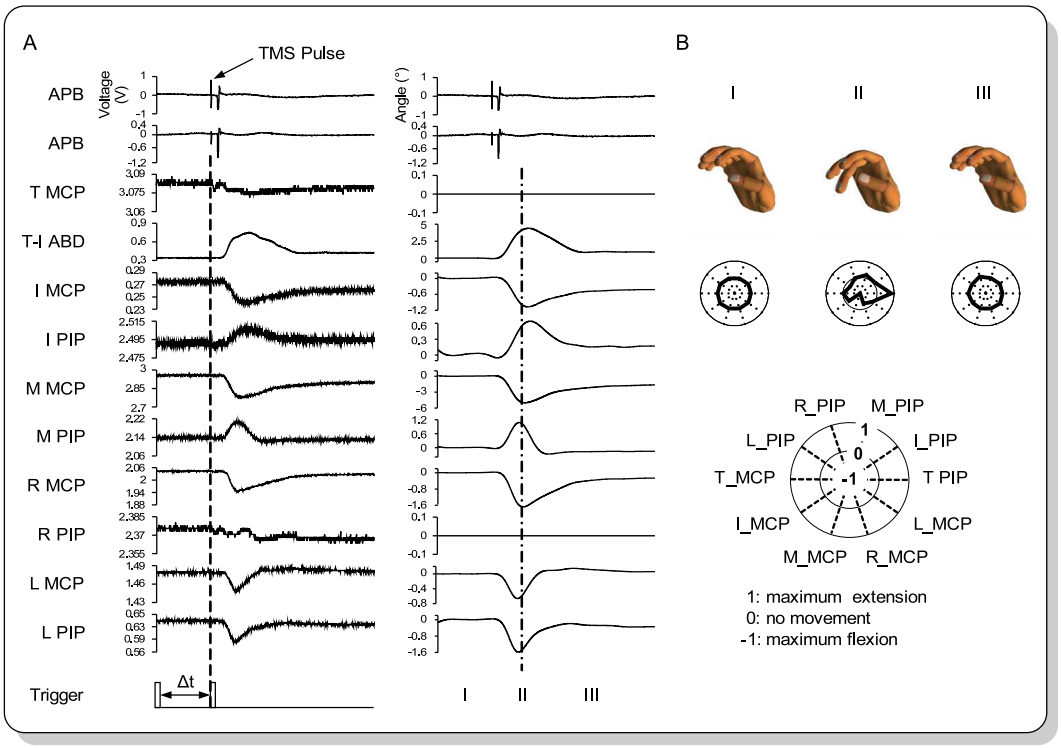

Figure 31: (A) Preprocessing of finger movements after TMS (dotted line in the left column indicates the time point at which the magnetic pulse was applied), recorded with the sensor glove. Signals are offset corrected, calibrated and filtered. Raw signals are shown on the left and preprocessed signals on the right. (B) TMS-evoked movements were defined as the hand posture present at the time of the maximum of the mean joint angular deviations from the baseline posture (indicated by the vertical dash-dotted line in the preprocessed signals in (A)). This movement index was termed posture vector (PV). Extension movements are displayed as outward deviations from the baseline position and flexion movements as inward deviations.

activity recordings from the APB and ADM muscle. After the delay Δt, the TMS pulse is applied (the dashed line indicates the time point of the TMS pulse). The artifact caused by the magnetic field can be seen as the sharp vertical line in the EMG channels. The activated neuronal populations project to the corresponding muscles and after a conduction delay, the muscle response occurs. The energy of the muscle contractions is transformed into mechanical actions resulting in finger twitches 20 - 30 ms after the MEP (lower 10 channels

in Figure 31A). After the movement, the fingers return to the initial static position. In the raw data, negative excursions indicate flexion and positive excursions indicate extension movements of the fingers. In a preprocessing step, the sensor recordings are offset-corrected and low-pass filtered using a 4^{th}-order Butterworth filter at 8 Hz. Then, the voltage signals are converted to joint angles according to the calibration values of the glove. Since the main information of TMS-evoked movements is represented in the spatial properties of the excursion, the entire time course is not considered for analysis. Instead, the movements are reduced to the relative static excursion around the resting position at the time point of maximum amplitude (dash-dotted line in Figure 31A) and extracted as a 10-dimensional vector for analysis. Here, positive values indicate extensions of the fingers and negative values indicate flexions. Data sets with completely zero values (i.e., no excursion around the resting position) are discarded from subsequent analysis. Figure 31B shows the static representation of the TMS-evoked movement from Figure 31A before the application of the TMS stimulus (I), at the time of maximum amplitude (II) and after returning to baseline (III). The vector representing the joint excursion at the time point of maximum amplitude is called the posture vector (PV). The PVs from each subject are stored in software structs for later analysis.

2.2.5 Spatial representation properties of finger movements

Several software functions to extract relevant measures, such as the size and the number of movements and the proportions between flexion and extension movements, exist. Especially, two relevant representational features of the cortical organization of movements [208] can be assessed.

Overlapping representations of fingers and movements

The first feature is the distributed representation of muscles belonging to certain body parts, indicating that the representations of any two smaller parts overlap extensively [208], as illustrated in Figure 32A. Furthermore, there should not be a major difference in the similarity of movements elicited from a single stimulation site and movements from other stimulation sites. In other words the within stimulation site variability of movements should be comparable to the between site variability of TMS-evoked movements.

To address these issues, two methods exist. The first method compares the similarity of PVs from one stimulation site to PVs obtained from other stimulation sites. The distance (or similarity) between two PVs is defined as the 1 minus the dot product of two normalized PVs which is identical to 1 minus the cosine distance:

$$d_{PV_1,PV_2} = 1 - \frac{\sum_{i=1}^{p} PV_{1,i} \cdot PV_{2,i}}{\sqrt{\sum_{i=1}^{p} PV_{1,i}^2} \cdot \sqrt{\sum_{i=1}^{p} PV_{2,i}^2}}, \tag{2.14}$$

where d_{PV_1,PV_2} designates the distance between the two $p = 10$ dimensional PVs, PV_1 and PV_2. Two identical PVs have a distance of 0, and PVs that are completely different (i.e. they point in opposite direction) have a distance of 2. Two PVs are defined as similar to each other if they have a maximum distance of $d_{PV_1,PV_2} = 0.2$. The algorithm computes

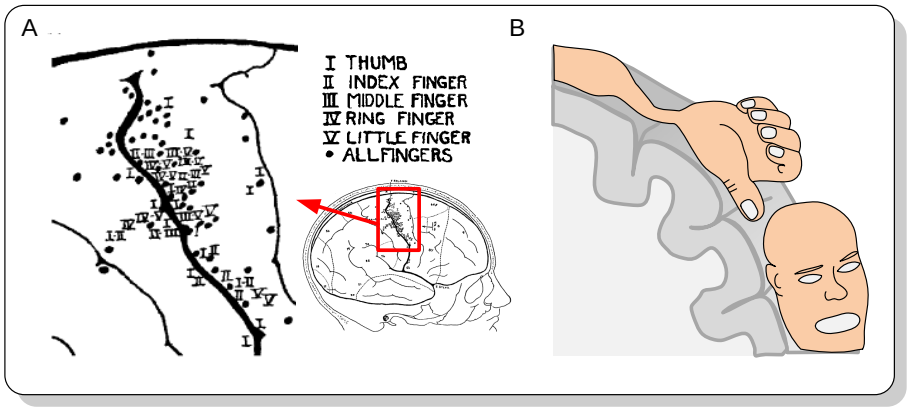

Figure 32: (A) Using electrical cortex stimulation, movements of a each fingers can be elicited from different stimulation sites. Image taken from [208]. (B) Despite this overlap, a somatotopic organization (as indexed by the homunculus [179]), with the thumb represented most laterally and the little finger represented most medially, can be identified.

the distance of all PVs obtained from a single stimulation site to each other resulting in $\binom{n}{k} = \frac{n\cdot(n-1)\cdot\ldots\cdot(n-k+1)}{k\cdot(k-1)\cdot\ldots\cdot1} = \frac{n!}{k!(n-k)!}$ distance values. Thus, for 15 PVs 105 combinations exist. Subsequently, for each PV of the same stimulation site, the distance to all PVs from different, randomly chosen stimulation sites are calculated, resulting in $15 \cdot 15 = 225$ combinations. For consistency, this calculation is repeated 10 times. The entire procedure is conducted for all 30 stimulation sites and the overall average distance of the within-site distance and between-site distance is calculated.

The second method computes matrices (one for each finger) of the summed absolute movement magnitude of a finger for all stimulation sites:

$$\vec{a}_k = \begin{pmatrix} a_{11,k} & \cdots & a_{15,k} \\ \vdots & \ddots & \vdots \\ a_{61,k} & \cdots & a_{65,k} \end{pmatrix}, \tag{2.15}$$

where $\vec{a}_k$ is defined as the activation matrix of finger k for all stimulation sites in one subject. The activation of finger k after 15 TMS-stimuli at a single stimulation site $a_{ij,k}$ with $i \in \{1, 6\}$ and $j \in \{1, 5\}$ (here 30 stimulation sites are assumed) is computed as:

$$a_{ij,k} = \sum_{m=1}^{15} \Big(\text{abs}(\text{PV}_{m,k,MCP}) + \text{abs}(\text{PV}_{m,k,PIP})\Big), \tag{2.16}$$

where $\text{abs}(\text{PV}_{m,k,MCP})$ and $\text{abs}(\text{PV}_{m,k,PIP})$ represent the MCP and PIP components of the m^{th} PV from finger k.

Somatotopical gradient

However, despite the intermingled representation of individual muscles and fingers, a subtle somatotopical gradient (Figure 32B) with the thumb represented most laterally and the little finger represented most medially [208] exists, a pattern which was previously summarized with the motor homunculus [179, 178, 82]. In contrast to these earlier stimulation studies, here, the somatotopical representation can be computed quantitatively as the centre of grav-

ities (CoGs) from the activation maps of individual fingers. For each finger k, the CoG is computed from the activation matrix $\vec{a}_k$ as:

$$\vec{g_k} = \begin{pmatrix} CoG_{x,k} \\ CoG_{y,k} \end{pmatrix} = \frac{1}{\sum_{i=1}^{6}\sum_{j=1}^{5} a_{ij,k}} \cdot \begin{pmatrix} \sum_{i=1}^{6}\sum_{j=1}^{5} i \cdot a_{ij,k} \\ \sum_{i=1}^{6}\sum_{j=1}^{5} j \cdot a_{ij,k} \end{pmatrix}. \tag{2.17}$$

For analysis of the somatotopical representation of individual muscles, an interactive graphical user interface was developed. EMG signals are assessed by a CED 1401 A/D converter and a corresponding software program (CED Signal2). Within this system the muscle activities are stored in a proprietary format (.cfs-files) which can be accessed via a .dll. To

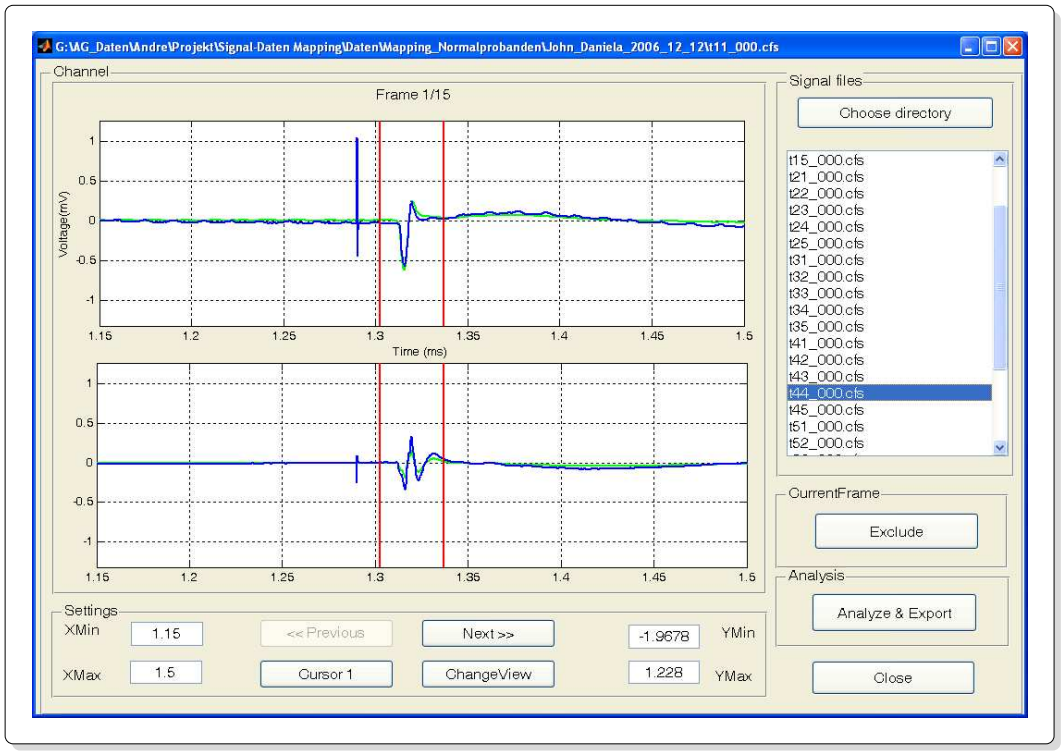

Figure 33: Graphical user interface for semi-automatic analysis of electromyographic signals.

automatize the analysis of muscle signals, a Matlab graphical user interface was developed. Using the .dll functionality, Matlab functions for reading data from the .cfs file format were created. (These functions were also used for loading and analyzing sensor glove data saved in this file format, see Chapters 3.2, 3.3 and 3.4.) The graphical user interface was designed to interactively analyze the data. First, all files present in the selected directory are loaded into the workspace and are displayed in a listbox (Figure 33 right). A file contains the electromyographic data from the trials of one stimulation site. These trials are called data frames. If a user selects a file from the listbox, the first frame is visualized in a time-amplitude plot. The user can now parse through the frames ('Previous' or 'Next' button, respectively) and can exclude ('Exclude' button) trials in which the muscles were not relaxed. For analysis, two vertical lines must be set by clicking into the data window (red lines in Figure 33). If the 'Analysis' button is pressed, the mean peak-to-peak signal amplitude in the region of interest across frames of both muscles is calculated and written into an Excel sheet by use of the Active-X mechanism. This calculation is repeated for all files in the directory, resulting

in an activation matrix of muscle signals similar as explained above. The CoGs are then calculated according to equation 2.17. The analysis of one experiment with the graphical user interface takes about 5 minutes, 5-10 times shorter than analyzing the data manually.

2.2.6 Movement groups

To study the similarity of TMS-evoked movements and to identify similar groups of movements, methods using hierarchical cluster analysis are implemented [32, 97]. In general, the purpose of hierarchical cluster analysis is to iteratively build groups of observations from a dataset until a single group containing all observations exist. The cluster algorithm is initiated with n clusters, each containing a single PV. A $n \times n$ distance matrix (using the distance measure from (2.14)) of similarities,

$$\mathbf{D}_n = \begin{pmatrix} 0 & d_{PV_1,PV_2} & \dots & d_{PV_1,PV_n} \\ d_{PV_2,PV_1} & 0 & \dots & d_{PV_2,PV_n} \\ \vdots & \vdots & \ddots & \vdots \\ d_{PV_n,PV_1} & d_{PV_n,PV_2} & \dots & 0 \end{pmatrix},$$

then is calculated, and the pair of clusters closest to each other is identified. These are merged to form a new cluster. Then the new $(n-1) \times (n-1)$ distance matrix

$$\mathbf{D}_{n-1} = \begin{pmatrix} 0 & d_{\{PV_1,PV_2\},PV_3} & \dots & d_{\{PV_1,PV_2\},PV_n} \\ d_{PV_3,\{PV_1,PV_2\}} & 0 & \dots & d_{PV_3,PV_n} \\ \vdots & \vdots & \ddots & \vdots \\ d_{PV_n,\{PV_1,PV_2\}} & d_{PV_n,PV_3} & \dots & 0 \end{pmatrix},$$

is calculated, where $\{PV_1, PV_2\}$ denotes the most similar PV pairs grouped into one cluster in the previous iteration. Subsequently, the next step of clustering is performed, etc., until all PVs are merged into one cluster. Several methods to calculate the distance between clusters exist. If n_r is the number of objects (PVs) in cluster r and n_s is the number of objects in cluster s, and x_{ri} is the i^{th} object in cluster r, the definitions of three important measurements are as follows:

- The single-linkage method (also known as nearest neighbor) is defined as the smallest distance between elements in the two clusters.

$$d_{r,s} = \min\left(d_{x_{ri},x_{sj}}\right),\ i \in (1 \dots n_r),\ j \in (1 \dots n_s)$$

- The complete-linkage method (also known as furthest neighbor) uses the largest distance between elements in the two clusters.

$$d_{r,s} = \max\left(d_{x_{ri},x_{sj}}\right),\ i \in (1 \dots n_r),\ j \in (1 \dots n_s)$$

- The average-linkage method uses the average distance between all pairs of objects in cluster r and cluster s.

$$d_{r,s} = \frac{1}{n_r \cdot n_s} \sum_{i=1}^{n_r} \sum_{j=1}^{n_s} d_{x_{ri},x_{sj}}$$

Here, the complete-linkage method is used. For each cluster a distance d^* exist at which it has been merged from two different clusters. The matrix $\mathbf{D}^*$ contains all linkage-distances and is called the cophenetic matrix. The entire clustering process can be visualized in a dendogram, which displays the elements of the cophenetic matrix [97]. Posture groups (PGs) are defined as clusters linked together at a maximum distance of d = 0.2 [227]; i.e., the maximum distance of the TMS-PVs belonging to a PG was d = 0.2. Furthermore, the spatial origin of the PVs in a PG can be traced back.

2.2.7 Modularity

As explained in Chapter 1.7, a module can be passively activated by TMS. Since neuronal networks may overlap extensively, a single magnetic stimulus may excite several networks at a time. A TMS evoked movement is therefore believed to represent the blended kinematic output of several activated modules (see Figure 34).

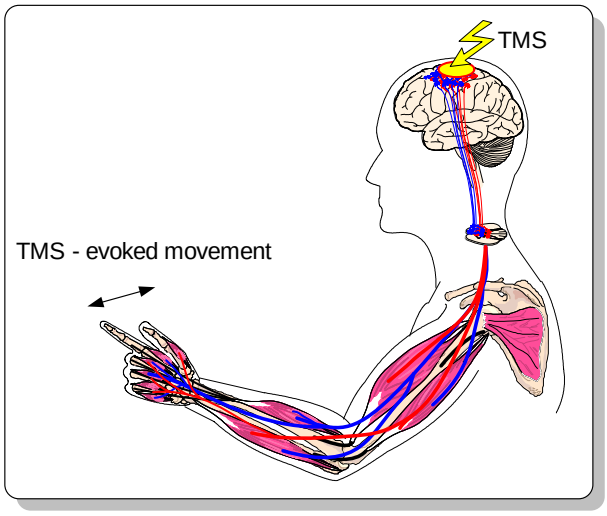

Figure 34: A single TMS pulse may activate several modules at a time. The resulting movement is a blend of the activated modules.

Thus, the generation of the j^{th} TMS-evoked movement, PV_j, can be modeled as a linear combination of n kinematic modules:

$$PV_j = \sum_{i=1}^{n} c_{ij}\vec{m}_i = c_{1j} \cdot \begin{pmatrix} m_{11} \\ \vdots \\ m_{1p} \end{pmatrix} + \ldots + c_{nj} \cdot \begin{pmatrix} m_{n1} \\ \vdots \\ m_{np} \end{pmatrix} = \mathbf{M} \cdot \begin{pmatrix} c_{1j} \\ \vdots \\ c_{nj} \end{pmatrix} \tag{2.18}$$

where $\vec{m}_i$ denotes the i^{th} p-dimensional module and c_{ij} the corresponding scaling coefficient. For all PVs this equation can be written in matrix notation as

$$\underbrace{\mathbf{PV}}_{p\times k} = \underbrace{\mathbf{M}}_{p\times n} \cdot \underbrace{\mathbf{C}}_{n\times k} \tag{2.19}$$

where **PV** has p rows (the number of joints or variables in general) and k columns (the total number of TMS-evoked postures), **M** has p rows and n columns (the number of modules) and **C** has n rows and k columns.

The task for further analysis is to identify modules from the set of TMS-evoked movements. Several mathematical methods [242] for module extraction exist. A widely used technique

is principal component analysis (PCA) wherein the module extraction is based on the correlations between joint movements [119].

Principal component analysis

Principal component analysis (PCA) was independently developed by Pearson and Hotelling in the early 20$^{\text{th}}$ century and is one of the oldest and best known technique of multivariate analysis. The central idea of PCA is to reduce the dimensionality of a dataset in which there are a large number of interrelated variables, while retaining as much as possible variation present in the data set [119].

This reduction is achieved by the transformation to a new set of variables, the principal components (PCs). The PCs are uncorrelated and ordered so that the first few retain most of the variation present in all of the original variables. In a first step, the mean of each variable is subtracted from the dataset (see transition from x_1' to x_1 and x_2' to x_2 in the two dimensional example in Figure 35). The second step in PCA is to search for a linear function $\vec{a}_1^T\vec{x}$ of the elements of the p-dimensional random variable $\vec{x}$ for which the variance $\text{var}(\vec{a}_1^T\vec{x}) = \vec{a}_1^T\text{var}(\vec{x})\vec{a}_1 = \vec{a}_1^T\mathbf{\Sigma}\vec{a}_1$ is maximized. $\mathbf{\Sigma}$ denotes the $p \times p$ variance-covariance matrix of $\vec{x}$. To ensure that a maximum can be achieved with finite $\vec{a}_1$, the constraint that the sum of squares of $\vec{a}_1$ equals 1 is introduced. Thus, the optimization problem

$$\max_{\vec{a}_1}\left(\text{var}(\vec{a}_1^T\vec{x})\right) = \max_{\vec{a}_1}\left(\vec{a}_1^T\mathbf{\Sigma}\vec{a}_1\right) \tag{2.20}$$

subject to

$$\vec{a}_1^T\vec{a}_1 = 1 \tag{2.21}$$

must be solved. The standard approach to solve these kind of optimization problems is to use the technique of Lagrangian multipliers [9]. The general result is that the minimum point of the Lagrangian $L(\vec{a}, \lambda_1, \ldots, \lambda_n) = \sum_{i=1}^{n}\lambda_i H_i(\vec{a})$, where its gradient is zero with respect to both $\vec{a}$ and all the λ_i gives the solution to the original constraint optimization problem (2.20) [97]. Here, the Lagrangian function is:

$$L(\vec{a}_1, \lambda) = \vec{a}_1^T\mathbf{\Sigma}\vec{a}_1 - \lambda(\vec{a}_1^T\vec{a}_1 - 1), \tag{2.22}$$

and its partial derivate calculate to:

$$\frac{\delta}{\delta\vec{a}_1}L(\vec{a}_1, \lambda) = 2\mathbf{\Sigma}\vec{a}_1 - 2\lambda\vec{a}_1 \tag{2.23}$$

$$\frac{\delta}{\delta\lambda}L(\vec{a}_1, \lambda) = 1 - \vec{a}_1^T\vec{a}_1 \tag{2.24}$$

The vector $\vec{a}_1$ fulfills all necessary conditions for a maximum, if

$$(\mathbf{\Sigma} - \lambda\mathbf{I}_p)\vec{a}_1 = 0 \tag{2.25}$$

$$\vec{a}^T\vec{a}_1 = 1, \tag{2.26}$$

where $\mathbf{I}_p$ is the $(p \times p)$ identity matrix. Equation 2.25 is an eigenvalue problem, where λ is an eigenvalue of $\mathbf{\Sigma}$. Thus, the necessary conditions for a maximum of (2.20) subject to

(2.21) are fulfilled by the normalized eigenvectors of $\mathbf{\Sigma}$. Generally, for a $p \times p$ matrix, p orthogonal eigenvectors and eigenvalues exist. To decide which of the p eigenvectors gives $\vec{a}_1^T \vec{x}$ with maximum variance it must be noted that the quantity to be maximized is

$$\vec{a}_1^T \mathbf{\Sigma} \vec{a}_1 = \vec{a}_1^T \lambda \vec{a}_1 = \lambda, \tag{2.27}$$

so λ must be as large as possible. Thus, $\vec{a}_1$ is the eigenvector corresponding to the largest eigenvalue of $\mathbf{\Sigma}$ and $\text{var}(\vec{a}_1 \vec{x}) = \vec{a}_1^T \mathbf{\Sigma} \vec{a}_1 = \lambda_1$, the largest eigenvalue. Subsequently, $\vec{a}_1$ is defined as the 1st PC (note that sometimes the term $\vec{a}_1^T \vec{x}$ is defined as the 1st PC), which is the most important PC, explaining more variance than any other PC. An example for $p = 2$ and $\vec{a}_1 = (a_{11}\ a_{12})^T$ is shown in Figure 35A.

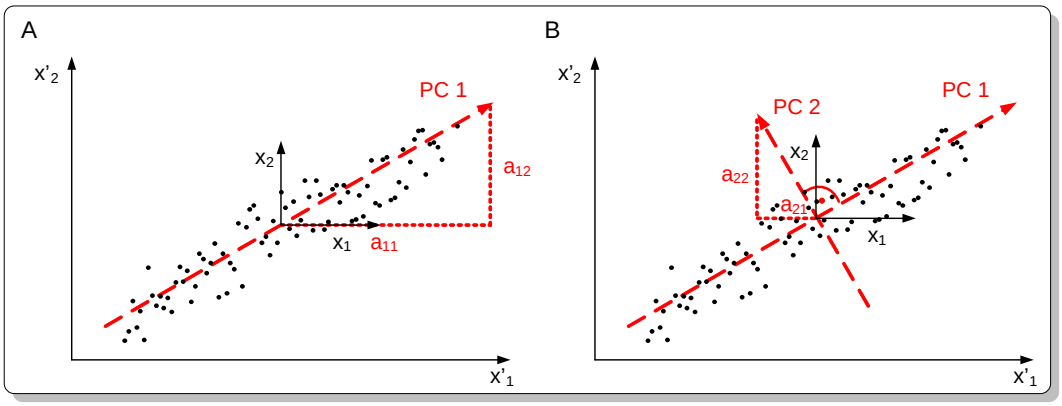

Figure 35: Two dimensional example of principal component analysis (PCA). (A) The first PC is selected to explain as much data variance as possible. (B) Similarly, the second PC is specified to explain as much data variance as possible with the constraint to be orthogonal to the first PC.

The next step is to determine the second PC maximizing $\vec{a}_2^T \vec{x}$ subject to being uncorrelated with $\vec{a}_1^T \vec{x}$, or equivalent to $\text{cov}(\vec{a}_1^T \vec{x}, \vec{a}_2^T \vec{x}) = 0$, where cov denotes the covariance. Applying the technique of Lagrange multipliers again, it can be shown [97] that the second PC simply is the eigenvector corresponding to the second largest eigenvalue of $\mathbf{\Sigma}$, which is orthogonal to $\vec{a}_1$ (see Figure 35B as an example for $p = 2$). Similarly it can be derived, that the third, fourth, ..., p^{th} PCs are the eigenvectors of $\mathbf{\Sigma}$ corresponding to the third, fourth, ..., and smallest eigenvalues, respectively [119].

In summary, to obtain linear combinations $\vec{a}^T \vec{x}$ with the largest variance, the eigenvalues and eigenvectors of the variance-covariance matrix $\mathbf{\Sigma}$ of $\vec{x}$ must be determined. The normalized eigenvector $\vec{a}_1$, which corresponds to the largest eigenvalue λ_1, is called the first PC and states the weights for the linear combination searched for. The eigenvector $\vec{a}_2$, which corresponds to the second largest eigenvalue λ_2, forms the coefficients of the linear combination with largest variance from all vectors being orthogonal to $\vec{a}_1$. All other eigenvectors can be interpreted analogously. The PCs from the TMS-evoked movements (PVs) are computed from the $p \times n$ dimensional matrix $\mathbf{PV}$ containing all non-zero PVs. The extracted PCs can be thought of as hand shape deformations which, scaled by the proper weighting coefficients, can be combined to reconstruct the entire set of postures. In the remainder of the thesis, the termination 'PC' will be used equivalent to 'module' or 'kinematic module'.

Number of modules for PCA

As discussed in Chapter 1.7, computational costs may be a driving factor of organization and re-organization of the modules. Mathematically, computational costs to execute a set of voluntary behavior (such as grasping movements) may be inferred in two ways. In the first approach, all PCs derived from TMS-evoked movements are used for generation of the behavior and the computational costs are given by the size of the weighting coefficients. The second approach is to look only at subset of modules, explaining most of the data variance. Then, the similarity of the subspace spanned by the selected set of modules and the behavior is a marker for computational costs to generate this behavior. For example, in Chapter 3.2, it was found that modules in violin players are adapted to the typical trained movement repertoire. These trained movements may then be generated at less computational costs because a smaller number of module combinations is necessary. In the thesis, mainly the second approach is used in the sense, that an adaptation of the modules to the behavior is a marker of less computational and energetic cost.

Within this approach, the question arises, how many modules (or PCs in this case) should be retained. The problem of estimating the number of relevant PCs has been addressed by many researchers and a large number of different criteria have been proposed [119, 242]. In general, each method attempts to determine the number of PCs that captures the structural variation in a data set. As described in the previous chapter, the first module (or PC) corresponds to the largest eigenvalue and therefore covers more data variation than any other module. Figure 36A and B, respectively, illustrate typical drawings of the relative and cumulative data variation explained by 10 PCs (calculated from a set of 10-dimensional PVs).

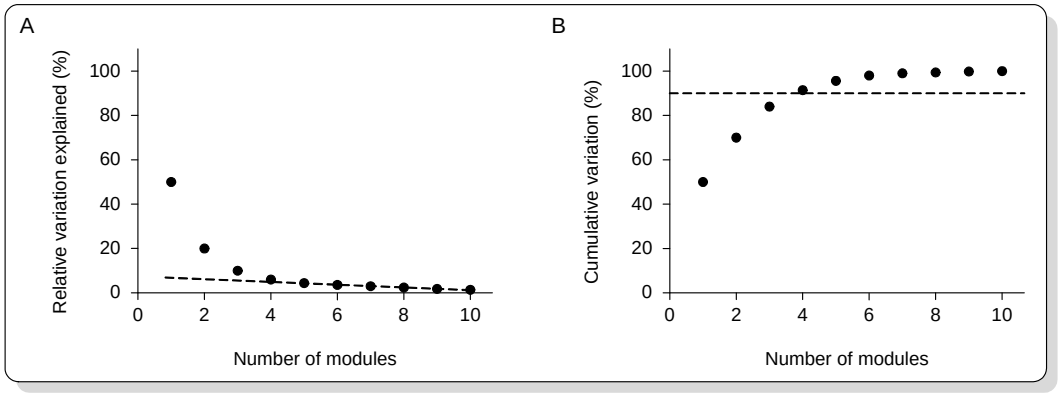

Figure 36: (A) The eigenvalues of each PC are normalized to the total variation of the data set. Each eigenvalue indicates how much relative variance the corresponding PC represents. At the point where the relationship becomes linear (dashed line), PCs are believed to mainly represent unstructured features and the increase of variation is due to the increasing number of dimensions. (B) Cumulative variation explained by subsequently adding the relative contributions of each PC from (A). The dashed line represents the number of PCs needed to account for $\geq$90% of the data variation.

A commonly used technique for choosing the number of PCs is to retain the first n PCs which explain most of the (cumulative) percentage of total variation, for example 90%. Mathematically, the term

$$t_m = 100 \cdot \frac{\sum_{i=1}^{n} \lambda_i}{\sum_{j=1}^{p} \lambda_j} \tag{2.28}$$

must be iteratively computed for increasing n until $t_m \geq 90\%$. If this threshold is exceeded, the first n PCs are retained (in Figure 36B, 4 PCs are chosen according to this criterion).

A second method is to observe changes in the slope in the plot of the variation explained by the PCs versus the number of PCs [242]. This method is often referred to as the scree-graph method [97]. It involves looking at a plot of λ_i against i and deciding at which value of i the slopes of lines joining the plotted point changes from 'steep' to 'not steep' and 'constant'. The value of i, defining an 'elbow' in the graph is then taken to be the number of components n to be retained. The rationale behind this idea is that PCs beyond this point capture only unstructured data and a small additional fraction of data variation. The explained variation then increases almost linearly with additional number of PCs, mainly because of the increasing dimensionality. To estimate the number of PCs n objectively, portions of the eigenvalue curve (relative variation explained by each PC, see Figure 36A) are fitted to straight lines using a standard least-squares technique [141]. First, all data points on the curve are included in the fit, and then the 2^{nd} to 10^{th} points, and so on, until only the 9^{th} and 10^{th} points are included. As the range of the fit moves toward the right side of the curve, the mean squared error (MSE) of the fit is expected to decrease because the curve approaches a straight line as the number of PCs increases. The correct number of PCs is estimated as the first point on the eigenvalue curve at which the linear fit of all points from that point to the 10^{th} point produces a small MSE [46]. Here the first point on the curve for which the corresponding MSE falls below 0.00001 is selected as the correct number of PCs (4 PCs according to Figure 36A). In the thesis, mainly the first method is used.

Limitations of PCA

Some limitations concerning the appropriateness of PCA and many other techniques exist. In Chapter 1.7 it was noted that modules with the same or similar kinematic output may exist several times to account for the adaptability and flexibility of human movements. With the PCA technique applied here, the maximum number of modules is equal to the number of recorded joints. Thus, it is not possible to extract more modules than number of measured joints or to identify redundant modules. However, since a module explains a certain amount of variance it can be assumed that the more data variance a module explains, the more redundant it may represented. Given this limitation, main emphasis is given to the shape of the modules. Furthermore, if a small number of PCs is investigated it will not be interpreted as a dimension reduction strategy to simplify the control problem at the kinematic level. Second, using PCA, modules are allowed to have negative weighting coefficients for reconstruction of the PVs. Given that neuronal signals cannot be negative, this feature of PCA may not fit optimal into biological reality. Nevertheless, it has been shown previously, that PCA, despite these limitations, leads to similar results as biologically more adequate techniques [242]. In the next section, an alternative technique for module extraction is presented, which constrains the module weighting coefficients to be positive.

Semi non-negative matrix factorization

Non-negative matrix factorization (NMF) techniques [142] are commonly applied for extraction of muscle synergies during natural behavior [243, 52, 46]. While these techniques do not allow negative muscle activations and, in addition, do not allow negative weighting coefficient, the extraction algorithm developed here is less stringent. Since negative components of the PVs (extracted from TMS-evoked movements) represent flexion and positive extension movements, the modules are not constrained to be positive. However, the excitation of these modules comes from neuronal networks and therefore the weighting coefficients cannot be negative (i.e. the kinematic output of a module cannot be inverted). Thus, the method developed here is referred to as 'semi non-negative matrix factorization', or SMF. Within this approach, an observed PV (PV_j^{obs}) can be expressed as a positive linear combination of the modules:

$$PV_j^{obs} \approx PV_j^{pre} = \sum_{i=1}^{n} c_{ij}\vec{m}_i, \quad c_{ij} > 0, \tag{2.29}$$

where PV_j^{pre} is the predicted PV resulting from the linear combination of the modules.

The algorithm is started by selecting a number of modules and initializing the modules with random values between -1 and 1. Then, the set of best-fit weighting coefficients, $c_{ij,new}$, for each PV_j^{obs} is found using a non-negative least-squares algorithm [141] by solving

$$\min_{c_{ij}} \left(\left\| \sum_{i=1}^{n} c_{ij}\vec{m}_i - PV_j^{obs} \right\|^2 \right) \tag{2.30}$$

subject to $c_{ij} > 0$. Once the weighting coefficients $c_{ij,new}$ were calculated, the modules $\vec{m}_i$ are updated by minimizing

$$\min_{\vec{m}_i} \left(\left\| \sum_{i=1}^{n} c_{ij,new}\vec{m}_i - PV_j^{obs} \right\|^2 \right) \tag{2.31}$$

without a non-negativity constraint. After updating the synergies, they are normalized so that the vector norm of each synergy is equal to one. The best-fit weighting coefficients are then again calculated using these new synergies, the synergies updated, and the process repeated. This algorithm is applied to 90 % of the PVs from one subject, chosen randomly from the PV set obtained after TMS over the 30 (or 36) scalp sites. After each iteration, the ability of the synergies found by the algorithm to predict the remaining 10 % of responses is assessed. If the amount of variance explained by the derived modules in this set of test data decreased below a threeshold of 0.2 the algorithm is considered to have converged. In case of no convergence, the algorithm is stopped after 500 iterations. In addition, the number of modules capturing most of the data structure can be assessed by cross-validation methods [37], as described by [46] and similar to the method for extraction of the number of relevant PCs as explained above.

Module similarity

The modules derived from different measurements each define a lower-dimensional subspace within the 10-dimensional joint space. Modules of different datasets can be similar in the

weaker sense that their subspaces overlap each other or in the stronger sense that the actual module bases of the two sets of modules are similar [46]. For example, consider data from a glove with 3 sensors and resulting 3-dimensional PVs, as illustrated in Figure 37. Then, two modules of each dataset (represented by solid and dashed arrows, respectively) can be different in their structure, but nonetheless can span the same 2-dimensional subspace within the 3-dimensional joint space.

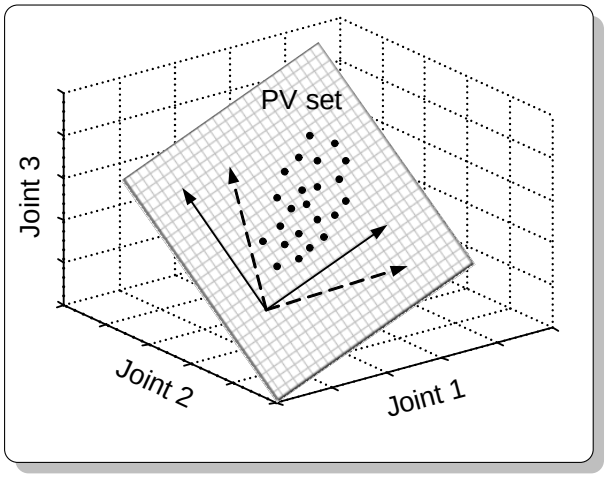

Figure 37: Hypothetical example of sets of PVs obtained from a sensor glove recording movements of three joints. PVs from two different subjects are described by two different sets of modules, indicated by solid and dashed arrows, respectively. Despite having different structures, these two sets of modules span the same two dimensional subspace within the three dimensional joint space and can describe the sets of TMS-evoked movements equally well (adapted from [46]).

Methods for assessing both types of similarity are available. First, the similarity of subspaces spanned by the modules is quantified by computing the principal angles [90]. If, for instance, the modules from two subjects share a 3-dimensional common subspace, the cosines of the first three principal angles are close to one. Here, the number of principal angles with cosines > 0.9 is defined as the shared subspace dimensionality between two sets of modules [46].

The second method of assessing similarity between modules derived from different data sets evaluates the degree of similarity between the modules using 1 minus the dot product as a distance measure between two modules (see equation 2.14). The algorithm matches each module from one set to all modules from the other set and the pair with the lowest distance is selected as the best matching module. Then this pair is removed and again the most similar pairs are identified until all modules from one set are matched to the modules from the other set. The number of best matching modules with a distance >0.8 is defined as the number of shared modules between two data sets.

The third approach serves to address the rank order consistency between modules from different datasets. Best-matching pairs of modules are computed as before and the rank order of the module pairs is entered in a 2D histogram. For example, if module 1 of a subject corresponds best to module 2 of another subject, the 2D histogram is incremented at the coordinates (1, 2). For completeness, all ten modules of each subject are considered. The result of this procedure is influenced by the sequence of subjects. To eliminate this effect, a second histogram, mirror-symmetric to the first one, is generated by repeating the procedure after reversing the sequence of subjects. The final histogram, which allows the display of all occurrences in a triangular matrix, is then constructed by the mean of both

mirror-symmetric histograms. This approach provides complementary information about similarity, since the rank order of a module reflects the amount of variation explained by this module (at least with PCA) and therefore is an indicator of structural similarity of the datasets.

In the experimental part of the thesis, modules are extracted from TMS-evoked movements and from voluntary behaviors such as grasping movements. The similarity measures are used to compare the movement space between individual subjects and between TMS evoked movements and voluntary movements. The next chapter describes the framework to assess grasping movements.

2.3 The grasp assessment framework

This part of the measurement framework serves to address the analysis of kinematic couplings during daily activities. Since grasping for objects is one of the most frequently conducted activities, a software system for analysis of the grasping movements was developed. Unlike in earlier experimental designs [197, 198, 151, 33], here the analysis is not only restricted to the movements themselves but also allows the comparison of grasping movement features to features of TMS-evoked finger movements. When grasping a real object, the hand posture is

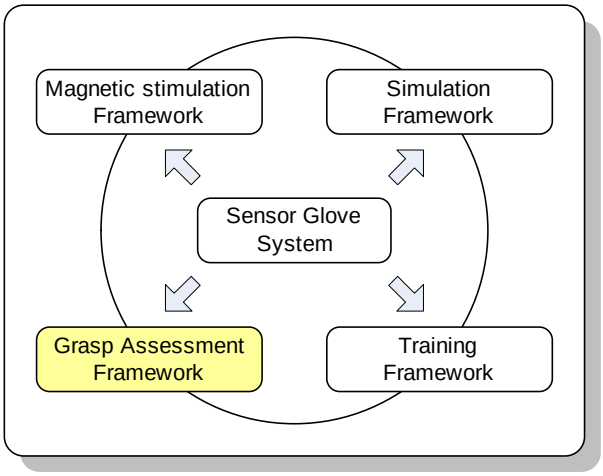

not only a consequence of central control signals but also of the mechanical interaction of the hand with the object. To exclude that the task was confounded by the latter it was suggested not to grasp for real objects but to imitate grasping movements to imagined objects [197]. Despite it was shown that hand postures are similar between grasping real and imagined objects [198], the software system here was developed for grasping imagined objects seen as photographs. This has the additional advantages, that the experimental protocol does not depend on real objects and ensures a consistent, repeatable perspective from which the subjects see the objects to be grasped. In this chapter the basic features of the software system for recording and storing grasping movements with a sensor glove are described.

2.3.1 Grasp assessment software system

The purpose of the grasp assessment software is to represent the subject images of objects to be grasped and to handle the data acquisition. Fourtyeight images of objects with differing shape and size were photographed from a right (Figure 38A) and left (not shown) perspective. The images are consistently named after the object which they represent and reside in specific data folders. Analogous to the software system for magnetic stimulation, the name of the subject, the base storage data path, the path where the object images are located and the number of desired grasping trials for each object must be specified. To accomplish this, the graphical user interface (Figure 38B) is equipped with appropriate menue items. After completion, the subject specific storage path is generated using the base storage path, the name and first name of the subject followed by the date (see right path structure in Figure 38C). The software system then parses the file names of the image objects and instantiates Java objects for each image. A Java object contains the filename of the image and the number how often it has already been grasped (0 in the beginning).

All Java objects are aggregated in a linked list, from which they can be accessed by their

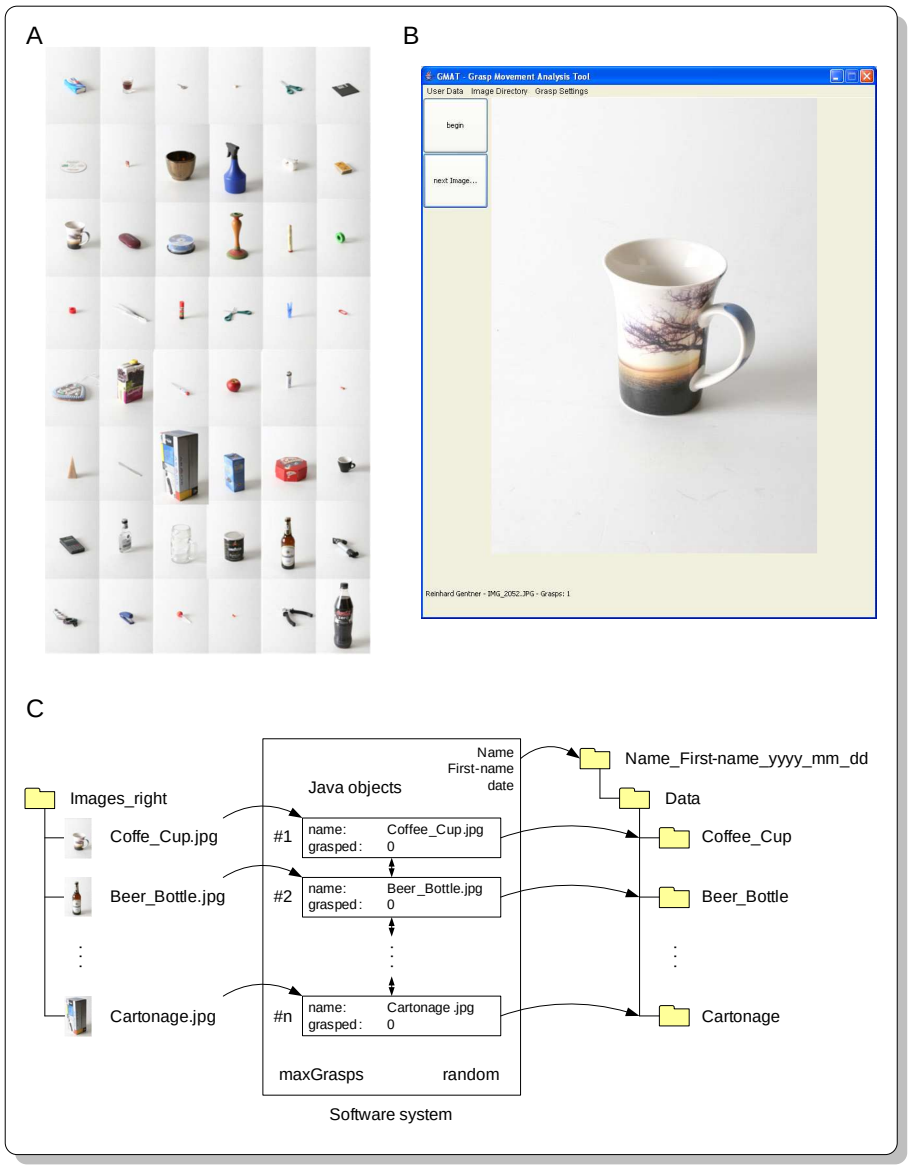

Figure 38: (A) Photographs of the objects to be grasped. (B) Graphical user interface to present the photographs to the subject in a random order. (C) Internal structure of the software system. Objects are loaded into Java classes and presented to the subjects by the graphical user interface (B). For each object, a data folder for storage of sensor glove data is created.

index. Additionally, a data storage folder for each image is generated according to the filename. For example, if the image displays a coffee cup and its filename is 'Coffee_Cup.jpg' the folder name will be 'Coffee_Cup'. The entire process is illustrated in Figure 38C. The variable 'maxGrasps' represents the specified number of trials per object and the variable 'random' represent a random index number used for displaying objects from the linked list. By clicking the button 'Next image', a new random index is generated (Figure 39, step 1) and the corresponding object in the list is identified and displayed in the graphical user interface (Figure 39, step 2). The grasping trial can then be initiated by clicking on the 'Start' button. At this time an auditory 'Go'-signal occurs and the sensor glove starts collecting data for 3 s. During the trial the data from the sensor glove is streamed to an -ascii file located in the appropriate folder as illustrated in Figure 39 (step 3). After the 3 s have elapsed, a second auditory tone signals the subject the end of the trial.

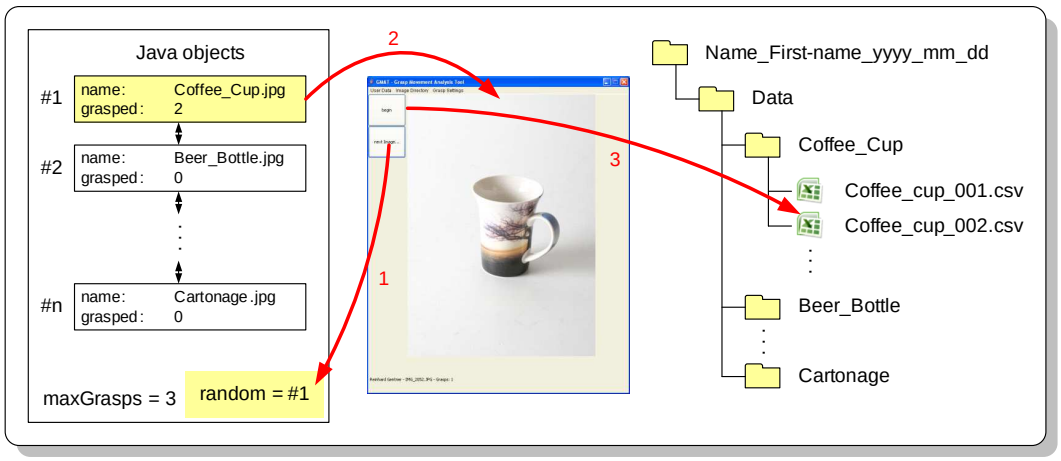

Figure 39: If the 'Next item' button is selected, a random index is selected and the corresponding image is displayed. By clicking the 'Start' button, the data from the sensor glove is collected and stored in corresponding data folders.

Additionally the variable 'grasped' (not illustrated in Figure 39) of the actual object is increased. By clicking the 'Next item' button a new image is randomly selected and a new trial can be started. If an object is selected which has already been grasped 'maxGrasp' times, the object is removed from the list. The entire procedure can be repeated until all objects have been removed from the list and 'maxGrasp' files exist for each object. Currently, the software works with the **Wii**-Glove, the TUB-Glove and the 5DT-Glove family. Since the data structure is analogous to the data structure of the magnetic stimulation environment, the same analysis software routines can be used here.

2.3.2 Experimental procedure

The subject must be comfortably seated with the hand at a semipronated position in a cast with the elbow joint in a flexed position such that the hand is approximately 30 cm in front of the chest. Subjects should imagine the displayed object floating at about 50 cm in front of them. After the 'Go'-signal they should perform grasping movements toward the imagined object without contacting any real object. The end grasp posture should be maintained until the recording is stopped after 3 s. Afterwards the subject should return to the resting position. Between two consecutive trials a pause of 2-3 s is desirable. In addition to the assessment of grasping movement, a finger movement training system is part of the measurement framework to analyze the modular organization after motor learning. This system is described in the next chapter.

2.4 The finger movement training framework

In this chapter, the development of a virtual-reality based finger movement training system is described. The system is based on the a sensor glove and contrasts to previously developed

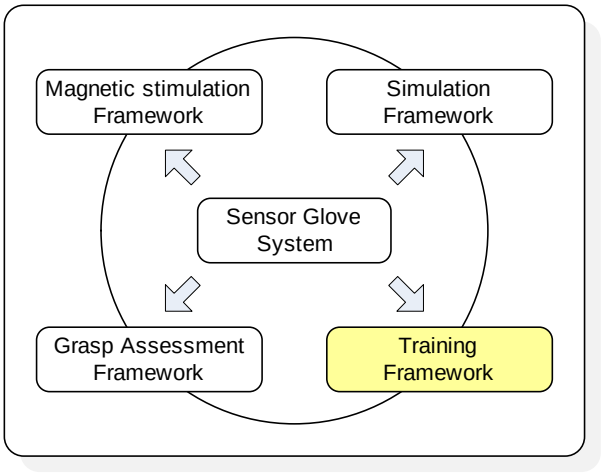

finger training systems with its training objective, which is the augmented repetition of kinematic movement profiles. In combination with the TMS stimulation environment, the cortical reorganization effect of a finger movement training can be assessed, providing an objective test of the effectiveness of a movement training. In the following chapters the rationale and the technical characteristics of the training system are described. The emphasis is here on the main features of the system and not on its detailed implementation. To explain the logical interrelations of the database concept and the Java software routines, entity relationship diagrams [126] and class diagrams from the unified modeling language (UML) are used [28].

2.4.1 Background

Several prototype virtual reality environments for finger and arm movement learning were developed and evaluated in the last 10 years [250, 157, 134, 50, 2, 26, 112]. One of these system was developed with the intention to enhance recovery after stroke [101, 102]. The system consists of an electromagnetic motion tracking device, desktop computer display, and VR software. The VR software contains a basic 3-D graphics editor which allows the user (therapist) to create 'scenes' designed to be therapeutically meaningful to the targeted patients. Usually, a scene shows some simple task (e.g., place an envelope in a slot, hit a nail with a hammer, move a ball through a ring, or lift a cup to the mouth). Following the basic scene creation, the motion tracking device is used to pre-record normal participants performing the desired activities, within the context of the VR scene. These prerecorded trajectories then serve as the 'virtual teacher' for the patient to watch and copy during the VR therapy practice (see Figure 40A). The degree of match with the teacher trajectory provides augmented feedback in a visual context to the participant during practice. This feedback is presented to the participant as a 'score', or paired with verbal cues.

A second system makes use of the commercially available CyberGlove to monitor hand position and to provide feedback about kinematics of hand movement during training, and a laboratory-built glove, Rutgers Master II, to provide haptic monitoring and feedback combined with position sensing [183]. Within this system four different types of exercises can

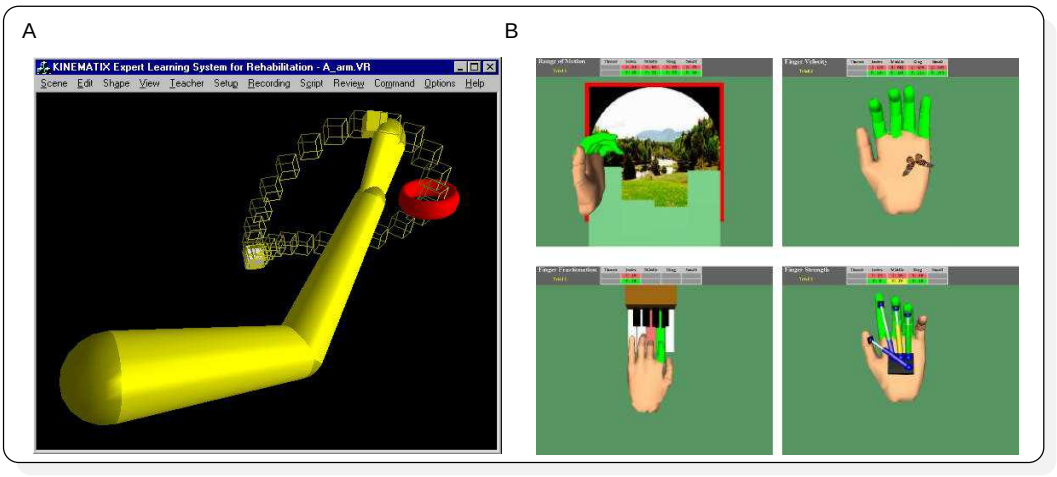

Figure 40: (A) A virtual reality system to train arm movements by imitation of the trajectory of a virtual teacher. (B) A stroke rehabilitation system to train basic finger movements, finger strength and reaction time.

be executed (Figure 40), namely finger fractionation training (upper left panel), reaction time training (upper right panel), individual finger movement training (lower left panel), and finger strength training [112, 26, 2].

However, no training system for training of spatio-temporal finger movement profiles exists. Here, the two presented approaches are merged into a virtual-reality based training system for finger movements. A system is required, which allows subjects (or patients) to repetitively train finger movement pattern with all the benefits of virtual-reality. In the end, the training consists of a visual representation of a movement to be trained (virtual teacher), and a representation of the actual movement conducted by the subject. Each movement is defined as a trial, whereas multiple trials constitute a block and several blocks constitute a session in which the subject trains. The system is based on a MySQL database [126] connected to the training computer via the Internet. The training computer hosts the training software programmed in Java and Java3D [41]. As an input device, the **Wii**-Glove family and the 5DT-Glove family can be used. The advantage of the **Wii**-Glove is that it provides high reliable finger joint measurements at low costs (≈500 €, the price for the 5DT glove is ≈4700 €) removing a major barrier for commercialization of such systems. The main components of the system are shown in Figure 41.

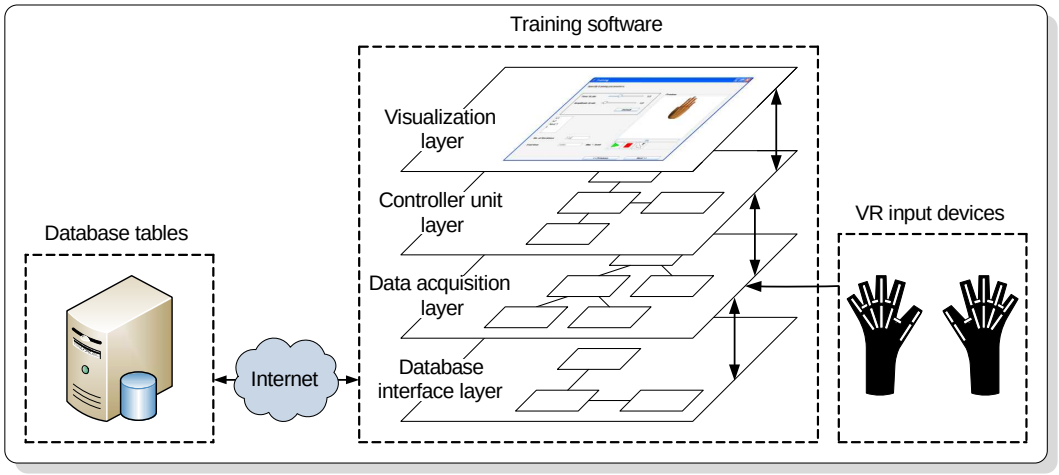

Figure 41: Overview of the training system components.

The training software consists of several interconnected hierarchical layers. The communication between Java objects and database tables is specified in the 'Database interface layer'. The 'Data acquisition layer' consists of several classes to interface sensor gloves, read stored sensor glove data from the database (the movement to be trained) and to write sensor glove data to the database. The pacemakers for these classes are defined in the 'Controller unit layer'. Here, the temporal aspects of the training system such as the specification of the sample rate or the invocation of the routines for retrieving data from the sensor glove, are defined. The 'Visualization layer' provides graphical user interfaces to allow the user to interact with the other layers. For example, user interfaces to create new database entries, and visualize the periodic sampling of sensor glove data exist. While the entire training system consists of > 200 Java classes, only the key classes of each layer are explained in the following chapters.

2.4.2 Database design

A modular MySQL database, similar to [112], was developed, which reflected elements and their dependencies as they are structured in the real world. Information about a subject (or patient) is entered as a new row (i.e. database entry) in the 'subject' table containing fields for the name, age, address, handedness, etc., as illustrated in Figure 42A. For identification, an unique identification number (UID) is assigned to each subject ('subjectID'). A subject

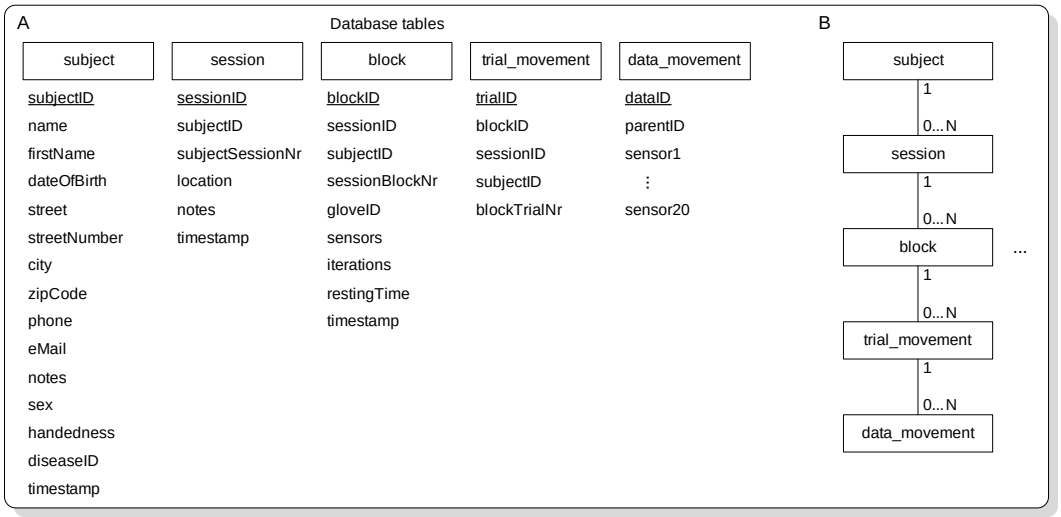

Figure 42: Database tables.

can participate in N training sessions, separated, for example, by some days. Consequently, a session is allocated only to a single subject. This relationship is reflected by the field 'subjectID' in the 'session' table, which represents the UID of the corresponding subject (see Figure 42A). The number of training sessions conducted by the subject is stored in the field 'subjectSessionNumber'. Further fields specify the date, the time, and the location of a training session. In a training session, N training blocks can be conducted (a block is specified within the 'block' table). Each block is linked to the corresponding session ('sessionID'), and additionally to the corresponding subject ('subjectID'). The multiple linkage was added to enhance the speed of database queries for later analysis. For example, all training blocks across sessions of a single subject can be easily identified by the 'subjectID' number of the blocks without the need for identifying all sessions before. The block table contains all necessary specifications regarding the training movement, such as the resting time between

trials (field 'restingTime'), the number of trials (field 'iterations'), the sensor glove used (field 'gloveID'), and the movement to be trained. A block consists of N trials, where a trial is a single movement to be trained. (After the training 'iteration' trials are linked to a block). Again, a trial contains references to the corresponding block ('blockID'), the corresponding session ('sessionID') and the corresponding subject ('subjectID'). The number of the trial is stored in the 'blockTrialNr' field. Finally, a trial consists of N data samples. At each time step the actual sensor values of the glove is stored as a new row in the 'data_movement' table. For instance, if the movement to be trained lasts 2 s and the sampling rate is 20 Hz, 40 entries in the 'data_movement' table are linked (by the field 'parentID') to this trial (i.e. the trial consists of 40 time points). The dependencies between these tables are illustrated in Figure 42B.

To specify the movement to be trained (the movement visualized by the virtual teacher), additional tables are linked to the 'block' table (Figure 43). The table 'gloves' contains

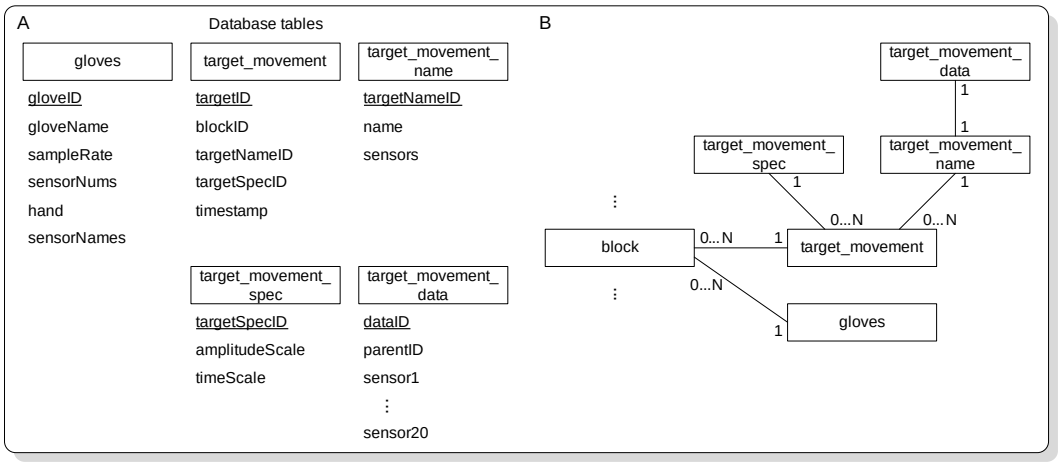

Figure 43: Database tables.

descriptions of the sensor gloves (such as the name of the glove, the associated sample rate, the number of sensors, their positioning, and if the glove is for the left or right hand) used for training. Each block contains a reference to the UID ('gloveID') of the selected glove. The movement to be trained is specified by an entry in the 'target_movement' table, which can be linked to different training blocks (Figure 43B) with an entry in the 'targetID' field of the appropriate block. A target movement (presented to the subject by the virtual teacher) consists of a link to an entry from the 'target_movement_name' table with the corresponding kinematic data stored in the 'target_movement_data' table and the 'target_movement_spec' table (see Figure 43B). Entries in the 'target_movement_spec' table modify the target movement presented to the subject during training. A target movement specification can be associated with N different target movements. Currently the speed (field 'timeScale'), and the amplitude (field 'amplitudeScale') of the target movement can be manipulated. Most of the data tables contain a timestamp to identify the date and time when the corresponding entry was created. Additionally, data tables for storing the notes (see 'subject' and 'session' tables) and disease categories exist. The database system is implemented on a central database server, accessible by the training software. The next section describes the mechanisms of interfacing the database with the Java based training software.

2.4.3 The database interface layer

The database and the training software reside on different computers and interact via the Internet with the help of the 'Java Database Connectivity' (JDBC) module (Figure 44 [126]). The physical separation of data storage and training system was selected to enhance flexibil-

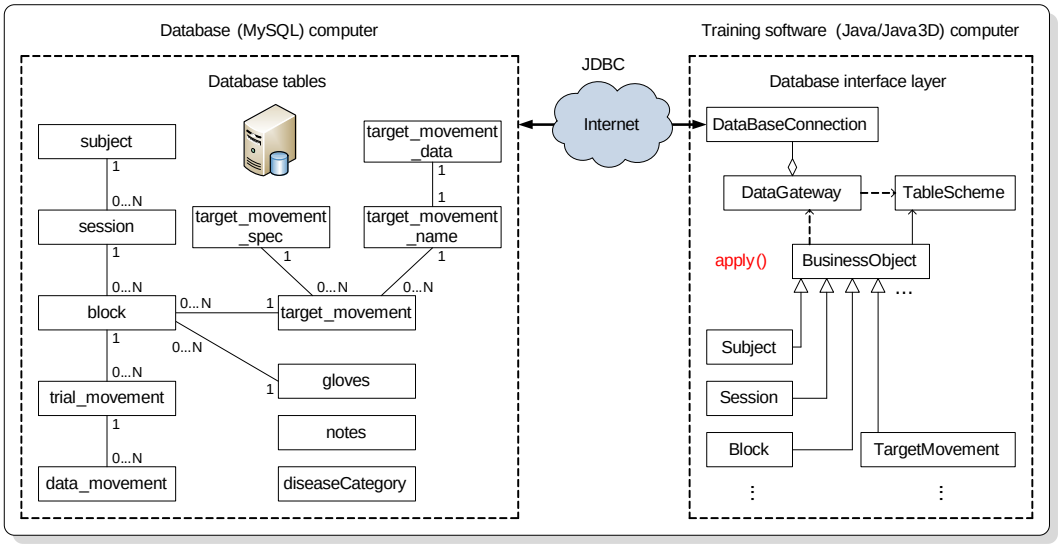

Figure 44: The database interface layer. The database is hosted on a central database server which the training software can access via the Internet.

ity of training location without the need to synchronize different databases. With the JDBC interface, SQL database queries can be formulated and sent to the database server via the Internet. Thus, database entries can be remotely created, modified, updated and deleted via Java classes and methods. The main class implemented for these tasks is the 'DataGateway', which is aggregated by the class 'BusinessObject'. The abstract 'BusinessObject' class implements a state machine and manages the synchronization between the database tables and the training software [98]. Child classes of 'BusinessObject', such as 'Subject' or 'Session', represent entries of the corresponding database tables described in Chapter 2.4.2. If the content of one of these classes is modified or a new instance is created, the database is updated by invoking the 'apply()' method, specified in the class 'BusinessObject'. This method uses the functionality from the 'DataGateway', explained in the following chapter.

Communication with the database

Communication with the database is handled by the final class 'DataGateway'. An instance of the 'DataGateway' is initialized with an instance of the 'DataBaseConnection' class (see Figure 44). This class uses the JDBC methods to connect (using the IP address of the database server, the login and the password) and disconnect to the database computer. Furthermore, methods for executing SQL queries (relevant for the queries using the 'SELECT' statement) and updating the database (relevant for the queries using 'INSERT', 'DELETE' and 'UPDATE') exist. The 'DataGateway' class uses this unspecific functionality to provide specialized methods relevant for the training system. In particular, static methods for inserting, updating, deleting, and retrieving database records are implemented. It is common to these methods that their SQL query string is composed by table informations from a 'TableScheme' instance. The 'TableScheme' class specifies table name and field information

of the child classes derived from 'BusinessObjects' such as 'Subject' or 'Session'.

Representation of the database in the training software

One of the common problems in applications utilizing databases is the need to define an object-relational mapping to allow transparent access to the database by dealing with database rows as objects. Previously, a mapping technique was described [98], where each row is represented by an object that maintains its state and issues appropriate database queries after commitment (here a slightly modified concept is used). Such an object is called a 'Business Object' and its implemented state machine is shown in Figure 45. The database communication ('Save in DB' and 'Delete from DB') is performed by invoking the appropriate static methods from the 'DataGateway' class. These actions (written in blue) are not invoked explicitly by other objects. Rather, other objects invoke an 'apply()' method which in turn invokes the appropriate action based on the current state. A Java business

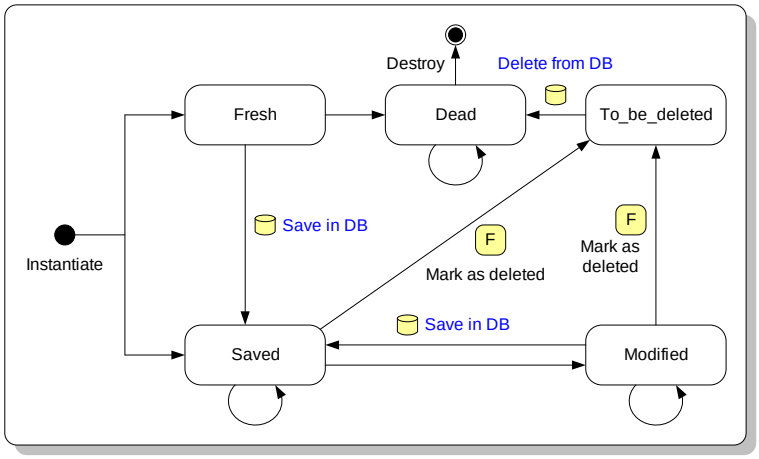

Figure 45: State machine of a BusinessObject.

object is instantiated and initialized with information entered into the graphical user interface by the user. In this case, the state of the business object is set to 'Fresh', because no corresponding database record exists. During this state, the database information is not consistent with the software representation of the object. With invoking the 'apply' method, the information of an object in 'Fresh' state is saved as a new database record and its state changes to 'Saved'. Thus, information carried by Java objects in 'Saved' state is always consistent with the corresponding database entry. If an object in 'Fresh' state is deleted, no database entries must be deleted and its state is set to 'Dead'. Dead objects are destroyed. An object can also be instantiated with information from database entries. Then the object represents this saved database entry and its state is 'Saved'. Objects in 'Saved' state can be modified. For example, consider a database table representing personal information from a subject (e.g. name, age, sex, and address). Then, by loading the subject information into the software system, a 'Business Object' is created whose information correspond to the information provided by the database entry. If the experimenter uses the software to change the address of the subject, the information carried by the object and the information in the database are not consistent any more. Thus, the state of the object is set to 'Modified'. By invoking the 'apply()' method, the database record is updated by calling methods from the 'DataGateway', and the state of the object returns to 'Saved'. Objects in 'Saved' and 'Modified' state can be deleted by setting their state to 'To_Be_Deleted' by the function call

'Mark as deleted'. With the next 'apply()' call, all objects in this state are set to 'Dead' and their corresponding database entries are deleted.

As mentioned earlier, for each database table, a child class of 'Business Object' is specified, having a 'TableScheme' corresponding to the fields of the database table. In the end >15 child classes of 'BusinessObject' were created.

2.4.4 The data acquisition layer

The purpose of the 'Data acquisition layer' is to handle the data exchange between the input devices, the database and the visualization of the data. The class 'Sensor' represents any kind of data source, which may be a virtual device to retrieve data from the 'target_movement_data' table of the database (class 'StoredMovementSensor') or real sensor glove. Currently, child classes for interfacing with the **Wii**-Glove and the 5DT Glove are provided. Observers (see Chapter A.3) of the type 'ISensorObserver' can be dynamically added, updated or removed from the 'Sensor' class using the appropriate method (Figure 46). The implementations of 'ISensorObserver' may belong to the 'visualization layer' to present the actual joint angles to the subject or may belong to the 'database interface layer' to write sensor values to the database.

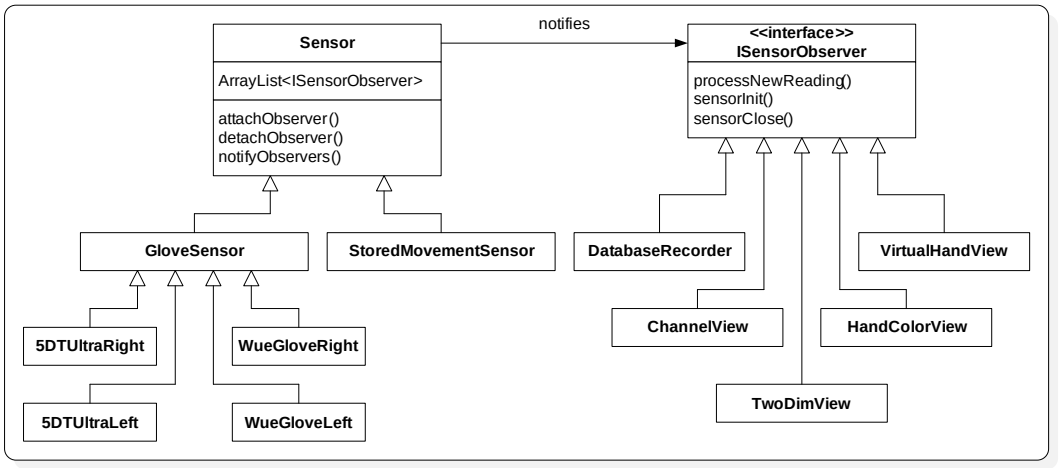

Figure 46: Class diagram of the data aquisition layer.

For example, a sensor of the type 'WueGloveRight' is instantiated and an instance of 'DatabaseRecorder' and 'VirtualHandView' is added to the sensor. If the 'getValues()' method is called, the sensor retrieves the actual joint angles from the **Wii**-Glove and invokes the 'notifyObservers()' method. Then the 'update()' method of each attached observer is invoked with the actual sensor readings as argument. The 'VirtualHandView' object adjusts the hand model with the current joint angles and the 'DatabaseRecorder' buffers the joint data for later storage in the database. Thus, the 'data acquisition layer' implements the Observer pattern combined with the MVC pattern (the 'Sensor' class represents the model), as described in Chapter A.3.

2.4.5 The controller unit layer

A controller represents a scheduler which periodically triggers sensor updates. The core functionality is implemented in the abstract class 'Controller' (see Figure 47). It contains

a list of 'Sensor' objects that can be dynamically added to an array list. Furthermore, the controller notifies classes on start and stop, that implement the 'IControllerListener' interface. Objects from these classes are also stored in an array list.

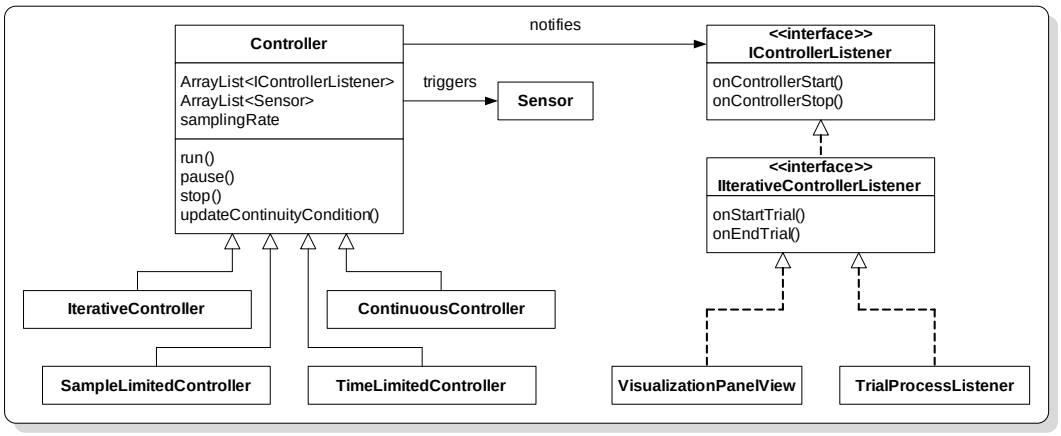

Figure 47: Class diagram of the controller unit layer.

The field 'samplingRate' specifies how often per second the attached sensors are updated. The controller is started by invoking the 'start()' method. At this time the sensors are initialized and the observers are notified. Then a Thread, which runs 'quasi' parallel to the main process [224], is created and the periodical sensor update is performed until the 'continuity condition' is violated. Afterwards the Thread is destroyed and the stop event is sent to the observers. The 'continuity condition' varies between different child classes of 'Controller'. The class 'ContinuousController' triggers the sensors continuously until the controller is stopped externally. In contrast the 'SampleLimitedController' and the 'TimeLimitedController' perform updates for a certain amount of samples and time, respectively. The most important controller for the training system is the 'IterativeController', which has a reference to the movement to be trained (i.e. the data for the virtual teacher) and allows sampling of a specified number of these movement (a repetition of this movement is defined as a trial, see Chapter 2.4.2). Each time the movement to be trained starts and ends, a 'start trial' and 'end trial' event is created and passed to all attached 'IIterativeControllerListener'. The classes that implement this interface ('VisualizationPanelView' and 'TrialProcessListener') perform appropriate actions, such as writing the finished trial to the database or updating the view. Thus, the controller classes correspond to the classical 'Controller' in the MVC Pattern discussed in Chapter A.3.

2.4.6 The visualization layer

The visualization layer (the view component in the MVC Pattern) consists of three different entities. The first contains classes to specify the training parameters and to set up the training environment using a wizard design. The second is the visualization of the training movement and the movements conducted by the subject, and the third provides classes to manage the database and to analyze the training success.

Training setup wizard

The graphical user interfaces (GUIs) to set up a training are presented in logical order. The GUIs are designed as a setup wizard which guides the user through all steps necessary to

start a training. The class diagram of the Wizard is visualized in Figure 48. To provide easy, flexible, and extensible methods to manage different states of the training wizard and to provide the ability to add new wizards or add new states to the current wizard, the State Pattern (see Chapter A.3) was used. The main idea in the State Pattern is that each state in a multi-state context is defined as a separate object. Here, the context is the wizard,

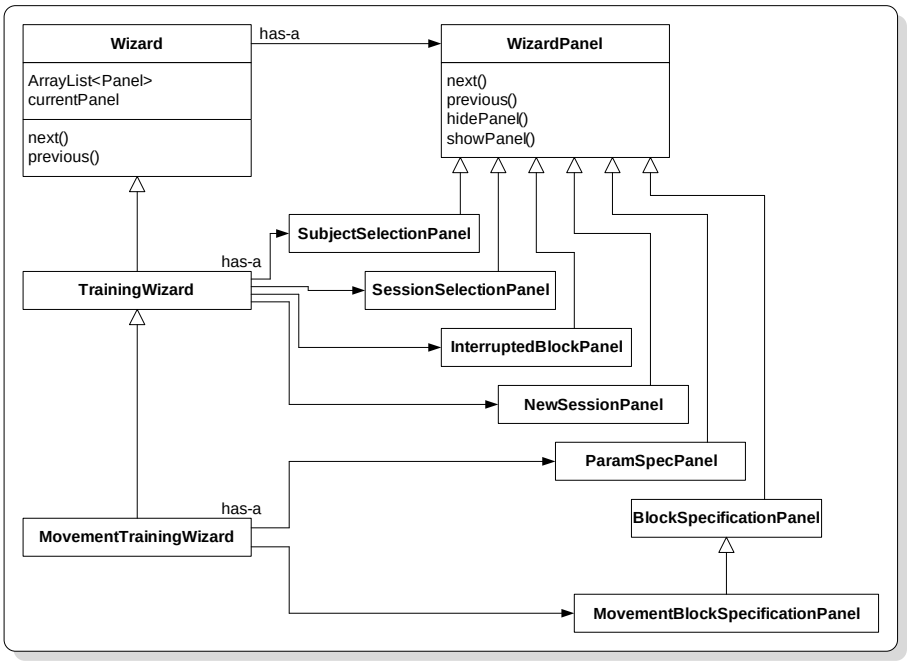

Figure 48: Class diagram of the experiment setup wizard.

the state is the step or the screen currently appearing (such as the 'SubjectSelectionPanel'), and the request is either 'next()' or 'previous()'. Each step is represented by a subclass of 'WizardPanel'. 'TrainingWizard' is a base class for all training wizards. It implements common steps such as subject and session specification. Training wizards of different types are derived from this class and each of them defines its own steps. Here, the 'MovementTraining-Wizard' is described. If a training is not aborted correctly (i.e. the database information is inconsistent), an additional panel ('InterruptedBlockPanel') exists to fix the inconsistencies in the database by either restarting the training block or deleting it.

In the first GUI (called the 'SubjectSelectionPanel'), the subjects who already performed a training are loaded from the database using 'Subject' Business Objects. The experimenter can select an already created subject or can create a new subject. If the 'next' button is clicked, a new 'Subject' instance is created (state 'Fresh') or the existing one is used for training (state 'Saved' or 'Modified' if adjustments were made).

In the following GUI, the session information must be specified (Figure 50). If the subject has already trained before, the last training session is loaded from the database and can be continued ('SessionSelectionPanel') or a new session can be started ('NewSessionPanel'). If the subject has not trained before, a new session must be started.

As a third step, training related parameters ('MovementBlockSpecificationPanel') must be entered (Figure 51A). The information of all gloves stored in the database is loaded into 'Glove' Business object and displayed in a drop-down menu. The user can select the appropriate glove and can enable or disable the glove specific sensors that are used for training by clicking on the '...' button. As response, a modal dialog appears, where enabled sensors are represented as green circles and disabled sensors as red circles. By clicking on a green

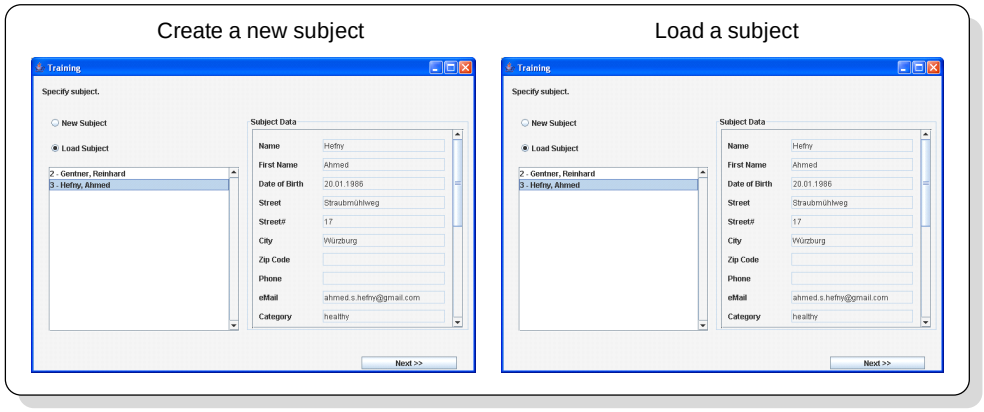

Figure 49: Grapical user interface (GUI) to create a new subject entry or load a subject data from the database.

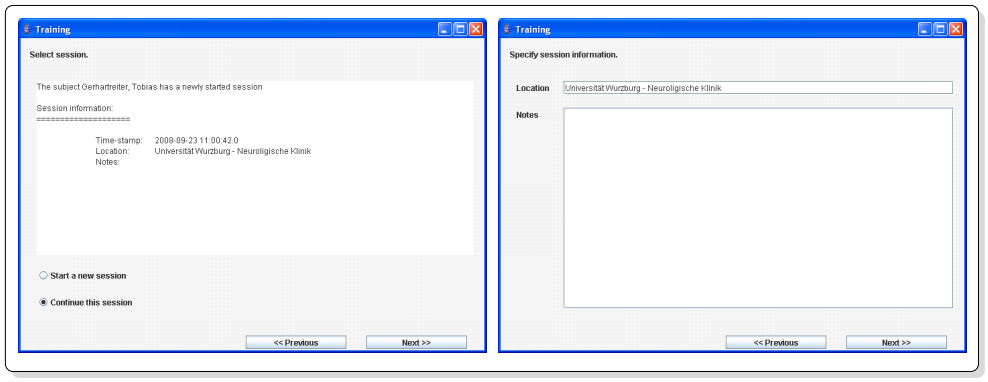

Figure 50: Session specification GUI.

circle, the color changes to red and the sensor is marked as disabled. However, at the current stage, the analysis and training routines always use all sensors, regardless, which have been disabled. Afterwards, the movement to be imitated must be selected. The user can load a

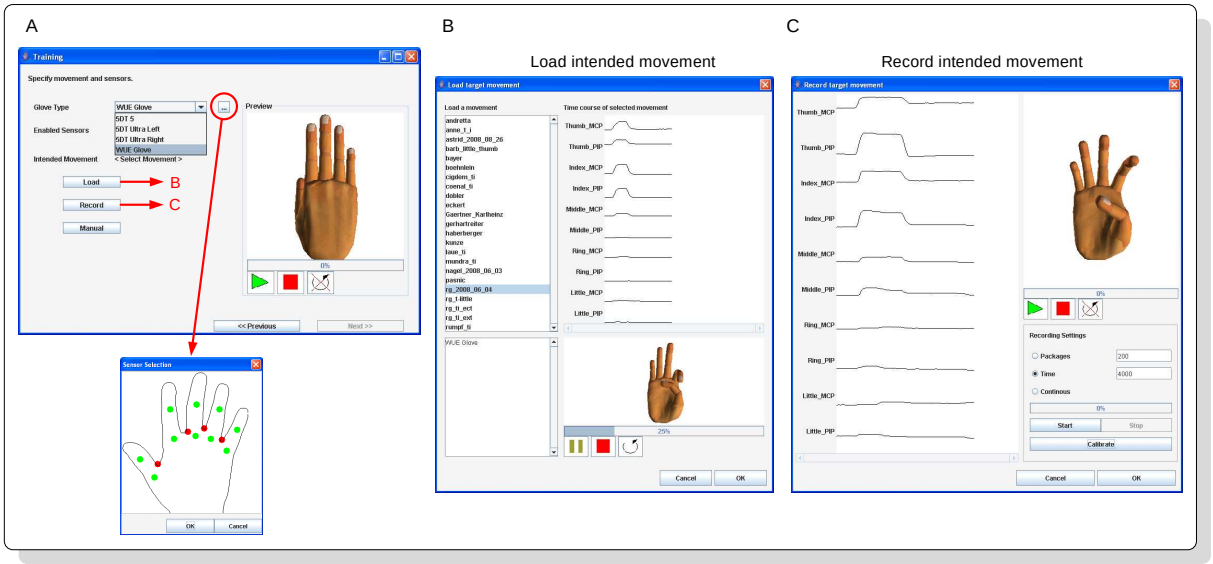

Figure 51: Block setup GUI. (A) A sensor glove can be selected from the list and sensors can be enabled and disabled. (B and C) A target movement to be trained can be loaded from the database (C) or recorded with the sensor glove (D).

movement already stored in the database (Figure 51B) or can record a new movement and

store it in the database (Figure 51C). In both cases, the movement is visualized by a virtual hand, and as a signal time course of each sensor. Before recording, the glove calibration must be conducted with the help of the calibration user interface (see Chapter A.5). A movement can be recorded for a certain amount of time (with a 'TimeLimitedController'), samples (using a 'SampleLimitedController') or until the 'Stop' button is clicked (with a 'ContinousController'). By clicking the 'OK' button, the recorded movement is stored in the database and the 'Next' button of the Wizard is enabled.

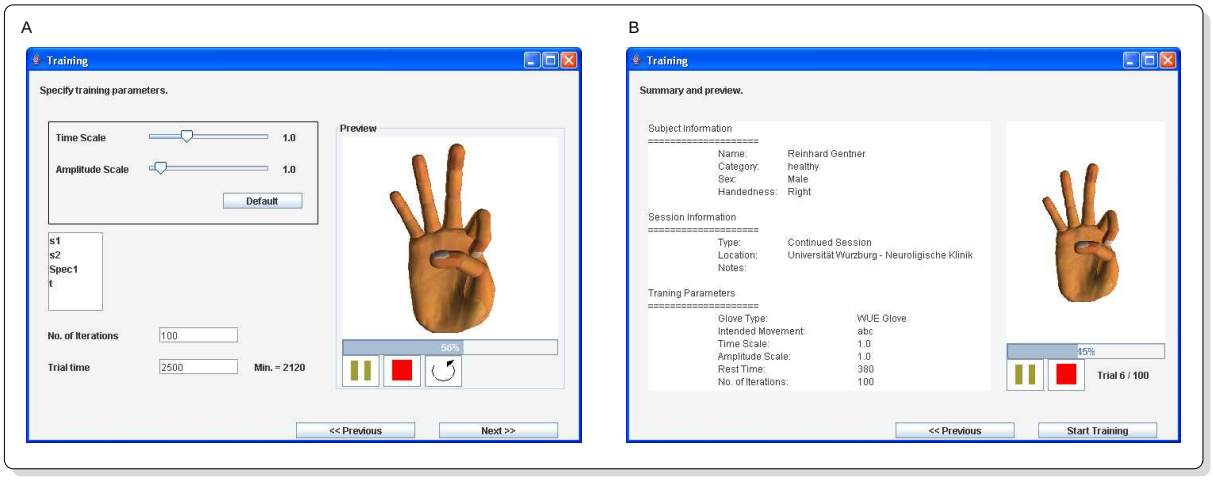

Figure 52: (A) GUI for adjustments of the target movement specification for amplitude and speed. (B) Finally, a summary of the parameters specified with the wizard is shown.

In the following training parameters panel ('ParamSpecPanel') shown in Figure 52 (left panel), the user can specify the following parameters:

- Timescale s: A parameter that takes a value between 0.1 and 1.0 (Precision of 0.1). It controls how fast the target movement is played back.
- Amplitude Scale a: A parameter that takes a value between 0.1 and 1.0 (Precision of 0.1) to increase or decrease the movement amplitude. The resulting movement is modified using these two parameters according to the model

$$y(t) = ax(st), \tag{2.32}$$

  where $x(t)$ represents the movement data (of the intended movement) of one sensor and y(t) its mapping into the new representation using the parameters a and s. Previously defined parameters can be loaded from the database.
- Number of trials: Specifies how many times the subject should try to imitate the target movement.
- Trial time: Specifies how long each trial would take (in milliseconds). This option provides the ability to add some resting time after each trial. The purpose of this rest time is to allow the system to perform linear interpolation between initial and final hand postures of the target movement. This avoids sudden posture changes at the end of each trial. Sensor data captured during resting time is not saved to the database.

Finally, a summary window of the training subject, the session, the movement to be trained, the amplitude and timescale, the number of trials and the trial time is given (Figure 52 right

panel). After clicking the 'Start training' button, the wizard is closed, all Business objects write their data to the database (using the 'apply()' method) and the training user interface is opened.

Movement training visualization

After specification of all necessary training parameters, the training user interface is started. It consists of a menu containing several buttons to calibrate the glove (by either opening the calibration dialog or by loading a previously conducted calibration file) and to start, stop and pause the training and the training visualization panel. Because the imitation of finger movements requires the concurrent control of several joint, an appropriate visualization of the target movement and the conducted movement is crucial for the training system. Here three different presentation techniques are implemented:

- **Concurrent view of virtual teacher and subject.** Subjects see two virtual hands, one displaying the target movement (the virtual teacher hand) and the other displaying the actual movement conducted by the subject. The task of the subject is to monitor the virtual teacher hand and to imitate the spatio-temporal movement pattern. The visualization is realized by two instances of 'VirtualHandView', where one is attached as an observer to the 'StoredMovementSensor' object and the other is attached to the appropriate 'GloveSensor' object (for example 'WueGloveRight'). Both sensors are updated by an 'IterativeController'.

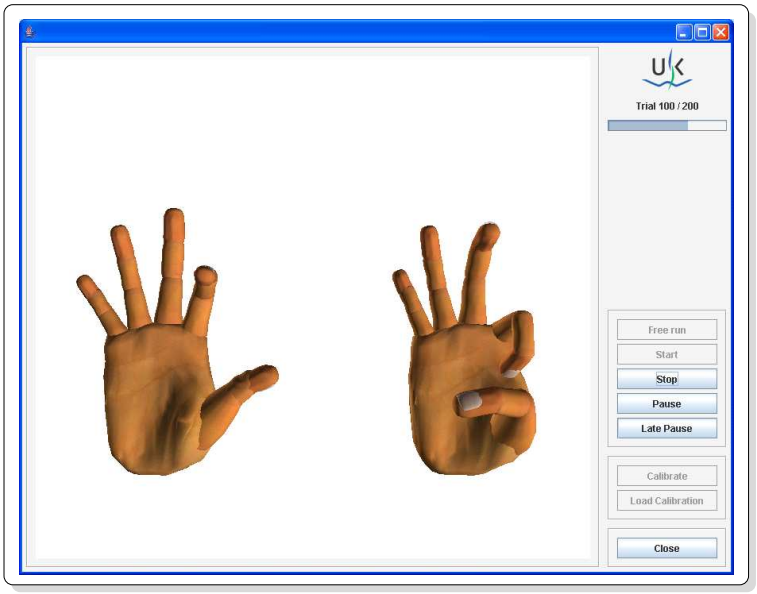

Figure 53: Training visualization. Concurrent view of virtual teacher and subject.

- **2D Mapping of finger movements.** This visualization technique maps the signals of the 10 sensors to an Euclidean 2-dimensional space. Previous studies have shown that subjects are able to conduct purposeful movements and learn within such a visualization

technique. The space was defined using the linear transformation

$$\begin{pmatrix} x \\ y \end{pmatrix} = \begin{pmatrix} a_{x,1} & a_{x,2} & \cdots & a_{x,10} \\ a_{y,1} & a_{y,2} & \cdots & a_{y,10} \end{pmatrix} \begin{pmatrix} h_1 \\ h_2 \\ \vdots \\ h_{10} \end{pmatrix} = \mathbf{A}\vec{h}, \tag{2.33}$$

where $\vec{p} = (x, y)^T$ indicates the point on the monitor, $\vec{h} = (h_1, h_2, \ldots, h_{10})^T$ is the 'glove signal vector', and $\mathbf{A}$ is the matrix of mapping coefficients with $(\mathbf{A})_{i,j} = a_{i,j}$. Four different calibration postures were used to determine the matrix $\mathbf{A}$ and thus to define the two dimensional movement space (Figure 54).

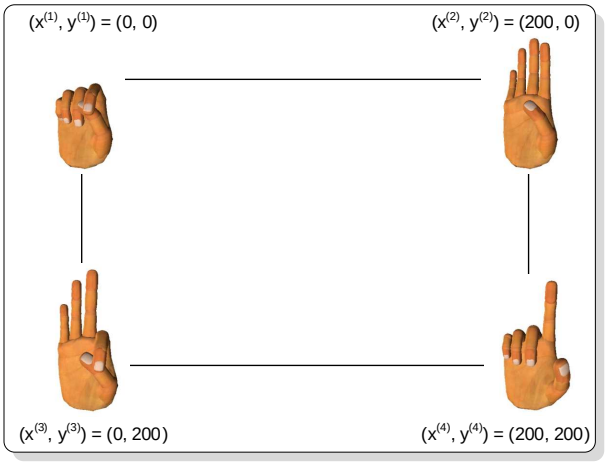

Figure 54: Reference postures to define the two dimensional mapping space.

With

$$\vec{P} = (\vec{p}^{(1)}, \vec{p}^{(2)}, \vec{p}^{(3)}, \vec{p}^{(4)})^T = (x^{(1)}, y^{(1)}, x^{(2)}, y^{(2)}, \ldots, x^{(4)}, y^{(4)})^T$$

representing the eight dimensional vector of screen coordinates and $\vec{h}^{(1)}, \vec{h}^{(2)}, \ldots, \vec{h}^{(4)}$ indicating the corresponding 10-dimensional glove signal vectors at these postures, a 8 $\times$ 20 data matrix $\mathbf{H}$ can be formulated as

$$\mathbf{H} = \begin{pmatrix} h_1^{(1)} & \cdots & h_{10}^{(1)} & 0 & \cdots & 0 \\ 0 & \cdots & 0 & h_1^{(1)} & \cdots & h_{10}^{(1)} \\ \cdots & \cdots & \cdots & \cdots & \cdots & \cdots \\ \cdots & \cdots & \cdots & \cdots & \cdots & \cdots \\ h_1^{(4)} & \cdots & h_{10}^{(4)} & 0 & \cdots & 0 \\ 0 & \cdots & 0 & h_1^{(4)} & \cdots & h_{10}^{(4)} \end{pmatrix}. \tag{2.34}$$

Similarly, the unknown coefficients $a_{i,j}$ of matrix $\mathbf{A}$ can be written as the 20-dimensional vector

$$\vec{a} = (a_{x,1}, \ldots, a_{x,10}, a_{y,1}, \ldots, a_{y,10})^T.$$

Using these notations, equation 2.33 can be written for the four reference points as

$$\begin{pmatrix} x^{(1)} \\ y^{(1)} \\ \vdots \\ x^{(4)} \\ y^{(4)} \end{pmatrix} = \begin{pmatrix} h_1^{(1)} & \cdots & h_{10}^{(1)} & 0 & \cdots & 0 \\ 0 & \cdots & 0 & h_1^{(1)} & \cdots & h_{10}^{(1)} \\ \cdots & \cdots & \cdots & \cdots & \cdots & \cdots \\ \cdots & \cdots & \cdots & \cdots & \cdots & \cdots \\ h_1^{(4)} & \cdots & h_{10}^{(4)} & 0 & \cdots & 0 \\ 0 & \cdots & 0 & h_1^{(4)} & \cdots & h_{10}^{(4)} \end{pmatrix} \begin{pmatrix} a_{x,1} \\ \vdots \\ a_{x,10} \\ a_{y,1} \\ \vdots \\ a_{y,10} \end{pmatrix} \tag{2.35}$$

and the coefficients $a_{i,j}$ are estimated by

$$\vec{a} = \mathbf{H}^{+}\mathbf{P},$$

where $\mathbf{H}^{+}$ is the Penrose pseudoinverse of H [162, 9]. This procedure corresponds to the selection of the minimum norm parameter vector $\vec{a}$, consistent with the reference postures [162]. Within this visualization, the history of the movement is visible as line. In this case, a redundant mapping existed, i.e. the visualized movement path can be generated from an infinitive number of joint constellations. Hence, this visualization technique is abstract and does not show the target movement directly to the subject. Here, one instance of the class 'TwoDimView' (which performs the mapping and the

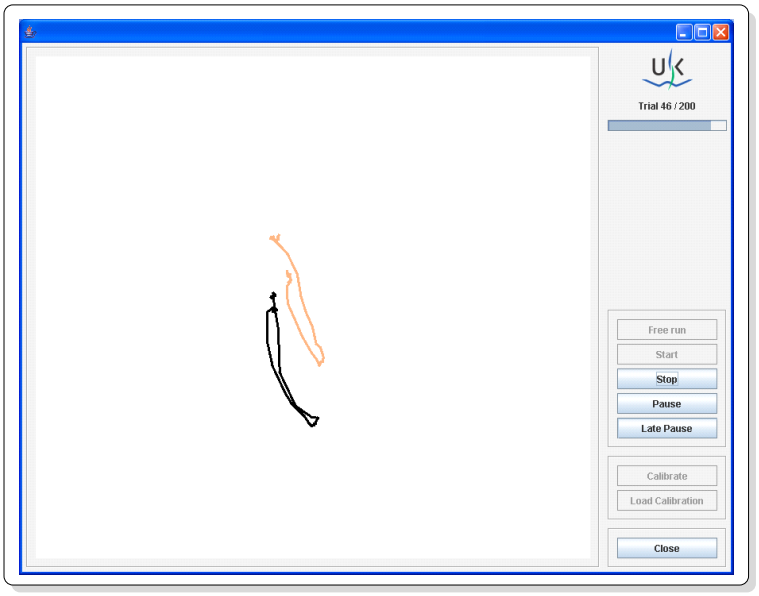

Figure 55: Training visualization. Mapping of the 10 signals from the virtual teacher (orange) and the subject (black) onto the two dimensional space.

visualization of the line) is attached to the 'StoredMovementSensor' object and another instance is attached to the 'GloveSensor' object.

- **Virtual teacher with changing color.** Only one virtual hand displaying the target movements is visualized. During a trial, the virtual hand changes its color in a continuum from normal hand colors (identical, correct movement) to red (opposite movement) if the subject's movement differs from the target movement. To accomplish the online adjustment of hand color, at each time step, a correlation coefficient between the actual joint positions and the angle values of the target movement is calculated and the corresponding hand color is chosen from a custom defined RGB value look-up table. One advantage of this visualization is that the target movement is visualized and the subject can indirectly see how the conducted movements are consistent with the target movement.

The storage of the trial data is handled by an observer, which does not belong to the view component ('DatabaseRecorder', see Figure 46). However, it is simply attached to the sensor as an observer and adds new data to a Java buffer. If the 'end trial' event is raised, the 'DatabaseRecorder' starts a Thread, writes the data buffer to the database and empties the buffer for the next trial.

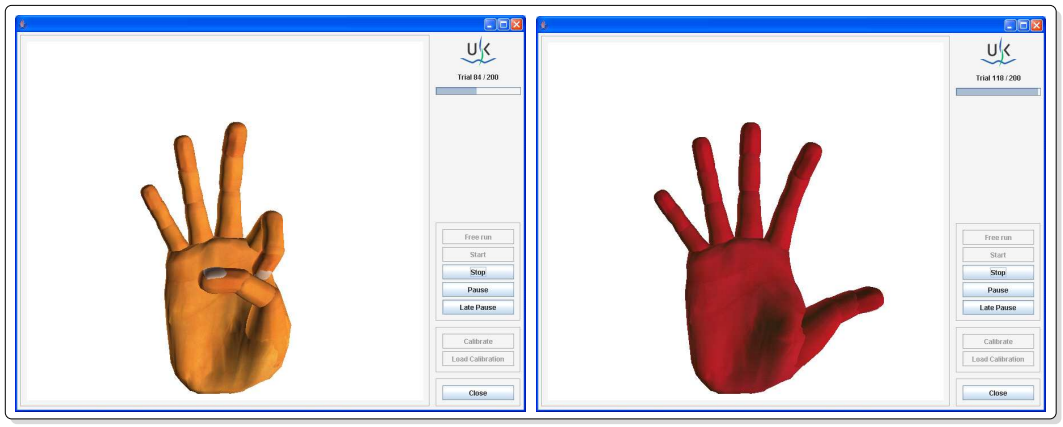

Figure 56: Training visualization. The virtual hand displays the movement of the virtual teacher and the color of the hand codes the correspondence of the posture adopted by the subject at each time point. Normal hand color indicates good correspondence.

Performance feedback is an important factor to drive neural plasticity and learning [213]. Therefore, the mean correlation coefficient of the last n trials can be fed back to the subjects via the 'PerformanceFeedback' class. Every n trials the class adds the actual bar to the feedback so that the subject can monitor the temporal evolution of imitation performance. The correlation coefficient (see Chapter A.6) is calculated after each trial (i.e. after the 'end

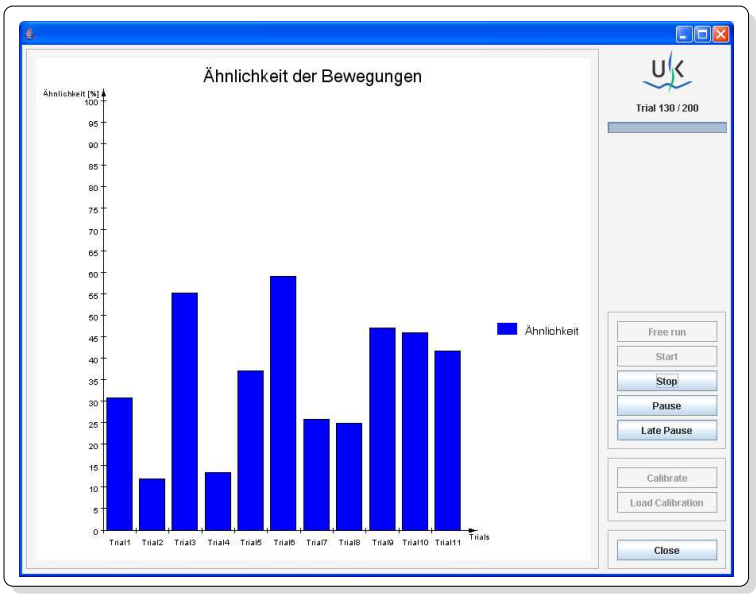

Figure 57: Performance feedback of the last n trials calculated as a correlation coefficient between the conducted movement and the target movement.

trial' event is raised by the controller) using the data from the intended movement and the actual conducted movement. Figure 57 shows the feedback of blocks of 10 trials. Since 110 trials are finished, the diagram consists of 11 performance bars.

The training system can be configured dynamically with the four views using the 'Training-Configurator' class. Each visualization is represented as an image. By clicking on it, the image (and the name of the corresponding visualization class) is added to a list. For example, in Figure 58 the training visualization is configured to show the 'ColorView' the first 10 trials. Then a performance feedback with $n = 10$ is given. The next 10 trials are shown as the 'TwoHandView' and again a performance feedback is given. In the following 10 trials,

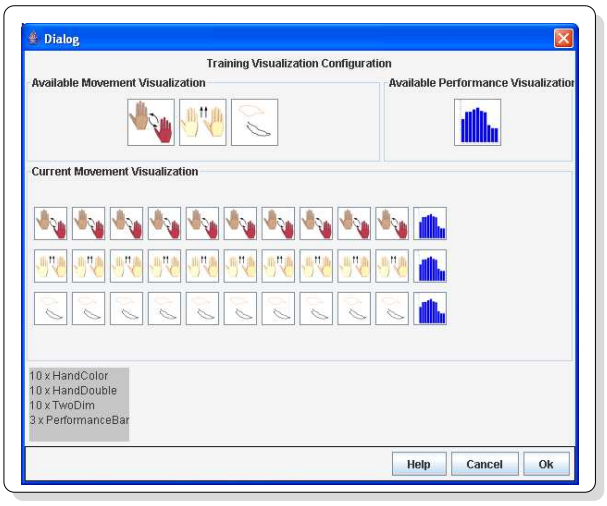

Figure 58: GUI to configure the visualization techniques during the training.

the subject sees a mapping of the movement in the 2-dimensional plane and the feedback after these 10 trials. If the number of trials exceeds the defined pattern, the visualization starts from the beginning. The view can be changed dynamically during program execution. This is realized by the instantiation of the view objects via the reflection mechanism. After a training is finished the data can be analyzed with the analysis framework.

Analysis Framework

More than one analysis method may be necessary to determine the training performance. To provide an extensible offline analysis framework, each analysis method is represented by a class (see Figure 59). An object of each class handles the analysis of a particular trial or

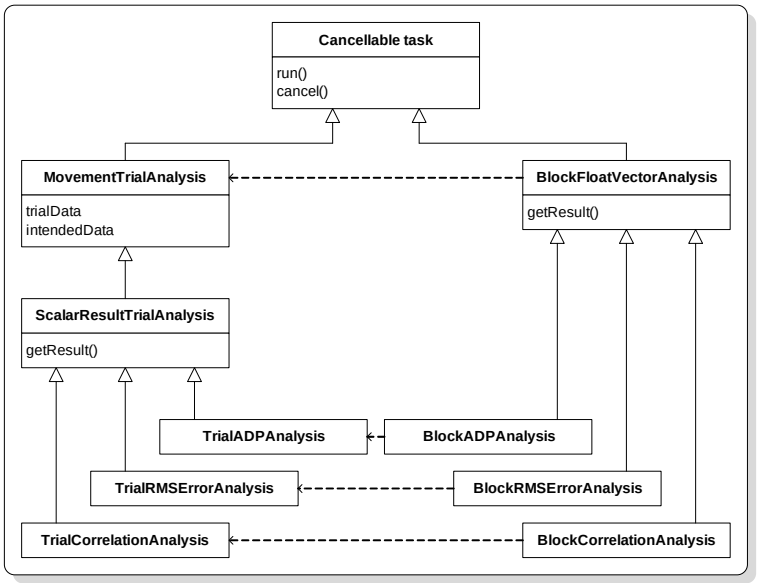

Figure 59: Class diagram of the analysis framework.

block. The base class of all analysis tasks is 'CancellableTask', which represents a cancellable Thread. Analysis tasks are derived from this class, because the user should have the ability to cancel a long analysis task. For movement training, 'MovementTrialAnalysis' is the base class for trial-level analysis. This class can import trial data from the database using appropriate

Business objects. Since a trial analysis results in a scalar value, the 'ScalarResultTrialAnalysis' class was defined. From this class three child classes are derived, each specifying the three analysis methods currently used. The 'BlockFloatVectorAnalysis' class represents a block-level analysis task that results in a scalar value for each trial. It creates and runs a 'ScalarResultTrialAnalysis' for each trial. Classes derived from this class ('BlockADPAnalysis', 'BlockRMSErrorAnalysis', and 'BlockCorrelationAnalysis') need only to implement the 'createAnalysis()' method, which builds the appropriate 'MovementTrialAnalysis' child object ('TrialADPAnalysis', 'TrialRMSErrorAnalysis', or 'TrialCorellationAnalysis'). The three types of analysis methods are defined as follows:

- **Average Dot Product (ADP):** As the name implies, this measurement depends on calculating the dot product between target movement and recorded samples on a sample-by-sample basis, and then taking the average value. The posture vectors used here are relative vectors, not absolute ones, which means their values are relative to initial posture. The ADP varies between -1 and 1, where values close to 1 indicate good performance.
- **Root Mean Squared (RMS) Error:** This measurement depends on the difference between target and recorded sensor values. It is also based on sample-by-sample comparison between target and recorded movements. For each pair of samples, a difference vector is obtained, from which a single root-mean-square error value is calculated. The RMS is normalized to values between -1 and 1, where higher values indicate better performance.
- **Correlation coefficient of vector fields:** Shadmehr and Mussa-Ivaldi defined vector versions of mathematical operations that enables the calculation of correlation coefficients between two ordered sets of vectors [219]. The value lie in the same range as in the previous two calculations. The algorithm is described in Chapter A.6.

Figure 60 shows the user interface of the analysis framework. On the left side, the database entries are listed as a tree. The user can expand the subject by double clicking on it. Then all training sessions are listed by identifying all block table entries from the database linked to the session. By clicking on a training session, the training blocks conducted in this session are identified and listed, and so on. Each of the three tabs in the right side is responsible for one of the three implemented analysis methods. By clicking on the 'Calculate' button, the whole block is analyzed according to the chosen method (in Figure 60 the correlation measure is displayed for all trials). If a single trial is selected in the left side, only the trial will be analyzed. The tab 'VirtualHand' can be clicked to visualize the selected trial with the virtual hand and the 'ChannelView' tab shows the time course of the sensors. The selected session, block or trial can be deleted ('Delete' button) or exported to -ascii files using the 'Export' button.

In summary, the training setup and visualization is programmed as flexible and as extensible as possible using single Design Patterns and the MVC concept as a composite Pattern. Especially, new gloves and glove drivers can be added by creating a database entry for a new glove and providing classes for interfacing with the glove. Furthermore, new kind of trainings, for example fractionation training [2, 26, 112], can be added without changing the code of the existing system. Finally additional training visualizations, performance feedback visualizations and analysis methods can easily integrated into the existing training system.

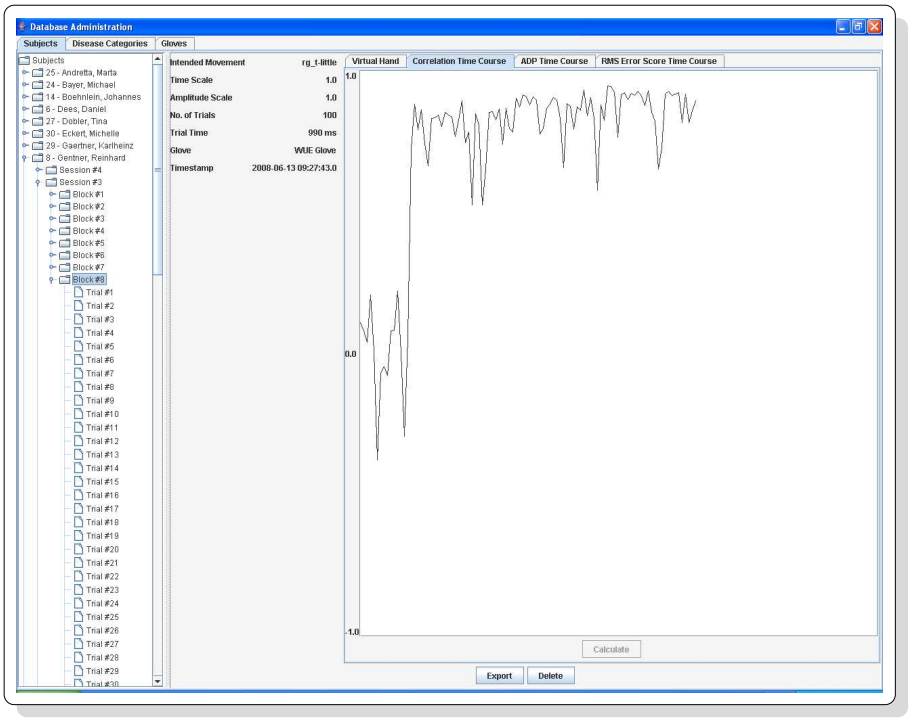

Figure 60: GUI of the analysis framework.

A valuable future development may be to translate the system into a web application, so that subjects or even patients can perform training movements at their homes.

The last component of the measurement framework is a dynamic model of the human hand to simulate finger movements and, in future, to incorporate learning related effects into neural network models.

2.5 The simulation framework

Since the anatomy of the hand in each individual varies according to their size, tendons, muscle structure, skin and bone properties, and changes during life, a globally 'correct' model of the human hand does not exist. Here a hand model is developed which approximates the biomechanical system of the human fingers. Key features are the agonist / antagonist innervation mechanisms of the muscles to move the joints, the existence of a resting (or equilibrium) position, where extension and flexion torques at one joint cancel each other and the convergence (several muscles act at one joint) and divergence (one muscle acts on several joints) of muscle forces.

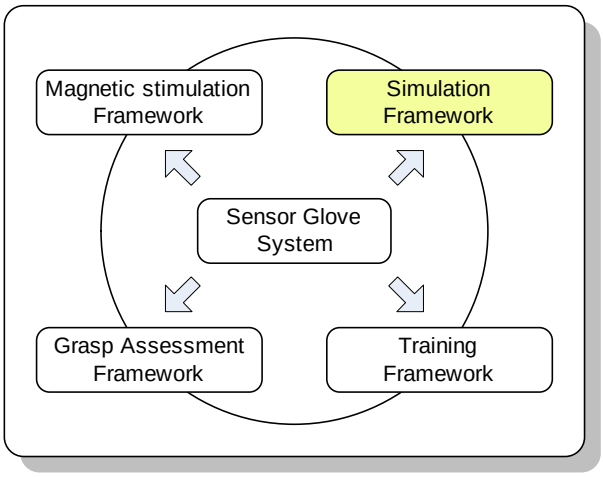

The model described here is not a realistic model of the human hand and muscles. However, the aim at this stage is not to provide a realistic model, but to have a model of approximately the same complexity as the human hand as a proof of principle for the results from brain stimulation. Therefore, the modeling is constrained to the joints which were measured by the sensor glove. More detailed models have been developed for single fingers [246] or the entire hand [246, 247, 249]. The dynamic model developed here is described in more detail in the following chapters.

2.5.1 Dynamic equations of a two-link kinematic chain

The basic effectors of the fingers are the bones consisting of the proximal phalanx (flexion/extension and abduction/adduction movements about the MCP joint), the medial phalanx (flexion/extension movements about the PIP joint) and the distal phalanx (flexion/extension movements about the DIP joint). The bones are modeled as cylinders with a certain length, radius and mass. Abduction/Adduction movements at the metacarpophalangeal joint and the distal phalanx are not considered (Figure 61A). Thus, a finger is reduced to a planar manipulator with two revolute joints (extension/flexion movements) as illustrated in Figure 61B. Each finger segment has the mass m, the length l, and the rotation angle q. The variable τ indicates torques acting on the joints.

The aim of the modeling is to find a mathematical description of the system relating torques acting on the joints to the joint angles. Principally, this kind of problem is covered by Newtonian mechanics and can be solved using the Euler-Lagrange equations

$$\frac{d}{dt}\frac{\partial \mathcal{L}}{\partial \dot{q}_k} - \frac{\partial \mathcal{L}}{\partial q_k} = \tau_k; \quad k = 1, ..., n \tag{2.36}$$

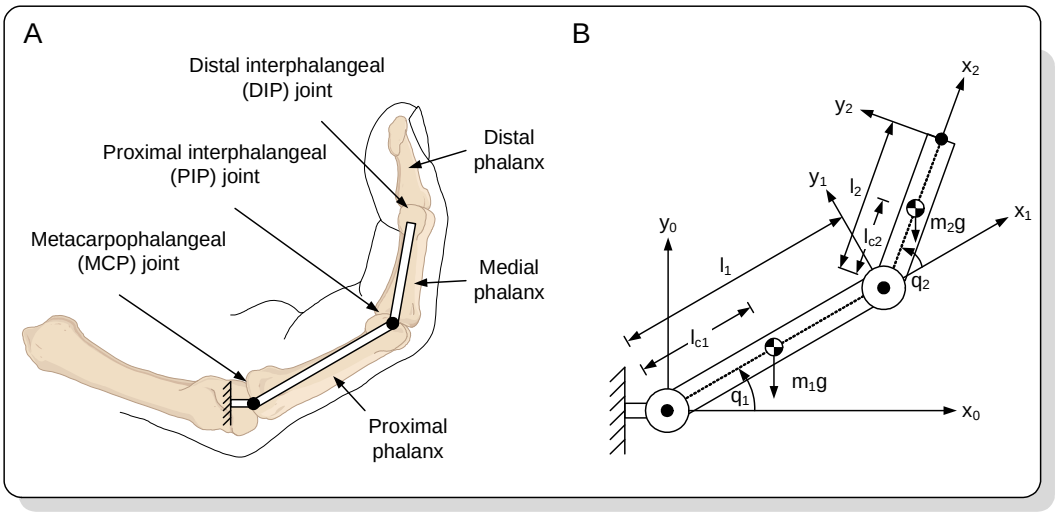

Figure 61: (A) Modeling of the fingers as rigid cylinders. (B) Geometrical definitions of the finger models.

where the Lagrangian $\mathcal{L}$ of the system denotes the difference between the kinetic energy $\mathcal{K}$ and the potential energy $\mathcal{P}$ and τ_k is the (generalized) force associated with the generalized coordinate q_k. Here the generalized forces are the torques about the joints and the generalized coordinates (minimum number of independent variables to describe the system) are the joint angles. Application of the Euler-Lagrange equations leads to a set of coupled second-order ordinary differential equations of motions equivalent to those derived using Newton's second law. The dynamic equations were determined according to Chapter A.2.

Kinetic energy contributions

To determine the kinetic energy of the system, the translational and angular velocities must be known. The translational velocity of the first link is given by $v_{c1} = \mathbf{J}_{v_{c1}}(\vec{q})\dot{\vec{q}}$, where

$$\mathbf{J}_{v_{c1}}(\vec{q}) = \begin{pmatrix} -l_{c1}sin(q_1) & 0 \\ l_{c1}cos(q_1) & 0 \\ 0 & 0 \end{pmatrix} \tag{2.37}$$

is the 3×2 Jacobian matrix relating velocity of the first joint to translational velocity of the center of the first link. Similarly, the translational velocity of the center of the second link is $v_{c2} = \mathbf{J}_{v_{c2}}(\vec{q})\dot{\vec{q}}$ with

$$\mathbf{J}_{v_{c2}}(\vec{q}) = \begin{pmatrix} -l_1sin(q_1) - l_{c2}sin(q_1+q_2) & -l_{c2}sin(q_1+q_2) \\ l_1cos(q_1) + l_{c2}cos(q_1+q_2) & l_{c2}cos(q_1+q_2) \\ 0 & 0 \end{pmatrix}. \tag{2.38}$$

Hence, the translational part of the kinetic energy is

$$\frac{1}{2}\dot{\vec{q}}^T \left(m_1 \mathbf{J}_{v_{c1}}^T(\vec{q})\mathbf{J}_{v_{c1}}(\vec{q}) + m_2 \mathbf{J}_{v_{c2}}^T(\vec{q})\mathbf{J}_{v_{c2}}(\vec{q}) \right) \dot{\vec{q}}. \tag{2.39}$$

The angular velocity of the first and second link expressed in the inertial frame is

$$\omega_1 = \dot{q}_1\vec{e}_z, \quad \omega_2 = (\dot{q}_1 + \dot{q}_2)\vec{e}_z, \tag{2.40}$$

respectively. Since the link can only rotate about the z-axis, the inertial tensor simplifies to a scalar inertia I_{zz} and the rotational kinetic energy is $I_{zz,i}\omega_i^2$, or

$$\frac{1}{2}\dot{\vec{q}}^T \left(I_{zz,1} \begin{pmatrix} 1 & 0 \\ 0 & 0 \end{pmatrix} + I_{zz,2} \begin{pmatrix} 1 & 1 \\ 1 & 1 \end{pmatrix} \right) \dot{\vec{q}}. \tag{2.41}$$

The inertia of a cylinder rotated about its center is given by

$$I_{zz,i} = \frac{1}{4} m_i r_i^2 + \frac{1}{12} m_i l_i^2 + m_i \left(\frac{l_i}{2} \right)^2, \tag{2.42}$$

where r is the radius of the cylinder, m the mass, and l its length. The rotational contributions to the kinetic energy can then be written as

$$\frac{1}{2}\dot{\vec{q}}^T \left(I_{zz,1} \begin{pmatrix} 1 & 0 \\ 0 & 0 \end{pmatrix} + I_{zz,2} \begin{pmatrix} 1 & 1 \\ 1 & 1 \end{pmatrix} \right) \dot{\vec{q}}. \tag{2.43}$$

Thus, the entire kinetic energy is given by

$$\mathcal{K} = \frac{1}{2}\dot{\vec{q}}^T \left(m_1 \mathbf{J}_{v_{c1}}^T(\vec{q}) \mathbf{J}_{v_{c1}}(\vec{q}) + m_2 \mathbf{J}_{v_{c2}}^T(\vec{q}) \mathbf{J}_{v_{c2}}(\vec{q}) + \begin{pmatrix} I_{zz,1} + I_{zz,2} & I_{zz,2} \\ I_{zz,2} & I_{zz,2} \end{pmatrix} \right) \dot{\vec{q}}. \tag{2.44}$$

Carrying out the multiplications (and using standard trigonometric identities) leads to

$$\begin{aligned} d_{11} &= m_1 l_{c1}^2 + m_2 (l_1^2 + l_{c2}^2 + 2 l_1 l_{c2} cos(q_2)) + I_{zz,1} + I_{zz,2} \\ d_{12} &= d_{21} = m_2 (l_{c2}^2 + l_1 l_{c2} cos(q_2)) + I_{zz,2} \\ d_{22} &= m_2 l_{c2}^2 + I_{zz,2}, \end{aligned} \tag{2.45}$$

which denote the elements of the matrix $\mathbf{D}(\vec{q})$ of the kinetic energy. The Christoffel symbols then compute to

$$\begin{aligned} c_{111} &= \frac{1}{2} \frac{\partial d_{11}}{\partial q_1} = 0 \\ c_{121} = c_{211} &= \frac{1}{2} \frac{\partial d_{11}}{\partial q_2} = -m_2 l_1 l_{c2} sin(q_2) = h \\ c_{221} &= \frac{\partial d_{12}}{\partial q_2} - \frac{1}{2} \frac{\partial d_{22}}{\partial q_1} = h \\ c_{112} &= \frac{\partial d_{21}}{\partial q_1} - \frac{1}{2} \frac{\partial d_{11}}{\partial q_2} = -h \\ c_{122} = c_{212} &= \frac{1}{2} \frac{\partial d_{22}}{\partial q_1} = 0 \\ c_{222} &= \frac{1}{2} \frac{\partial d_{22}}{\partial q_2} = 0. \end{aligned}$$

Potential energy contributions

The potential energy of the manipulator is the sum of the potential energy of the two links

$$\mathcal{P} = \mathcal{P}_1 + \mathcal{P}_2 = m_1 g l_{c1} sin(q_1) + m_2 g (l_1 sin(q_1) + l_{c2} sin(q_1 + q_2)) \tag{2.46}$$

and the functions $g_k(\vec{q})$ compute to

$$\begin{aligned} g_1 &= \frac{\partial \mathcal{P}}{\partial q_1} = g(m_1 l_{c1} + m_2 l_1) cos(q_1) + g m_2 l_{c2} cos(q_1 + q_2) \\ g_2 &= \frac{\partial \mathcal{P}}{\partial q_2} = g m_2 l_{c2} cos(q_1 + q_2). \end{aligned}$$

Dynamical equations of the system

With the contributions of the kinetic and potential energy, the dynamic equations of the system can be written as

$$d_{11}\ddot{q}_1 + d_{12}\ddot{q}_2 + c_{121}\dot{q}_1\dot{q}_2 + c_{211}\dot{q}_2\dot{q}_1 + c_{221}\dot{q}_2^2 + g_1 = \tau_1 \tag{2.47}$$

$$d_{21}\ddot{q}_1 + d_{22}\ddot{q}_2 + c_{112}\dot{q}_1^2 + g_2 = \tau_2. \tag{2.48}$$

Implementation in Matlab/Simulink

Equations 2.47 and 2.48 completely specify the dynamic behavior of the coupled cylinder system, which serves as a model for a human finger. However, since the model should describe the fingers in the same position as in the TMS-experimental setup (semipronated), the gravity direction in this special case is perpendicular to the joints and thus is not considered in the actual simulation. Furthermore, to simplify the implementation of the model in Matlab/Simulink, the dynamic equations were rewritten to

$$\begin{aligned}\ddot{q}_1 &= \frac{(\tau_1 - B_1)A_{22} - (\tau_2 - B_2)A_{12}}{(A_{11}A_{22} - A_{12}A_{21})} \\ \ddot{q}_2 &= \frac{(\tau_2 - B_2)A_{11} - (\tau_1 - B_1)A_{21}}{(A_{11}A_{22} - A_{12}A_{21})},\end{aligned} \tag{2.49}$$

where

$$\begin{aligned}A_{11} &= I_{zz,1} + I_{zz,2} + m_1 l_{c1}^2 + m_2(l_1^2 + l_{c2}^2 + 2l_1 l_{c2} cos(q_2)) \\ A_{12} &= I_2 + m_2(l_{c2}^2 l_1 l_{c2} cos(q_2)) \\ A_{21} &= A_{12} \\ A_{22} &= I_2 + m_2 l_{c2}^2,\end{aligned} \tag{2.50}$$

and

$$\begin{aligned}B_1 &= -m_2 l_1 l_{c2}\dot{q}_2^2 sin(q_2) - 2m_2 l_1 l_{c2}\dot{q}_1\dot{q}_2 sin(q_2) \\ B_2 &= m_2 l_1 l_{c2}\dot{q}_1^2 sin(q_2).\end{aligned} \tag{2.51}$$

Figure 62 shows the implementation of the dynamic equations of a finger in Simulink. In the sub-model 'Dynamics w/o gravity' the geometry and the mass of the finger is specified and equations 2.49 - 2.51 are implemented. The outputs of the sub-model are the joint angle accelerations $\ddot{q}_1$ and $\ddot{q}_2$, respectively, which are integrated to obtain the actual joint angles. The blue marked blocks ensure the anatomically constrained range of joint angles. If the external torque is would rotate the joint apart the anatomical limit (specified as saturation limit in the second integrators), the internal state of the first integrator is resetted and its input is switched to 0. As a consequence, the joint position outputs of the model, q_1 and q_2, remain constant and the corresponding joint velocity outputs $\dot{q}_1$ and $\dot{q}_2$ become 0. The inputs of the model are the external joint torques τ_1 and τ_2 applied by the muscles. The entire block is the basic dynamic model of a finger, whose purpose is to calculates the joint angles after externally applied torques. Note that in this model the external torques can be applied at each joint independently which is not the case in real human fingers. As a next step the torque generation by the muscles is modeled.

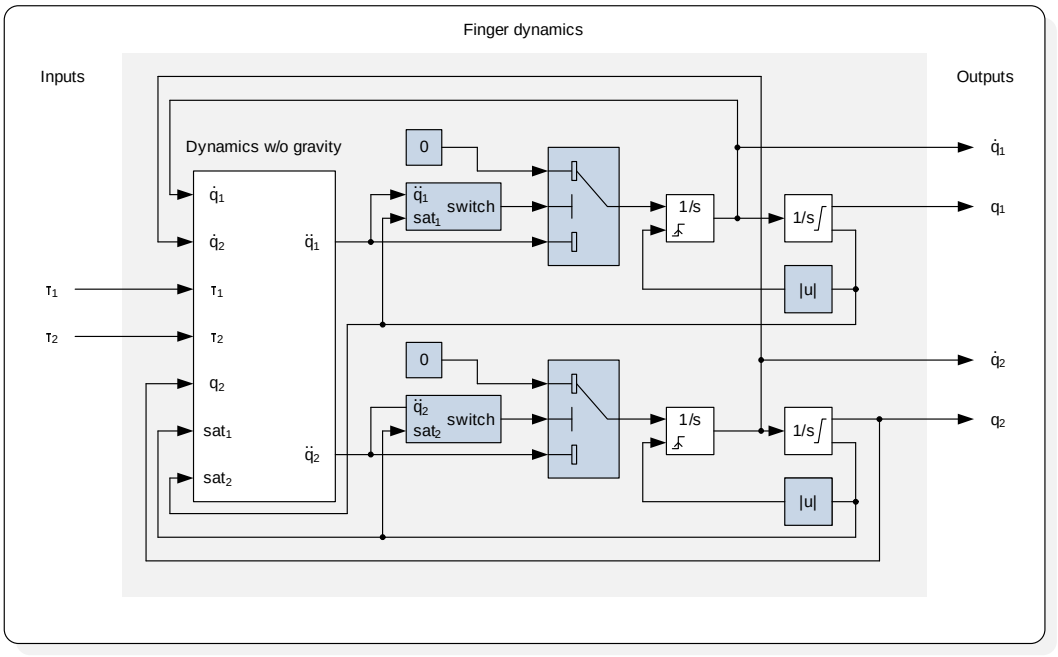

Figure 62: Simulink block diagram of the dynamic equations. Blue blocks indicate mechanical constraints.

2.5.2 Torque generation and equilibrium

The external torques to rotate the finger are generated by the muscles, which transmit their forces by tendons to the finger segments (see Figure 63A). In mathematical terms, muscles can be thought of as springlike actuators that produce forces dependent on the actual muscle length and recent usage, growth and other factors (Shadmehr Wise 2005). In the model developed here, a finger segment is moved by a pair of 'virtual muscles', one acting as agonist and the other as antagonist (Figure 63B). A virtual muscle is a spring-damper contractile element (with viscosity b and stiffness k), contracted by the summed input force ($\sum F_{ext}$ and $\sum F_{flex}$, respectively) from several muscles. Thus, the model simplifies the

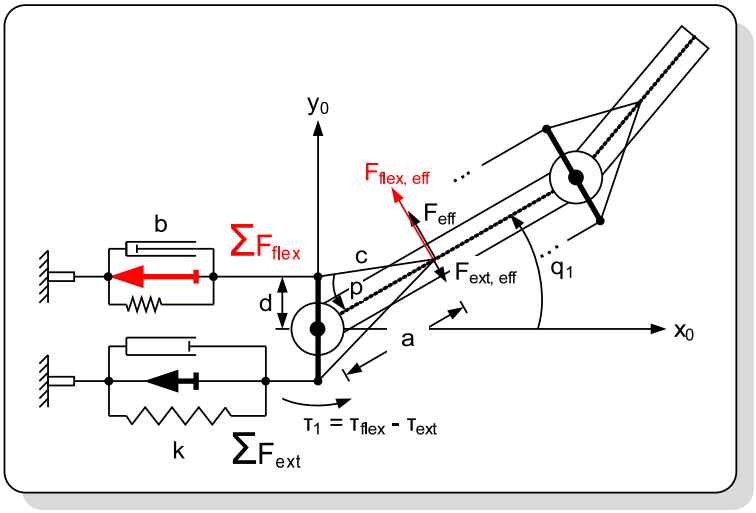

Figure 63: Torque generation by a pair of virtual muscles.

muscle dynamics of several muscles acting on a joint to a single system, the virtual muscle. In this chapter, the relationship between the force produced by a virtual muscle and the

resulting torque τ_1 at the proximal joint is described representatively.

The torque τ_1 is generated by the moment arm a of the virtual muscle and the effective force F_{eff} acting perpendicular on the finger segment. The finger segment is in its equilibrium position ($F_{eff} = 0$) if the virtual muscle produces no active forces and the spring forces cancel each other. If a virtual muscle, for example the one acting in flexion direction, is contracted, the effective force $F_{eff} = F_{eff,flex} - F_{eff,ext}$ consists of the force exerted by the active muscle but also on the passive (or active) force exerted by the antagonist muscle. Hence, the torque $\tau_1 = \tau_{flex} - \tau_{ext}$ is the result of action and reaction forces from the virtual muscles. In the example here, the effective force $F_{eff,flex}$ is given by

$$F_{eff,flex} = \left(\sum F_{flex} + F_{spring} + F_{damper}\right) sin(p), \tag{2.52}$$

where F_{spring} is the configuration dependent force of the spring and F_{damper} the velocity dependent force of the damper element, both acting in the opposite direction to $\sum F_{flex}$. The resulting torque is given by

$$\tau_{flex} = \left(\sum F_{flex} + F_{spring} + F_{damper}\right) sin(p)\ a. \tag{2.53}$$

Using the basic trigonometric relationships

$$\begin{aligned} sin(p) &= \frac{d}{c} sin(90° - q_1) = \frac{d}{c} cos(q_1) \\ c &= \sqrt{a^2 + d^2 - 2ad\ cos(90° - q_1)} = \sqrt{a^2 + d^2 - 2ad\ sin(q_1)}, \end{aligned}$$

the torque can be rewritten as a function of q_1 as

$$\tau_{flex} = \left(\sum F_{flex} + F_{spring} + F_{damper}\right) \frac{ad\ cos(q_1)}{\sqrt{a^2 + d^2 - 2ad\ sin(q_1)}}. \tag{2.54}$$

Furthermore, the spring force is defined to be zero, if the angle q_1 is zero (later, q_1 gets an offset of 45°, so that the equilibrium position is 45° flexion for all joints) and is thus given by the change of c with respect to its neutral length:

$$F_{spring} = k\left(c(q_1) - c(q1 = 0°)\right) = k\left(\sqrt{a^2 + d^2 - 2ad\ sin(q_1)} - \sqrt{a^2 + d^2}\right). \tag{2.55}$$

Note that the spring force is negative and thus acts against the active flexion force produced by the virtual muscle. Similarly, the damping forces compute to

$$F_{damper} = -2bad\ cos(q_1)\dot{q}_1. \tag{2.56}$$

In summary, the torque τ_{flex} in flexion direction produced only by the virtual muscle that acts in flexion direction is given by

$$\tau_{flex} = \frac{\left(\sum F_{flex} + k\left(\sqrt{a^2 + d^2 - 2ad\ sin(q_1)} - \sqrt{a^2 + d^2}\right) - 2bad\ cos(q_1)\dot{q}_1\right) ad\ cos(q_1)}{\sqrt{a^2 + d^2 - 2ad\ sin(q_1)}}. \tag{2.57}$$

With the torque exerted by the antagonist muscle in extension direction, which can be derived analogously, the resulting torque at the proximal joint is then computed as

$$\tau_1 = \tau_{flex} - \tau_{ext}. \tag{2.58}$$

The proposed model of torque generation shares several features of real human fingers. First, a joint is moved by the action of several muscles. Second, an equilibrium position

exist, defined as the position of the joint where the passive torques cancel each other. Since the viscosity b, the stiffness k, and the geometry of the moment arm is set equal for both, the agonist and antagonist virtual muscle, the equilibrium position is at $q_1 = 0°$. However, to obtain a physiologically plausible equilibrium position, an offset of 45° is added to q_1 resulting in an equilibrium position of 45° flexion of each joint. Third, the agonist-antagonist configuration of the virtual muscles implicate that the muscles can only produce forces in one direction and that the torques at a joint are always composed of the combined action of agonist and antagonist virtual muscle.

Implementation in Matlab/Simulink

The implementation of the virtual muscle concept is shown in Figure 64. In each sub-model (flexion torque proximal, extension torque proximal, and flexion torque distal, extension torque distal), equation 2.57 is implemented for the appropriate movement direction and joint. The resulting torques τ_1 and τ_2 are fed as external torques into the finger dynamics

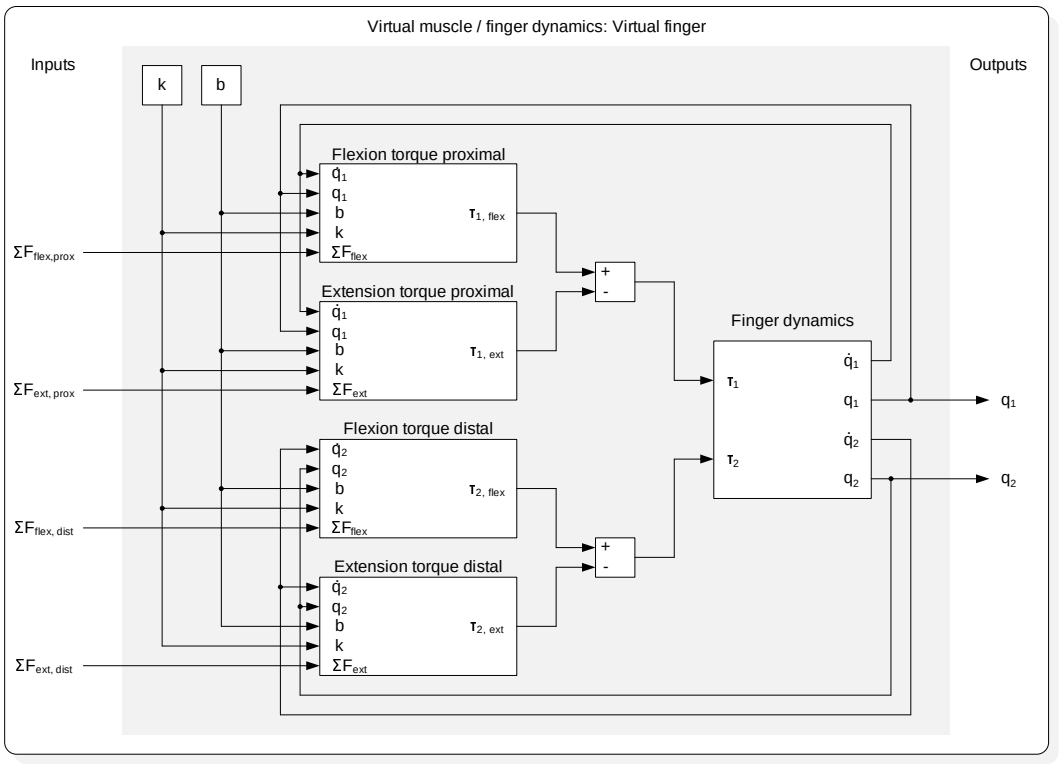

Figure 64: Simulink model of virtual muscles acting on the dynamic finger model.

model (see Figure 64). The four sub-models and the finger dynamics model represent the dynamics of the finger model and the external torques generated by the virtual muscles. Virtual muscles are defined as systems, which actively generate forces according to the summed input from several muscles innervating the appropriate joint. In the next chapter, the complete hand model consisting of four fingers and the thumb (i.e., five 'Virtual muscle / finger dynamics' models) is composed. As a last step, the contribution of anatomically distinct muscles to the appropriate virtual muscles are defined.

2.5.3 Composition of the hand and muscle innervations

For each finger, a 'Virtual finger' model was created using plausible geometrical and dynamic properties of each segment and finger. The parameters of each finger and finger segment are summarized in Table 5. Note that at the current status, these parameters were selected to

	Thumb		Index		Middle		Ring		Little	
	prox.	dist.	prox.	dist.	prox.	dist.	prox.	dist.	prox.	dist.
Joint name	MCP	IP	MCP	PIP	MCP	PIP	MCP	PIP	MCP	PIP
l [cm]	3.5	3	5	3	6	3.5	5	3	4.5	2.5
m [g]	30	30	30	20	35	25	30	20	20	15
a [cm]	3.5	3	5	3	6	3.5	5	3	4.5	2.5
d [cm]	1.5	1.5	1	1	1	1	1	1	0.8	0.8
k	50	50	50	50	50	50	50	50	50	50
b	110	110	110	110	110	110	110	110	110	110

Table 5: Parameters of the finger model.

approximately match the relationships between fingers. In future, these parameters should be adapted to experimentally identified values.

Based on the five virtual fingers, the muscles innervating the fingers were specified (see Table 6) and their contribution to extension and flexion of the appropriate finger was defined. This procedure essentially consists of choosing the weighting coefficients between the mapping of the contraction force of a specific muscle and its contributions to the virtual muscle force moving a finger segment. As mentioned before, a muscle can contribute to the torque at a single finger joint (for example the force generated by the extensor pollicis brevis muscle is transmitted fully to the virtual muscle acting producing extension torques around the proximal thumb segment) or to torques at several fingers and/or finger joints (for example the flexor digitorum profundus muscle transmits 40% its force to the proximal and 60% to the distal segment of the index, middle, ring and little finger in flexion direction). The complete mappings of the 24 muscles considered are summarized in Table 6, where 'e' and 'f' indicate contribution to the extension and flexion torques, respectively. Here again, the magnitude of the coefficients are selected to approximately match the neuroanatomy of muscle innervations. Note also that several muscles considered here mainly contribute to abduction or adduction movements, which are not considered in the actual dynamic model of the hand. The contribution of all muscles to a single segment in extension and flexion movements are then summed together and define the force generated by the appropriate virtual muscle.

The complete model of the hand is visualized in Figure 65. The forces generated by the 24 muscles are the inputs of the model and the resulting joint angles the outputs. The muscle forces are mapped onto the flexion and extension forces of the proximal and distal segment of each finger, where the mapping coefficients are taken from Table 6. The summed forces are then fed into the 'Virtual finger' models of each finger and the joint configurations are calculated. The output of the model is processed into Matlab and stored in data arrays for analysis and storage.

	Thumb		Index		Middle		Ring		Little	
	prox.	dist.	prox.	dist.	prox.	dist.	prox.	dist.	prox.	dist.
Joint name	MCP	IP	MCP	PIP	MCP	PIP	MCP	PIP	MCP	PIP
Extensor pollicis brevis	1.0e	0	0	0	0	0	0	0	0	0
Extensor pollicis longus	0.2e	0.8e	0	0	0	0	0	0	0	0
Abductor pollicis brevis	0.3e	0	0	0	0	0	0	0	0	0
Adductor pollicis	0.3f	0	0	0	0	0	0	0	0	0
Flexor pollicis brevis	1.0f	0	0	0	0	0	0	0	0	0
Flexor pollicis longus	0.2f	0.8f	0	0	0	0	0	0	0	0
Extensor indicis	0	0	0.5f	0.5f	0	0	0	0	0	0
Interosseus dorsalis I	0	0	0.6f	0.2e	0	0	0	0	0	0
Interosseus palmaris I	0	0	0.6f	0.2e	0	0	0	0	0	0
Lumbricalis I	0	0	0.1f	0	0	0	0	0	0	0
Interosseus dorsalis II	0	0	0	0	0.6f	0.2e	0	0	0	0
Interosseus dorsalis III	0	0	0	0	0.6f	0.2e	0	0	0	0
Lumbricalis II	0	0	0	0	0.1f	0	0	0	0	0
Interosseus dorsalis IV	0	0	0	0	0	0	0.6f	0.2e	0	0
Interosseus palmaris II	0	0	0	0	0	0	0.6f	0.2e	0	0
Lumbricalis III	0	0	0	0	0	0	0.1f	0	0	0
Extensor digiti minimi	0	0	0	0	0	0	0	0	0.5e	0.5e
Abductor digiti minimi	0	0	0	0	0	0	0	0	0.2f	0.2e
Interosseus palmaris III	0	0	0	0	0	0	0	0	0.2f	0.2e
Lumbricalis IV	0	0	0	0	0	0	0	0	0.1f	0
Flexor digiti minimi br.	0	0	0	0	0	0	0	0	0.9f	0
Extensor digitorum	0	0	0.6e	0.4e	0.6e	0.4e	0.6e	0.4e	0.6e	0.4e
Flexor digitorum superf.	0	0	0.4f	0.6f	0.4f	0.6f	0.4f	0.6f	0.4f	0.6f
Flexor digitorum prof.	0	0	0.4f	0.6f	0.4f	0.6f	0.4f	0.6f	0.4f	0.6f

Table 6: Muscle contributions to the force produced by the virtual muscles. Values were selected by inspection.

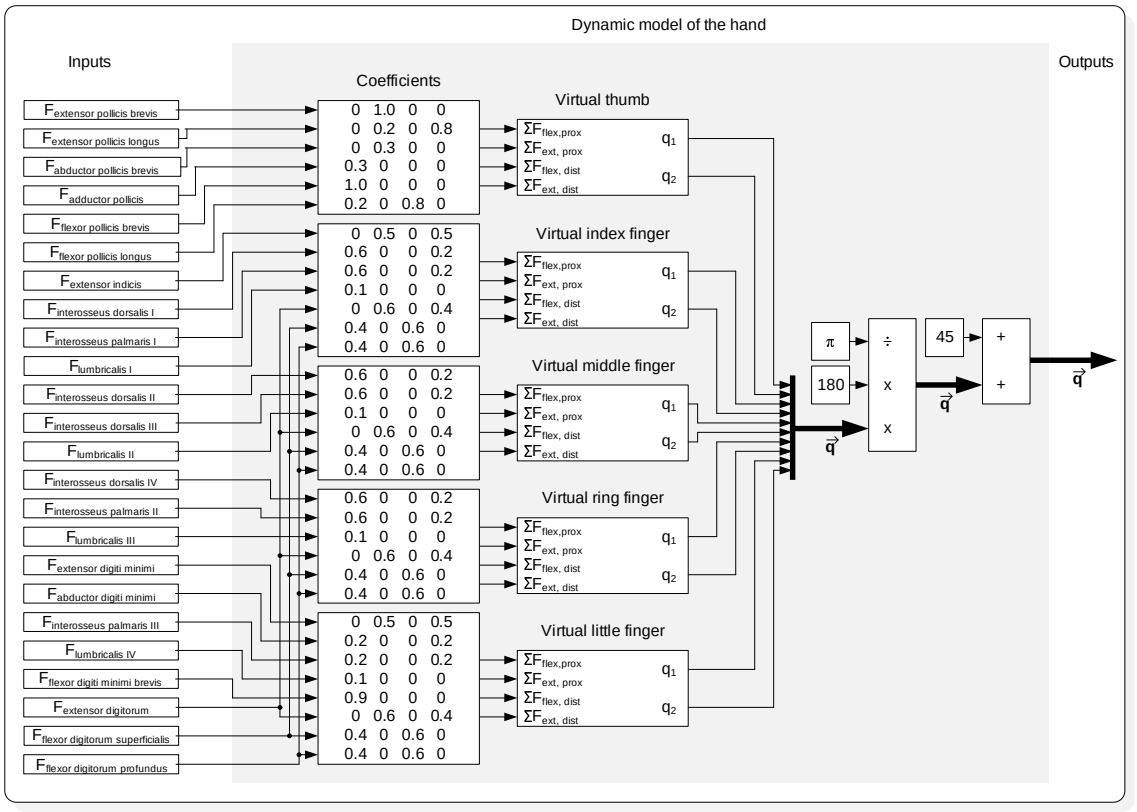

Figure 65: Contribution of real muscles to virtual muscles of the fingers.

3 Application of the measurement system

The second part of the thesis consists of four empirical studies to examine the modular organization using the developed measurement framework. The first study (Chapter 3.1) describes the modular organization of finger movements healthy adults and provides support for the module developed in Chapter 1.7. The second study in Chapter 3.2 addresses the effect of learning a musical instrument on the modular organization. In the third study (Chapter 3.3), the developed finger movement training system is evaluated and the effect of short term learning of finger movements on the modular organization is described. Finally in the fourth study presented in Chapter 3.4, the simulation environment is evaluated. The modular structure of finger movements after random muscle activity is investigated and compared to the results of empirical obtained data.

3.1 Description of the modular organization of finger movements

The mapping and grasping elements of the developed measurement system were used to investigate the modular organization described in Chapter 1.4 in healthy subjects. In this study, the TUB-Glove was used for the acquisition of finger movements. As outlined in

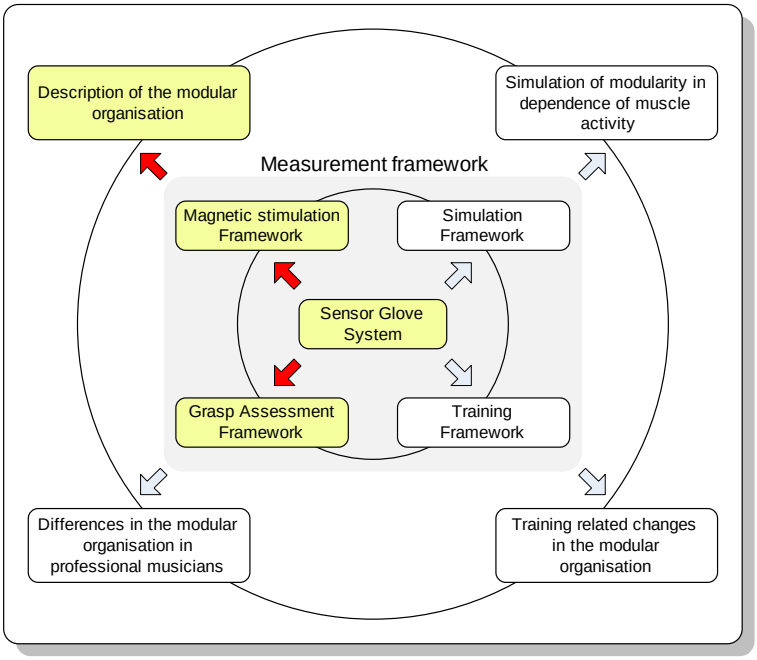

Chapter 1.4, the motor system may generate automated movements, such as walking, by combining modular spinal motor synergies. However, it remains unknown whether a modular neuronal architecture is sufficient to generate the unique flexibility of human finger movements, which rely on cortical structures. Here we show that finger movements evoked by transcranial magnetic stimulation (TMS) of the primary motor cortex reproduced distinctive features of the spatial representation of voluntary movements as identified in previous neuroimaging studies [17, 100, 29], consistent with naturalistic activation of neuronal elements. Principal component analysis revealed that TMS-evoked movements can be described as a linear combination of a small number of modules (or principal components), explaining most of the data variance. Modules extracted from TMS-induced finger movements resembled those derived from end-postures of voluntary movements performed to grasp imagined objects, and a small subset of them was sufficient to reconstruct these movements with

remarkable fidelity. Thus, the motor system may coordinate even the most dexterous movements by using a modular architecture involving cortical components.

3.1.1 Background

It has been proposed that a set of neuromotor synergies, termed 'modules', may represent a possible basis for intentional as well as automatic actions [78, 181, 229]. Despite experimental support for a modular organization of motor system (see Chapter 1.4), it is unclear whether this modularity has a causal relationship to neuronal operation, and if so, at which locations in the motor system this modularity is implemented. This uncertainty arises because the rules that govern neuronal activity for generating movements cannot be inferred directly through the analysis of the kinematics or muscle activation patterns due to the inverse problem. For example, tremulous motion may originate from the activity of an independent neuronal pacemaker, but it is equally possible that it may originate from reflexively organized neuronal activity or biomechanical properties [57].

Strong causal evidence for a modular operation of the central nervous system (CNS) in movement control is provided if similar modular principles are revealed by direct stimulation of the nervous system. Although intraspinal microstimulation experiments in mammals [241] and amphibians [51] revealed similar results, experimental support for functional modular organization was notably absent in spinalized cats [8, 164]. It is possible, then that modular neuronal organization of intentional dexterous movements, if at all present in higher-order animals and in humans, may depend on the motor cortex.

Here, the magnetic stimulation framework (Chapter 2.2) is used to test this hypothesis directly in awake humans. First, critical evidence in favor of TMS activation as an experimental paradigm that can reproduce features of natural activation of the primary motor cortex is added. Secondly, the question of whether TMS-evoked finger movements may show modular properties is examined, and if so, whether they are similar to grasping movements, an extensively well characterized family of dexterous finger movements whose modular kinematic properties have been documented previously [197]. For the assessment of grasping movements, the grasping framework was used (see Chapter 2.3).

3.1.2 Methods

The study was approved by the Ethics committee of the University of Wuerzburg, and written informed consent was obtained from all participants. Experiments were performed on 21 healthy volunteers (9 men and 12 women, age 24 $\pm$ 4 years). Three subjects were excluded, because no finger movements could be obtained at a low stimulation intensity. TMS mapping was applied as explained in Chapter 2.2.2.

Magnetic brachial plexus stimulation

Additionally, magnetic brachial plexus stimulation performed in five subjects. The subject's right hand was positioned in the same position as in the brain mapping experiments. Approximately 100 stimuli were applied with the coil positioned over the right brachial plexus. Stimulation intensity was chosen to ensure that the amplitude of evoked finger movements matched those evoked by TMS.

Biomechanical constraints

Six subjects took part in this experiment. The hand and fingers were positioned as in the brain mapping experiments. In each trial the experimenter moved a single joint by ≈10° in either flexion or extension direction. Concomitantly, passive movements of the remaining joints were recorded. For any subject, this resulted in 20 trials (2 for each recorded finger joint). The end-posture was maintained until the recording was stopped after 2 s. Subjects were told to relax during passive movements and let the experimenter move the finger.

Structureless-PVs

Structureless-PVs were generated by randomly reshuffling PV components from TMS-PVs across samples of each subject. A set of Structureless-PVs contained the same number of elements as the set of TMS-PVs of the corresponding subject. This procedure served to remove correlations between joints without changing the variance of each data set. For each subject, five different sets of Structureless-PVs were generated.

Reconstruction of grasp postures

Grasp end postures were reconstructed by finding the best solution $\mathbf{X}$ to the equation $\mathbf{AX} = \mathbf{B}$, using a standard least squares algorithm. The matrix $\mathbf{B} \in 10 \times$ (number of Grasp-PVs) contained the normalized (Euclidean-norm) Grasp-PVs, and the matrix $\mathbf{A} \in 10 \times$ n contained n basis vectors (the first n modules). The number n of basis vectors was defined as the number of modules needed to account for >90% of variation of the appropriate data set. Modules derived from TMS-PVs, Structureless Structureless-PVs, and Grasp-PVs themselves were used as basis vectors to reconstruct Grasp-PVs. In the case of Structureless-PVs, the number of modules was set as equal to the computed number of modules derived from TMS-evoked movements of the corresponding subject. The reconstruction quality of a specific Grasp-PV, B_i, was expressed as a percentage value of the normalized Euclidean distance between $\mathbf{A}X_i$ and B_i (100% indicated the largest reconstruction error and was equivalent to the maximum Euclidean distance).

3.1.3 Results

Pattern of finger movements evoked by TMS

Across all subjects and all joints, the mean flexion angle was 2.0° ± 1.7° and the mean extension angle was 1.9° ± 1.6°. Movements occurred around single joints, joints of a single finger, or multiple joints, in both extension and flexion. Of all finger movements, isolated thumb movements were evoked most frequently (14% ± 13% of movements across 18 subjects), followed by movements of the index (10% ± 10%), middle (7% ± 7%), little (4% ± 4%), and ring finger (2% ± 2%). Although isolated finger movements were observable on multiple occasions, it was more common for TMS to elicit movements of several fingers simultaneously (63% ± 16% of evoked movements across 18 subjects). All movements (isolated or as part of composite finger movements) considered, thumb movements, index finger movements, and middle finger movements were evoked with similar frequencies (50% ± 22%; 59% ± 19%; 56% ± 18%, respectively) whereas ring finger movements (41% ± 22%) and

little finger movements (38% ± 21%) were elicited somewhat less frequently.

Overlap and somatotopic gradient of movement representations

Movements evoked by TMS over different scalp positions did not display a prominent systematic topographic pattern. Similar finger movements could be evoked from spatially separate stimulation sites and dissimilar movements could be evoked from stimulation of the same site. This is visualized in Figure 66A and B, which show matrices of pairwise distances of all TMS-evoked movements recorded in two subjects. Figure 66C displays a segment of the matrix of one subject (Figure 66A) and illustrates pairs of individual similar and dissimilar posture vectors derived from TMS-evoked movements (TMS-PVs). To assess the spatial gradient of movement similarity, all TMS-PVs were matched to two randomly selected TMS-PVs obtained through stimulation of (1) the same site or (2) a distant site. The similarity of the resulting pairs of local TMS-PVs was compared with the similarity of the pairs of distant TMS-PVs across all subjects. Although the mean similarity of local TMS-PV pairs was significantly higher (i.e., the distance was smaller) than the similarity of distant TMS-PV pairs ($p < 0.001$; two-tailed paired t-test), the mean similarity differed only by 0.08 ± 0.58 (Figure 66D). This 'isotropy' of movement representation on a macroscopic scale is consistent with findings obtained with a large variety of investigational methods ranging from anatomical study [186], intracortical microstimulation (ICMS) [135, 234], and recorded activity of single neurons [182, 158] to functional magnetic resonance imaging (MRI) [17, 100, 130, 195]. Scalp sites from which movements of individual fingers (mostly as part of composite finger movements) could be evoked overlapped extensively. Figure 67A displays the topographical distribution of the movements of each individual finger as summarized by its activation map (see Chapter 2.2.5).

Peak activations were located near the grand center of gravity (CoG) of all finger movements. The location of the CoG of individual fingers is illustrated in Figure 67B. The lateral position of the CoG of different fingers differed significantly (analysis of variance (ANOVA); $F(4, 85) = 2.5$; $p = 0.049$). With reference to the CoG of little finger movements, the CoG of thumb movements was 2.3 ± 3.4 mm ($p = 0.011$; two-tailed paired t-test) more lateral, and the CoG of index finger movements was 3.1 ± 2.8 mm ($p < 0.001$; two-tailed paired t-test) more lateral. The CoGs derived from motor-evoked potential (MEP) amplitudes recorded from the abductor pollicis brevis (APB) muscle and adductor digiti minimi (ADM) muscle were comparable in distance and location to the CoGs of the corresponding finger movement. The APB muscle was located 3.0 ± 1.5 mm more laterally than the ADM muscle ($p < 0.001$; two-tailed paired t-test). Projected at the level of the cortex, the mean 3D distance of CoGs of thumb and index finger to little finger amounted to ≈3.4 - 3.7 mm, in excellent agreement with findings obtained from neuroimaging studies [17, 100]. In these studies, the 3D distance obtained after voluntary individual finger movements was found to be 1.7 - 5.4 mm.

Variability of TMS-evoked movements is constrained by neuronal factors

To obtain a more detailed view of the properties of the output of the primary motor cortex as revealed by TMS, the analysis of individual fingers was extended to the analysis of entire TMS-evoked movements. Although a large variety of movements were evoked by TMS, many movements appeared to share a limited number of mutually similar postures. Hierarchical cluster analysis was used to allocate TMS-PVs to posture groups (PGs), which were defined

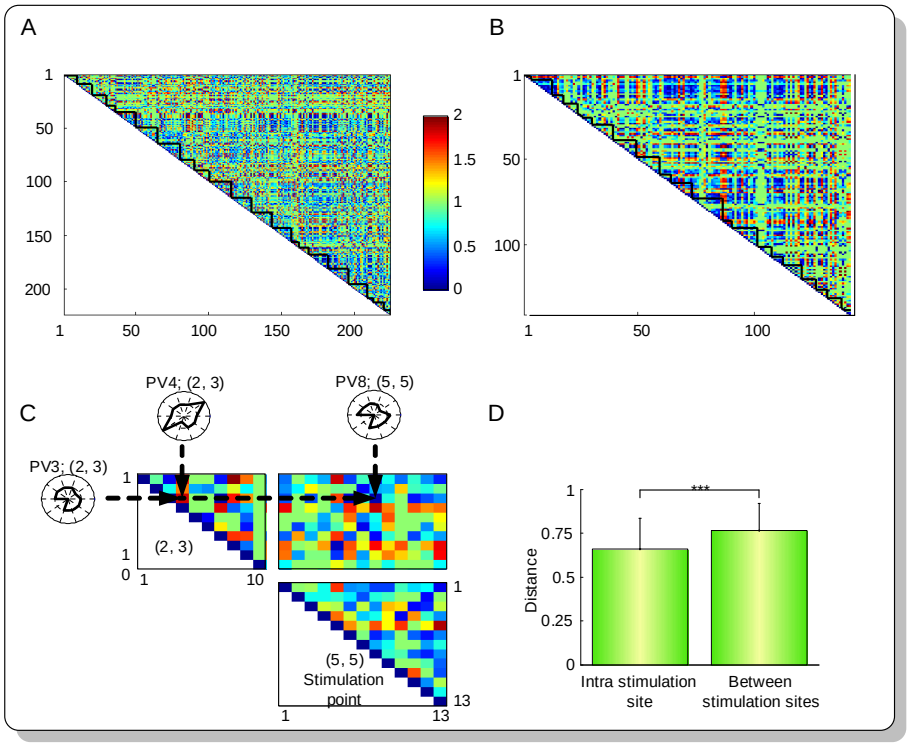

Figure 66: Mapping of scalp positions onto TMS-evoked finger movements. (A and B) Distance matrices of PVs indexing TMS-evoked movements for two representative subjects. The distance between any two ten-dimensional PVs is coded on a color scale ranging from 0 (dark blue, implying identity) to 2 (dark red, indicating strongest possible dissimilarity, i.e., the vectors pointed in opposite directions). Because the matrices are symmetric, only the upper triangular part is shown. The leftmost diagonal represents the distance of two identical PVs. The black bold triangles along the diagonal refer to pairs of PVs derived from movements evoked from the same stimulation point. The different sizes of triangles indicate that at some stimulation sites, fewer than 15 movements were evoked by TMS. (C) Selected segments of the distance matrix computed from PVs of two arbitrarily selected, spatially distant stimulation sites (2, 3) and (5, 5) from subject AA, whose complete matrix is displayed in (A). The inset illustrates individual PVs obtained from site (2, 3) and (5, 5). The third TMS pulse delivered over point (2, 3) and the eighth TMS pulse delivered over point (5, 5) evoked flexions of the I_MCP and I_PIP joint. The distance of their corresponding PVs was small (d = 0.072), implying high similarity. In contrast, the fourth TMS pulse delivered over point (2, 3) evoked a movement consisting of extension of I_MCP and I_PIP and flexion of M_MCP. The distance of its corresponding PV from the PV evoked by the third stimulus was large (d = 1.840), implying dissimilarity. (D) Distance of PVs to randomly selected PVs of the same stimulation site (left bar) and to randomly selected PVs from different stimulation sites (right bar). Values are presented as mean ± SD.

by the minimal distance of their group members (Chapter 2.2.6). Visualization of these groups revealed that several movements contained motion elements observable in natural motor behavior, such as thumb and index finger opposition or opening and closing of the hand. Examples are shown in Figure 68A, in which 8 (of a total of 73) different PGs derived from TMS-PVs in one subject (AA) are rendered. Figure 68B summarizes the results of the clustering process of the TMS-PVs for all 18 subjects. Across all subjects, the mean number of PGs was 47 ± 17,indicating that TMS-evoked movements exhibited

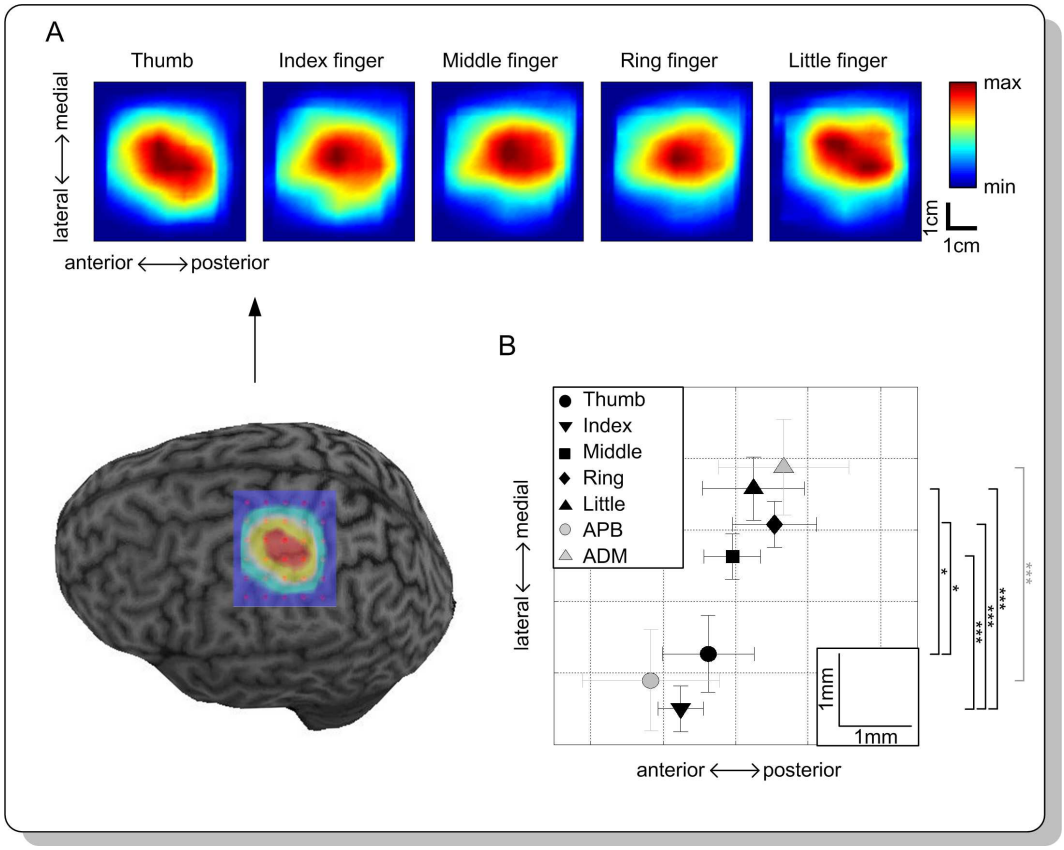

Figure 67: Somatotopical gradient of finger movement representations. (A) Scalp sites from which movements of individual fingers could be evoked overlapped extensively. Summed normalized activation maps of each finger were aligned to the center of gravity (CoG) of all fingers (18 subjects). (B) Somatotopical gradient of finger movement representation and intrinsic hand muscle (APB, ADM, eight subjects) representation. CoGs of finger movements (black symbols) and muscle activations (gray symbols) were normalized to the position of the CoG of all finger movements. Despite overlapping areas, finger movements exhibited a somatotopical gradient, with thumb and index finger movements represented most laterally and little finger movements represented most medially. *$p < 0.05$; ***$p < 0.001$.

considerable variability. The variability of TMS-PVs was compared with the variability of Structureless-PVs, which were generated from randomly shuffling the TMS-PV components of each subject. TMS-PVs were also compared with movements evoked by magnetic brachial plexus stimulation (as indexed by Plexus-PVs) to illustrate the variability of TMS-evoked movements in relation to movements evoked by synchronous stimulation of a peripheral part of the nervous system. Cluster analysis yielded a different number of PGs for the three conditions (TMS, Structureless-PVs, and Plexus-PVs) in each subject. This is illustrated in Figure 4C, which displays PGs derived from subject AA. For comparison of the results across subjects, the number of PGs was normalized by the total number of PVs to generate a cluster index (CI) that was independent of the total number of PVs. The computed CIs differed significantly between the three conditions (ANOVA; $F(2, 15) = 60.50$; $p < 0.001$; Figure 68D). CIs derived from TMS-PVs were intermediate between those obtained from Structureless-PVs and Plexus-PVs. These results indicate that the variability of TMS-evoked movements is likely to be influenced to a major extent by factors upstream of biomechanics, and thus, probably by neuronal factors related to the organization of the corticospinal system.

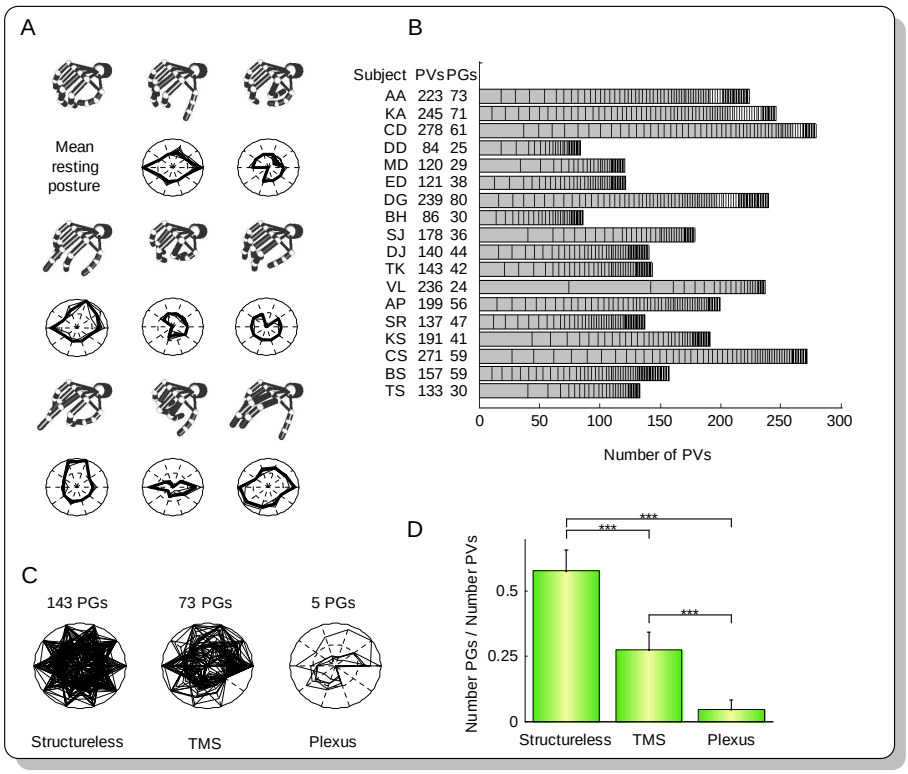

Figure 68: Grouping of Similar PVs by cluster analysis. (A) Examples of eight different posture groups (PGs) of one subject. The resting position before application of the TMS pulse is shown in the upper left. (B) Summary of the clustering process. The length of horizontal bars corresponds to the number of PVs (as indicated in the middle column). Each horizontal bar is segmented to indicate posture groups (PGs, right column). PGs were obtained by clustering similar PVs into groups. The number of PVs in a PG is represented by the length of the segment. PGs are sorted in descending order of elements. (C) All PGs of one subject for structureless datasets, TMS-evoked movements, and brachial plexus stimulation-evoked movements. (D) Group data. Variability of TMS-PVs, Structureless-PVs, and PVs resulting from brachial plexus stimulation as indicated by the number of PGs normalized by the number of PVs (mean ± SD). Variability of TMS-PVs was reduced if compared to Structureless-PVs, but variability was larger than in PVs resulting from brachial plexus stimulation. ***p < 0.001.

Modular Composition of TMS-Evoked Movements

To analyze the data with respect to the model described in Chapter 1.7, PCA, a widely used matrix factorization technique, was applied (see Chapter 2.2.7). The resulting PCs are termed modules. On average, the first four modules accounted for ≈89.3% of the variance, with the first two accounting for ≈72.6% of the variance (Figure 5A). Therefore, the number of the most prominent modules (as defined by the number of modules accounting for ≈90% of the variance) inherent in the TMS-PVs amounted to approximately four, indicating that the a large portion of the kinematic output of the primary motor cortex can be explained by linear combinations of four modules. In contrast, approximately eight PCs were needed to account for ≈89% of the total variance of Structureless-PVs (Figure 69A). The number of relevant modules derived from TMS-evoked movements was significantly lower than in Structureless-PVs ($p < 0.001$, two-tailed t-test). This difference would indicate a property

of the cortical motor system, unless this specific pattern was not already present due to mechanical properties of the human hand.

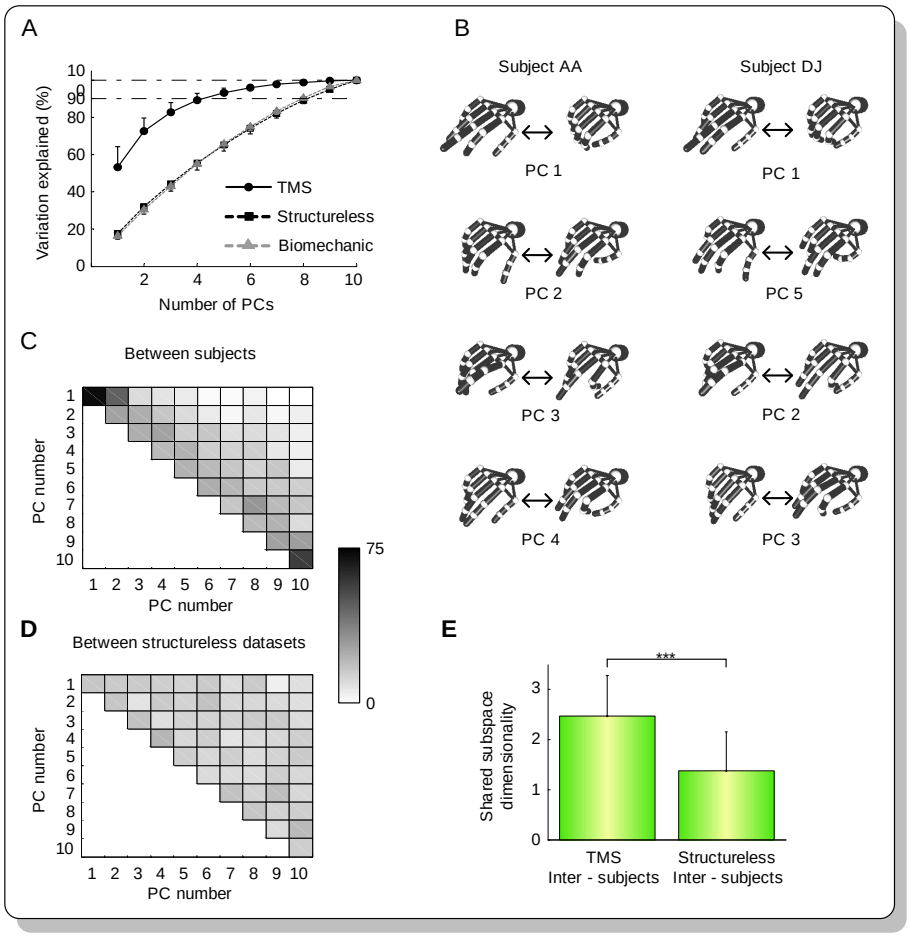

Figure 69: Modular composition of TMS-evoked movements. (A) Results of principal component analysis (PCA). The cumulative fraction of total variation explained by the principal components (PCs or modules) of TMS-PVs (solid line), Structureless- PVs (black dashed line), and Biomechanical-PVs (gray dashed line) are shown (mean ± SD). Approximately four modules resulting from TMS were needed to reconstruct the real data at high fidelity. In contrast, approximately eight modules from the Structureless-PVs and from the Biomechanical-PVs were needed to obtain the same reconstruction accuracy. (B) Interindividual similarity of extracted modules. The first four modules from subject AA are displayed in the left panel. The best-matching modules in relation to subject AA were computed for subject DJ (right panel). Note that the rank order differed between some best matching module pairs. (C and D) Histograms of the rank order of best matching pairs of TMS-modules (C) and of Structureless-modules (D) as an indicator of structural similarity between sets of modules. Dark cells denote frequently occurring best-matching module assignments between subjects. The histogram of all possible combinations from 18 subjects is shown. TMS-modules exhibited a greater consistency, which was expressed as a larger number of entries near the diagonal axis of the histogram. The first modules especially corresponded most often with one another between subjects. (E) The shared subspace dimensionality of TMS-modules between subjects was significantly higher than that between sets of Structureless-modules. Values are presented as mean ± SD. ***$p < 0.001$.

Indeed, Lang and Schieber [138] have demonstrated biomechanical constraints for passive

large-arc (≈40° - 80°) finger movements. To address the degree to which the variance of the modules explained could be attributed to biomechanical constraints, we performed passive individuated movements of every single recorded finger joint of the right hand in six subjects. The range of these joint motions was 23.2° ± 2.8° and, thus, considerably larger than that of the TMS-evoked movements (mean range of joint motions 3.9°, see above). PCA of these individuated passive movements showed that eight modules accounted for ≈90.0% of the variance, similar to modules derived from Structureless-PVs (Figure 69A). Therefore, the modular structure of finger movements evoked by TMS of primary motor cortex cannot be explained by tested biomechanical factors. However, simple passive movements of the fingers mainly detect couplings of skin tissue and thus do not cover the whole spectrum of biomechanical constraints further involving muscle and tendon couplings as well as couplings from incomplete segregation of muscle compartments [211]. To address this issue in more detail, muscles could be selectively stimulated by intramuscular electrodes. Alternatively, the hand could be modeled and the influence of biomechanical couplings could be analyzed by simulations. A first attempt to the second approach has been taken Chapter 3.4.

Similarity of modules

To address the question of similarity between modules derived from different subjects, best-matching pairs (see Chapter 2.2.7) of modules were computed. Figure 69B shows the best-matching module pairs of two subjects. Note that the members of best-matching modules did not necessarily have the same rank order. A complete overview of the rank order assignments of best-matching pairs of modules between all subjects is displayed in the 2D histogram of Figure 69C. The module with rank order 1 (i.e. the first PC explaining most of the data variance), and 2 showed the best consistency between subjects, i.e., the best matching counterpart of module 1 from one subject was most often module 1 or module 2 of another subject. In several cases, module components of a pair of best-matching modules had a different rank order with regard to the relative amount of variance they explained in each data set.

Surprisingly, module 10 of one subject frequently corresponded best to module 10 of another subject. Subsequent detailed analysis revealed a small-amplitude mechanical artifact as the likely origin of this module. Due to the fact that module 10 accounted for less than 0.1% of the data variance, the above conclusions are not affected by this artifact. In contrast to TMS-modules, modules derived from Structureless-PVs did not show any consistent rank order assignments (Figure 69D). Additionally, to quantify the similarity of different sets of modules, the shared subspace dimensionality between subjects was computed. A subspace was defined by the first n modules, where n corresponded to the number of modules necessary to account for ≈90% of the data variance in each subject. In contrast to best-matching module pairs, this measure is insensitive to variations in the rank order of modules. Between subjects, the shared subspace dimensionality of modules derived from TMS-PVs (TMS-modules) was 2.5 ± 0.8, indicating a substantial overlap when compared with the dimensionality of approximately four modules necessary to explain ≈90% of the variance (Figure 69E). The shared subspace dimensionality between TMS-modules exceeded the shared subspace dimensionality between Structureless-modules (1.4 ± 0.6; $p < 0.001$, two-tailed t-test). Although TMS-modules between subjects showed considerable overlap, there was also interindividual variability, possibly as a result of differences in the biomechanical properties of the hands, or of interindividual differences in the neural system. Therefore,

one might predict intraindividual similarity of the modules to be greater than interindividual similarity. To address this issue, five subjects took part in additional mapping sessions, 2 months after the first session and 1 week after the second session. Results indicate a high degree of consistency of the rank order of best-matching pairs of PCs in the same subject after three mapping sessions (Figure 70A).

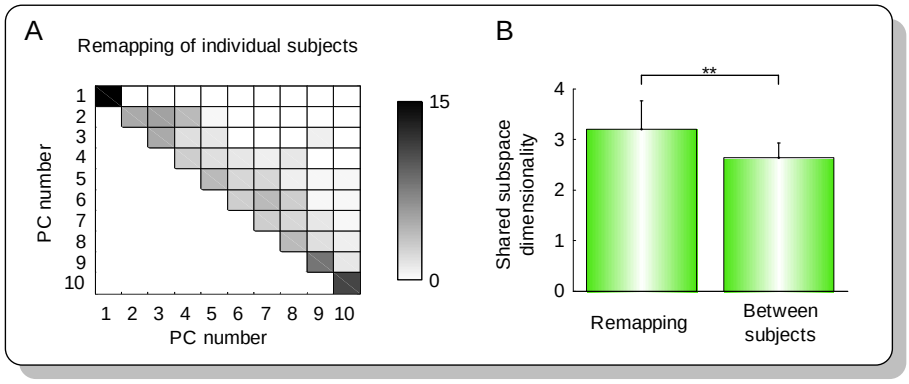

Figure 70: Similarity of modules after remapping. (A) Histogram of intra-individually best-matching module pairs (three sessions). The first modules (PC1) between sessions were always most similar to each other, indicating a high structural similarity of the modules after remapping. (B) Intra-individually and inter-individually shared subspace dimensionality (mean ± SD). **p < 0.01.

Module 1 computed from the first session always corresponded best to Module 1 in subsequent mapping sessions. Moreover, the shared subspace dimensionality (Figure 70B) was significantly higher intra-individually, between different sessions in the same subject, (3.2 ± 0.7) than inter-individually, between subjects, (2.6 ± 0.8; p = 0.007, two-tailed t-test). Therefore, the modules extracted from TMS-evoked movements likely contain individually specific features of movement organization.

Structural similarity of modules derived from TMS and grasping movements

PCA revealed that modularity was different in TMS-PVs with respect to Structureless-PVs and that the modules overlapped considerably between subjects. However, it remains unknown whether the modules derived from TMS-PVs bear any relationship to natural motor behavior. To address this question, six subjects performed grasping movements toward 28 imagined different objects displayed as images presented on a computer screen in front of them. Analysis of grasping end-postures (Grasp-PVs) generated a set of ten modules, with four of them accounting for ≈91.7% of the data variance. The variation explained by the first four modules is similar to that reported previously by Santello and coworkers [197] and similar to the results from TMS-evoked movements. TMS-modules were more similar to modules derived from grasping movements than to Structureless-modules. The histograms of the rank order assignments of bestmatching modules showed a higher degree of consistency between TMS-modules and Grasp-modules (Figure 71A) than between Structureless-modules and Grasp-modules (Figure 71B).

The shared subspace dimensionality between the TMS-module subspaces and the subspaces spanned by the Grasp-modules was 2.0 ± 0.6; i.e., two of approximately four dimensions of the TMS-modules subspace were shared with their corresponding Grasp-module subspace. Across all six subjects, the shared subspace dimensionality between Structureless-modules

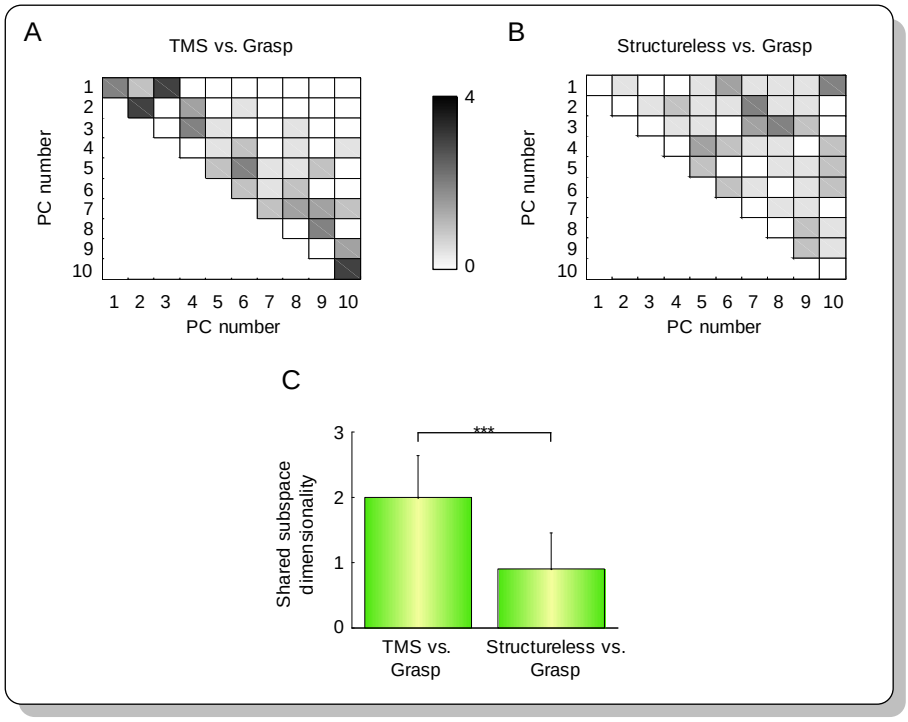

Figure 71: Similarity between Grasp-modules, TMS-modules, and Structureless-modules. (A and B) Histograms of the rank order assignments of best-matching pairs of Grasp-modules and TMS-modules, and Grasp-modules and Structureless-modules, respectively. (C) The dimensionality of shared subspaces between Grasp-modules and TMS-modules was significantly higher than that between Grasp-modules and Structureless-modules. Values are presented as mean ± SD. ***$p < 0.001$.

and Grasp-modules was 0.9 ± 0.5, and significantly lower ($p < 0.001$, two-tailed t-test) than the shared subspace dimensionality between TMS-modules and Grasp-modules.

The biological significance of modules derived from TMS-evoked movements would gain additional strong support if the TMS-modules could be used to reproduce hand postures that resulted from voluntary grasping movements. The performance of modules computed from TMS-PVs in reconstructing static grasp end-postures was compared with that of Structureless-PVs and Grasp-PVs . Figure 72A illustrates examples of reconstruction of different hand shapes adopted when grasping two different objects. As expected, reconstruction error was minimal when using Grasp-modules. The quality of reconstruction differed between Grasp-modules, TMS-modules, and Structureless-modules (ANOVA; $F(2, 39) = 46.71$; $p < 0.001$; Figure 72B). Reconstruction error associated with TMS-modules was significantly smaller than that of Structureless-modules ($p < 0.001$, two-tailed t-test), and larger than that of Grasp-modules ($p < 0.001$, two-tailed paired t-test; Figure 72B).

3.1.4 Discussion

The present study used magnetic stimulation to examine the mapping between the motor cortex and finger movements in humans. PCA revealed that a small set of approximately four modules accounted for much of the data variance of TMS-evoked movements as indexed by their posture vectors, whereas approximately eight modules were needed to approximate the data variance when the biomechanical part of the motor system was examined in isolation. Before we consider the biological significance of this finding, we have to ensure that the

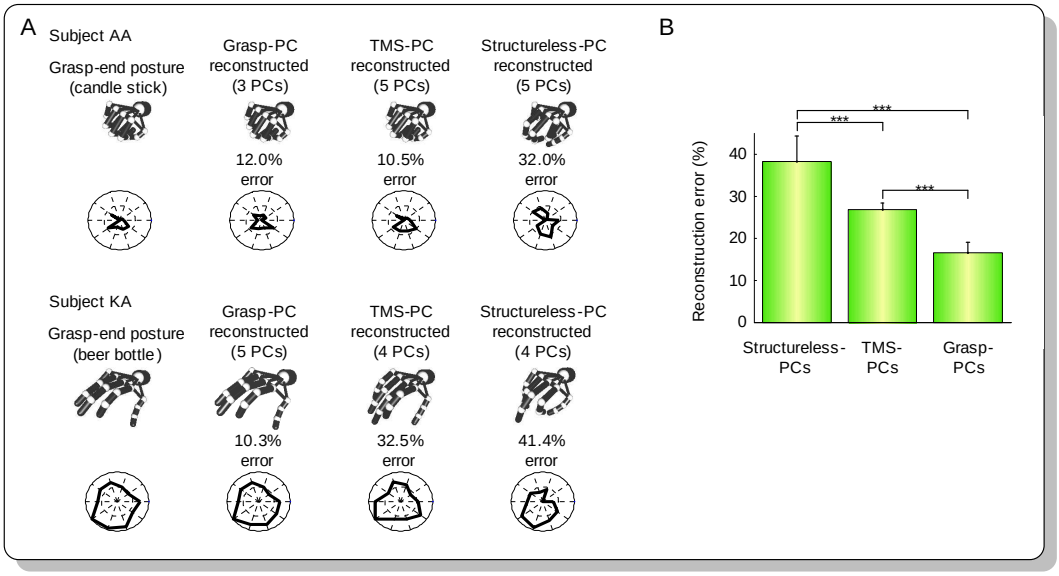

Figure 72: Reconstruction of grasping end-postures from modules. (A) Examples of reconstruction of two different postures (from subjects AA and KA) with small reconstruction errors (top row) and large reconstruction errors (bottom row). The number of modules used for reconstruction was chosen according to the number of modules necessary to explain >90% of the variance. In the case of Structureless-modules, the number was set as equal to the number of TMS-modules. (B) Mean reconstruction error (± SD, six subjects) was lowest using modules directly derived from grasping end-postures. Using TMS-modules, the reconstruction error was significantly smaller than the reconstruction error using Structureless-modules. ***$p < 0.001$.

artificial stimulation of the primary motor cortex by TMS reproduces important properties of natural movements (c.f. [233]). At least two lines of evidence support this assumption. First, TMS-evoked movements displayed properties which may be considered idiosyncratic hallmarks of the spatial representation of voluntary finger movements. Although movements evoked by TMS from different scalp positions did not display a prominent topographical organization, the spatial sampling resolution of the TMS technique was sufficient to reproduce the topographical order and dimensions of the fine somatotopical gradient found in functional MRI studies of voluntary finger movements [17, 100, 130] and in studies of non-human primates utilizing neuronal recording and stimulation techniques [208]. Secondly, previous observations demonstrated that TMS-evoked movements retain kinematic properties of recently performed movements [47]. Such phenotypical homology implies that neuronal ensembles that determine important kinematic properties of voluntary movements are physiologically similarly activated by TMS.

If these considerations supply indirect evidence for naturalistic activation of motor cortex by TMS, then the modular characteristics of TMS-evoked movements has implications for the understanding of how the primary motor cortex is engaged in the control of movements. That the finding of a small number of relevant modules is not just an artifact of the stimulation technique (despite its physiological properties) is strongly supported by the finding that modules derived from TMS-evoked movements were similar to modules derived from grasping movements. Because TMS-evoked movements and voluntary movements each comprised a wide variety of diverse end-postures, it is unlikely that this similarity arose by chance. Furthermore, the end-postures of natural grasping movements could be reconstructed with remarkable fidelity from TMS-derived modules. Based on these observations, we propose

that the structural properties of TMS-evoked movements not only unveil modularity in the ultimate output of the primary motor cortex, but also indicate that this modularity is used for movement control. In this way, our findings provide direct, and causal, evidence to suggest that the modular structure of natural grasping movements [151, 197], or signing gestures in American sign language [117], are indeed signatures of a modular principle of operation of the CNS.

Previous studies in frogs have shown that a small set of muscle activation patterns was sufficient to describe the muscle activity associated with mechanically triggered kick reflexes [243]. These muscular activation patterns were similar between different behaviors such as swimming, jumping, and walking [52]. Because they persisted even after deafferentation [46], it was concluded that complex locomotor behaviors in frogs may arise from spinal modules that are provided with the proper weighting coefficients by afferent and / or supraspinal commands [46]. When spinal structures were activated by medullo-spinal projections through vestibular nerve stimulation [51], the dimensionality of the kinematic output was similarly reduced when compared with spinal preparations. The study by d'Avella and Bizzi therefore extended the evidence of modular organization of motor behavior to subcortical, reflexively organized neuronal circuits. Because TMS activates cortical elements, the present results suggest that modular organization in neuronal systems generalizes to cortical control of movements. Therefore, the present findings indicate that the most dexterous intentional movements of higher-order mammals may share similar principles with elementary automated movements in amphibians. Our findings do not allow us to make detailed inferences about the anatomical identity and location of the TMS-derived movement modules. Given the enormous sophistication of the spinal interneuronal circuitry in primates [75], it appears unlikely that coordination of grasping movements rests exclusively upon transmission of descending corticospinal commands from the primary motor cortex onto spinal motoneurons. Although intracortical neuronal elements likely play a special role, corticospinal projection neurons, spinal interneurons, and the peripheral part of the motor system all determine the final appearance of the extracted modules (see Chapter 1.7). This may explain why Poliakov and Schieber [182] failed to find evidence for functional grouping of motor cortical neurons into modules. These authors examined discharge properties of sets of motor cortical neurons sampled from multiple distributed sites during a set of skilled, individuated finger movements. Such movements likely require the combination of multiple overlapping corticospinal modules. It is possible that the structure of these modules might not be revealed through recording exclusively the activity of a small number of cortical neurons, which may themselves be members of multiple and overlapping modules. Consistent with the idea that modularity is a property of the wholeness of the cortico-muscular system, stimulation of two motor cortical points in anesthetized cats led to vectorial summation of the responses obtained at each point individually [72], whereas intraspinal microstimulation of two points in spinalized cats did not [164].

It is noteworthy that TMS-derived modules were similar to those derived from grasping movements, despite the fact that grasping movements were indexed only by their final posture. Results obtained by Graziano and coworkers [4, 94, 93] may help to explain this finding. These authors used ICMS and recordings from single neurons of the motor cortex in monkeys to investigate principles of neuronal control of diverse and naturalistic upper limb movements. ICMS of the precentral motor cortex induced multijoint complex arm movements, with some of them resembling feeding and grasping movements [94, 93]. Centrally directed hand movements in conjunction with formations of grip postures of the fingers were clustered around

the central sulcus [93], a region overlapping the primary motor cortex in humans. A large fraction of the variance in recordings of neuronal firing behavior with natural movements was explained by neuronal tuning to preferred end-postures [4]. This model accounted substantially better for the data variance than models of neuronal tuning to direction or a variety of different alternative movement parameters. Importantly, the end-postures preferred by the neurons significantly matched the final postures evoked by ICMS of the same cortical sites. Our observations are in accord with the emerging view that neuronal tuning to final posture plays an important role in the control of movement [4, 89, 94], and they suggest that this principle may apply to the most distal upper limb movements. TMS induces only short-lasting activity (10 to 15 ms [59]) in corticospinal projections. This may be one factor that explains why the duration and amplitude of TMS-evoked finger movements differ from the ICMS-evoked full-scale complex multijoint movements, which appear to require long (typically 500 ms) stimulation trains [4, 94]. The induction of fragments of grasping movements by TMS over the primary motor cortex is consistent with the idea that different components of movements have different induction thresholds and do not necessarily depend on the duration of the stimulation. This view is supported by the facts that the distinctive features of ICMS-induced movement or muscle activation patterns may become evident already at some 80 ms into the stimulation train [93] and even after single ICMS pulses, and by previous observations that TMS at a weaker intensity than that used in the present study has a higher probability of evoking individuated thumb movements [47]. TMS-evoked movements over the motor cortex obviously lacked the arm component, which is necessary to transport the hand to the final destination. The above considerations predict that physiological signatures of such specific arm movements should be induced by TMS applied at the same sites. TMS may be particularly suited to stimulate neuronal circuits naturalistically because it activates an extended brain region through activation of intracortical horizontal fibers [191].

The results obtained here provide possibly the most direct support to date for the conjecture that a set of movement modules constitute building blocks of the most complex, highly flexible motions; they also provide evidence in favor of models of neuronal tuning to end-posture. The findings may contribute to a deeper understanding of the human motor system and may inform the design of novel neuro-rehabilitative strategies. As has been noted before [20, 181, 229], modular neuronal control may afford computational savings over approaches that rely on extraction of a number of individual movement parameters from large numbers of individual neurons. Therefore, consideration of modular principles of neural control may be of value for the design of neural prostheses driving electrical stimulation of hand muscles and the development of brain-machine interfaces that control the movements of artificial prosthetic devices [171].

The second study was conducted with the help of professional violin players and addressed how the modular structure changes after to learning of musical skills.

3.2 How skills shape the modular organization in musicians

This study addresses the effect of learning how to play a musical instrument on the modular organization of finger movements. The sensor glove, the magnetic stimulation paradigm and the grasp assessment tool are used in this investigation.

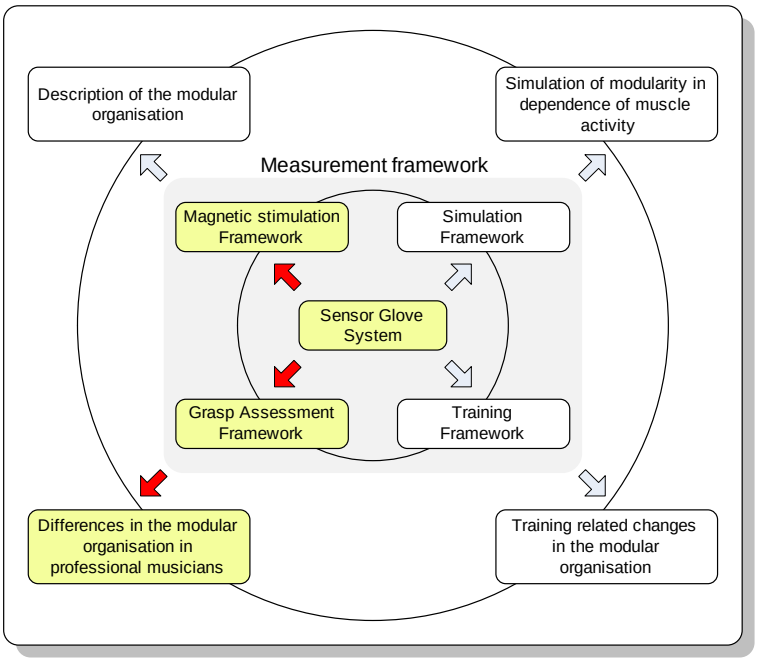

Although it is well established that the motor cortex and several other brain areas in musicians show an altered organization pattern, the significance of this reorganization pattern in relation to the trained movement repertoire and possible underlying motor control theories is still largely unclear. We combined transcranial magnetic stimulation and finger movement recordings to analyze the kinematic output of the primary motor cortex in professional and amateur violin players. We first show that the somatotopy in the right motor cortex in musicians is enlarged. Further, assuming that finger movements are generated as a linear combination of synergistic joint correlation patterns, or modules, we provide evidence that modules derived from TMS-evoked movements reflect spatial properties of typical violinist's movements in dependence of training intensity. These findings illustrate highly specific functional motor system reorganization in response to long-term training and provide strong further support for the contention that the nervous system may co-ordinate even the dexterous movements by using a modular architecture involving cortical components.

3.2.1 Background

If we applaud at the end of a classical concert we acknowledge the performance of the musicians during the concert. What we do not consider at that moment is that the way to perfect and virtuous performance requires years of intensive, continuous training and discipline.

Investigations of the neural underpinnings of sports [177] and musical skills over the last decades [18] have found structural [7, 85, 19] and functional adaptations [69, 215, 177] as well as correlates of unique, instrument specific, musical abilities [13]. Professional violin players show a pronounced left-right asymmetry in terms of the cortical separation between

thumb and little finger in the right somatosensory cortex [215, 69], the morphology of the motor cortex [13, 7], the position of the primary motor cortex output map in the right hemisphere [215], and an increased hand skill of the left hand [115]. Because partially differing results were found between violin and keyboard players [13, 115], it seems plausible that the reorganization pattern is instrument specific.

While these findings highlight the neural structures undergoing training dependent plasticity, only limited knowledge exists about the mechanisms of reorganization, the relationship to the trained movements and, especially, how these changes can be viewed with respect to possible motor control theories. In humans, TMS is a promising technique to study effect on training non-invasively and painlessly in humans [47]. Studies using this technique have shown that the cortical representation of muscles change during training [1, 110, 176] but the examination of a single or a small number of muscles or movements of a single digit may be of limited value to draw conclusions about the benefit of this reorganization in terms motor control. In the previous chapter, evidence for a modular organization has been found and its key characteristics were described. Here we investigated if training related changes can be identified and are consistent with the ideas of a modular model. Principally, musical training might lead to a reorganization of the present modules and / or to additional modules.

Here we show for violin players that, in addition to an altered somatotopical representation in the primary motor cortex, the modules derived from TMS-evoked movements of the right hemisphere adapt their shape to the trained movement repertoire and that this adaptation is linearly related to long term practice history. Therefore, our results do not only give an answer to how the motor cortex reorganizes due to learning but also provides further support that a modular architecture may underlie the control of finger movements.

3.2.2 Methods

The study was approved by the Ethics committee of the University of Wuerzburg, and written informed consent was obtained from all participants.

Participants

Finger movements were recorded after transcranial magnetic stimulation from 36 different sites over the scalp in 17 neurologically healthy right handed violin players (4 males, mean age 24.4 ± 2.2 years) and 17 controls matched for age (mean age 24.8±3.8 years), sex and handedness ('non-musicians'). Non-musicians occasionally played an instrument such as keyboard, but none of them did this regularly longer than 1h per day. Especially none of this group had ever practiced violin or viola playing. Musicians started playing their instrument at a mean age of 6.8 ± 4.0 years, only 5 of them after the assumed sensitive period in childhood for the motor component of musical training [254]. Since for violin playing especially skilled movements of the left fingers are required [115, 215], emphasis was on the right hemisphere. Musicians were divided into two groups according to their training intensity, one with low training intensity ('amateur musicians', N = 8) and the other with high training intensity ('professional musicians', N = 9). All professional musicians studied violin playing to be an orchestral musician or played a leading role in an orchestra. Additionally, musicians were asked if there was a time point where they significantly intensified their training intensity and if so, how many years this was ago. The average daily practice hours refers to

the average practice duration since this time. In comparison to amateur players, professional musicians had a higher average daily practice (3.4 ± 0.8 vs. 0.8 ± 0.5 h per day, $p < 0.001$), practiced longer the week (3.7 ± 1.7 h vs. 0.8 ± 0.6 h; $p < 0.001$) and the day (3.3 ± 2.0 h vs. 1.1 ± 1.8 h; $p = 0.03$) before the measurement.

Mapping

TMS mapping was performed as described in Chapter 2.2.2. The stimulation intensity for recording finger movements was set to 1.3 times RMT. Finger movements were recorded by a left **Wii**-Glove (a resolution of 0.2° was used) in all 17 musicians and non-musicians after stimulation of the right hemisphere, and additionally by a right **Wii**-Glove in 8 musicians and 9 non-musicians after stimulation of the left hemisphere. Glove signals were sampled at 2 kHz together with electromyographic recordings of the abductor pollicis brevis (APB) and abductor digiti minimi (ADM) muscle of the appropriate hand. Sensors considered for analysis were located over the proximal interphalangeal (PIP) and metacarpal-interphalangeal (MCP) of the index (I), middle (M), ring (R), little (L) finger joints. For the thumb (T), sensors over the MCP and interphalangeal (IP) joints were considered.

Somatotopical representation of finger movements

To estimate the extent to which a single finger moved at each stimulation site, an activation map for each finger was calculated (see Chapter 2.2.5). The extent of the somatotopical representation was quantified as the distance between the thumb CoG and the little finger CoG.

Modularity analysis

Principal component analysis (PCA) was used to represent the PVs as a small set of principal components (PCs, modules) that can be linearly combined to reconstruct the original dataset. The movement action of a module was visualized using a virtual model of the human hand by adding to and subtracting the module coefficients (scaled by a factor of 40) from the mean resting position across all subjects. To rule out that the results were influenced by the statistical assumptions underlying PCA, we additionally analyzed some of the results with the SMF technique (Chapter 2.2.7). With this method, the number of extracted modules was set to 4, because PCA revealed ≈4 modules to explain most of the data variance.

Reconstruction of violin exercises

The modular approach to motor control states that complex movements are generated as (linear) combinations of the modules. Here we considered the modules derived after TMS as the building blocks (bases) of complex movements and assessed how well they were suited for reconstruction of movements, typically for violin playing. 8 of the 9 professional musicians had their instrument with them and played 20 s of two standard musical exercises with the glove worn on their left hand. The movements were reconstructed by finding the optimal weighting coefficients $\mathbf{C}$ to solve the equation

$$\mathbf{WC} = \mathbf{M},$$

where **W** contains the modules derived from TMS-evoked movements and **M** the time course of the active violin exercise. As a measure of similarity between the original violin movements, **M**, and the reconstructed movements, **WC**, the two dimensional correlation coefficient described in Chapter A.6 was used. A correlation coefficient of 1 indicated a perfect reconstruction of the violin exercises. In addition to the violin exercises, grasping movements were assessed using the grasping framework described in Chapter 2.3.

Statistical Analysis

Analysis of variance (ANOVA) were used to compare the CoGs of different fingers, the results of module similarity and the comparison of reconstruction of violin exercises. Two-tailed t-tests and paired t-tests were used where appropriate. All values are presented as mean ± S.D. unless indicated otherwise.

3.2.3 Results

Basic physiological parameters

Resting motor threshold (RMT) and the stimulation intensity, were similar (ANOVA, F = 0.98, p = 0.388) between non-musicians (N = 17, RMT of 39.1±5.5% of the maximum stimulator output; 50.1±7.1% stimulation intensity), amateur musicians (N = 8, RMT of 42.1±6.7%; 54.8±8.7% stim. int.) and professional musicians (N = 9, RMT of 42.0±7.2%; 54.6±9.4% stim. int.). Except one professional musician, who reported mild headaches after TMS, there were no reports or observations of any discomfort or adverse effects during and after TMS. There was no difference in the number and the size of TMS-evoked movements between groups. Furthermore in all groups approximately the same number of individual finger movements could be evoked.

Somatotopical representation of finger movements

Previous studies have shown an increased separation of the thumb and little finger in the somatosensory cortex of the left hemisphere of professional violinists [215]. Here we extend these findings to the motor cortex. The CoGs of movement representations of individual fingers in the right hemisphere differed significantly in non-musicians (ANOVA, F = 8.38, p < 0.0001), amateur musicians (ANOVA, F = 6, p = 0.0009) and professional musicians (Figure 73).

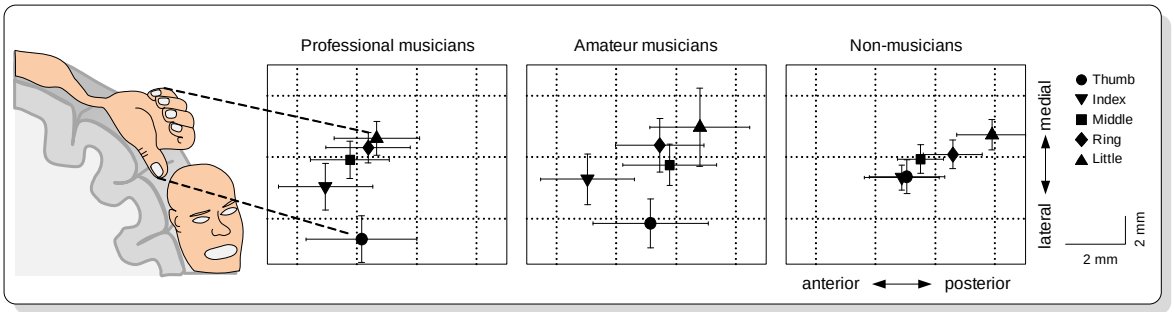

Figure 73: The somatotopic separation between the thumb and the little finger was enlarged in professional violinists.

The distance between thumb and little finger CoGs, a commonly used marker for the size of the somatotopic segregation [17, 215] was enlarged in professional musicians (6.6±3.1 mm) when compared to non-musicians (2.7±3.1 mm, p = 0.006). The segregation of thumb and little finger in amateur musicians did not differ significantly to the other groups (6.3±6.0 mm). In the left hemisphere, the separation was similar to the right hemisphere but there were no differences between groups (ANOVA, F = 0.51, p = 0.61). Thus, the results support previous findings of an asymmetric cortical representation of individual fingers. Here we could additionally show that this asymmetry is also present in the primary motor cortex. The functional role of the separation is unclear, but indicates that the left motor cortex has undergone reorganization due to learning. In the next section we ask if the kinematic reorganization patterns can be identified using a modular approach.

Number of modules explaining most of the data variance

As hypothesized by the modular model presented in Chapter 1.7, training of motor skills might lead to the adaptation of existing modules and / or to the build up of new modules. As shown in Figure 74, the cumulative variance explained by the modules did not differ significantly between non-musicians, amateur musicians and professional musicians, suggesting that the basic modular structure as identified by PCA is only weakly affected by musical practice.

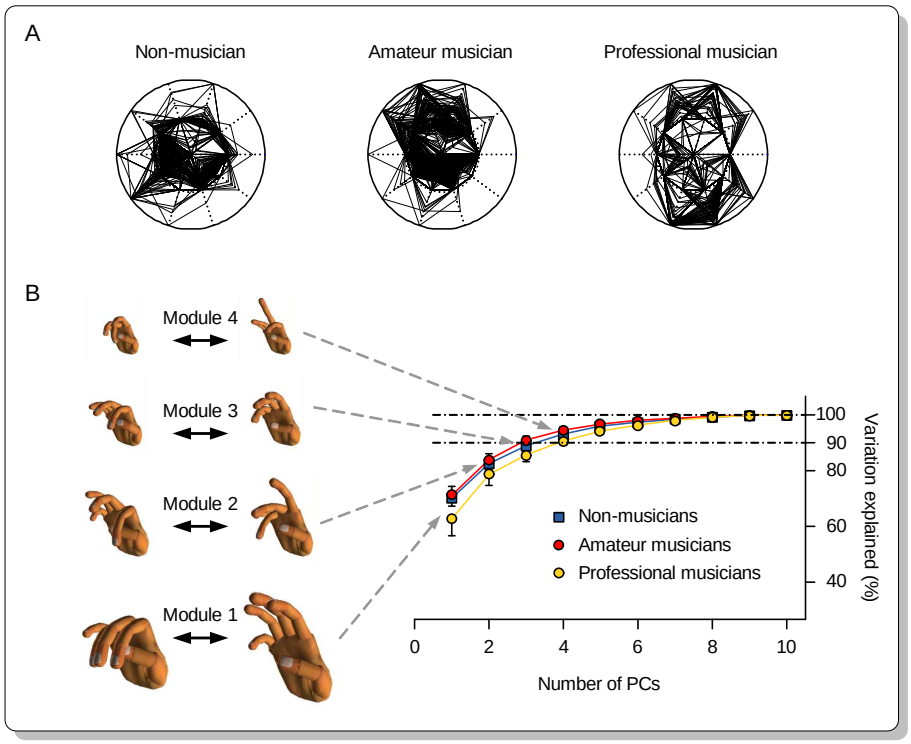

Figure 74: The cumulative variance explained by the modules was similar between groups. In professional violin players, a single modules explained slightly less variance as compared to the other groups.

To quantify the number of relevant modules needed to explain most of the data variance, the first n modules that explained > 90% of the data variance were retrieved. There was no difference in the number of modules between the groups (ANOVA, F = 0.98, p = 0.39). For non-musicians 3.5±1.2, for amateur musicians 3.3±0.7 and for professional musicians, 4.0±1.3 modules were needed to account for > 90% of the data variance. We also tried several

other methods to extract the number of modules, such as the fractal number of modules needed to account for $> 90\%$ of the variance, the Kaiser criteria [97], cross-validation of the reconstruction quality, and a scree-test like method similar to the method used by [46]. No method revealed a significant difference in the number of modules. Thus, in terms of a modular architecture investigated with PCA, violin learning did not lead to an increase in the number of modules. A second possibility might be that modules reorganize to possibly simplify the conduction of skill related movements 1.7.

Training related reorganization of existing movement modules

Training of musical skills might lead to a reorganization of existing modules. Using PCA this would indicate that neurally coded joint correlations change, possibly mimicking joint correlations of the musical skill. This kind of reorganization would indicate that the structure of the primary motor cortex reorganizes to generate skill related movements more efficiently and faster in a feed-forward manner. To address this question, 8 of the 9 musicians professional musicians played two typical training pieces (taken from Flesch: Das Skalensystem and Kreutzer: 42 Etueden oder Capricen) for 20 s with a metronome paced speed of 1 Hz on their own violin. These are common violin training exercises, which are normally executed before concerts and during training lessons. In fact, all musicians knew these pieces and could play them without any difficulty. The movements of the left hand were recorded with the sensor glove worn during playing. Figure 75B (green lines) illustrates an example of a musical exercise played by a musician.

Joint excursion about the resting position before the start of the movements, are visualized in the time-angle plots. The time course of the joint excursions was reconstructed from TMS-modules (Figure 75A) by a standard least squares algorithm using the first four modules from non-musicians, amateur musicians and professional musicians as a basis. This reconstruction procedure is a generative model how the neural controller could combine modules derived from TMS-evoked movements to construct complex voluntary behaviors. The quality of reconstruction of the violin exercises by combinations of the first four modules was expressed as a correlation coefficient (see Chapter A.6) between the reconstructed data set and the original movements.

The group correlation coefficient was calculated as the mean across the two musical exercises for all possible combinations of subjects and musical exercises. For example for the non-musicians, $17 \cdot 8 = 136$ different mean correlation coefficients across the two exercises existed. For musicians, comparisons of the same subjects were not considered in this analysis. If the first four modules derived from TMS-evoked movements of the left hand were considered, a significant difference in reconstruction quality between groups existed (ANOVA, $F = 6.84$, $p = 0.0013$). There was no difference in reconstruction quality between non-musicians (correlation coefficient of 0.65 ± 0.09) and amateur musicians (0.64 ± 1.03, $p = 0.61$). However, the reconstruction quality of the musical exercises using modules from professional violin players (0.69 ± 0.07) was significantly higher than in non-musicians ($p = 0.0005$) and in amateur musicians ($p = 0.0017$). Group data is shown in Figure 76A.

The same qualitative results were found if three (ANOVA, $F = 6.62$, $p = 0.0016$) modules or four modules computed with the SMF technique were used for reconstruction (ANOVA, $F = 13.38$, $p < 0.0001$). Thus, if the number of modules is kept constant for analysis, training of musical skills leads to an adaption of the modular structure to the kinematic demands of the

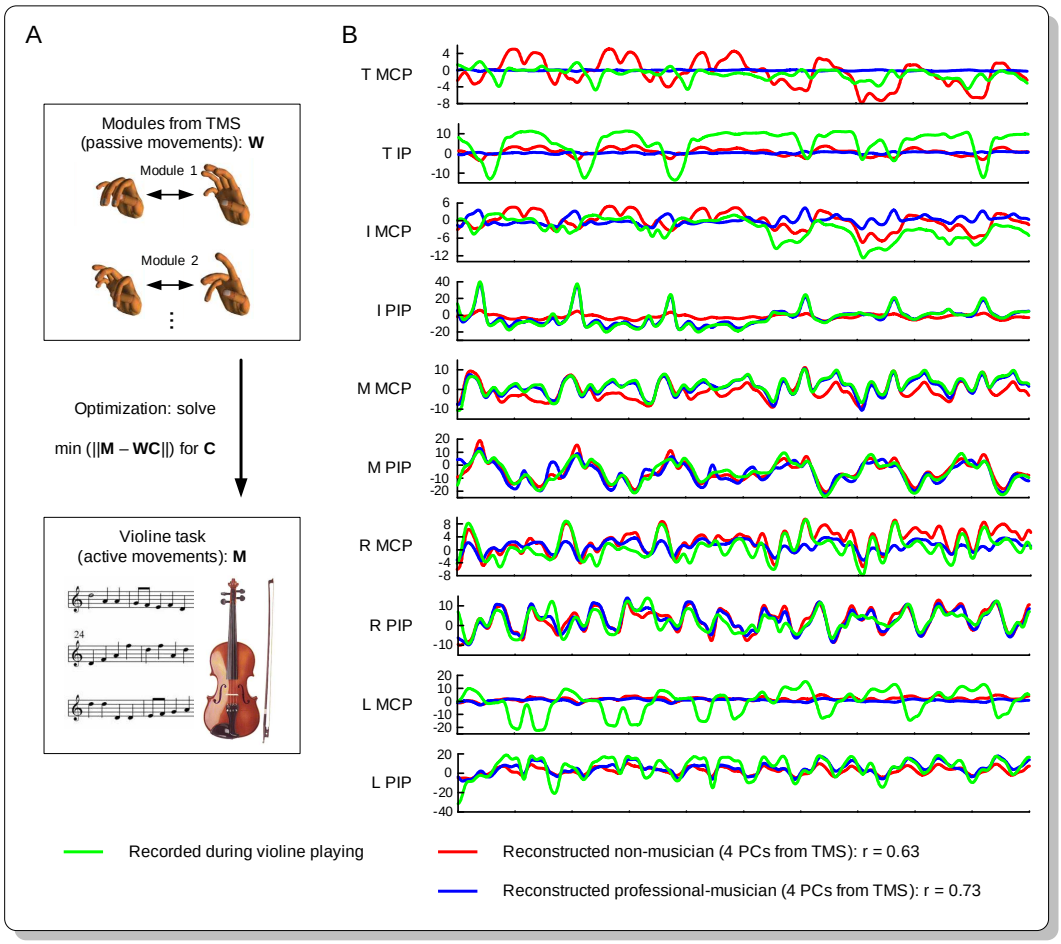

Figure 75: The time course of the recorded violin exercises was reconstructed by finding the best linear combinations of the first four modules from violinists and non-musicians. Examples from one violinists and one non-musician are shown.

motor skill. If the violin exercises were reconstructed using the first four modules obtained from TMS of the left hemisphere (i.e. movements of the right hand, 9 healthy subjects and 8 musicians, 4 professional musicians) a similar pattern resulted (ANOVA, $F = 3.06$, $p = 0.05$, see Figure 76B). The reconstruction quality was higher in professional musicians (0.70 ± 0.06) compared to amateur musicians (0.65 ± 0.09, $p = 0.02$) and non-musicians (0.66 ± 0.08, $p = 0.02$) indicating that also the left hemisphere, which is not as heavily engaged in violin playing as the right hemisphere, had adapted its structure to the kinematics of the skill trained with the left hand. However, this happened to a lesser degree because the differences were not evident if 3 modules were considered. This result suggests that some transfer between the hemispheres has taken place, consistent with the finding that the ipsilateral hemisphere influences finger movement control [11] and motor learning [67]. A hypothesis that emerges is that violin players may be able to play their instrument with the other hand.

Specific reorganization of the most important modules beyond biomechanics

The influence of biomechanics was quantified by comparing the reconstruction quality of violin exercises from the corresponding professional with the mean reconstruction qualities of violin exercise from the other musicians. The reconstruction quality was slightly higher in individual comparisons (0.72 ± 0.10) than in comparisons between subjects (0.69 ± 0.05) but not statistically different ($p = 0.33$, two-tailed paired t-test). Thus, the influence of individual

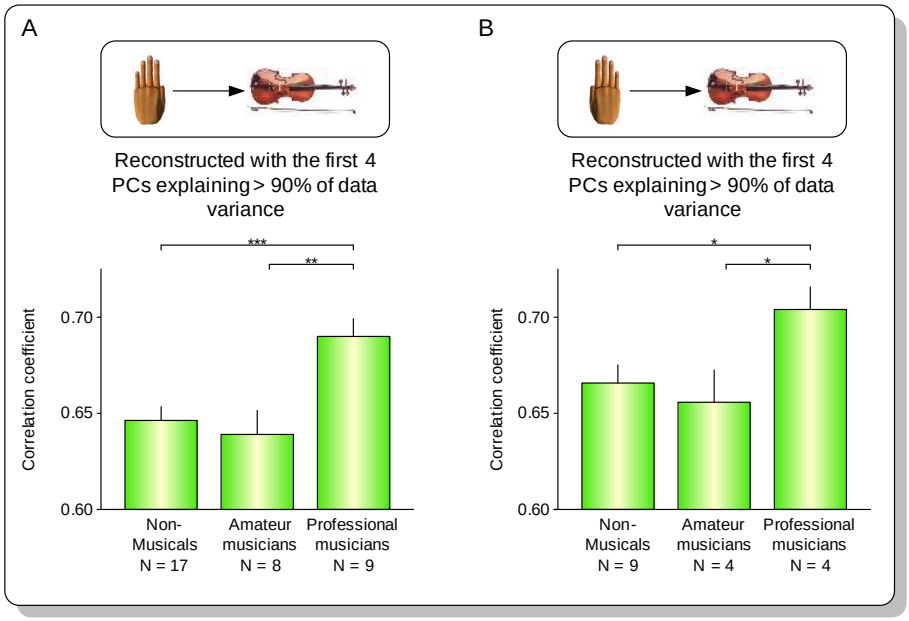

Figure 76: (A) Generally, the reconstruction quality was best using modules from professional violinists. Reconstruction quality with modules from amateur musicians was similar to non-musicians. (B) Using modules obtained from TMS-evoked movements of the right hand, similar results could be identified.

biomechanics with regard to the reconstruction quality of violin movements appears to be low. Taken together with the fact that there were no differences in the biometric measures of hand size between the groups, it is unlikely that the results may be an artifact of greater similarity of the peripheral motor apparatus in professional musicians.

Similarly, to rule out that the reconstruction quality did not increase because an unspecific reshaping of the modules, the reconstruction procedure was repeated with shuffled datasets. For each musician, the posture vectors were shuffled between trials but without shuffling between the joints. This ensured that the variance of each joint (and thus the entire variance) did not change. The first four modules from the shuffled datasets were used to reconstruct the violin exercise movements. The reconstruction performance in the shuffled datasets was significantly ($p << 0.001$) worse compared to the reconstruction with modules from the original dataset, indicating that an unspecific reshaping does not lead to a superior reconstruction quality of a trained motor skill (Figure 77A). Furthermore no significant differences between the three groups in terms of the reconstruction quality existed (ANOVA, $F = 2.81$, $p = 0.06$).

We additionally investigated if the training related reorganization was evident in the higher order modules. The reconstruction of violin exercises was repeated using the last four (which accounted for $< 10\%$ of the data variance) instead of the first four modules. Again the reconstruction was worse in all three groups (non-musicians: 0.61 ± 0.08, $p < 0.001$, amateur musicians: 0.60 ± 0.10, $p = 0.01$, professional musicians: 0.59 ± 0.11, $p < 0.001$) compared to the reconstruction using the first four modules. However, more importantly, there was no difference in reconstruction quality between non-musicians, amateur musicians and professional musicians (ANOVA, $F = 1.71$, $p = 0.1828$) indicating that training related reorganization is only expressed in a small number of modules explaining most of the data variance (Figure 77B). Similar results were found if the last three modules were used (ANOVA, $F = 0.03$, $p = 0.97$). Thus, musical skills are reflected mainly in the first modules explaining most of the

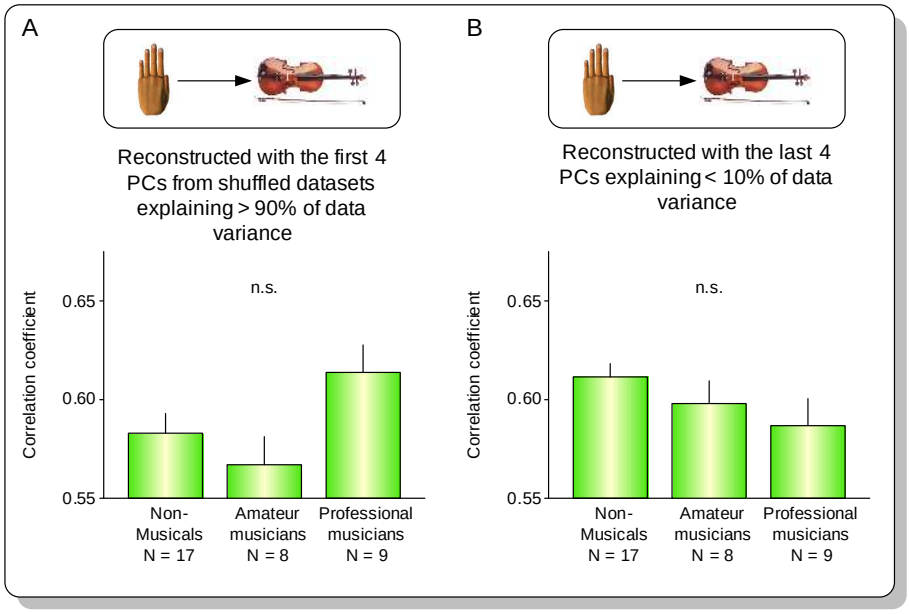

Figure 77: (A) Training related effects were absent if modules calculated from shuffled datasets were used or (B) the last 4 modules explaining < 10 % of the data variance were used for reconstruction.

data variance as identified by PCA.

Relevance of the reorganization for grasping movements

We further asked how the skill dependent reorganization of the right hemisphere is related to voluntary grasping movements of the left hand. Grasping movements of professional violin players to 51 different virtual objects were reconstructed using the first four modules (Figure 78). There was no difference in the reconstruction quality between groups (ANOVA, $F = 0.01$, $p = 0.993$).

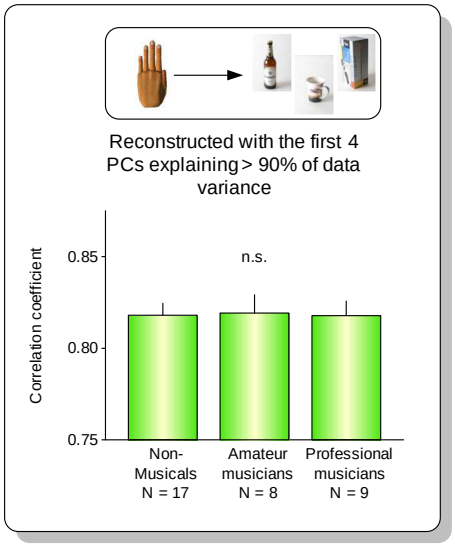

Figure 78: No differences with respect to the reconstruction quality of grasping movements existed.

Additionally, the reconstruction quality was significantly higher (0.82 ± 0.08 for all groups,

p << 0.001) compared to the reconstruction of the violin exercises indicating that grasping movements are different from violin movements and a smaller number of modules are necessary to obtain the same reconstruction quality as with the violin exercises.

Dependence of the reorganization on previous training history

Finally we asked how the mean reconstruction quality for each professional musician across violin exercises depends on the previous history of practice (only the left hand was considered). Since none of the violin players had practiced on the day of the measurement, short term plasticity effects are not likely to be involved. Rather the reorganization might be long-lasting and might depend on the daily training duration. This, however, was not the case. There was no correlation to the practice duration on the day before the measurement, no correlation between the average practice duration on the week before the measurement and also no correlation if the overall average daily practice duration was considered (Figure 79).

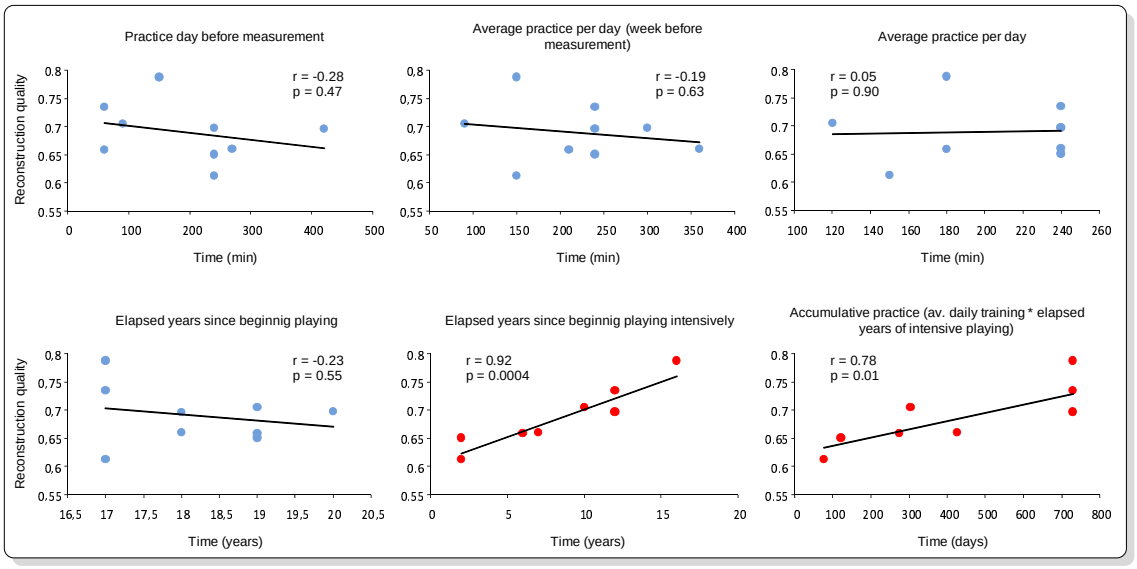

Figure 79: Reconstruction quality in profession violinists depended on the years of intensive practice and the accumulated practice duration.

However, if the number of elapsed years of intensive practicing (3.4±0.8 h per day) was considered (8.8±4.8 years ago), there was a strong correlation to the mean reconstruction quality (r = 0.92, p = 0.0004). Similarly, the accumulated practice duration (calculated as the product of the elapsed years at which each musician started professional playing and the average practice duration per day) strongly correlated with the reconstruction quality (r = 0.78, p = 0.0123). The results suggest that the reorganization of the primary motor cortex for these skilled movements depend on the long term history of intensive practice and consequently on the accumulated amount of practice. The recent training history of the day and week before does not significantly influence the organization of the motor cortex.

3.2.4 Discussion

We investigated how long term learning of musical skills affects the modular organization of TMS-evoked finger movements. First we found that the somatotopical separation between thumb and little finger is asymmetrically enlarged in the right hemisphere. Second,

the structure of TMS-modules explaining most data variance adapted to the typical violin movements. Grasping movements were not affected indicating that these are different to violin movements. Unspecific reshaping of the modules does not account for the greater reconstruction quality. Training related adaptation is not reflected in higher order modules describing only a small fraction of variance. Finally, the adaptation of the TMS-modules to the trained movement repertoire as a marker of plasticity significantly correlated with the accumulated practice over the years and not with the recent training history.

Naturalistic activation

Critical for the reliability of our findings is that TMS activates the motor system naturally. In support for this pre-requisite we found that the somatotopical separation closely resembles findings obtained during active finger movements using functional resonance imaging [17, 100, 130]. Furthermore, the asymmetric enlarged somatotopical separation in the right hemisphere of the motor cortex is in accordance with the same asymmetry in the somatosensory cortex [215, 69] and consistent with functional alterations of grey matter thickness and different anatomical alterations of the sulcus length in the right hemisphere of violin players [13]. The increased separation between thumb and little finger did not correlate significantly with any training related parameter. However, we found a reduced somatotopical separation in multiple sclerosis patients with poor hand function using the same experimental paradigm. Thus, the somatotopical separation appears to represent a rather unspecific measure for adaptive and maladaptive plasticity.

Training related changes in a modular architecture

We further asked how this asymmetric reorganization is related to the pattern of TMS-evoked finger movements and, if so, how it is related to the trained movement repertoire. Within the modular approach, finger joints are not considered to be controlled individually, but by the combination of synergistic movement patterns, or modules. Training of violin did not result in additional modules which would be equivalent to an increased degrees of freedom that allow more individual control of finger joints. In contrast, the existing modules adapted to the trained movement kinematics. Since modules extracted with PCA reflect multi-joint correlations, our results indicate that simultaneous moving joints (or simultaneous co-contracting muscles) in the behavior come to be represented together in the cortex to build up a neurophysiological correlate of a motor skill. Similar conclusions were drawn in studies of muscle excitability in humans [1, 110] and monkeys [172, 3]. However, the results obtained here represent a significant departure from these earlier studies. First, we performed the experiments in humans in conjunction with real life motor learning and not with learning in experimental conditions. Second, because of the quantitative data recording of finger kinematics, the results could be statistically analyzed and compared to the trained motor skill. Doing so, we found differences between the left and right hand, between grasping and typical trained movements and could relate these results to the amount of training. Third, our approach does not only highlight neurophysiological changes due to motor learning but also gives new insights into the control architecture of the CNS.

Implications for motor control

In terms of a single optimal control process the control signals for movement execution are generated dynamically and flexibly. Within this framework muscle and kinematic modules observed during voluntary movements may be a consequence of the optimal control process [239]. Here we provide evidence that the existence of modules have a neurophysiological correlate, related to the acquired motor skills and therefore may not be the only consequence of the control process, at least for finger movements. The finding that these training related effects are represented in modules favors the control of the hand as a unit [197, 151] and not in terms of single joints, fingers [117] or muscles [248]. Importantly, the adaptation of the modules is compatible with the concept of generalization, which distinguishes motor skills from elementary motor memories [181]. Generalization represents the ability to apply what has been learned from limited experience to new situations: although none of the violinists had extensively trained the exact movements required to play the compositions, their modules allowed a better reconstruction than these of non-musicians. The re-organization of the modules, which may be viewed similar to the problem of fitting a multivariate function to a certain number of measurement data, possibly reduces the computations necessary to execute movements associated with the motor skill (see Chapter 1.7). A consequence may be that the required movements can be executed faster, and more automatically freeing up cortical resources for other processes [213].

Skilled violin playing movements do not appear to have strong correlates in normal motor behavior and the maintenance of motor skills usually affords continuous and extended training. One reason for this may be to encounter genetic and other processes [4, 92] which continuously [175] re-adapt the organization back to a representation sufficient to account for evolutionary developed movements, such as grasping. We also found evidence for transfer of the re-organization to the left hemisphere, which suggest that the training of one hand may have consequences for the control of the other hand and may explain the sometimes reported transference of musicians' Dystonia from one hand to the other [256].

Our results are relevant for the motor learning in terms of adaptation of the CNS as a marker for plasticity and its relation to the training intensity. Since none of the musicians practiced on the day of the measurement, the re-organization is likely a sort of long term plasticity [118, 3]. Indeed, results on training piano exercises suggest that the effects of one-week training have a correlate of several days in the motor cortex [1]. We found that the degree of adaptation of the modules depends on the accumulated long term training history, especially on the elapsed years where musicians started to practice intensively. Short term practice duration the day before the measurement and the week before did not significantly influence the adaptation. Thus, the elapsed years of intensively practicing an instrument is a predictor for the adaptation of the motor cortex to the kinematics of the motor skill. Our concept might be highly relevant for all forms of learning and may have a direct practical application to objectively assess the success of a motor training embedded in a theoretically and practically well founded control architecture. With this approach, rehabilitative settings and procedures may be optimized to distinguish between different methods and parameters.

Conclusions

Using TMS we found a neurophysiological correlate of violin playing in professional musicians. Adaptation of the cortical organization due to behaviorally co-contraction has been

proposed earlier [172]. Here we provide quantitative evidence in humans that these suggestions may be correct. In terms of joint correlations, the kinematics of the trained movements are neuronally coded in the motor cortex possibly to allow faster and more automated execution of trained movements freeing cortical resources to other processes [213]. Further, we were able to link this representation to the amount of practice in professional musicians. Based on these results, the question arises whether the structure of modules may also be malleable in the short-term. This issue was addressed in the third study.

3.3 Short term training affects the modular architecture

Based on the results of the study how musical skills affects the modular organization, this study addressed if and how the modules adapt to repetitively conducted movements.

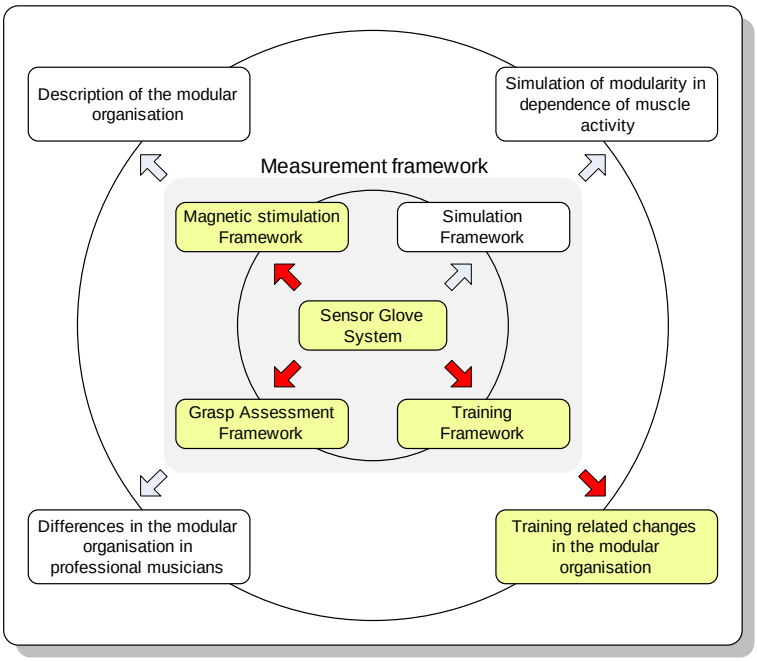

Extensive training involving repetition of movements and actions is required to acquire many motor skills. Cortico-muscular motor synergies may be viewed as storage devices for such motor skills. Repetition of stereotyped elementary movements triggers temporary representational changes in the motor cortex, a kind of motor memory, which specifically reflect kinematic details of the trained movement. It remains unknown how repetitive movements relate to motor skill acquisition. Here we show that repetition of complex movements specifically shapes movement modules. These findings establish a link between repetition-induced formation of short-term motor memory and skill learning. Subjects trained on a highly constrained combined index-finger and thumb flexion movement. Finger movements were evoked at rest by transcranial magnetic stimulation (TMS) delivered over the primary motor cortex. Voluntary training movements, simple grasping movements, and TMS-evoked finger movements were recorded by an instrumented glove. The training target movement was reconstructed from principal components (PCs), derived from TMS-evoked finger movements. The training effect was quantified by comparing the quality of reconstruction from PCs obtained before and after the training. Following the training, reconstruction fidelity of the training target movement increased, while reconstruction fidelity of elementary grasping movements remained constant. Reconstruction quality correlated linearly with overall training performance, but not with the performance gain recorded at the end of training. These findings suggest that the cortico-spinal system builds specific memory traces of recently practiced movements of considerable complexity.

3.3.1 Background

The acquisition of new motor skills requires frequent repetition which leads to performance improvements. It has been suggested that short lasting traces of recently practiced movements in the primary motor cortex may represent one of the steps preliminary to the acquisi-

tion of a motor skill [131, 67]. Especially the repetition of stereotyped elementary movements triggers representational changes which specifically reflect kinematic details of the trained movements [47]. These changes require the repetition of active movements [122], depend on neuromodulating transmitters [40, 201, 199, 200, 154, 81], become already manifest during motor observation [231, 43], or can be enhanced by concurrent observation of one other's movements [230], are less pronounced in older adults [81, 201] and proximal upper limbs [133], influence the ipsilateral hemisphere [67] and may be accomplished by the formation of an efficient network in the primary motor cortex that is specific for the trained movement direction [161]. Despite this wealth of information on plasticity it remains unknown whether kinematic specificity of plasticity is retained also with complex movements and how this plasticity is related to motor skill acquisition. Furthermore many influencing factors are well established but it is not known how the reorganization depends on factors directly related to the training, such as behavioral performance gains or on the spatio-temporal consistency of movement repetition. Understanding the neurophysiological underpinnings of movement repetition may also be important for optimizing rehabilitation strategies [38]. Here, the measurement framework is used to identify the determinants of plasticity after repetition of complex finger movements and to embed the findings in the modular model introduced in Chapter 1.7. Assuming that finger movements are generated by the combinations of modules, we show that the modules adapt their shape to the intended target training movement, a similar effect that occurs after years of skill acquisition. Additionally, we provide evidence that the quality of the training, i.e. the spatio-temporal consistency of the trained movement, is a crucial factor for building up specific memory traces of recently practiced movements of considerable complexity.

3.3.2 Methods

The study was approved by the local ethics committee and written informed consent was obtained from every participant. None of the participants had neurological, psychiatric, or other medical problems or any contraindication to TMS. Twenty one healthy volunteers (9 females, mean age 27.3 $\pm$ 6.0 years) participated in this study.

Experimental procedures

A **Wii**-glove for the right hand was used to record finger movements after transcranial magnetic stimulation (TMS). The subject's right arm was fixed in a cast in a semipronated position with the hand approximately 40 cm in front of the chest. The optimal position of the magnetic coil for eliciting motor evoked potential (MEPs) in the resting APB muscle was assessed at a moderately suprathreshold stimulation intensity. At this site, termed hotspot, the resting motor threshold (RMT) was determined as the lowest stimulation intensity needed to produce a MEP greater than 50 μV in at least 5 out of 10 trials. The glove was put on and the TMS coil was positioned over the hostpot to apply 120 stimuli applied at a rate of 0.2 ($\pm$ 10%) Hz (Figure 80). After the baseline measurement, the subjects performed grasping movements to 51 imagined objects seen on a computer screen in front of them. Then, information on the subject was entered into the database of the training system and a new training session was created. For each subject an individual training target movement was recorded consisting of a synergistic flexion of the thumb and index finger. Figure 81 shows example movements from three subjects. Afterwards the training was started. The

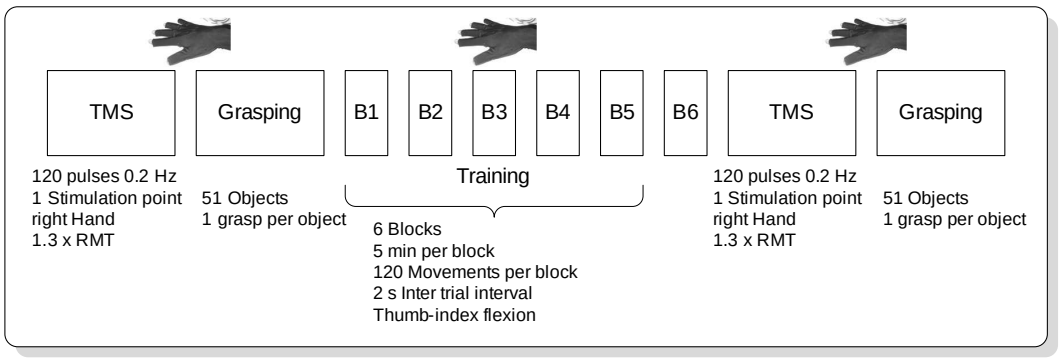

Figure 80: Experimental procedure. 120 TMS-evoked finger movements were recorded from one stimulation site. Additionally, subjects performed grasping movements to 51 different objects. The training consisted of 6 blocks, each lasting 5 min. The target movement was a synergistic flexion of the thumb and index finger, recorded individually for each subject. After the training, finger movement recording after TMS and grasping was repeated.

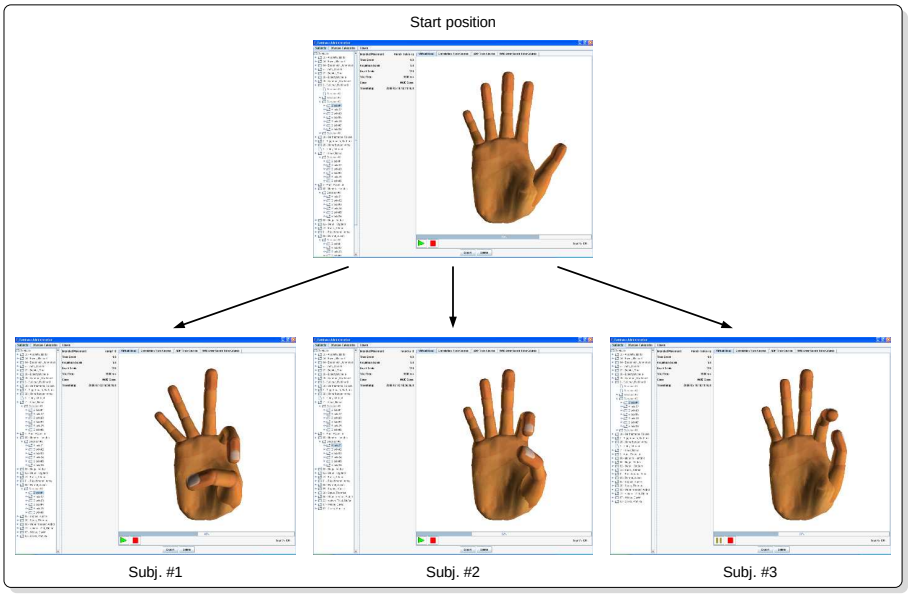

Figure 81: The target movement consisted of synergistic flexion movements of the index finger and the thumb. After the movement, subject returned to the start position. Examples from three subjects are shown.

training session was divided in 6 training blocks each separated with a pause of 1 min. A block consisted of 120 trials repeated every 2 s. In each trial, the target movement was presented to the subject by a virtual teacher [101]. Subjects also saw their own movements in real time in the computer screen and could therefore adapt their movements to the virtual teacher. Every 10 trials, the visualization changed between the HandColorInterpolator, the Two-Hand-View and the Two-Dim-Mapping view. After every 10 trials a performance bar indicated the mean performance (correlation coefficient) over the last 10 trials. The subjects were instructed to imitate the target movement of the virtual teacher as exactly as possible.

After the last block, TMS was applied again to elicit 120 finger movements, recorded by the sensor glove. Finally, the grasping procedure was repeated (Figure 80).

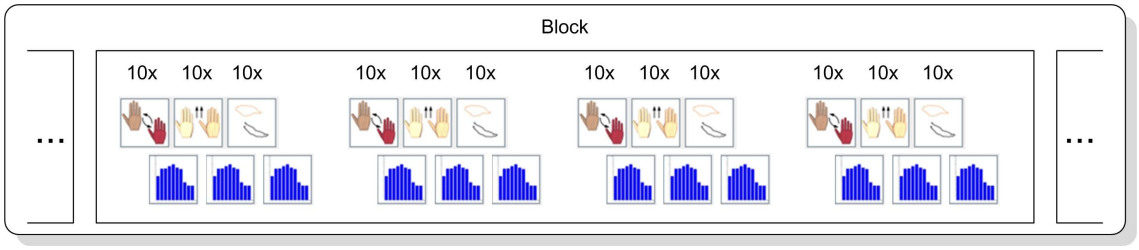

Figure 82: Every 10 trials the visualization changed between the HandColorInterpolator, the Two-Hand-View and the Two-Dim-Mapping view. After every 10 trials a performance bar indicated the mean performance (correlation coefficient) over the last 10 trials.

Statistical Analysis

Two-tailed t-tests and paired t-tests were used where appropriate. All values are presented as mean ± S.D. unless indicated otherwise.

Reconstruction of the target movements

The modular approach to motor control is that complex movements are generated as (linear) combinations of the modules. Here we considered the modules derived by PCA after TMS as the building blocks of complex movements and assess how well they were suited for reconstruction of the target movement before and after training. The target movements were reconstructed by finding the optimal weighting coefficients $\mathbf{C}$ to solve the equation

$$\mathbf{WC} = \mathbf{M},$$

where $\mathbf{W}$ contains the modules derived from TMS-evoked movements (without any voluntary movement) and $\mathbf{M}$ the time course of the active conducted target movements. The target movements were reconstructed with modules from the corresponding subject. As a measure of similarity between the original target movements $\mathbf{M}$ and the reconstructed target movements $\mathbf{WC}$ the two dimensional correlation coefficient introduced in Chapter A.6 was used. A correlation coefficient of 1 indicated a perfect reconstruction of the violin exercises.

3.3.3 Results

None of the participants reported any discomfort or adverse effects during and after TMS. The resting motor threshold was 39.7 ± 5.9% of the maximum stimulator output and the mean stimulation intensity used for TMS was 51.6 ± 7.6%.

Evaluation of training visualization

The first aim was to identify (for further studies), which training visualization is best suited to imitate the target movement and how the visualizations are related to subjective feelings of the subjects. The similarity of each trial to the individual recorded target movement was quantified as a correlation coefficient of two matrices. The mean correlation coefficients across blocks are visualized in Figure 83A. Subjects significantly increased their performance during the training from 0.52 ± 0.14 in the 1^{st} block to 0.70 ± 0.10 in the 6^{th} block ($p << 0.001$), indicating that the task to imitate the virtual teacher spatially and temporally

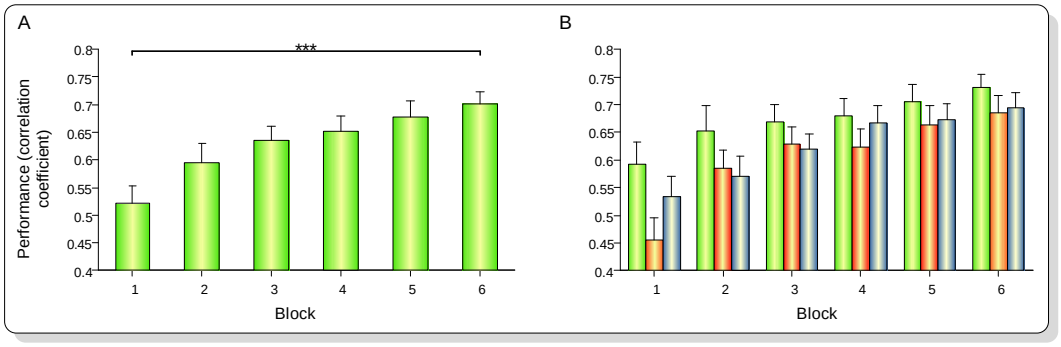

Figure 83: Similarity between the target movement and the conducted movements steadily increased during training. (A) Mean correlation coefficients for each blocks across visualizations are shown. (B) Mean correlation coefficients for each block and for each visualization. Performance increased for all visualizations. Green bars: Color Interpolator; red bars: Two hand; blue bars: Two Dim Mapping

congruent was learned during the training. To analyze the task performance for each visualization technique, the mean correlation coefficient for the same visualization (40 trials per block) was calculated for each block. The correlation coefficient did not differ significantly between the three visualization techniques in the first (ANOVA, $F = 3.06$, $p = 0.054$) and in the last block (ANOVA, $F = 0.76$, $p = 0.47$). However, the performance with the Color Interpolator visualization tended to be somewhat superior to the other two visualization techniques (Figure 83B). With all three visualizations, the performance was better in the 6^{th} block when compared to the 1^{st} block ($p < 0.001$).

In addition to objective performance analysis, the subjects were asked to judge the visualization techniques with 1 coding the best and 3 the worst. This subjective rating was done to investigate if a training method is rated bad or good in dependence of the performance, or if a method is generally not preferred.

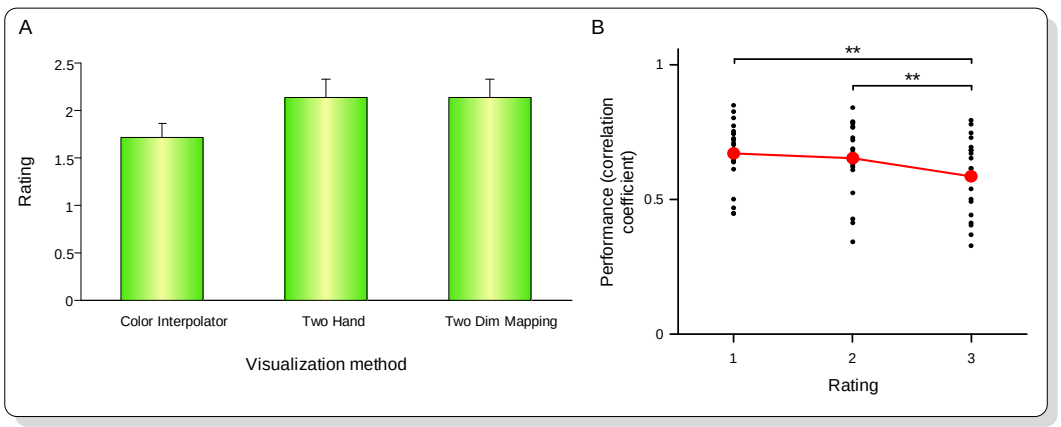

Figure 84: (A) Subjective ratings of visualization methods by the subjects. There was no preference for a certain visualization technique in general. (B) Rather, the visualization method, in which a good performance was achieved was rated best.

No differences in the rank order between visualization techniques existed, suggesting that the visualization technique is preferred with which a good training performance is achieved (Figure 84A). This was quantified by assigning of the normalized mean training performance for each subject to the ratings. A significant performance difference between the ratings existed (ANOVA, $F = 6.26$, $p = 0.0024$). The performance in the best rated visualization

was significantly larger than the performance in the worst rated visualization ($p = 0.003$) and the performance in the second best rated visualization differed significantly from the worst rated visualization ($p = 0.013$, see (Figure 84B). These results indicate, that no visualization is a priori good or bad. It depends on the subjects and how they perform in a certain visualization technique.

Adaptation of the cortical organization to the target movement

We have shown that modular description can describe disease related reorganization and long term reorganization due to intensive musical skill learning. Here we investigated, if and how repetition of short duration of simple movements leads to a re-organization of the modular organization. Further we evaluate how this is related to training performance. Short term training might affect the number of modules or the shape of the modules.

Since only one scalp site was stimulated the number of modules was somewhat smaller than in our previous mapping studies where 30-36 points were stimulated. However, there was no difference between pre and post training. Before training, 2.8 ± 0.9 modules were needed to explain > 90 % of the data variance, after training 2.7 ± 0.7 ($p = 0.79$). Several methods did not result in a different number of modules. In musicians we could show that the organization of the motor cortex adapts to the trained movement skill and that this reorganization is related to long term practice. Here we investigated if movement repetition leads to a short term memory of a similar nature. For each subject, the target training movement was reconstructed by finding the best fitting coefficients to minimize the reconstruction error. A correlation between the reconstructed target movement (by the modules) and the target movement served as a measure of how the primary motor cortex has adapted to the kinematic profile of the target movement.

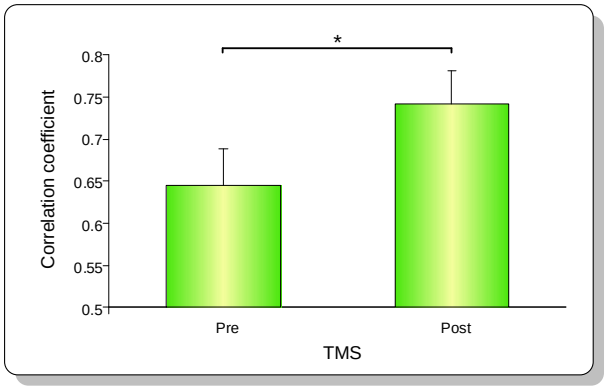

Figure 85: Reconstruction quality (as index by a correlation coefficient) of the target movement by modules derived from TMS-evoked movements increased after training.

Using 4 PCs, the reconstruction quality of the target movement before training was 0.65 ± 0.20. After training, the target movement could be reconstructed significantly ($p = 0.015$, paired t-test) better from the modules derived from TMS-evoked movements (0.74 ± 0.18), indicating that the structure of the primary motor cortex has adapted to the spatial structure of the trained target movement (Figure 85). There were no differences in reconstruction quality of grasping movements ($p = 0.12$).

Determinants of training-dependent plasticity

In previous studies examining the kinematic changes after repetitive execution of simple movements could not identify determinants of training dependent plasticity with regard to the trained movements. Using this training system, a target movement could be defined and training related parameters such as the performance or the increase of performance during the training could be assessed quantitatively. Here we examined how two relevant parameters affected the amount of adaptation of the primary motor cortex to the target movement. The amount of adaptation was defined as the difference between the reconstruction quality of the target movement (by TMS modules) before and after training (rec_post - rec_pre). Thus, a higher positive value indicated a higher amount of adaptation. First, it may be that the performance gain, i.e. the increase of the similarity of the conducted movement to the target movement in the last block compared to the first training block, determines the amount of adaptation. However this measure did not correlate significantly with the amount of adaptation (r = -0.05, p = 0.85), suggesting that for motor repetition, the increase of performance gain is not a crucial factor triggering the amount of plasticity in the primary motor cortex.

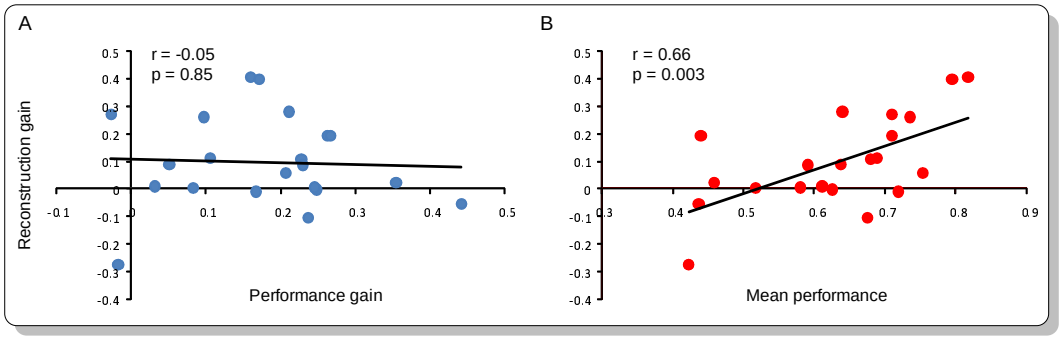

Figure 86: (A) There was no relationship between the increase in reconstruction quality and the performance gain. (B) A significant correlation between the increase in reconstruction quality and mean performance across blocks existed.

Second, not the increase of performance, but the mean absolute performance during the training, i.e. the quality of reproducing the target movement might trigger cortical plasticity to adapt to this movement. As a measure of performance, the mean performance across all six blocks was calculated. In contrast to the performance gain, the mean performance during the training significantly correlated with the amount of adaptation (r = 0.62, p = 0.003). Similarly, if only the performance of the last block was considered, a comparable correlation resulted (r = 0.56, p = 0.008).

3.3.4 Discussion

We showed that subjects were able to train complex synergistic thumb-index flexion movements with the help of the training system. The reconstruction quality of the target movement from modules derived from TMS after the training was significantly enhanced compared to the reconstruction quality from modules obtained before the training. The increase of reconstruction quality was correlated to the training performance.

The training system allowed a visualization of the target movement and the presentation of performance feedback during the training, increasing the motivation and driving plas-

ticity mechanisms [213]. Furthermore, for the first time a performance measure of the spatio-temporal characteristics of the finger movements to be trained could be calculated and compared to the actual conducted movements. The finding that all subjects enhanced their ability to imitate the spatio-temporal characteristics of the target movement at the training with all visualization methods indicates, that a motivation was high and a sort of learning has occurred. Visualizations were not rated as good or bad a priori but rather depended on the individual performance. Since the rating of the HandColor interpolator visualization was slightly better than the others, and also positively influences plasticity by activating the mirror neuron system [231, 188], this method might be the preferred choice in future experiments. Further developments of the training system could include optimizing the visualization techniques and the testing of alternative techniques to present the target movement, for example using auditory feedback.

What is stored in the motor cortex?

The increase of the reconstruction quality of the target movement with TMS-derived modules after training indicates an adaptation of the cortical structure to spatial characteristics of the target movement. Our findings are consistent with earlier studies showing that the direction of TMS induced thumb and index finger movements change according to the training direction. However, the results obtained here represent a significant departure from the analysis of simple movements. With the repetition of simple movements [47] and using intracortical recordings [88] it was suggested that the movement direction is neuronally coded. The present results suggest, that it is not the movement direction per se but repeated muscle activation patterns. This notion is not a contradiction but a generalization of the storage of movement direction: If a movement in a certain direction is trained, the muscle patterns used during training are strengthened and the resulting TMS-evoked movement is a necessary consequence of this. In contrast, the movement direction coding hypothesis cannot explain cortical reorganization, which might occur if not a certain movement direction is trained but co-movements of different fingers. In summary, our results provide the first quantitative evidence in humans that lower movement parameters in terms of muscle cocontractions resulting in finger joint couplings are the building blocks of movement induced plasticity. The reconstruction of grasping movements was not affected by the training. This finding can be interpreted 1.) that the reorganization that occurs during movement repetition is constrained by maintaining phylogenetically older behaviors and 2.) that grasping movements, which are believed to consist of only two fundamentally movement pattern [167], can be executed by different organizational structures of the primary motor cortex.

A link to motor skill learning

Little is known up to date how movement induced short term plasticity is related to motor skill learning and long term plasticity. In professional violin players we have found an enhancement of the reconstruction quality of typical violin associated movements restored from TMS-derived modules. The reconstruction quality did not correlate with recent training history of the day before the measurement or the average training duration in the week before the measurement. Rather, there was a highly significant relationship between the reconstruction quality and the accumulated practice over years. Interestingly the nature of this plasticity was similar to the results obtained in the current study: an adaptation of the

organization of the primary motor cortex to the kinematics of the trained movement. Thus, short term plasticity might be related to the acquisition of a motor skill in the sense that a correlate of a trained movement is directly and temporarily stored in the motor cortex. If a motor skill, consisting of not only one movement, but a whole repertoire of movements [213] is trained, the short term memory traces might be reinforced and optimized for the motor skill to become robust and persist permanently, as seen in professional musicians. Furthermore the fact that these training related effects can be efficiently and plausibly described by the adaptation of principal components, provides further evidence for a modular organization of finger movements.

The results are not only important for the understanding of motor learning and motor control in general. They also have consequences for motor learning in real life. If we learn a musical instrument, the adaptation of the motor cortex to the skill might be best if we try to repetitively repeat the typical required movement. Doing so, the goodness of the spatio-temporal repetition profile, i.e. the consistency of the repetitive execution of the movement to be learned (and the amount of repetition) is crucial for its storage in the CNS. Finally, the finding that the adaptation of the reconstruction quality of the target movement correlated with the mean performance and not with the performance gain indicates that functional improvements might not be the crucial factor driving the storage of new motor skills. Rather functional improvements, or the minimization of variability, might be a first step to modulate cortical plasticity. This notion is equivalent to the 1st step of the Bernstein theory of skill acquisition [170, 20]. In the last study, the effect of random muscle activity on TMS-evoked movements and the modular organization is investigated.

3.4 Modular properties are determined by neuronal organization

The simulation system was used to investigate to which degree TMS-evoked movements are constrained by biomechanical couplings. Furthermore, it was assessed to which degree voluntary grasping movements can be reconstructed from kinematic modules computed from joint excursions after random muscle activity compared to physiologically obtained modules.

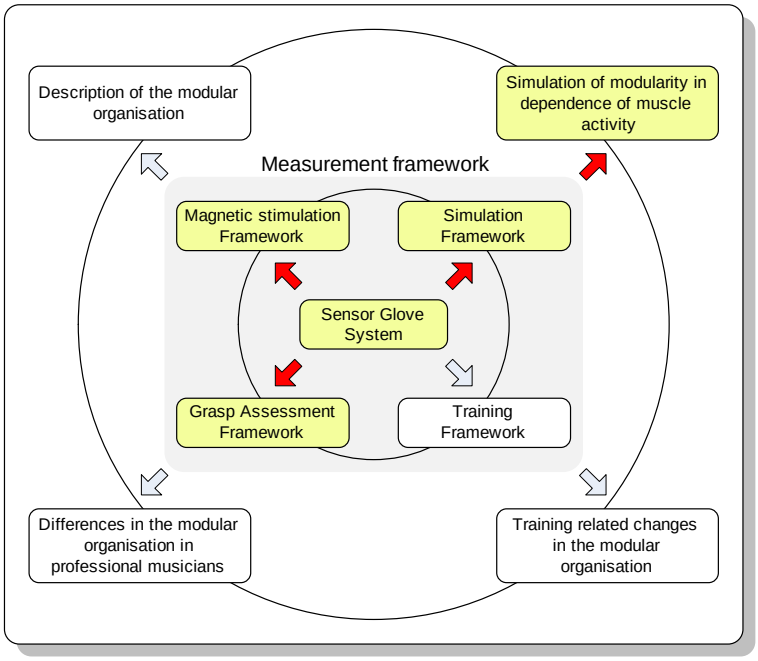

3.4.1 Background

The aim of the simulation is to understand the results of modular properties of TMS-evoked finger movements. Since the link between muscle activity and finger movements cannot be addressed by solely recording finger movements and the recording of a large set finger muscles is methodologically complex, this relationship was investigated using the dynamic hand model introduced in Chapter 2.2.4. Specifically it was evaluated, which properties kinematic modules would exhibit after random excitation of muscles and how these modules are related to modules derived from TMS-evoked movements.

3.4.2 Methods

Finger movement simulation

A Matlab control script was implemented, which iteratively simulated the resulting movements from different muscle activation profiles. After a simulation run had stopped, the posture vector of the simulated joint excursions was extracted and stored in a similar data structure as TMS-evoked movements (Figure 87). The simulation conditions were chosen to approximately match the conditions from the TMS stimulation. The simulation duration was set to 800 ms. After 200 ms without an action (baseline), an abrupt muscle contraction (100 ms) of one or several muscles was simulated. The simulation stopped 500 ms after the end of the muscle contraction (Figure 87). During this period, the fingers returned to baseline because of the equilibrium mechanism implemented in the model. The magnitude

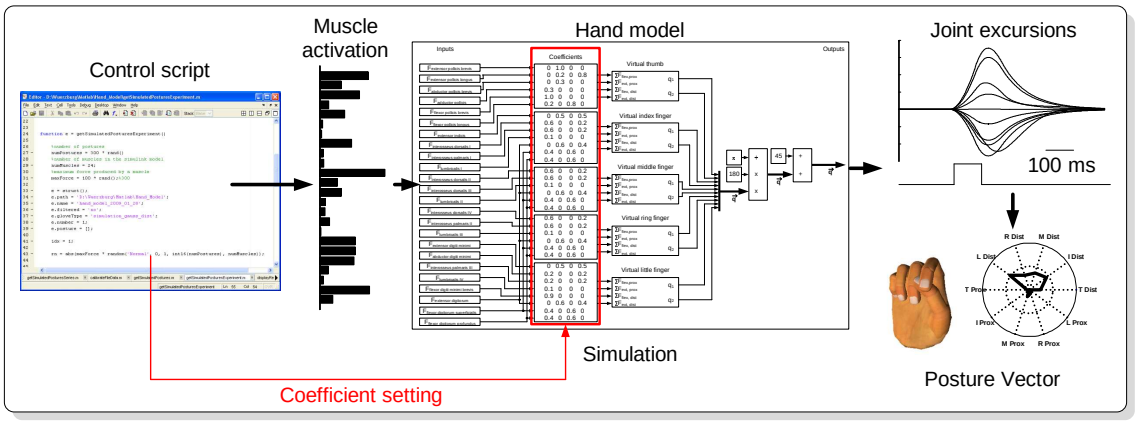

Figure 87: Simulation setup. A control script generates random muscle activation pattern and feeds them into the simulation model. From the simulated movement, a posture vector is extracted and stored in data-structs. To simulate different hand anatomies, the muscle connection coefficients were changed for different datasets.

of the muscle forces was chosen to result in movements of approximately the same size as in the TMS experiments. Fifteen datasets consisting of a random number (normally distributed) of simulated movements (and resulting posture vectors) were created. To account for the fact that human finger and hand anatomy individually varies, the muscle connection parameters (i.e. the muscle force - joint torque relationships) were modified by adding or subtracting a random, normally distributed constant to the constant weighting coefficients (Figure 87 red rectangle) for each dataset. Note that this modification did not change the connection pattern of the muscles but only the amount of force transferred to the joints. The generation of a dataset consisting of 150 posture vectors (i.e. 150 simulation runs) took about 15 minutes. The random muscle force pattern for a simulation run was generated from a right sided Gaussian distribution with zero mean and a standard deviation of one (Figure 88A and B).

Recording of TMS-evoked finger movements

To compare simulated datasets with experimentally obtained data, TMS mapping was performed as described in Chapter 2.2.2 in 15 healthy, right handed subjects. Eight of the 15 subjects also performed grasping movements to 51 different objects as described in Chapter 2.3.

Statistical Analysis

Analysis of variance (ANOVA), paired t-tests and Pearson's correlation coefficient were used where appropriate. All values are presented as mean±S.D. unless indicated otherwise

3.4.3 Results

The dynamic simulation model approximately matched the human hand and the number and location of the sensors mounted on the sensor glove. Thus, the simulated data sets could be analyzed exactly the same way as the datasets obtained after TMS. Since TMS-evoked movements and simulated movements were small (≈1-2°), it was assumed that several char-

acteristics not considered in the hand model (such as muscle dynamics or tissue couplings) did not significantly influence the types of movements recorded here. Furthermore, the human hand has much more and sophisticated tendon, muscle (compartments), and dynamic interactions [211], perhaps allowing a more complex joint innervation scheme as described here. Thus, the results may represent a lower bound scenario as obtained with more detailed hand models.

Basic movement parameters

Fifteen datasets were created. Figure 88 shows an exemplary muscle activation profile, which was iteratively fed into the dynamic hand model. For simulation of finger movements after random muscle activation (Figure 88: 70 simulations), each muscle was activated with Gaussian normal distributed values (Figure 88B). The resulting temporal pattern of finger movements after simulation (Figure 88C) and TMS (Figure 88D) were similar both in magnitude and duration. From the time point of maximum amplitude (dotted lines), the posture vectors (see Chapter 2.2.4) were extracted. Three resulting hand posture vectors from each

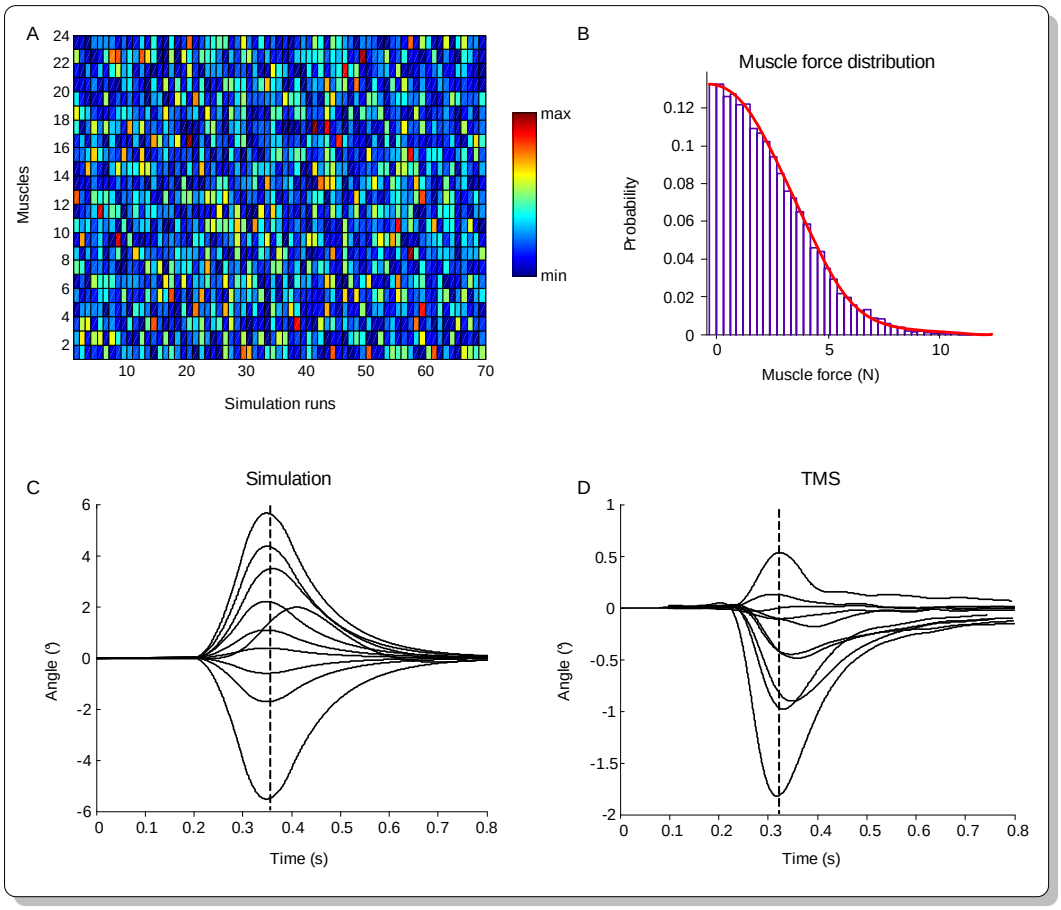

Figure 88: (A) Activity patterns of the 24 muscles for generation of a dataset consisting of 70 simulated movements. (B) Random values for each muscle were chosen from a Gaussian normal distribution. (C) Example joint excursions of one simulated movement. The temporal and spatial profile of simulated movements was similar to TMS-evoked movements (D).

group are shown in Figure 89. For better visualization, the posture vectors were scaled by a factor of 40 and added to a resting position that approximately matched the position of the hand during assessment of finger movements with TMS. Generally, there was no difference

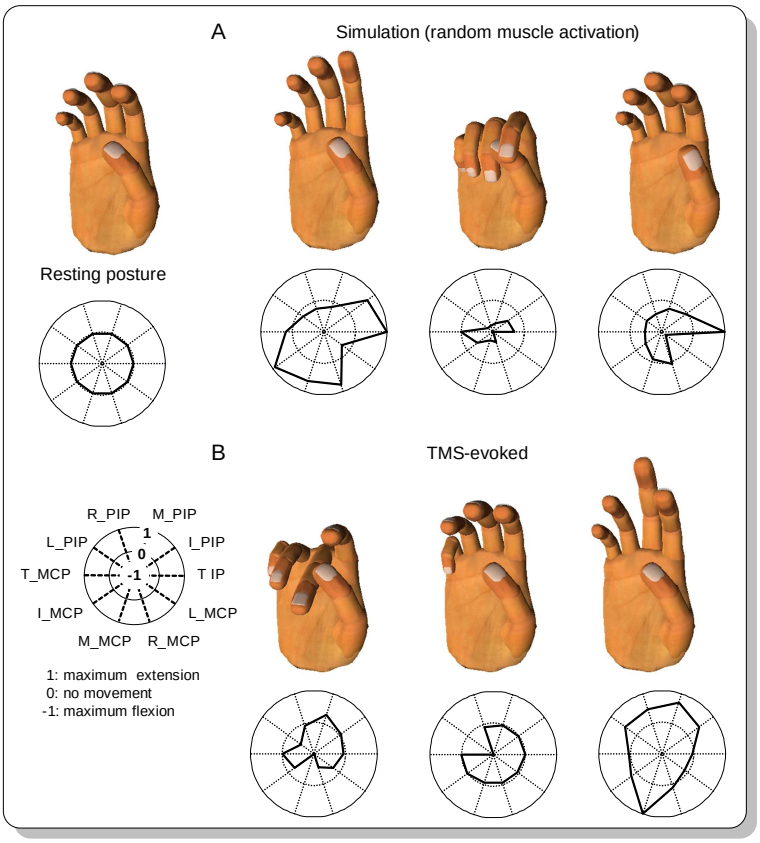

Figure 89: Examples of posture vectors obtained from simulated (A) and TMS-evoked (B) movements.

($p = 0.29$) in magnitude of the evoked movements (random muscle: $2.31 \pm 3.55°$, TMS: $2.29 \pm 2.46°$), no difference ($p = 0.12$) in the number of movements (random muscle: 183.27 ± 77.09, TMS: 222.67 ± 54.57) and no difference in the movement duration (see Figure 88C and D). As a next step, the modular properties inherent in the posture vectors were analyzed.

Module similarity between group members

Principal component analysis was used to extract kinematic modules from the PVs obtained from simulated datasets and TMS-evoked movements (Figure 90A). As a measure of intra-group variability, the shared subspace dimensionality (ssd), using the first 4 modules was computed. With respect to this measure there was no difference ($p = 0.19$) between simulated (1.86 ± 0.63) and physiologically (1.97 ± 0.64) obtained datasets (Figure 90B). Furthermore, the allocation consistency of most similar module pairs between data sets of each group (Figure 90C and D, respectively) was comparable. These two measures indicate, that the coefficient variation in the simulated datasets mimicked intra-subject variations of modules derived from finger movements evoked by TMS and validate the assumptions taken during the modeling process of the hand.

Variance explained by the modules

Since the groups were not different in structural variability of their datasets, it was assumed that they were comparable and mainly differ in the mode of muscle excitation. As a measure

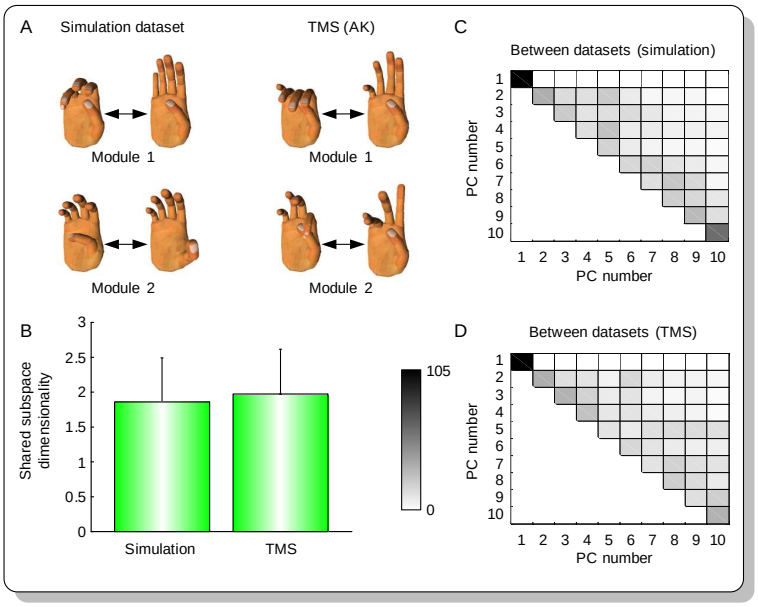

Figure 90: Intra-group similarity of modules. (A) Visualization of the first (PC1) and second (PC2) module. (B) The shared subspace dimensionality did not differ between groups. (C and D) The rank order assignments of best matching module pairs were similar between groups. These results indicate that the variation parameters of the simulated datasets matched anatomical variations between subjects.

of how random muscle activation contributed to the relative variance explained by the modules, the eigenvalues of each module were summed and plotted against their number. For the individual and random muscle activation datasets, less variance was explained by the first modules, resulting in a less steep curve compared to TMS-evoked movements (Figure 91A). As illustrated in Figure 91B, the number of modules necessary to explain > 90% of the data

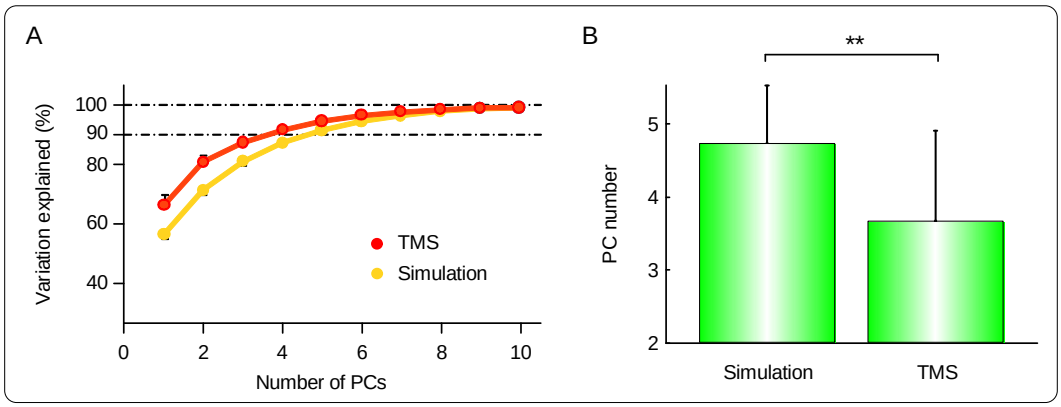

Figure 91: (A) Visualization of the cumulative variance explained by the modules. For modules derived from simulated datasets, the curve was less steep, indicating that most of the variance is shared among a larger number of modules. (B) The number of relevant modules was quantified by the 90 % method. A significantly larger number of modules were needed to account for > 90 % of the variance in simulated datasets than in TMS datasets.

variance differed significantly ($p = 0.009$) between simulated random muscle activation (4.73 ± 0.80) datasets and TMS-evoked movements (3.66 ± 1.23). The variance explained by the first modules derived from simulation tended to be less as compared to experimental data. These results suggest, that TMS-evoked finger movements contain constraints imposed by

the cortical system and not only by biomechanics [137] (see Chapter 1.4). Furthermore we asked if the structure of the most important modules differ in their capacity to reconstruct voluntary movements.

Relationship to grasping movements

It was investigated how the modules were suited to reconstruct voluntary grasping movements. Eight of the 15 healthy subjects performed grasping movements to 51 different objects. The first 4 modules from each dataset were used for reconstruction of grasping movements. Figure 92 shows that the reconstruction quality of grasping movements was sig-

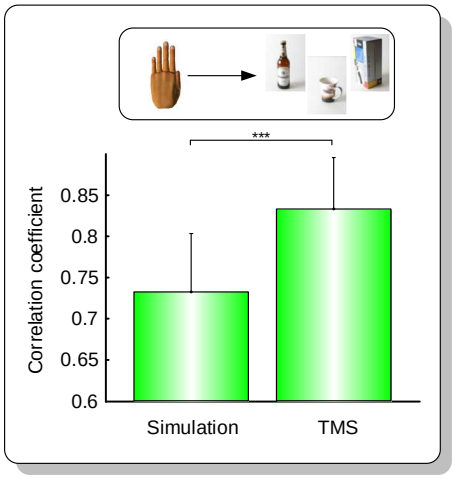

Figure 92: Reconstruction of grasping movements was significantly worse with the first 4 modules from simulated datasets as compared to TMS-modules.

nificantly lower ($p << 0.001$) using modules from the random muscle activation simulation ($r = 0.73 \pm 0.07$) as compared to modules from TMS-evoked movements ($r = 0.83 \pm 0.06$). Thus, despite similar modular properties across datasets, finger movements resulting from random muscle activations were not sufficient to reconstruct voluntary grasping movements with a sufficient quality. The capability to produce the correct kinematic pattern of grasping movements, therefore, is likely to be stored in neuronal networks beyond biomechanics.

3.4.4 Discussion

Using an approximative hand-like simulation model and appropriate simulation conditions, macroscopically similar movements could be generated with respect to TMS-evoked movements. Intra-individual variations due to different biomechanics were mimicked by varying the muscle connection patterns as revealed by the similar shared subspace dimensionality and similar module allocations in the groups. The simulation gave insights into the muscle activation patterns that caused the movements.

TMS modules are shaped by neuronal and biomechanical couplings

By feeding the model with random muscle activation, less variance was explained by the first modules as compared to modules derived from TMS-evoked movements. The findings obtained here support the hypothesis that, principally, the CNS is able to weaken

and strengthen the representation of the output modules, i.e. that biomechanics couplings (see Chapter 1.4) are not the only constraints inherent in TMS-evoked finger movements. Candidate mechanism for the adaptation of the kinematic output structure are short term plasticity (LTP and LTD), reactivation of silent synapses, or synaptogenesis [160, 3]. All these mechanisms may change the connections between neuronal structures and muscle excitation and finally kinematics. The re-organization may be triggered by learning of musical skills (see Chapter 3.2), or repetition of movements (Chapter 3.3). For example, if a desired skill to be learned would be completely independent movements of single finger joints, one strategy to neurally simplify the execution of those movements may be to weaken the cortical representation of the flexor digitorum profundus, the flexor digitorum superficialies and the extensor digitorum, which move several fingers and joints at a time [206]. The rationale behind this idea is that co-movements of other fingers do not have to be compensated any more during individual finger movements. We modeled such a scenario by creating 10 new simulated datasets (random muscle activations), in which the muscle force produced by the aforementioned muscles were decreased by a factor of 20. Such a modification could

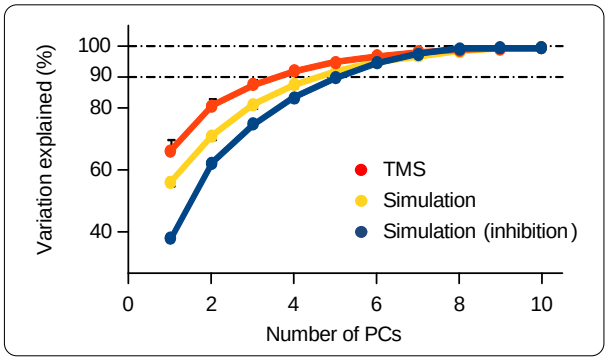

Figure 93: Example of changing the modular structure by inhibiting muscle activities of extrinsic finger muscles.

mimic neuronal inhibition of the representation of those muscles. As would be predicted, the variance explained by each module and the similarity (ssd) between dataset decreased, indicating that neural reorganization changed the kinematic output without a change of the biomechanical components (Figure 93). Conceptually similar processes may have happened in musicians during years of practice or during short term movement repetition. However, in real life motor learning, the capacity of such reorganization may be more complex than inhibiting single muscle representations and is likely not entirely flexible but constrained by homeostatic, genetic, behavioral and other factors [4].

Neuronal networks are necessary to produce human behavior

The results obtained here indicate that TMS-evoked movements in healthy subjects contain modules with cortical components relevant for generating typical human behavior. In healthy subjects, musicians and multiple sclerorsis patients, the capability to reconstruct grasping movements at a high fidelity was found to be present in TMS-evoked movements. In all groups, widely differing in hand function, the reconstruction was higher than with the modules derived from random muscle excitation. Thus, distinct physically present modules mediate human grasping behavior and this capability is maintained during motor skill learning and during injuries of the cortical nervous system, such as in multiple sclerosis.

We observed changes in the modular structure in musicians and in healthy subjects after movement repetition. Interestingly, the proportion of variance explained by the extracted modules did not systematically change in any condition. Motor learning, therefore, cannot generally be associated with a change in the variance explained by the extracted modules. Rather, the nature of re-organization in terms of variation explained by the extracted modules may be dependent on the task to be learned.

In summary, the simulation environment is capable of building a bridge in the understanding of TMS-evoked finger movements and muscle patterns producing finger movements. It is a useful tool to systematically study the effect of muscle activations on evoked finger movements and may also have a practical application for motor learning. Furthermore, pathologic changes can be described in order to optimize rehabilitational strategies.

4 Conclusions

The aim of this thesis was to develop a measurement framework to investigate hand motor control from different perspectives and to investigate the hypothesized underlying modular organization of finger movements. In four different, but related studies, strong experimental support for a modular organization of finger movements was identified. The results provide evidence that TMS reveals properties of voluntary movements and motor skills. Therefore, the components of the measurement framework are an ideal system to study the mapping between the structure of the nervous system and its function:

- TMS reproduces important characteristics of natural movements, indicating that neuronal ensembles which determine important kinematic properties of voluntary movements are physiologically similarly activated by TMS (Study 1, Study 2, Study 3).
- Consistent with brain activation patterns during voluntary movements, a somatotopic separation (indexed by the CoG of the activation across stimulation points) with the thumb represented most laterally and the little finger represented most medially can be identified on top of overlapping areas with respect to individual finger movements (Study 1).
- Similar to results using fMRI, the separation of the thumb and little finger CoG is enlarged in professional violin players as compared to healthy subjects (Study 2).
- The activation of the muscles after TMS, i.e. the neuronal signal sent to the muscles, is not random but contains motor skill related information (Study 2, 3 and 4).
- Consequently, the variability of TMS-evoked finger movements is not only constrained by biomechanics but also by neuronal factors inculding the primary motor cortex(Study 1).
- Consistent with the notion that the substrate of dexterous finger movements is a distributed and overlapping organization of the primary motor cortex, finger movements evoked by TMS from different scalp positions do not display a prominent topographical pattern (Study 1).

Furthermore, important properties of kinematic modules derived from TMS-evoked finger movements could be identified which fit perfectly in the concept of a modular control architecture (Wolpert1998):

- A small number of kinematic modules is sufficient to account for most of the data variance (Study 1, 2, 3 and 4). Since with computational techniques only as much as modules as output variables can be extracted (and not more) it is possible that the prominent modules contain the effects of different neural systems which produce similar kinematic outputs. Thus, the variance explained by a module might also be a marker of redundant representation of neural networks producing similar kinematic output.
- The cortical components of the most prominent modules is adapted to frequently conducted movements and motor skills, possibly to reduce computational cost and minimize energy consumption (Study 2, 3 and 4).
- Plasticity mechanisms and structural adaptations could be mechanisms to sculpt the modules (Study 4).

- Modules contain both, shared and individually specific features of movement organization (Study 1).
- The shape of the most prominent module resembles in most cases a phylogenetic old, power grasp like synergistic movement of all fingers (Study 1, 4).
- Modules derived from TMS-evoked movements are sufficient to reconstruct grasping movements (Study 1, 2, 3).
- Adaptation of the modules due to motor learning is constrained by maintaining the ability to efficiently execute grasping movements (Study 2 and 3).
- Neural networks as part of the cortical and spinal components of kinematic modules are necessary to generate grasping movements (Study 4). Grasping therefore represents a skilled behavior mediated by the nervous system.
- However, the modules derived here may not indicate the full spectrum of operation of the CNS. The neural controller might have possibilities to use feedback, other cortical mechanisms such as surround inhibition [16], and alternative pathways [188] to generate dexterous finger movements.

In summary, the developed measurement framework in combination with a modular approach to analyze finger movements represents a powerful tool to study cortical mechanisms underlying finger control. A challenge for the future is to translate the knowledge and principles to applicable systems to enhance learning strategies for musical instruments, sports, and rehabilitation. Finally, the system brings the diverse areas of research a step closer together to formulate a cohesive framework to understand the function of the most complex biological system in nature.

A Appendix

A.1 Physiological basics of neuronal communication

The working unit of the brain is a neuron, a specialized cell designed to transmit information to other nerve cells or muscles (Figure 94A). Basically, a neuron consists of a cell body containing the nucleus and an electricity-conducting fiber, the axon, which also gives rise to many smaller axon branches before ending at nerve terminals (for a detailed description of the neuron, see [212]). Additional cell processes, dendrites, extend from the neuron cell body and receive messages from other neurons. The dendrites and cell body are covered with synapses which are contact points formed by axon terminals from other neurons and ion channels passing through the neuron's membrane (yellow objects in Figure 94A). In rest-

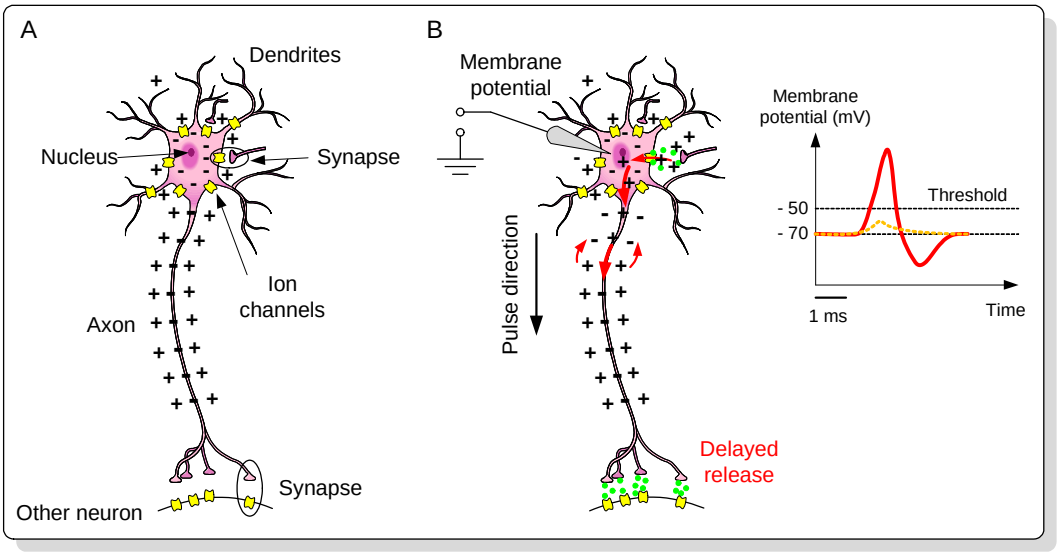

Figure 94: The neuronal communication. (A) Elements of a neuron. (B) Basic mechanism of information transmission between neurons.

ing state (or dynamic equilibrium), a neuron has a negative membrane potential (≈-70 mV) with respect to the extracellular space determined by the permeability of the ion channels and other chemical and electrical processes [212]. A neuron transmits information if it is globally depolarized, i.e. the electrical potential is raised (mainly) by the influx of positive ions (above all Na^+ ions). The influx is initiated at the synapses, where neurotransmitters (green dots in Figure 94B) from the axon terminals of other neurons are released into the synaptic junction. The neurotransmitters bind at the ion channels and force them to change their conductivity for specific positive charged ions entering the cell (Figure 94B). The result, called the excitatory postsynaptic potential, is a local depolarization of the neuron. If a certain threshold is exceeded (≈-50 mV), a huge number of ion channels open, leading to a global depolarization of the neuron (red line in diagram of Figure 94B). This sudden voltage increase, called action potential, then passes along the membrane of the axon to their terminals where neurotransmitters are released to depolarize connected neurons (Figure 94B). In this way, neurons transmit their information in an 'all or nothing' manner to other neurons. Immediately after the depolarization, cellular processes (involving K^+ ions) bring the neuron back to the dynamic equilibrium. However, if the threshold for global depolarization of the neuron is not exceeded, the dynamic equilibrium is reinstalled without generation of an action potential (see orange dotted line in diagram of Figure 94B) and therefore without

information transmission. Normally, an action potential is generated by the summed excitatory postsynaptic potentials (EPSP) from several neurons and the information is transmitted to a large number of neurons [212]. Besides synapses where information is transmitted by neurotransmitters (chemical synapses), other types of synapses exist such as synapses that respond to electrical potential changes (electrical synapses). While the explained mechanism leads to an exchange of information between neurons, the opposite, i.e. the inhibition of information transmission by hyperpolarization of neurons (inhibitory postsynaptic potentials, IPSPs), is also possible. Complex human behaviors such as moving the fingers are generated by the coordinated excitation and inhibition of thousands of interconnected neurons.

A.2 The Euler Lagrange equations

The Euler Lagrange equations

$$\frac{d}{dt}\frac{\partial \mathcal{L}}{\partial \dot{q}_k} - \frac{\partial \mathcal{L}}{\partial q_k} \;=\; \tau_k; \quad k = 1, ..., n, \tag{A.59}$$

where $\mathcal{L} = \mathcal{K} - \mathcal{P}$ is the Lagrangian of the system, and τ_k is the force associated with the coordinate q_k can be used to derive the dynamical equations if it is possible to express the kinetic $\mathcal{K}$ and potential $\mathcal{P}$ energy of the system in terms of a set of generalized coordinates. In the following sections, the formulas for the kinetic energy and potential energy of a robot with rigid links using the Denavit-Hartenberg joint variables as generalized coordinates are derived [228].

Kinetic energy

The kinetic energy of a rigid body is given as

$$\mathcal{K} = \frac{1}{2} m \vec{v}^T \vec{v} + \frac{1}{2} \vec{\omega}^T \mathcal{I} \vec{\omega}, \tag{A.60}$$

where m is the total mass of the object, $\vec{v}$ and $\vec{\omega}$ are the linear and angular velocity vectors, respectively, and $\mathcal{I}$ is a symmetric 3×3 matrix called the inertia tensor. Since $\vec{v}$ and $\vec{\omega}$ are expressed in the inertial frame by the transformation $\mathbf{R}$, it is also necessary to express the inertial tensor $\mathcal{I}$ in the inertial frame. If $\mathbf{I}$ denotes the inertia tensor expressed in the body attached frame, then the two matrices are related to each other according to

$$\mathcal{I} = \mathbf{R}\mathbf{I}\mathbf{R}^T. \tag{A.61}$$

The inertia tensor in the body attached frame is computed as

$$\mathbf{I} = \begin{pmatrix} I_{xx} & I_{xy} & I_{xz} \\ I_{yx} & I_{yy} & I_{yx} \\ I_{zx} & I_{zy} & I_{zz} \end{pmatrix}. \tag{A.62}$$

The diagonal elements, I_{xx}, I_{yy}, I_{zz} are called the principal elements of inertia about the x, y, and z axes, respectively and the off-diagonal elements I_{xy}, I_{xz}, etc., are called the cross products of inertia. If the mass density of the object can be described as a function of

position, $\rho(x, y, z)$, the elements of the inertia tensor are given by

$$I_{xx} = \int\int\int (y^2 + z^2)\rho(x, y, z)dxdydz$$
$$I_{yy} = \int\int\int (x^2 + z^2)\rho(x, y, z)dxdydz$$
$$I_{zz} = \int\int\int (x^2 + y^2)\rho(x, y, z)dxdydz$$

and

$$I_{xy} = I_{yx} = -\int\int\int xy\rho(x, y, z)dxdydz$$
$$I_{xz} = I_{zx} = -\int\int\int xz\rho(x, y, z)dxdydz$$
$$I_{yz} = I_{zy} = -\int\int\int yz\rho(x, y, z)dxdydz.$$

If a robotic manipulator with n links is considered, the linear and angular velocities at link i can be expressed in terms of the Jacobian matrices $\mathbf{J}_{v_i}$, $\mathbf{J}_{\omega_i}$ and the derivatives of the joint variables:

$$v_i = \mathbf{J}_{v_i}(\vec{q})\dot{\vec{q}}, \quad \omega_i = \mathbf{J}_{\omega_i}(\vec{q})\dot{\vec{q}}. \tag{A.63}$$

With the mass m_i and the inertia tensor $\mathbf{I}$ of link i, the overall kinetic energy of the manipulator equals

$$\mathcal{K} = \frac{1}{2}\dot{\vec{q}}^T \left(\sum_{i=1}^{n} \left[m_i \mathbf{J}_{v_i}(\vec{q})^T \mathbf{J}_{v_i}(\vec{q}) + \mathbf{J}_{\omega_i}(\vec{q})^T \mathbf{R}_i(\vec{q}) \mathbf{I}_i \mathbf{R}_i(\vec{q})^T \mathbf{J}_{\omega_i}(\vec{q}) \right] \right) \dot{\vec{q}} = \frac{1}{2}\dot{\vec{q}}^T \mathbf{D}(\vec{q})\dot{\vec{q}}, \tag{A.64}$$

where $D(\vec{q})$ is an n × n symmetric and positive definite configuration dependent matrix, called the inertia matrix [228].

Potential energy

In case of rigid dynamics, the only source of potential energy is gravity. The potential energy of link i can be computed by assuming that the mass of the entire object is concentrated at its center of mass and is given by

$$\mathcal{P}(\vec{q}) = \sum_{i=1}^{n} m_i \vec{g}^T \vec{r}_{ci}(\vec{q}), \tag{A.65}$$

where g is the vector giving the direction of gravity in the inertial frame and r_{ci} gives the coordinates of the center of mass of link i. In the case that elastic elements, such as muscles, are present, the potential energy will include terms containing the energy stored in the elastic elements [228].

Equations of motion

Using the kinetic and potential energy, the Lagrangian can be written as

$$\mathcal{L} = \mathcal{K} - \mathcal{P} = \frac{1}{2}\dot{\vec{q}}^T \mathbf{D}(\vec{q})\dot{\vec{q}} - \sum_{i=1}^{n} m_i \vec{g}^T \vec{r}_{ci}(\vec{q}) = \frac{1}{2}\sum_{i,j=1}^{n} d_{ij}(\vec{q})\dot{q}_i\dot{q}_j - \sum_{i=1}^{n} m_i \vec{g}^T \vec{r}_{ci}(\vec{q}), \tag{A.66}$$

where d_{ij} are the entries of the n × n inertia matrix $\mathbf{D}(\vec{q})$. The partial derivatives of the Lagrangian with respect to the velocity of joint k is given by

$$\frac{\partial \mathcal{L}}{\partial \dot{q}_k} = \sum_{j=1}^{n} d_{kj}(\vec{q})\dot{q}_j, \tag{A.67}$$

and therefore

$$\frac{d}{dt}\frac{\partial \mathcal{L}}{\partial \dot{q}_k} = \sum_{j=1}^{n} d_{kj}(\vec{q})\ddot{q}_j + \sum_{j=1}^{n} \frac{d}{dt} d_{kj}(\vec{q})\dot{q}_j = \sum_{j=1}^{n} d_{kj}(\vec{q})\ddot{q}_j + \sum_{i,j=1}^{n} \frac{\partial d_{kj}(\vec{q})}{\partial q_i}\dot{q}_i\dot{q}_j. \tag{A.68}$$

Similarly, the derivative with respect to the position of joint k is

$$\frac{\partial \mathcal{L}}{\partial q_k} = \frac{1}{2}\sum_{i,j=1}^{n} \frac{\partial d_{ij}(\vec{q})}{\partial q_k}\dot{q}_i\dot{q}_j - \sum_{i=1}^{n} m_i \vec{g}^T \frac{\partial \vec{r}_{ci}(\vec{q})}{\partial q_k}. \tag{A.69}$$

Thus, the Euler-Lagrange equations can be written as

$$\sum_{j=1}^{n} d_{kj}(\vec{q})\ddot{q}_j + \sum_{i,j=1}^{n} \left(\frac{\partial d_{kj}(\vec{q})}{\partial q_i} - \frac{1}{2}\frac{\partial d_{ij}(\vec{q})}{\partial q_k} \right) \dot{q}_i\dot{q}_j + \sum_{i=1}^{n} m_i \vec{g}^T \frac{\partial \vec{r}_{ci}(\vec{q})}{\partial q_k} = \tau_k. \tag{A.70}$$

Using the notation

$$c_{ijk} = \frac{1}{2}\left(\frac{\partial d_{kj}(\vec{q})}{\partial q_i} + \frac{\partial d_{ki}(\vec{q})}{\partial q_j} - \frac{\partial d_{ij}(\vec{q})}{\partial q_k} \right) \tag{A.71}$$

and

$$g_k(\vec{q}) = \sum_{i=1}^{n} m_i \vec{g}^T \frac{\partial \vec{r}_{ci}(\vec{q})}{\partial q_k} = \frac{\partial \mathcal{P}(\vec{q})}{\partial q_k}, \tag{A.72}$$

where the c_{ijk} are called the Christoffel symbols of the first kind and the $\vec{g}_k(\vec{q})$ is the gravity vector, equation A.70 can be rewritten as

$$\sum_{j=1}^{n} d_{kj}(\vec{q})\ddot{q}_j + \sum_{i=1}^{n}\sum_{j=1}^{n} c_{ijk}(q)\dot{q}_i\dot{q}_j + g_k(\vec{q}) = \tau_k, \quad k = 1, ..., n. \tag{A.73}$$

It is common to express the above equation in matrix notation:

$$\mathbf{D}(\vec{q})\ddot{\vec{q}} + \mathbf{C}(\vec{q}, \dot{\vec{q}})\dot{\vec{q}} + \vec{g}(\vec{q}) = \vec{\tau}. \tag{A.74}$$

A.3 Object-oriented design patterns

Java is an object oriented programming language such as C++, C#, or Python. In contrast to procedural languages (such as C), the aim of object orientation is to create flexible, modular structures that mimic real world objects close to the programming problem. In such a design, independent software modules can be linked to each other by clearly defined functionalities. The basic software module is called a 'class', which consists of attributes and methods (Figure 95).

While attributes specify the properties of the class (for example if a class represents a car, an attribute might be 'kilometers driven'), methods specify appropriate class specific actions (in the example one method might be 'drive()'; then the attribute 'kilometers driven' is appropriately increased). Thus, a class is a coded scheme mirroring the structure of an object. During software runtime, physical representations of a class are instantiated. These

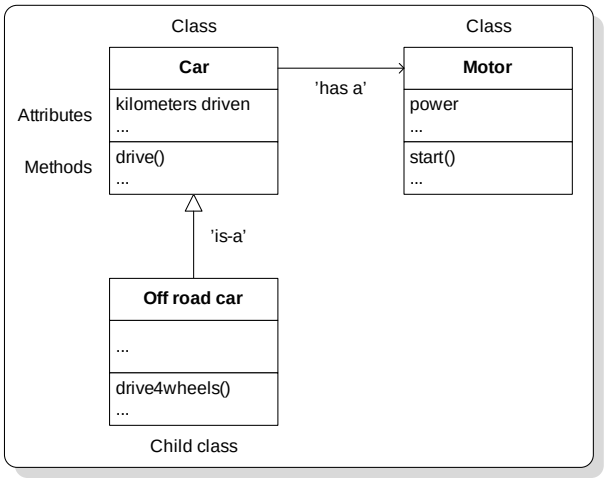

Figure 95: UML class diagrams explaining typical object oriented design methods.

representations are defined as objects. Generally an infinitive number of objects can be instantiated, which are stored in the Heap during software execution. For example, an instance of a 'Car' object might represent a new car with 'kilometers driven' set to zero and a second object might represent an used car with already 100 kilometers driven. Classes that inherit attributes and methods from other classes are called 'child classes' and represent specializations of the parent class ('is-a' relationship). In the example, a child of the class 'Car' might be the class 'Off road car' with the additional method 'drive4wheels()'. Furthermore, a class might use the functionality of other classes by aggregation. This behavior is referred to as a 'has-a' relationship (for example a car 'has-a' 'Motor'). While these relationships are key concepts of object oriented design, a number of other principles and programming concepts exist [224]. Basically, Java provides predefined classes stored in packages or libraries (such as the javax.comm packages), which can be aggregated or extended to fulfill the needs of the actual programming problem.

However, to obtain a flexible, maintainable and extensible source code, the class concept must be applied in a structured way. Design Patterns, higher level than classes and libraries, provide a framework how to structure classes and their interaction to solve a certain software design problem [84]. In the following chapters, some Design Patterns used in the training system are presented.

The State Pattern

The State Pattern allows an object to have many different behaviors based on its internal states. The UML class diagram is shown in Figure 96. The 'Context' is the class that can have a number of internal states and a method ('request()') that is delegated to the state class to handle. The state interface defines a common interface for all concrete states [84].

Concrete states handle requests from the 'Context'. Each 'ConcreteState' class provides its own implementation for a request. In this way, when the 'Context' changes state, its behavior will change as well. Alternatively, in non-complex classes, the states of an object can be defined as attributes of the type 'final static int'. Different behaviors are then coded in the 'Context' class by 'if' statements.

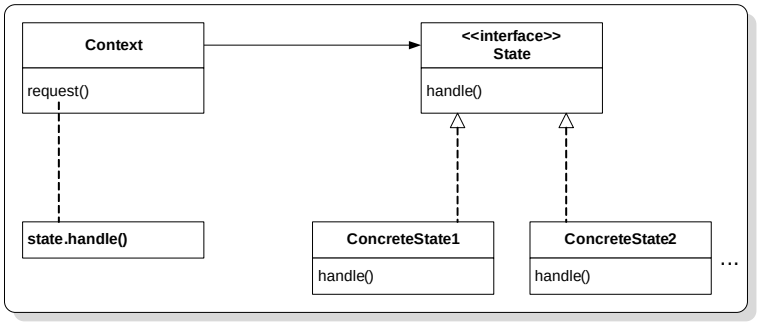

Figure 96: UML diagram of the State Pattern.

The Observer Pattern

The Observer Pattern defines a one-to-many dependency between objects so that if one object changes its state, all of its dependents are notified and updated automatically. The one-to-many relationship is defined by objects called subjects and observers. If the subject changes its state, the observers get notified. Depending on the style of notification, the observer may also be updated with new values. Thus, the Observer Pattern provides a design where subjects and observers are loosely coupled (Figure 97).

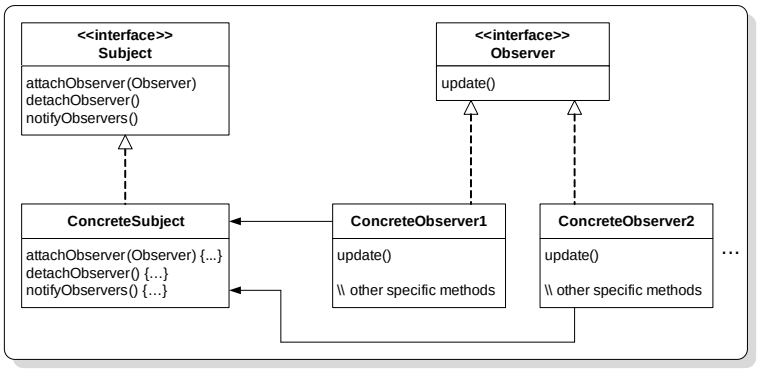

Figure 97: UML diagram of the Observer Pattern.

The only thing the subject knows about an observer is that it implements a certain interface. Because the subject only depends on a list of objects that implement the Observer interface, new observers can be added ('attachObserver(Observer)'), replaced, or removed ('detachObserver()') at any time during runtime. Since all observers implement the same interface, the subject never needs to be modified in order to add new types of observers. An additional advantage of this pattern is that the subjects and observers can be reused independently of each other so that changes to either the subject or an observer will not affect the other. In summary, loosely coupled designs allow building flexible object oriented systems, which can handle change because they minimize the interdependency between objects [84].

The Model View Controller (MVC) Pattern

The Model View Controller (MVC) Pattern (Figure 98) is used in almost every modern software application and is a composite of several other patterns such as the Observer Pattern and the State Pattern.

The 'Model' holds all the data, state and application logic and is oblivious to the view and controller, although it provides an interface to manipulate and retrieve its state. Furthermore

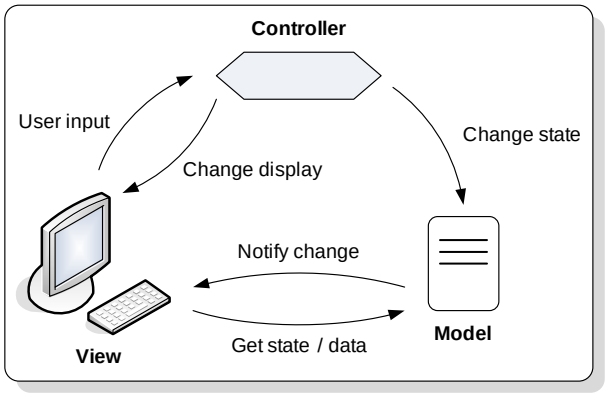

Figure 98: The Model View Controller concept.

it can send notifications of state changes to observers (such as 'View' classes). The 'View' gives a presentation of the 'Model' and usually retrieves the state and data it needs to display directly from the model. When the user does something to the view, for example clicking a button, then the 'View' notifies the 'Controller' about the action. Thus the 'Controller' represents a middle layer between the 'View' and the 'Model'. It takes user input and figures out what that means and how the 'Model' should be manipulated based on that action. In addition, the 'Controller' may also ask the view to change (such as enabling or disabling buttons). In the training system, the 'Database interface layer' and the 'Data acquisition layer' represent the 'Model', whereas the 'Controller unit layer' and the 'Visualization layer' represent the 'Controller' and the 'View', respectively (see Figure 41). A detailed discussion of the MVC and other Design Patterns can be found in [84].

A.4 The virtual hand

To visualize the data from the sensor glove, a virtual hand was developed. To integrate the virtual hand in the training system a Java compatible 3-D modeling language, the Java3D application programming interface (API) was selected.

The Java3D API

The Java3D API is an interface for writing programs to display and interact with three-dimensional graphics. The API contains a collection of high-level constructs for creating and manipulating 3D geometry and structures for rendering that geometry. Java3D provides the functions for creation of imagery, visualizations, animations, and interactive 3D graphics application programs [41].

Every Java3D program is assembled from objects from the Java3D class hierarchy. This collection of objects describes a 'virtual universe', which refers to the three dimensional virtual space Java3D objects populate (Figure 99). A Java3D virtual universe is created from a scene graph and a scene graph is created using instances of Java3D classes. Each scene graph has a single 'VirtualUniverse'. The 'VirtualUniverse' object usually has a single 'Locale' object that establishes a virtual world Cartesian coordinate system. A 'Locale' object may serve as the root of multiple subgraphs of the scene graph. A 'BranchGroup' object (BG) is the root of a subgraph, or branch graph. There are two different categories of scene subgraphs: the view branch graph (Figure 99, right) and the content branch graph

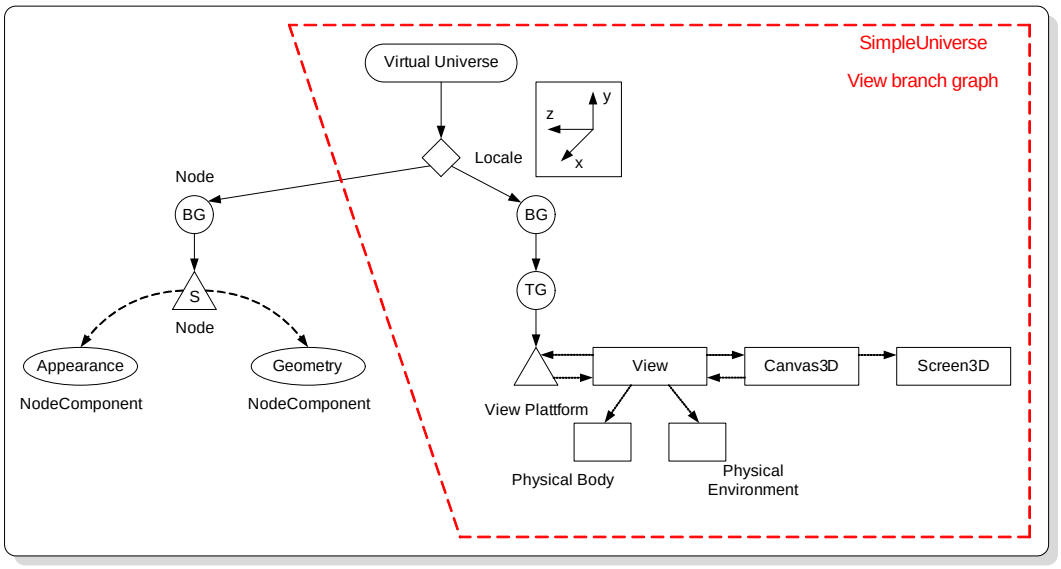

Figure 99: Java3D scene graph model.

(Figure 99, left). The content branch graph specifies the contents of the virtual universe - geometry, appearance, behavior, location, sound, and lights. The view branch graph specifies the viewing parameters such as the viewing location and direction. Here, a standard view branch graph is created by using the 'SimpleUniverse' class. Specifically, this class creates 'Locale', 'VirtualUniverse', 'ViewingPlatform', and 'Viewer' objects. The creation of the virtual hand, represented as objects in the content branch graph, is described in the remainder of this chapter.

Objects of the content branch graph are subclasses of the 'ScreenGraphObject' class. An important subclass is the 'Node' class. It is an abstract superclass of 'Group' (such as 'BranchGroup') and 'Leaf' (such as 'Shape3D') classes and defines common methods for its subclasses. The most common relationship in the content branch graph is a parent-child relationship. A 'Group' node can have any number of children but only one parent. A 'Leaf' node can have one parent and no children. The other relationship is a reference (dotted line in Figure 99). A reference associates a 'NodeComponent' object with a scene graph Node. 'NodeComponent' is the superclass used in specifying the geometry, appearance, texture, and material properties of a 'Shape3D' node. A Java 3D scene graphs is constructed of Node objects in parent-child relationships forming a tree structure. Each scene graph path in the tree completely specifies the state information of its 'Leaf'. State information includes the location, orientation, and size of a visual object. Consequently, the visual attributes of each visual object depend only on its scene graph path.

The virtual hand scene graph

The scene graph for the virtual hand was constructed by embedding Java3D objects in Java classes to provide a flexible structure for rotating, changing the color, the transparency, the shape and the material properties of the fingers. The base class is the 'KinematicChainElement', which encapsulates the 'Node' and 'NodeComponents' of a finger segment (Figure 100A). The object on top of the finger segment tree structure is a 'TransformGroup' (TG) that defines rotations of the finger segment about the xyz axis. The second transformation is a translation to the end of the finger segment. Objects attached to this TG are then located

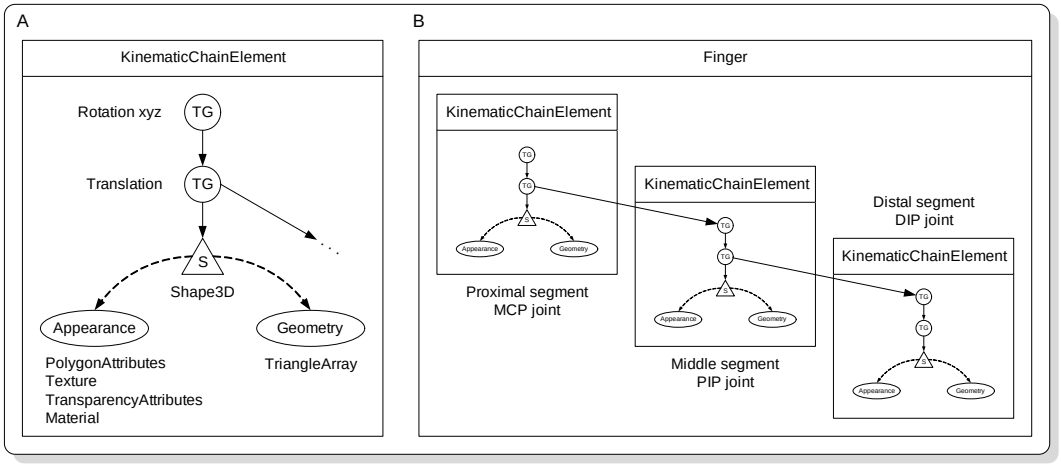

Figure 100: Scene graph elements of the developed virtual hand are embedded in Java classes. (A) Basic element of the hand model. (B) Chains of the basic elements define a finger.

at the end of the finger segment. The 'Leaf' node of the a finger segment, a 'Shape3D' object, references the 'Geometry' and the 'Appearance' of the finger segment. The 'Geometry' defines the visual shape of the finger segment and is imported as a 'TriangleArray' from realistic, custom built VRML models (see below). The visualization properties of the finger segment shape is determined by the 'Appearance' objects. Specifically, the following elements exist:

- **PolygonAttributes**: Allows to visualize the polygons of the shape filled or not filled.
- **Texture**: With the texture element, a texture image file can be loaded to create a more realistic appearance.
- **TransparencyAttributes**: The transparency of the finger segment can be specified.
- **Material**: This element determines the color of the finger segment.

A method to modify each element is implemented in the 'KinematicChainElement' class. A finger is modeled as a chain of finger segments (Figure 100B). The first 'KinematicChainElement' represents the proximal finger segment and describes rotations about the MCP joint. The rotation TG of the second element (the middle segment) is attached to the translation TG of the proximal finger segment. Thus, the shape of the middle finger segment is located at the end of the proximal finger segment and the rotations and translations depend on the angle proximal segment (Euler transformations). Analogously, the distal segment is attached to the translation TG of the middle segment. Furthermore, the 'Finger' class defines the same methods as the 'KinematicChainElement', but the methods can also affect all finger segments in the same way. For example if the 'setColor()' method of the 'Finger' class is invoked, all finger segments change their colors. Regarding rotation movements, the MCP joint is allowed to rotate in two dimensions (extension/flexion, adduction/abduction) and the PIP and DIP joints are restricted to flexion/extension movements. Since the glove cannot record rotations about the DIP joint, the angle value of the DIP joint is fixed to $\frac{1}{3}$ of the angle value of the PIP joint.

The class 'VirtualHand', implemented as observer, assembles the five 'Finger' objects and connects them to the palm, a 'KinematicChainElement'. In this class, a VRML model of

the human hand is loaded by the Java VRML-loader and imported as 'TriangleArray'. The model was custom designed with 'Art of Illusion', an open source graphics design program. Figure 101 shows the palm mesh of the hand created in 'Art of Illusion'. After completion of

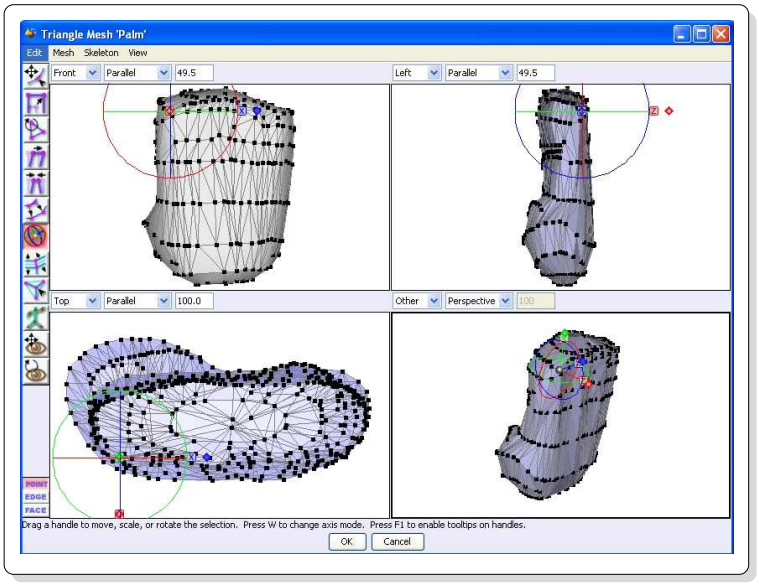

Figure 101: Design of the components of the virtual hand using a 3D modelling software.

loading of the VRML mesh, the finger segments and the palm are extracted and used to define the 'Geometry' of the 'Shape3D' element of the appropriate finger segment. Additionally, images of a human hand were taken to provide the texture attribute for rendering of the finger segments and the palm. The complete virtual hand in Java3D is visualized in Figure 102A. To visualize joint rotations, the 'rotate()' method takes 14 arguments (float values)

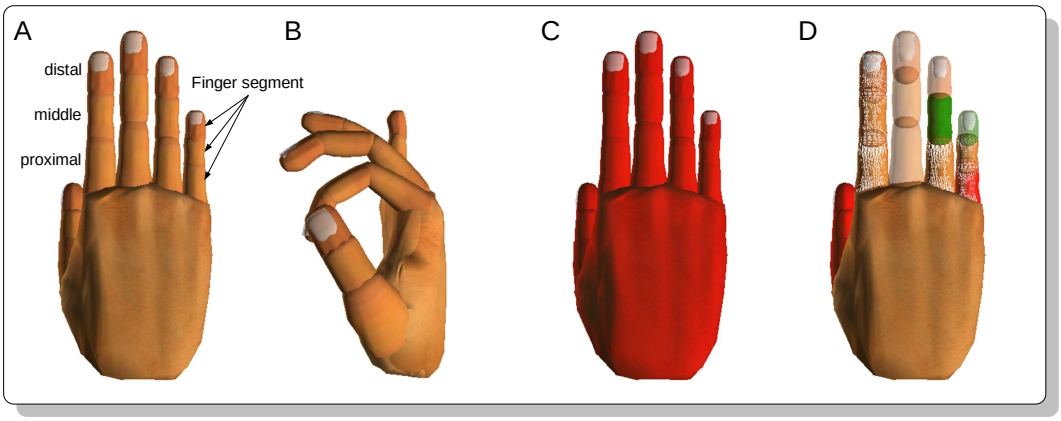

Figure 102: Images of the created virtual hand. (A) Resting posture. (B) Rotation of individual joints. (C) Color variation of the whole hand (used for example in the training system). (D) Visualization of each element of the virtual hand can be adjusted independently.

and maps them onto the appropriate finger joints as shown in Figure 102B. Additionally, methods to change the appearance of the hand exists. For example, the 'setColor()' method changes the color of all finger segments, as illustrated in Figure 102C. There are also methods to modify the appearance of each finger or finger segment individually. In Figure 102D, the thumb color is changed to red, the 'PolygonsAttributes' of the index finger are set to 'not filled' and the transparency of the middle finger is set to '0.4'. The appearance of the ring and little finger segments are set to different individual patterns.

In summary, the virtual hand developed here is an object oriented designed 3D model of the human hand which provides flexible visualization modifications and fully integrates in every Java environment such as the training system described in Chapter 2.4. The final underlying scene graph is shown in Figure 103. The scene is lighted with ambient and directional light

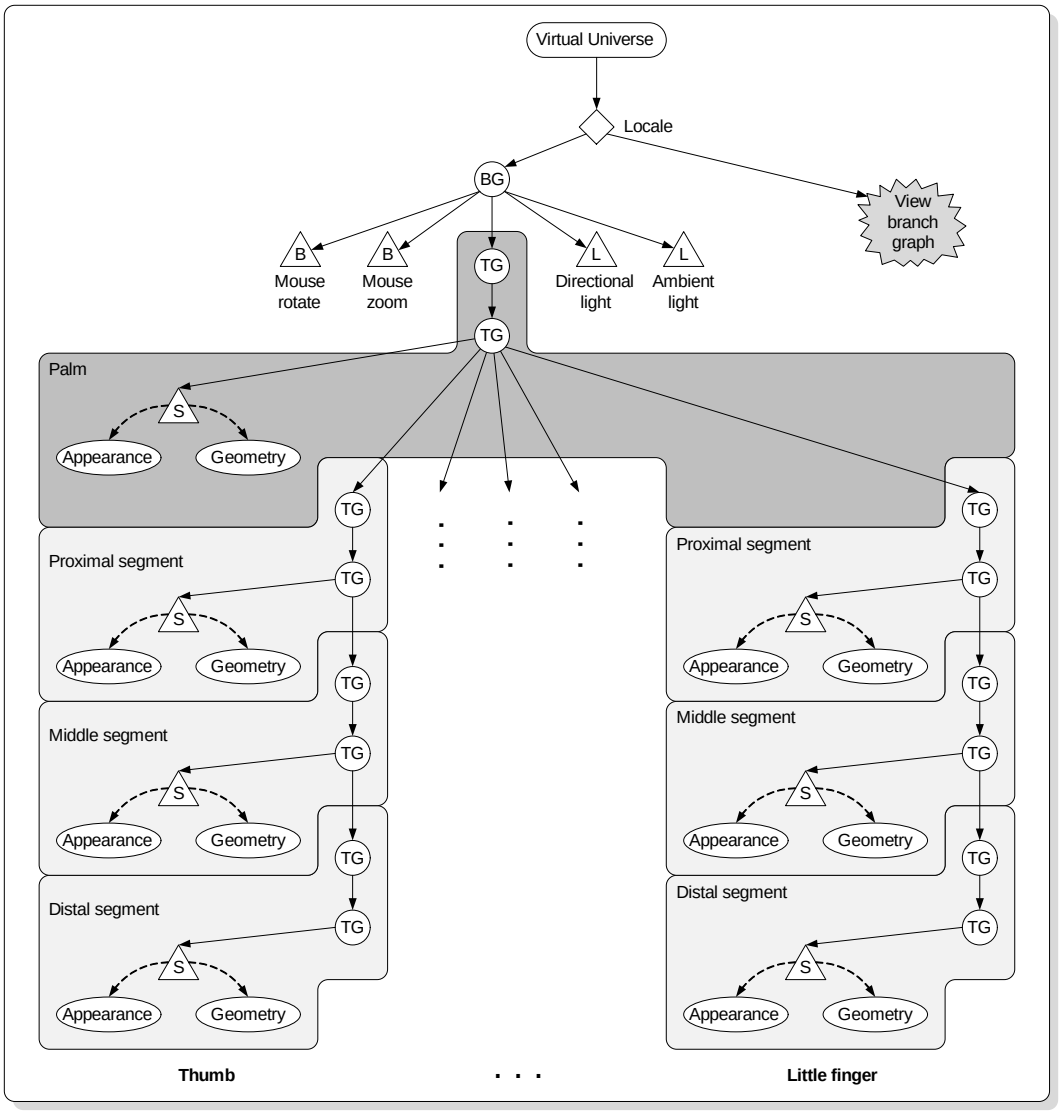

Figure 103: Complete scence graph of the virtual hand.

sources. To allow the user to interact with the model, a zoom and rotate option is added to the root BG.

A.5 The calibration user interface

This class represents a graphical user interface for sensor glove calibration. Calibration is necessary to map the maximum and minimum sensor voltage signals (which differ between individuals) into joint angles. Since the **Wii**-Glove and the 5DT-Glove have linear sensors (see Chapter 2.1), two values are sufficient for calibration. The driver of the 5DT-Glove and the developed driver of the **Wii**-Glove can provide sensor outputs in an automatic, linearly calibrated fashion. During every update, the raw value read from the sensor is compared to the current minimum and maximum raw values (raw_{min} and raw_{max}). If the current minimum and maximum values are exceeded, they are overwritten. The upper and lower calibration

values are therefore continuously pushed 'outwards'. The normalized output of a sensor is given by the first order equation

$$out = \frac{raw_{val} - raw_{min}}{raw_{max} - raw_{min}}, \tag{A.75}$$

which gives values between 0 an 1. By mapping the output onto physiologically plausible joint movement ranges or by adopting predefined postures (e.g. 90° flexion) the calibrated angle values are obtained. Figure 104 shows the graphical user interface developed for calibration. The core functionality is implemented by a 'ContinousController' which triggers a 'GloveSensor' object every 20 ms (50 Hz). The 'GloveSensor' has two observers attached, a 'VirtualHand' object and a 'ChannelView' object that are updated every time the 'GloveSensor' is triggered. The 'ContinousController' can be started by clicking the 'Start' button and stopped by clicking the 'Stop' button. Immediately after the start, the maximum and mini-

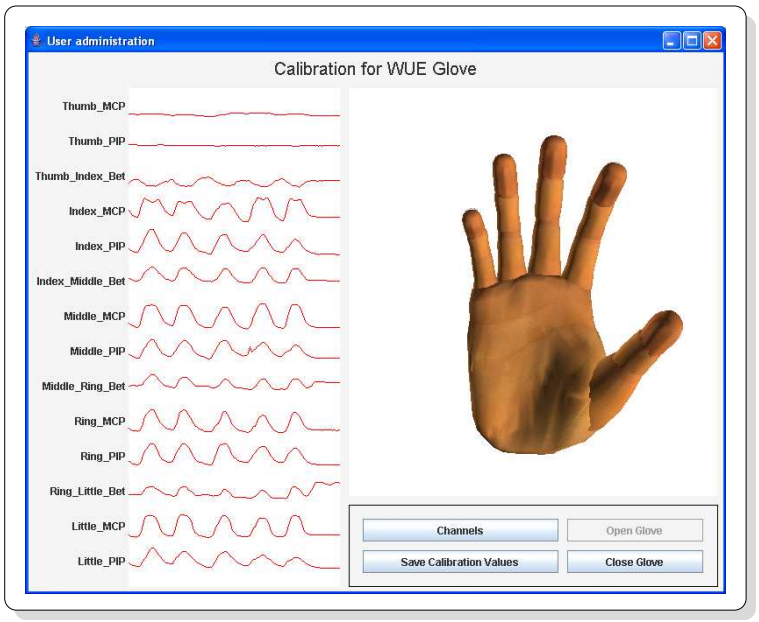

Figure 104: Graphical user interface for calibration.

mum values are set to 1 and 0, respectively. Doing a few flexing movements with the hand quickly sets the operating values for raw_{min} and raw_{max}, and calibrates the glove. If the glove is calibrated, the maximum and minimum values are stored as an array (used by the training system) or can be exported to -ascii files for off-line calibration (used for example in the grasping movement experiments).

A.6 The correlation coefficient of matrices

A correlation coefficient of matrices was developed to define a correlation coefficient between a time series of vectors [219]. Here it is used as a correlation coefficient between two matrices, each of which containing joint angles sampled over a period of time. Formally, the p-dimensional joint angle vector $\vec{u}_i$, sampled at each time instance $i \in \{1, \ldots, n\}$ can be written as a p × n dimensional matrix $\mathbf{U} = (\vec{u}_1, \vec{u}_2, \ldots, \vec{u}_n)$. Then the expected value of $\mathbf{U}$, denoted as $\epsilon(\mathbf{U})$, can be defined as

$$\epsilon(\mathbf{U}) = \left(\frac{1}{n} \sum_{j=1}^{n} \vec{u}_j, \ldots, \frac{1}{n} \sum_{j=1}^{n} \vec{u}_j \right) = (\vec{v}_1, \ldots, \vec{v}_n), \tag{A.76}$$

where $\vec{v}_i = \vec{v}_j,\ \forall i,j \in \{1,\ldots,n\}$. The inner product of two such matrices $\mathbf{U}$ and $\mathbf{Y}$ can be written as the scalar

$$< \mathbf{U}, \mathbf{Y} >= \sum_{i=1}^{n} \vec{u}_i \cdot \vec{y}_i, \tag{A.77}$$

where $\cdot$ represents the dot product between two vectors and the expected value of this inner product is

$$\epsilon(< \mathbf{U}, \mathbf{Y} >) = \frac{1}{n} < \mathbf{U}, \mathbf{Y} > . \tag{A.78}$$

With these expressions, the co-variance of two matrices can be defined as

$$\begin{aligned} \mathrm{Cov}(\mathbf{U}, \mathbf{Y}) &= \epsilon(< \mathbf{U} - \epsilon(\mathbf{U}), \mathbf{Y} - \epsilon(\mathbf{Y}) >) \\ &= \epsilon(< \mathbf{U}, \mathbf{Y} >) - < \epsilon(\mathbf{U}), \epsilon(\mathbf{Y}) > . \end{aligned} \tag{A.79}$$

Furthermore, the correlation coefficient between two matrices $\rho(\mathbf{U}, \mathbf{Y})$ is given by the ratio of the co-variance of the time series and the product of their standard deviations:

$$\rho(\mathbf{U}, \mathbf{Y}) = \frac{\mathrm{Cov}(\mathbf{U}, \mathbf{Y})}{\sigma(\mathbf{U})\sigma(\mathbf{Y})}, \tag{A.80}$$

where the standard deviation is the scalar

$$\sigma(\mathbf{U}) = \epsilon(\|\mathbf{U} - \epsilon(\mathbf{U})\|) \tag{A.81}$$

and $\|\mathbf{U}\|$ is defined as $\|\mathbf{U}\| = (< \mathbf{U}, \mathbf{U} >)^{1/2}$. With these definitions it follows that $-1 \leq \rho(\mathbf{U}, \mathbf{Y}) \leq 1$. This measure is used for example in the training system to compare the similarity between the intended movement and the actual conducted movement of a trial.

References

[1] Pascual-Leone A., Nguyet D., Cohen L.G., Brasil-Neto J.P., Cammarota A., and M. Hallett. Modulation of muscle responses evoked by transcranial magnetic stimulation during the acquisition of new fine motor skills. *J Neurophysiol*, 74(3):1037–45, 1995.

[2] S. V. Adamovich, A. S. Merians, R. Boian, M. Tremaine, G. S. Burdea, M. Recce, and H. Poizner. A virtual reality based exercise system for hand rehabilitation post-stroke: transfer to function. *Conf Proc IEEE Eng Med Biol Soc*, 7:4936–9, 2004.

[3] D. L. Adkins, J. Boychuk, M. S. Remple, and J. A. Kleim. Motor training induces experience-specific patterns of plasticity across motor cortex and spinal cord. *J Appl Physiol*, 101(6):1776–82, Dec 2006.

[4] T. N. Aflalo and M. S. Graziano. Possible origins of the complex topographic organization of motor cortex: reduction of a multidimensional space onto a two-dimensional array. *J Neurosci*, 26(23):6288–97, Jun 7 2006.

[5] E. Altenmueller. *Vom Spitzgriff zur Liszt-Sonate*. Spektrum Akademischer Verlag, 2005.

[6] V. E. Amassian, M. Stewart, G. J. Quirk, and J. L. Rosenthal. Physiological basis of motor effects of a transient stimulus to cerebral cortex. *Neurosurgery*, 20(1):74–93, Jan 1987.

[7] K. Amunts, G. Schlaug, A. Schleicher, H. Steinmetz, A. Dabringhaus, P. E. Roland, and K. Zilles. Asymmetry in the human motor cortex and handedness. *Neuroimage*, 4(3 Pt 1):216–22, Dec 1996.

[8] Y. Aoyagi, R. B. Stein, V. K. Mushahwar, and A. Prochazka. The role of neuromuscular properties in determining the end-point of a movement. *IEEE Trans Neural Syst Rehabil Eng*, 12(1):12–23, Mar 2004.

[9] T. Arens, F. Hettlich, Ch. Karpfinger, U. Kockelkorn, K. Lichtenegger, and H. Stachel. *Mathematik*. Spektrum Akademischer Verlag, 2008.

[10] A.C. Armstrong, W.C. Stokoe, and S.E. Wilcox. *Gesture and the Nature of Language*. Cambridge Univ. Press, 1995.

[11] L. Avanzino, M. Bove, C. Trompetto, A. Tacchino, C. Ogliastro, and G. Abbruzzese. 1-hz repetitive tms over ipsilateral motor cortex influences the performance of sequential finger movements of different complexity. *Eur J Neurosci*, 27(5):1285–91, Mar 2008.

[12] S. N. Baker, E. Olivier, and R. N. Lemon. An investigation of the intrinsic circuitry of the motor cortex of the monkey using intra-cortical microstimulation. *Exp Brain Res*, 123(4):397–411, Dec 1998.

[13] M. Bangert and G. Schlaug. Specialization of the specialized in features of external human brain morphology. *Eur J Neurosci*, 24(6):1832–4, Sep 2006.

[14] A. T. Barker, R. Jalinous, and I. L. Freeston. Non-invasive magnetic stimulation of human motor cortex. *Lancet*, 1(8437):1106–7., 1985.

[15] D.B. Beck, J.A. Sindt, and T.E. Danielson. Thin deflectable resistor, 2007.

[16] S. Beck, S. P. Richardson, E. A. Shamim, N. Dang, M. Schubert, and M. Hallett. Short intracortical and surround inhibition are selectively reduced during movement initiation in focal hand dystonia. *J Neurosci*, 28(41):10363–9, Oct 8 2008.

[17] R. Beisteiner, C. Windischberger, R. Lanzenberger, V. Edward, R. Cunnington, M. Erdler, A. Gartus, B. Streibl, E. Moser, and L. Deecke. Finger somatotopy in human motor cortex. *Neuroimage*, 13(6):1016–1026, JUN 2001.

[18] M. Bentivoglio. Musical skills and neural functions. the legacy of the brains of musicians. *Ann N Y Acad Sci*, 999:234–43, Nov 2003.

[19] P. Bermudez and R. J. Zatorre. Differences in gray matter between musicians and nonmusicians. *Ann N Y Acad Sci*, 1060:395–9, Dec 2005.

[20] N. Bernstein. *The co-ordination and regulation of movements*. Pergamon, 1967.

[21] B. Berret, F. Bonnetblanc, C. Papaxanthis, and T. Pozzo. Modular control of pointing beyond arm's length. *J Neurosci*, 29(1):191–205, Jan 7 2009.

[22] A. Bethe. Die plastizitaet (anpassungsfaehigkeit) des nervensystems. *Die Naturwissenschaften*, 2:214–21, 1933.

[23] E. Bizzi, V. C. Cheung, A. d'Avella, P. Saltiel, and M. Tresch. Combining modules for movement. *Brain Res Rev*, 57(1):125–33, Jan 2008.

[24] E. Bizzi, S. F. Giszter, E. Loeb, F. A. Mussa-Ivaldi, and P. Saltiel. Modular organization of motor behavior in the frog's spinal cord. *Trends Neurosci*, 18(10):442–6, Oct 1995.

[25] E. Bizzi, F. A. Mussa-Ivaldi, and S. Giszter. Computations underlying the execution of movement: a biological perspective. *Science*, 253(5017):287–91, Jul 19 1991.

[26] R. Boian, A. Sharma, C. Han, A. Merians, G. Burdea, S. Adamovich, M. Recce, M. Tremaine, and H. Poizner. Virtual reality-based post-stroke hand rehabilitation. *Stud Health Technol Inform*, 85:64–70, 2002.

[27] P. Bonato. Advances in wearable technology and applications in physical medicine and rehabilitation. *J Neuroeng Rehabil*, 2(1):2, Feb 25 2005.

[28] G. Booch, J. Rumbaugh, and I. acobson. *Unified Modeling Language User Guide*. Addison Wesley, 1999.

[29] B. Boroojerdi, H. Foltys, T. Krings, U. Spetzger, A. Thron, and R. Topper. Localization of the motor hand area using transcranial magnetic stimulation and functional magnetic resonance imaging. *Clin Neurophysiol*, 110(4):699–704, Apr 1999.

[30] B. Boroojerdi, L. Kopylev, F. Battaglia, S. Facchini, U. Ziemann, W. Muellbacher, and L. G. Cohen. Reproducibility of intracortical inhibition and facilitation using the paired-pulse paradigm. *Muscle Nerve*, 23(10):1594–7., 2000.

[31] G. A. Bortoff and P. L. Strick. Corticospinal terminations in 2 new-world primates - further evidence that corticomotoneuronal connections provide part of the neural substrate for manual dexterity. *Journal of Neuroscience*, 13(12):5105–5118, DEC 1993.

[32] J. Bortz. *Statistik: Für Human- und Sozialwissenschaftler*. Springer, 2005.

[33] P. Braido and X. Zhang. Quantitative analysis of finger motion coordination in hand manipulative and gestic acts. *Hum Mov Sci*, 22(6):661–78, Apr 2004.

[34] M. Brecht, M. Schneider, B. Sakmann, and T. W. Margrie. Whisker movements evoked by stimulation of single pyramidal cells in rat motor cortex. *Nature*, 427(6976):704–10, Feb 19 2004.

[35] T. Brochier, M. J. Boudreau, M. Pare, and A. M. Smith. The effects of muscimol inactivation of small regions of motor and somatosensory cortex on independent finger movements and force control in the precision grip. *Exp Brain Res*, 128(1-2):31–40, Sep 1999.

[36] T. Brochier, R. L. Spinks, M. A. Umilta, and R. N. Lemon. Patterns of muscle activity underlying object-specific grasp by the macaque monkey. *J Neurophysiol*, 92(3):1770–82, Sep 2004.

[37] M.W. Browne. Cross validation methods. *J Math Psychol*, 44:108 –132, 2000.

[38] C. Buetefisch, H. Hummelsheim, P. Denzler, and K. H. Mauritz. Repetitive training of isolated movements improves the outcome of motor rehabilitation of the centrally paretic hand. *J Neurol Sci*, 130(1):59–68, 1995.

[39] C. M. Buetefisch. Plasticity in the human cerebral cortex: lessons from the normal brain and from stroke. *Neuroscientist*, 10(2):163–73, Apr 2004.

[40] C. M. Buetefisch, B. C. Davis, S. P. Wise, L. Sawaki, L. Kopylev, J. Classen, and L. G. Cohen. Mechanisms of use-dependent plasticity in the human motor cortex. *Proc Natl Acad Sci U S A*, 97(7):3661–5, Mar 28 2000.

[41] G. Burdea and P. Coiffet. *Virtual Reality Technology*. Wiley, 2003.

[42] M. Butz, F. Worgotter, and A. van Ooyen. Activity-dependent structural plasticity. *Brain Res Rev*, Jan 6 2009.

[43] P. Celnik, B. Webster, D. M. Glasser, and L. G. Cohen. Effects of action observation on physical training after stroke. *Stroke*, 39(6):1814–20, Jun 2008.

[44] P. D. Cheney and E. E. Fetz. Comparable patterns of muscle facilitation evoked by individual corticomotoneuronal (cm) cells and by single intracortical microstimuli in primates - evidence for functional-groups of cm cells. *Journal of Neurophysiology*, 53(3):786–804, 1985.

[45] V. C. Cheung, A. d'Avella, and E. Bizzi. Adjustments of motor pattern for load compensation via modulated activations of muscle synergies during natural behaviors. *J Neurophysiol*, Dec 17 2008.

[46] V. C. Cheung, A. d'Avella, M. C. Tresch, and E. Bizzi. Central and sensory contributions to the activation and organization of muscle synergies during natural motor behaviors. *J Neurosci*, 25(27):6419–34, Jul 6 2005.

[47] J. Classen, J. Liepert, S. P. Wise, M. Hallett, and L. G. Cohen. Rapid plasticity of human cortical movement representation induced by practice. *J Neurophysiol*, 79(2):1117–23, Feb 1998.

[48] R. H. Clewley, J. M. Guckenheimer, and F. J. Valero-Cuevas. Estimating effective degrees of freedom in motor systems. *IEEE Trans Biomed Eng*, 55(2 Pt 1):430–42, Feb 2008.

[49] M.C. Corballis. *From Hand to Mouth. The Origins of Language.* Princeton Univ. Press, 2002.

[50] J. H. Crosbie, S. Lennon, M. D. McNeill, and S. M. McDonough. Virtual reality in the rehabilitation of the upper limb after stroke: the user's perspective. *Cyberpsychol Behav*, 9(2):137–41, Apr 2006.

[51] A. d'Avella and E. Bizzi. Low dimensionality of supraspinally induced force fields. *Proc Natl Acad Sci U S A*, 95(13):7711–4, Jun 23 1998.

[52] A. d'Avella and E. Bizzi. Shared and specific muscle synergies in natural motor behaviors. *Proc Natl Acad Sci U S A*, 102(8):3076–81, Feb 22 2005.

[53] A. d'Avella, L. Fernandez, A. Portone, and F. Lacquaniti. Modulation of phasic and tonic muscle synergies with reaching direction and speed. *J Neurophysiol*, 100(3):1433–54, Sep 2008.

[54] A. d'Avella, A. Portone, L. Fernandez, and F. Lacquaniti. Control of fast-reaching movements by muscle synergy combinations. *J Neurosci*, 26(30):7791–810, Jul 26 2006.

[55] A. d'Avella, P. Saltiel, and E. Bizzi. Combinations of muscle synergies in the construction of a natural motor behavior. *Nat Neurosci*, 6(3):300–8, Mar 2003.

[56] P. Dechent and J. Frahm. Functional somatotopy of finger representations in human primary motor cortex. *Hum Brain Mapp*, 18(4):272–83, Apr 2003.

[57] G. Deuschl, J. Raethjen, M. Lindemann, and P. Krack. The pathophysiology of tremor. *Muscle Nerve*, 24(6):716–35, Jun 2001.

[58] V. Di Lazzaro, A. Oliviero, P. Mazzone, A. Insola, F. Pilato, E. Saturno, A. Accurso, P. Tonali, and J. C. Rothwell. Comparison of descending volleys evoked by monophasic and biphasic magnetic stimulation of the motor cortex in conscious humans. *Exp Brain Res*, 141(1):121–7, Nov 2001.

[59] V. Di Lazzaro, A. Oliviero, F. Pilato, E. Saturno, M. Dileone, P. Mazzone, A. Insola, P. A. Tonali, and J. C. Rothwell. The physiological basis of transcranial motor cortex stimulation in conscious humans. *Clin Neurophysiol*, 115(2):255–66, Feb 2004.

[60] V. Di Lazzaro, A. Oliviero, F. Pilato, E. Saturno, A. Insola, P. Mazzone, P. A. Tonali, and J. C. Rothwell. Descending volleys evoked by transcranial magnetic stimulation of the brain in conscious humans: effects of coil shape. *Clin Neurophysiol*, 113(1):114–9, Jan 2002.

[61] V. Di Lazzaro, A. Oliviero, E. Saturno, F. Pilato, A. Insola, P. Mazzone, P. Profice, P. Tonali, and J. C. Rothwell. The effect on corticospinal volleys of reversing the direction of current induced in the motor cortex by transcranial magnetic stimulation. *Exp Brain Res*, 138(2):268–73, may 2001.

[62] V. Di Lazzaro, D. Restuccia, A. Oliviero, P. Profice, L. Ferrara, A. Insola, P. Mazzone, P. Tonali, and J. C. Rothwell. Magnetic transcranial stimulation at intensities below active motor threshold activates intracortical inhibitory circuits. *Exp Brain Res*, 119(2):265–8, Mar 1998.

[63] L. Dipietro, A. M. Sabatini, and P. Dario. Evaluation of an instrumented glove for hand-movement acquisition. *J Rehabil Res Dev*, 40(2):179–89, Mar-Apr 2003.

[64] B. H. Dobkin. Clinical practice. rehabilitation after stroke. *N Engl J Med*, 352(16):1677–84, Apr 21 2005.

[65] J. P. Donoghue, S. Leibovic, and J. N. Sanes. Organization of the forelimb area in squirrel monkey motor cortex: representation of digit, wrist, and elbow muscles. *Exp Brain Res*, 89(1):1–19, 1992.

[66] R. P. Dum and P. L. Strick. Frontal lobe inputs to the digit representations of the motor areas on the lateral surface of the hemisphere. *J Neurosci*, 25(6):1375–86, Feb 9 2005.

[67] J. Duque, R. Mazzocchio, K. Stefan, F. Hummel, E. Olivier, and L. G. Cohen. Memory formation in the motor cortex ipsilateral to a training hand. *Cereb Cortex*, 18(6):1395–406, Jun 2008.

[68] S. A. Edgley, J. A. Eyre, R. N. Lemon, and S. Miller. Excitation of the corticospinal tract by electromagnetic and electrical stimulation of the scalp in the macaque monkey. *J Physiol*, 425:301–20, Jun 1990.

[69] T. Elbert, C. Pantev, C. Wienbruch, B. Rockstroh, and E. Taub. Increased cortical representation of the fingers of the left hand in string players. *Science*, 270(5234):305–7, Oct 13 1995.

[70] Maynard E.M., Hatsopoulos N.G., Ojakangas C.L., Acuna B.D., Sanes J.N., Normann R.A., and J.P. Donoghue. Neuronal interactions improve cortical population coding of movement direction. *J Neurosci*, 19(18):8083–93, 1999.

[71] K. C. Engel, M. Flanders, and J. F. Soechting. Anticipatory and sequential motor control in piano playing. *Exp Brain Res*, 113(2):189–99, Feb 1997.

[72] C. Ethier, L. Brizzi, W. G. Darling, and C. Capaday. Linear summation of cat motor cortex outputs. *J Neurosci*, 26(20):5574–81, May 17 2006.

[73] J. A. Eyre, S. Miller, G. J. Clowry, E. A. Conway, and C. Watts. Functional corticospinal projections are established prenatally in the human foetus permitting involvement in the development of spinal motor centres. *Brain*, 123 (Pt 1):51–64, Jan 2000.

[74] E. E. Fetz and P. D. Cheney. Muscle fields of primate corticomotoneuronal cells. *J Physiol (Paris)*, 74(3):239–45, 1978.

[75] E. E. Fetz, S. I. Perlmutter, Y. Prut, K. Seki, and S. Votaw. Roles of primate spinal interneurons in preparation and execution of voluntary hand movement. *Brain Res Brain Res Rev*, 40(1-3):53–65, Oct 2002.

[76] U. M. Fietzek, F. Heinen, S. Berweck, S. Maute, A. Hufschmidt, J. Schulte-Monting, C. H. Lucking, and R. Korinthenberg. Development of the corticospinal system and hand motor function: central conduction times and motor performance tests. *Dev Med Child Neurol*, 42(4):220–7, Apr 2000.

[77] M. Flanders. Functional somatotopy in sensorimotor cortex. *Neuroreport*, 16(4):313–6, Mar 15 2005.

[78] T. Flash and B. Hochner. Motor primitives in vertebrates and invertebrates. *Curr Opin Neurobiol*, 15(6):660–6, Dec 2005.

[79] Flexpoint. Bend sensor technology, electronic interface design guide. Technical report, Draper, 1997.

[80] Flexpoint. Bend sensor technology, mechanical application design guide. Technical report, Draper, 1997.

[81] A. Floel, C. Breitenstein, F. Hummel, P. Celnik, C. Gingert, L. Sawaki, S. Knecht, and L. G. Cohen. Dopaminergic influences on formation of a motor memory. *Ann Neurol*, 58(1):121–30, Jul 2005.

[82] O. Foerster. *Motorische Felder und Bahnen*. Handbuch der Neurologie. Springer, 1936.

[83] S. Franco. *Design with Operational Amplifiers and Analog Integrated Circuits*. McGraw Hill, 2003.

[84] E. Freeman, E. Freeman, B. Bates, and K. Sierra. *Head First Design Patterns*. O'Reilly Media, 2004.

[85] C. Gaser and G. Schlaug. Gray matter differences between musicians and nonmusicians. *Ann N Y Acad Sci*, 999:514–7, Nov 2003.

[86] C.T. Gentile, M. Wallace, T.D. Avalon, S. Goodman, R. Fuller, and T. Hall. Angular displacement sensors, 1992.

[87] R. Gentner and J. Classen. Modular organization of finger movements by the human central nervous system. *Neuron*, 52(4):731–42, Nov 22 2006.

[88] A. P. Georgopoulos, J. F. Kalaska, R. Caminiti, and J. T. Massey. On the relations between the direction of two-dimensional arm movements and cell discharge in primate motor cortex. *J Neurosci*, 2(11):1527–37, Nov 1982.

[89] S. F. Giszter, F. A. MussaIvaldi, and E. Bizzi. Convergent force-fields organized in the frogs spinal-cord. *Journal of Neuroscience*, 13(2):467–491, FEB 1993.

[90] G.H. Golub and C.F. Van Loan. *Matrix computations*. Johns Hopkins University Press, 1996.

[91] M. Graziano. The organization of behavioral repertoire in motor cortex. *Annu Rev Neurosci*, 29:105–34, 2006.

[92] M. S. Graziano and T. N. Aflalo. Mapping behavioral repertoire onto the cortex. *Neuron*, 56(2):239–51, Oct 25 2007.

[93] M. S. Graziano, T. N. Aflalo, and D. F. Cooke. Arm movements evoked by electrical stimulation in the motor cortex of monkeys. *J Neurophysiol*, 94(6):4209–23, Dec 2005.

[94] M. S. Graziano, C. S. Taylor, T. Moore, and D. F. Cooke. The cortical control of movement revisited. *Neuron*, 36(3):349–62, Oct 24 2002.

[95] I. V. Grinyagin, E. V. Biryukova, and M. A. Maier. Kinematic and dynamic synergies of human precision-grip movements. *J Neurophysiol*, 94(4):2284–94, Oct 2005.

[96] C. Hager-Ross and M. H. Schieber. Quantifying the independence of human finger movements: comparisons of digits, hands, and movement frequencies. *J Neurosci*, 20(22):8542–50, Nov 15 2000.

[97] A. Handl. *Multivariate Verfahren*. Springer, 2002.

[98] M.S. Hefny. Business object model. Technical report, Al-Rivera, 2005.

[99] C.W. Hess. *Hirnstimulation – Historischer Überblick*. Springer, 2007.

[100] P. Hlustik, A. Solodkin, R. P. Gullapalli, D. C. Noll, and S. L. Small. Somatotopy in human primary motor and somatosensory hand representations revisited. *Cerebral Cortex*, 11(4):312–321, APR 2001.

[101] M. K. Holden. Virtual environments for motor rehabilitation: review. *Cyberpsychol Behav*, 8(3):187–211; discussion 212–9, Jun 2005.

[102] M.K. Holden and E. Todorov. *Use of virtual environments in motor learning and rehabilitation*. Lawrence Erlbaum Associates, 2002.

[103] G. Hommel, F. G. Hofmann, and J. Henz. The tu berlin high-precision sensor glove. *In Proceedings of the WWDU´94, Fourth International Scientific Conference, University of Milan*, 2, 1994.

[104] D. R. Humphrey. Representation of movements and muscles within the primate precentral motor cortex: historical and current perspectives. *Fed Proc*, 45(12):2687–99, Nov 1986.

[105] G. W. Huntley and E. G. Jones. Relationship of intrinsic connections to forelimb movement representations in monkey motor cortex - a correlative anatomic and physiological study. *Journal of Neurophysiology*, 66(2):390–413, AUG 1991.

[106] J. N. Ingram, K. P. Kording, I. S. Howard, and D. M. Wolpert. The statistics of natural hand movements. *Exp Brain Res*, 188(2):223–36, Jun 2008.

[107] Y. P. Ivanenko, G. Cappellini, N. Dominici, R. E. Poppele, and F. Lacquaniti. Coordination of locomotion with voluntary movements in humans. *Journal of Neuroscience*, 25(31):7238–7253, AUG 3 2005.

[108] Y. P. Ivanenko, G. Cappellini, R. E. Poppele, and F. Lacquaniti. Spatiotemporal organization of alpha-motoneuron activity in the human spinal cord during different gaits and gait transitions. *Eur J Neurosci*, 27(12):3351–68, Jun 2008.

[109] Y. P. Ivanenko, R. E. Poppele, and E. Lacquaniti. Five basic muscle activation patterns account for muscle activity during human locomotion. *Journal of Physiology-London*, 556(1):267–282, APR 1 2004.

[110] Liepert J., Terborg C., and C. Weiller. Motor plasticity induced by synchronized thumb and foot movements. *Exp Brain Res*, 125(4):435–9, 1999.

[111] Kleim J.A., Barbay S., and R.J. Nudo. Functional reorganization of the rat motor cortex following motor skill learning. *J Neurophysiol*, 80(6):3321–5, 1998.

[112] D. Jack, R. Boian, A. S. Merians, M. Tremaine, G. C. Burdea, S. V. Adamovich, M. Recce, and H. Poizner. Virtual reality-enhanced stroke rehabilitation. *IEEE Trans Neural Syst Rehabil Eng*, 9(3):308–18, Sep 2001.

[113] A. Jackson, V. J. Gee, S. N. Baker, and R. N. Lemon. Synchrony between neurons with similar muscle fields in monkey motor cortex. *Neuron*, 38(1):115–25, Apr 10 2003.

[114] R. Jalinous. *Principles of magnetic stimulator design*. Arnold, 2002.

[115] L. Jancke, G. Schlaug, and H. Steinmetz. Hand skill asymmetry in professional musicians. *Brain Cogn*, 34(3):424–32, Aug 1997.

[116] Rothwell J.C., Thompson P.D., Day B.L., Boyd S., and C.D. Marsden. Stimulation of the human motor cortex through the scalp. *Exp Physiol*, 76(2):159–200, 1991.

[117] T. E. Jerde, J. F. Soechting, and M. Flanders. Biological constraints simplify the recognition of hand shapes. *IEEE Trans Biomed Eng*, 50(2):265–9, Feb 2003.

[118] Sanes J.N. and J.P. Donoghue. Plasticity and primary motor cortex. *Annu Rev Neurosci*, 23:393–415, 2000.

[119] I.T. Joliffe. *Principal component analysis*. Springer, 2 edition, 2004.

[120] Brasil-Neto J.P., Valls-Sole J., Pascual-Leone A., Cammarota A., Amassian V.E., Cracco R., Maccabee P., Cracco J., Hallett M., and L.G. Cohen. Rapid modulation of human cortical motor outputs following ischaemic nerve block. *Brain*, 116(Pt 3):511–25, 1993.

[121] Donoghue J.P., Suner S., and J.N. Sanes. Dynamic organization of primary motor cortex output to target muscles in adult rats. ii. rapid reorganization following motor nerve lesions. *Exp Brain Res*, 79(3):492–503, 1990.

[122] A. Kaelin-Lang, L. Sawaki, and L. G. Cohen. Role of voluntary drive in encoding an elementary motor memory. *J Neurophysiol*, 93(2):1099–103, Feb 2005.

[123] B. Kainka. *Handbuch der PC-Mess- und Steuertechnik*. Franzis Verlag, 2001.

[124] T. Kammer and A. Thielscher. Physikalische und phyisologische grundlagen der transkraniellen magnetstimulation. *Nervenheilkunde*, 22:168–76, 2003.

[125] A. Keller. Intrinsic synaptic organization of the motor cortex. *Cereb Cortex*, 3(5):430–441, 1993.

[126] A. Kemper and A. Eickler. *Datenbanksysteme: Eine Einführung*. Oldenbourg, 2006.

[127] T. Kenny. *Electromagnetism in Sensing*. Newnes, 2005.

[128] G.D. Kessler, Hodges L., and Walker N. Evaluation of the cyber glove as a whole hand input device. *ACM Trans Comput Hum Interact*, 2(4):263–83, 1995.

[129] J. A. Kleim, T. M. Hogg, P. M. VandenBerg, N. R. Cooper, R. Bruneau, and M. Remple. Cortical synaptogenesis and motor map reorganization occur during late, but not early, phase of motor skill learning. *J Neurosci*, 24(3):628–33, Jan 21 2004.

[130] A. Kleinschmidt, M. F. Nitschke, and J. Frahm. Somatotopy in the human motor cortex hand area. a high-resolution functional mri study. *Eur J Neurosci*, 9(10):2178–86., 1997.

[131] J. W. Krakauer and R. Shadmehr. Consolidation of motor memory. *Trends Neurosci*, 29(1):58–64, Jan 2006.

[132] M. Kretschmar, S. Welsby, and L. Precision. *Capacitive and Inductive Displacement Sensors*. Newnes, 2005.

[133] M. A. Krutky and E. J. Perreault. Motor cortical measures of use-dependent plasticity are graded from distal to proximal in the human upper limb. *J Neurophysiol*, Oct 17 2007.

[134] M. Kuttuva, R. Boian, A. Merians, G. Burdea, M. Bouzit, J. Lewis, and D. Fensterheim. The rutgers arm, a rehabilitation system in virtual reality: a pilot study. *Cyberpsychol Behav*, 9(2):148–51, Apr 2006.

[135] H. C. Kwan, W. A. Mackay, J. T. Murphy, and Y. C. Wong. Spatial-organization of precentral cortex in awake primates .2. motor outputs. *Journal of Neurophysiology*, 41(5):1120–1131, 1978.

[136] C. E. Lang and M. H. Schieber. Differential impairment of individuated finger movements in humans after damage to the motor cortex or the corticospinal tract. *J Neurophysiol*, 90(2):1160–70, Aug 2003.

[137] C. E. Lang and M. H. Schieber. Human finger independence: limitations due to passive mechanical coupling versus active neuromuscular control. *J Neurophysiol*, 92(5):2802–10, Nov 2004.

[138] C. E. Lang and M. H. Schieber. Reduced muscle selectivity during individuated finger movements in humans after damage to the motor cortex or corticospinal tract. *J Neurophysiol*, 91(4):1722–33, Apr 2004.

[139] M. L. Latash, J. P. Scholz, and G. Schoner. Toward a new theory of motor synergies. *Motor Control*, 11(3):276–308, Jul 2007.

[140] D. G. Lawrence and H. G. Kuypers. The functional organization of the motor system in the monkey. i. the effects of bilateral pyramidal lesions. *Brain*, 91(1):1–14, Mar 1968.

[141] C. L. Lawson and R. J. Hanson. *Solving Least Squares Problems*. Prentice-Hall, 1974.

[142] D. D. Lee and H. S. Seung. Learning the parts of objects by non-negative matrix factorization. *Nature*, 401(6755):788–91, Oct 21 1999.

[143] J. N. Leijnse. Measuring force transfers in the deep flexors of the musician's hand: theoretical analysis, clinical examples. *J Biomech*, 30(9):873–82, Sep 1997.

[144] R. Lemon. *Basic physiology of transcranial magnetic stimulation*. Arnold, 2002.

[145] R. N. Lemon. Neural control of dexterity: what has been achieved? *Exp Brain Res*, 128(1-2):6–12, Sep 1999.

[146] R. N. Lemon, G. W. Mantel, and R. B. Muir. Corticospinal facilitation of hand muscles during voluntary movement in the conscious monkey. *J Physiol*, 381:497–527, Dec 1986.

[147] S. Liang. *Java(TM) Native Interface: Programmer's Guide and Specification*. Prentice Hall, 1999.

[148] D. Liu and E. Todorov. Evidence for the flexible sensorimotor strategies predicted by optimal feedback control. *J Neurosci*, 27(35):9354–68, Aug 29 2007.

[149] J. H. Martin. The corticospinal system: from development to motor control. *Neuroscientist*, 11(2):161–73, Apr 2005.

[150] M. W. Marzke and R. F. Marzke. Evolution of the human hand: approaches to acquiring, analysing and interpreting the anatomical evidence. *J Anat*, 197 (Pt 1):121–40, Jul 2000.

[151] C. R. Mason, J. E. Gomez, and T. J. Ebner. Hand synergies during reach-to-grasp. *J Neurophysiol*, 86(6):2896–910, Dec 2001.

[152] Maxim. A filter primer. Technical report, 2001.

[153] B. J. McKiernan, J. K. Marcario, J. H. Karrer, and P. D. Cheney. Corticomotoneuronal postspike effects in shoulder, elbow, wrist, digit, and intrinsic hand muscles during a reach and prehension task. *J Neurophysiol*, 80(4):1961–80, Oct 1998.

[154] F. Meintzschel and U. Ziemann. Modification of practice-dependent plasticity in human motor cortex by neuromodulators. *Cereb Cortex*, 16(8):1106–15, Aug 2006.

[155] J. M. Melgari, P. Pasqualetti, F. Pauri, and P. M. Rossini. Muscles in "concert": study of primary motor cortex upper limb functional topography. *PLoS ONE*, 3(8):e3069, 2008.

[156] M. Mentzel, F. Hofmann, T. Ebinger, B. Jatzold, L. Kinzl, and N. J. Wachter. Reproducibility of measuring the finger joint angle with a sensory glove. *Handchir Mikrochir Plast Chir*, 33(1):59–63; discussion 63–4, Jan 2001.

[157] A. S. Merians, H. Poizner, R. Boian, G. Burdea, and S. Adamovich. Sensorimotor training in a virtual reality environment: does it improve functional recovery post-stroke? *Neurorehabil Neural Repair*, 20(2):252–67, Jun 2006.

[158] Schieber M.H. and L.S. Hibbard. How somatotopic is the motor cortex hand area? *Science*, 261(5120):489–92, 1993.

[159] K. R. Mills, S. J. Boniface, and M. Schubert. Magnetic brain stimulation with a double coil: the importance of coil orientation. *Electroencephalogr Clin Neurophysiol*, 85(1):17–21, Feb 1992.

[160] M. H. Monfils, E. J. Plautz, and J. A. Kleim. In search of the motor engram: motor map plasticity as a mechanism for encoding motor experience. *Neuroscientist*, 11(5):471–83, Oct 2005.

[161] K. Morgen, N. Kadom, L. Sawaki, A. Tessitore, J. Ohayon, J. Frank, H. McFarland, R. Martin, and L. G. Cohen. Kinematic specificity of cortical reorganization associated with motor training. *Neuroimage*, 21(3):1182–7, Mar 2004.

[162] K. M. Mosier, R. A. Scheidt, S. Acosta, and F. A. Mussa-Ivaldi. Remapping hand movements in a novel geometrical environment. *J Neurophysiol*, 94(6):4362–72, Dec 2005.

[163] Rioult-Pedotti M.S., Friedman D., Hess G., and J.P. Donoghue. Strengthening of horizontal cortical connections following skill learning. *Nat Neurosci*, 1(3):230–4, 1998.

[164] V. K. Mushahwar, Y. Aoyagi, R. B. Stein, and A. Prochazka. Movements generated by intraspinal microstimulation in the intermediate gray matter of the anesthetized, decerebrate, and spinal cat. *Can J Physiol Pharmacol*, 82(8-9):702–14, Aug-Sep 2004.

[165] F. A. Mussa-Ivaldi and E. Bizzi. Motor learning through the combination of primitives. *Philos Trans R Soc Lond B Biol Sci*, 355(1404):1755–69, Dec 29 2000.

[166] F. A. Mussa-Ivaldi, S. F. Giszter, and E. Bizzi. Linear combinations of primitives in vertebrate motor control. *Proc Natl Acad Sci U S A*, 91(16):7534–8, Aug 2 1994.

[167] J. R. Napier. The prehensile movements of the human hand. *J Bone Joint Surg Br*, 38-B(4):902–13, Nov 1956.

[168] J. R. Napier and R. H. Tuttle. *Hands*. Princeton University Press, 1980.

[169] J.S. Neely and P.J. Restle. Capacitive bend sensors, 1997.

[170] K. M. Newell and D. E. Vaillancourt. Dimensional change in motor learning. *Hum Mov Sci*, 20(4-5):695–715, Nov 2001.

[171] M. A. L. Nicolelis. Brain-machine interfaces to restore motor function and probe neural circuits. *Nature Reviews Neuroscience*, 4(5):417–422, may 2003.

[172] R. J. Nudo, G. W. Milliken, W. M. Jenkins, and M. M. Merzenich. Use-dependent alterations of movement representations in primary motor cortex of adult squirrel monkeys. *J Neurosci*, 16(2):785–807, Jan 15 1996.

[173] S. A. Overduin, A. d'Avella, J. Roh, and E. Bizzi. Modulation of muscle synergy recruitment in primate grasping. *J Neurosci*, 28(4):880–92, Jan 23 2008.

[174] M. C. Park, A. Belhaj-Saif, M. Gordon, and P. D. Cheney. Consistent features in the forelimb representation of primary motor cortex in rhesus macaques. *Journal of Neuroscience*, 21(8):2784–2792, APR 15 2001.

[175] A. Pascual-Leone, A. Amedi, F. Fregni, and L. B. Merabet. The plastic human brain cortex. *Annu Rev Neurosci*, 28:377–401, 2005.

[176] A. Pascual-Leone, A. Cammarota, E. M. Wassermann, J. P. Brasil-Neto, L. G. Cohen, and M. Hallett. Modulation of motor cortical outputs to the reading hand of braille readers. *Ann Neurol*, 34(1):33–7., 1993.

[177] A. J. Pearce, G. W. Thickbroom, M. L. Byrnes, and F. L. Mastaglia. Functional reorganisation of the corticomotor projection to the hand in skilled racquet players. *Exp Brain Res*, 130(2):238–43., 2000.

[178] W. Penfield and E. Boldrey. Somatic motor and sensory representation in the cerebral cortex of man as studied by electrical stimulation. *Brain*, 37:389–443, 1937.

[179] W. Penfield and T. Rasmussen. *The Cerebral Cortex of Man. A Clinical Study of Localization of Function*. The Macmillan Comp., 1950.

[180] E. J. Plautz, G. W. Milliken, and R. J. Nudo. Effects of repetitive motor training on movement representations in adult squirrel monkeys: role of use versus learning. *Neurobiol Learn Mem*, 74(1):27–55, Jul 2000.

[181] T. Poggio and E. Bizzi. Generalization in vision and motor control. *Nature*, 431(7010):768–774, OCT 14 2004.

[182] A. V. Poliakov and M. H. Schieber. Limited functional grouping of neurons in the motor cortex hand area during individuated finger movements: A cluster analysis. *Journal of Neurophysiology*, 82(6):3488–3505, DEC 1999.

[183] V. G. Popescu, G. C. Burdea, M. Bouzit, and V. R. Hentz. A virtual-reality-based telerehabilitation system with force feedback. *IEEE Trans Inf Technol Biomed*, 4(1):45–51, Mar 2000.

[184] Porter R. and R. Lemon. *Corticospinal function and voluntary movement*, volume 45 of *Monographs of the Physiological Society*. Clarendon Press, 1993.

[185] P. Raghavan, E. Petra, J. W. Krakauer, and A. M. Gordon. Patterns of impairment in digit independence after subcortical stroke. *J Neurophysiol*, 95(1):369–78, Jan 2006.

[186] J. A. Rathelot and P. L. Strick. Muscle representation in the macaque motor cortex: an anatomical perspective. *Proc Natl Acad Sci U S A*, 103(21):8257–62, May 23 2006.

[187] K. T. Reilly and G. R. Hammond. Independence of force production by digits of the human hand. *Neurosci Lett*, 290(1):53–6, Aug 18 2000.

[188] G. Rizzolatti, L. Fogassi, and V. Gallese. Neurophysiological mechanisms underlying the understanding and imitation of action. *Nat Rev Neurosci*, 2(9):661–70, Sep 2001.

[189] B. Rohrer, S. Fasoli, H. I. Krebs, B. Volpe, W. R. Frontera, J. Stein, and N. Hogan. Submovements grow larger, fewer, and more blended during stroke recovery. *Motor Control*, 8(4):472–83, Oct 2004.

[190] P. M. Rossini, A. T. Barker, A. Berardelli, M. D. Caramia, G. Caruso, R. Q. Cracco, M. R. Dimitrijevic, M. Hallett, Y. Katayama, C. H. Lucking, A.L. Maertens de Noordhout, C.D. Marsden, N.M.F. Murray, J.C. Rothwell, M. Swash, and C. Tomberg. Non-invasive electrical and magnetic stimulation of the brain, spinal cord and roots: basic principles and procedures for routine clinical application. report of an ifcn committee. *Electroencephalogr Clin Neurophysiol*, 91(2):79–92., 1994.

[191] J.C. Rothwell. Techniques and mechanisms of action of transcranial stimulation of the human motor cortex. *J Neurosci Methods*, 74(2):113–122, 1997.

[192] J. Rouhonen. Trasncranial magnetic stimulation: modelling and new techniques. Master's thesis, Helsinki University of Technology, Finland, 1998.

[193] J. Rouhonen and R.J. Ilmoniemi. *Phyiscal principles for transcranial magnetic stimulation*. Arnold, 2002.

[194] P. Saltiel, M. C. Tresch, and E. Bizzi. Spinal cord modular organization and rhythm generation: an nmda iontophoretic study in the frog. *J Neurophysiol*, 80(5):2323–39, Nov 1998.

[195] J. N. Sanes, J. P. Donoghue, V. Thangaraj, R. R. Edelman, and S. Warach. Shared neural substrates controlling hand movements in human motor cortex. *Science*, 268(5218):1775–7, Jun 23 1995.

[196] J. N. Sanes, S. Suner, J. F. Lando, and J. P. Donoghue. Rapid reorganization of adult rat motor cortex somatic representation patterns after motor nerve injury. *Proc Natl Acad Sci U S A*, 85(6):2003–7, Mar 1988.

[197] M. Santello, M. Flanders, and J. F. Soechting. Postural hand synergies for tool use. *J Neurosci*, 18(23):10105–15, Dec 1 1998.

[198] M. Santello, M. Flanders, and J. F. Soechting. Patterns of hand motion during grasping and the influence of sensory guidance. *Journal of Neuroscience*, 22(4):1426–1435, FEB 15 2002.

[199] L. Sawaki, B. Boroojerdi, A. Kaelin-Lang, A. H. Burstein, C. M. Buetefisch, L. Kopylev, B. Davis, and L. G. Cohen. Cholinergic influences on use-dependent plasticity. *J Neurophysiol*, 87(1):166–71., 2002.

[200] L. Sawaki, L. G. Cohen, J. Classen, B. C. Davis, and C. M. Buetefisch. Enhancement of use-dependent plasticity by d-amphetamine. *Neurology*, 59(8):1262–4, Oct 22 2002.

[201] L. Sawaki, K. J. Werhahn, R. Barco, L. Kopylev, and L. G. Cohen. Effect of an alpha(1)-adrenergic blocker on plasticity elicited by motor training. *Exp Brain Res*, 148(4):504–8, Feb 2003.

[202] S. Schaal, A. Ijspeert, and A. Billard. Computational approaches to motor learning by imitation. *Philos Trans R Soc Lond B Biol Sci*, 358(1431):537–47, Mar 29 2003.

[203] S. Schaal and N. Schweighofer. Computational motor control in humans and robots. *Curr Opin Neurobiol*, 15(6):675–82, Dec 2005.

[204] M. H. Schieber. Individuated finger movements of rhesus monkeys: a means of quantifying the independence of the digits. *J Neurophysiol*, 65(6):1381–91, Jun 1991.

[205] M. H. Schieber. Muscular production of individuated finger movements: the roles of extrinsic finger muscles. *J Neurosci*, 15(1 Pt 1):284–97, Jan 1995.

[206] M. H. Schieber. *Individuated finger movements. Rejecting the labeled-line hypothesis.* Academic Press, 1996.

[207] M. H. Schieber. Somatotopic gradients in the distributed organization of the human primary motor cortex hand area: evidence from small infarcts. *Exp Brain Res*, 128(1-2):139–48, Sep 1999.

[208] M. H. Schieber. Constraints on somatotopic organization in the primary motor cortex. *Journal of Neurophysiology*, 86(5):2125–2143, NOV 2001.

[209] M. H. Schieber and A. V. Poliakov. Partial inactivation of the primary motor cortex hand area: effects on individuated finger movements. *J Neurosci*, 18(21):9038–54, Nov 1 1998.

[210] M. H. Schieber and M. Santello. Hand function: peripheral and central constraints on performance. *J Appl Physiol*, 96(6):2293–300, Jun 2004.

[211] M.H. Schieber, K.T. Reilly, and C.E. Lang. *Motor cortex control of a complex peripheral apparatus: The neuromuscular evolution of individuated finger movements*. CRC Press, 2005.

[212] R. Schmidt, G. Thews, and F. Lang. *Physiologie des Menschen*. Springer, 2000.

[213] R.A. Schmidt and T.D. Lee. *Motor control and learning*. Human Kinetics, 2003.

[214] J. P. Scholz and G. Schoner. The uncontrolled manifold concept: identifying control variables for a functional task. *Exp Brain Res*, 126(3):289–306, Jun 1999.

[215] P. Schwenkreis, S. El Tom, P. Ragert, B. Pleger, M. Tegenthoff, and H. R. Dinse. Assessment of sensorimotor cortical representation asymmetries and motor skills in violin players. *Eur J Neurosci*, 26(11):3291–302, Dec 2007.

[216] S. H. Scott. Optimal feedback control and the neural basis of volitional motor control. *Nat Rev Neurosci*, 5(7):532–46, Jul 2004.

[217] R. Shadmehr and H. H. Holcomb. Neural correlates of motor memory consolidation. *Science*, 277(5327):821–5, Aug 8 1997.

[218] R. Shadmehr and J. W. Krakauer. A computational neuroanatomy for motor control. *Exp Brain Res*, 185(3):359–81, Mar 2008.

[219] R. Shadmehr and F. A. Mussa-Ivaldi. Adaptive representation of dynamics during learning of a motor task. *J Neurosci*, 14(5 Pt 2):3208–24, may 1994.

[220] R. Shadmehr and S.P. Wise. *The computational biology of reaching and pointing*. The MIT Press, 2005.

[221] Y. Shinoda, J. I. Yokota, and T. Futami. Divergent projection of individual corticospinal axons to moto-neurons of multiple muscles in the monkey. *Neuroscience Letters*, 23(1):7–12, 1981.

[222] P.E. Shrout and J.L. Fleiss. Intraclass correlations: Uses in assessing rater reliabiltiy. *Psychological Bulletin*, 86(2):420–28, 1979.

[223] H.R. Siebner and U. Ziemann. *Hirnstimulation – Physiologische Grundlagen*. Springer, 2007.

[224] K. Sierra and B. Bates. *Head First Java*. O'Reilly Media, 2005.

[225] L. K. Simone and D. G. Kamper. Design considerations for a wearable monitor to measure finger posture. *J Neuroeng Rehabil*, 2(1):5, Mar 1 2005.

[226] L. K. Simone, N. Sundarrajan, X. Luo, Y. Jia, and D. G. Kamper. A low cost instrumented glove for extended monitoring and functional hand assessment. *J Neurosci Methods*, 160(2):335–48, Mar 15 2007.

[227] J. F. Soechting and M. Flanders. Flexibility and repeatability of finger movements during typing: Analysis of multiple degrees of freedom. *Journal of Computational Neuroscience*, 4(1):29–46, JAN 1997.

[228] M.W. Spong, S. Hutchinson, and M. Vidyasagar. *Robot modeling and control*. Wiley, 2005.

[229] O. Sporns and G. Edelman. Solving bernstein's problem: A proposal for the development of coordinated movement by selection. *Child development*, 64(4):960–981, AUG 1993.

[230] K. Stefan, J. Classen, P. Celnik, and L. G. Cohen. Concurrent action observation modulates practice-induced motor memory formation. *Eur J Neurosci*, 27(3):730–8, Feb 2008.

[231] K. Stefan, L. G. Cohen, J. Duque, R. Mazzocchio, P. Celnik, L. Sawaki, L. Ungerleider, and J. Classen. Formation of a motor memory by action observation. *J Neurosci*, 25(41):9339–46, Oct 12 2005.

[232] S. D. Stoney, W. D. Thompson, and H. Asanuma. Excitation of pyramidal tract cells by intracortical microstimulation - effective extent of stimulating current. *Journal of Neurophysiology*, 31(5):659–666, 1968.

[233] P. L. Strick. Stimulating research on motor cortex. *Nature Neuroscience*, 5(8):714–715, AUG 2002.

[234] P. L. Strick and J. B. Preston. 2 representations of the hand in area 4 of a primate .1. motor output organization. *Journal of Neurophysiology*, 48(1):139–149, 1982.

[235] G. Sumbre, G. Fiorito, T. Flash, and B. Hochner. Neurobiology: motor control of flexible octopus arms. *Nature*, 433(7026):595–6, Feb 10 2005.

[236] B.N. Tillmann. *Atlas der Anatomie des Menschen*. Springer, 2005.

[237] E. Todorov. Optimality principles in sensorimotor control. *Nat Neurosci*, 7(9):907–15, Sep 2004.

[238] E. Todorov. Analysis of the synergies underlying complex hand manipulation. *Annual International Conference of the IEEE Engineering in Biology and Medicine Society*, 2004a.

[239] E. Todorov and M. I. Jordan. Optimal feedback control as a theory of motor coordination. *Nat Neurosci*, 5(11):1226–35, Nov 2002.

[240] P. S. Tofts. The distribution of induced currents in magnetic stimulation of the nervous system. *Phys Med Biol*, 35(8):1119–28, Aug 1990.

[241] M. C. Tresch and E. Bizzi. Responses to spinal microstimulation in the chronically spinalized rat and their relationship to spinal systems activated by low threshold cutaneous stimulation. *Exp Brain Res*, 129(3):401–16, Dec 1999.

[242] M. C. Tresch, V. C. Cheung, and A. d'Avella. Matrix factorization algorithms for the identification of muscle synergies: evaluation on simulated and experimental data sets. *J Neurophysiol*, 95(4):2199–212, Apr 2006.

[243] M. C. Tresch, P. Saltiel, and E. Bizzi. The construction of movement by the spinal cord. *Nat Neurosci*, 2(2):162–7, Feb 1999.

[244] N.G. Tsagarakis, B. Kenward, K. Rosander, D.G. Caldwell, and C. von Hofsten. "babyglove": A device to study hand motion control development in infants. *EuroHaptics*, 2006.

[245] Di Lazzaro V., Oliviero A., Profice P., Saturno E., Pilato F., Insola A., Mazzone P., Tonali P., and J.C. Rothwell. Comparison of descending volleys evoked by transcranial magnetic and electric stimulation in conscious humans. *Electroencephalography and Clinical Neurophysiology*, 109:397–401, 1998.

[246] F. J. Valero-Cuevas, M. E. Johanson, and J. D. Towles. Towards a realistic biomechanical model of the thumb: the choice of kinematic description may be more critical than the solution method or the variability/uncertainty of musculoskeletal parameters. *J Biomech*, 36(7):1019–30, Jul 2003.

[247] F. J. Valero-Cuevas and H. Lipson. A computational environment to simulate complex tendinous topologies. *Conf Proc IEEE Eng Med Biol Soc*, 6:4653–6, 2004.

[248] F. J. Valero-Cuevas, M. Venkadesan, and E. Todorov. Structured variability of muscle activations supports the minimal intervention principle of motor control. *J Neurophysiol*, Apr 15 2009.

[249] F. J. Valero-Cuevas, J. W. Yi, D. Brown, 3rd McNamara R. V., C. Paul, and H. Lipson. The tendon network of the fingers performs anatomical computation at a macroscopic scale. *IEEE Trans Biomed Eng*, 54(6 Pt 2):1161–6, Jun 2007.

[250] A. Viau, A. G. Feldman, B. J. McFadyen, and M. F. Levin. Reaching in reality and virtual reality: a comparison of movement kinematics in healthy subjects and in adults with hemiparesis. *J Neuroeng Rehabil*, 1(1):11, Dec 14 2004.

[251] Muellbacher W., Ziemann U., Wissel J., Dang N., Kofler M., Facchini S., Boroojerdi B., Poewe W., and M. Hallett. Early consolidation in human primary motor cortex. *Nature*, 415(6872):640–4, 2002.

[252] T. Wagner, A. Valero-Cabre, and A. Pascual-Leone. Noninvasive human brain stimulation. *Annu Rev Biomed Eng*, 9:527–65, 2007.

[253] N. S. Ward, M. M. Brown, A. J. Thompson, and R. S. Frackowiak. Neural correlates of motor recovery after stroke: a longitudinal fmri study. *Brain*, 126(Pt 11):2476–96, Nov 2003.

[254] D. Watanabe, T. Savion-Lemieux, and V. B. Penhune. The effect of early musical training on adult motor performance: evidence for a sensitive period in motor learning. *Exp Brain Res*, 176(2):332–40, Jan 2007.

[255] T. Watkins. *Force, Load and Weight Sensors.* Newnes, 2005.

[256] A.H Watson. What can studying musicians tell us about motor control of the hand? *J.Anat.*, (208):527–542, 2006.

[257] E. J. Weiss and M. Flanders. Muscular and postural synergies of the human hand. *J Neurophysiol*, 92(1):523–35, Jul 2004.

[258] K. Wendicke. Optimierung von stimulationsspulen für die induktive nervenreizung. Master's thesis, Technical University of Munich, 2006.

[259] K. J. Werhahn, J. K. Fong, B. U. Meyer, A. Priori, J. C. Rothwell, B. L. Day, and P. D. Thompson. The effect of magnetic coil orientation on the latency of surface emg and single motor unit responses in the first dorsal interosseous muscle. *Electroencephalogr Clin Neurophysiol*, 93(2):138–46, Apr 1994.

[260] T. Weyh and H.R. Siebner. *Hirnstimulation – Technische Grundlagen*. Springer, 2007.

[261] M. Wiesendanger. Manual dexterity and the making of tools - an introduction from an evolutionary perspective. *Exp Brain Res*, 128(1-2):1–5, Sep 1999.

[262] N. W. Williams, J. M. Penrose, C. M. Caddy, E. Barnes, D. R. Hose, and P. Harley. A goniometric glove for clinical hand assessment. construction, calibration and validation. *J Hand Surg [Br]*, 25(2):200–7, Apr 2000.

[263] F. R. Wilson. *Mathematik*. Vintage, 1998.

[264] S. Wise, W. Gardner, E. Sabelman, E. Valainis, Y. Wong, K. Glass, J. Drace, and J. M. Rosen. Evaluation of a fiber optic glove for semi-automated goniometric measurements. *J Rehabil Res Dev*, 27(4):411–24, Fall 1990.

[265] C. Woolsey, J. Barnard, R. Butler, G. Crandall, J. Fay, R. Ostenso, P. Settlage, and A. Travis. Patterns of localization in somatic efferent and afferent systems of the cerebral cortex of the chimpanzee. *Federation Proceedings*, 11(1):176–176, 1952.

[266] C. N. Woolsey, T. C. Erickson, and W. E. Gilson. Localization in somatic sensory and motor areas of human cerebral-cortex as determined by direct recording of evoked-potentials and electrical-stimulation. *Journal of Neurosurgery*, 51(4):476–506, 1979.

[267] R. W. Young. Evolution of the human hand: the role of throwing and clubbing. *J Anat*, 202(1):165–74, Jan 2003.

[268] V. M. Zatsiorsky, Z. M. Li, and M. L. Latash. Enslaving effects in multi-finger force production. *Exp Brain Res*, 131(2):187–95, Mar 2000.

Peer reviewed papers

Classen J, Stefan K, Wolters A, Wycislo M, **Gentner R**, Zeller D, Schramm A, Sandbrink F, Litvak V, Schmidt A, Weise D. TMS-induzierte Plastizität: Ein Fenster zum Verständnis des motorischen Lernens? Klin Neurophysiol, 2005; 36: 178-85.

Gentner R, Classen J. Development and evaluation of a low-cost sensor glove for assessment of human finger movements in neurophysiological settings. J Neurosci Methods, 2009; 178: 138-47.

Gentner R, Classen J. Modular organization of finger movements by the human central nervous system. Neuron, 2006; 52: 731-42.

Gentner R, Wankerl K, Reinsberger C, Zeller D, Classen J. Depression of human corticospinal excitability induced by magnetic theta-burst stimulation: evidence of rapid polarity-reversing metaplasticity. Cereb Cortex, 2007; 18: 2046-2053.

Litvak V, Zeller D, Oostenveld R, Maris E, Cohen A, Schramm A, **Gentner R**, Zaaroor M, Pratt H, Classen J. LTP-like changes induced by paired associative stimulation of the primary somatosensory cortex in humans: source analysis and associated changes in behaviour. Eur J Neurosci, 2007; 25: 2862-74.

Stefan K, **Gentner R**, Zeller D, Dang S, Classen J. Theta-burst stimulation: remote physiological and local behavioral after-effects. Neuroimage, 2008; 40: 265-74.

Stefan K, Wycislo M, **Gentner R**, Schramm A, Naumann M, Reiners K, Classen J. Temporary occlusion of associative motor cortical plasticity by prior dynamic motor training. Cereb Cortex, 2006; 16: 376-85.

Conferences

Gentner R, Classen J. Development and evaluation of a low cost sensor glove for assessment of physiological parameters. Federation of the European Neuroscience Societies Meeting: Geneva, 2008.

Gentner R, Classen J. Modular organisation of hand movements by the human central nervous system: A transcranial magnetic stimulation study. German Society for Neuroscience Meeting: Mannheim, 2006.

Gentner R, Reinsberger C, Stefan K, Zeller D, . CJ. Magnetische Theta-Burst Stimulation: Rolle der vorangehenden Aktivierung des Motorkortex. German Society for Clinical Neurophysiology Meeting: Munich, 2007.

Gentner R, Stefan K, Arnold A, Kessler K, Gutsche A, Kramer H, Koch A, Classen J. Mapping finger movements by transcranial magnetic stimulation. German Society for Neuroscience Meeting: Mannheim, 2006.

Gentner R, Stefan K, Kessler K, Arnold A, Koch AW, Classen J. Finger movement pat-

terns elicited by transcranial magnetic stimulation of human primary motor cortex. Society for Neuroscience Meeting: Washington DC, 2005.

Gentner R, Weise D, Buttmann M, Classen J. Finger movement representation is shaped by long-term practice of musical skills. Third International Conference on Transcranial Magnetic and Direct Current Stimulation Goettingen, 2008.

Missitzi J, **Gentner R**, Geladas N, Classen J, Klissouras V. Genetic variation of plasticity in human motor cortex. Third International Conference on Transcranial Magnetic and Direct Current Stimulation Goettingen, 2008.

Nagel A, **Gentner R**, Classen J. Reduced degrees of freedom of finger movements in multiple sclerosis patients with impaired hand function - a TMS study. German Society for Neuroscience Meeting: Hamburg, 2008.

Nagel A, **Gentner R**, Zeller D, Reinsberger C, Classen J. Different modular characteristics of TMS-evoked finger movements in multiple sclerosis patients with impaired hand function. Third International Conference on Transcranial Magnetic and Direct Current Stimulation Goettingen, 2008.

Oenal C, **Gentner R**, Uebelmesser A, Classen J. Retention of performance increments in a serial reaction time task: Influence of post-training emotional interference. 5th Brain and Behaviour Days - Comparative Research on Emotion Processing: Kloster Bronnbach, 2007.

Wankerl K, **Gentner R**, Classen J. Inhibition of movement representation by Transcranial Magnetic Stimulation timed to Event Related Synchronisation. German Society for Neuroscience Meeting: Hamburg, 2008a.

Wankerl K, **Gentner R**, Weise D, Zeller D. Metaplasticity of cTBS-induced enhancement of corticospinal excitability: dependence on activation of L-Type voltage-gated Ca2+ channels. Third International Conference on Transcranial Magnetic and Direct Current Stimulation Goettingen, 2008b.

Wankerl K, **Gentner R**, Zeller D, Classen J. L-type voltage-gated Ca2+-channels link activity-dependent metaplasticity to human LTP/LTD-like plasticity. Federation of the European Neuroscience Societies Meeting: Geneva, 2008c.

Weise D, **Gentner R**, Classen J. Matching midbrain-sonography to its macroanatomic correlate. German Society for Clinical Neurophysiology Meeting: Magdeburg, 2008.

Zeller D, AufmKampe K, Stefan K, **Gentner R**, Toyka K, Rieckmann P, Classen J. Rapid onset central motor plasticity is not compromised in multiple sclerosis patients. European Neurological Society Meeting Nice, 2008.

Talks

Gentner R, Classen J. Magentic mapping of the human motor cortex. What does it tell us about the physiology and pathophysiology of finger movements? Santa Lucia Foundation: Rome, 2008.

Gentner R, Classen J. Mapping of finger movement synergies in human motor system by transcranial magnetic stimulation. 39th Annual Congress of the German Society for Biomedical Engineering Nuremberg, 2005.

List of figures

List of tables